Molecular Mode of Action of Flavonoids: From Neuroprotective Hybrids to Molecular Probes for Chemical Proteomics.

Wirkmechanismen von Flavonoiden: Von neuroprotektiven Hybriden zu Sonden für chemische Proteomik.

Doctoral thesis for a doctoral degree
at the Graduate School of Life Sciences,
Julius-Maximilians-Universität Würzburg,
Section Neuroscience
submitted by

Sandra Gunesch

from

Heilbronn

Würzburg, 2020

Submitted on: .....
Office stamp

Members of the Thesis Committee

Chairperson: Prof. Dr. Peter Jakob

Primary Supervisor: Prof. Dr. Michael Decker

Supervisor (Second): Prof. Dr. Dr. Lorenz Meinel

Supervisor (Third): Prof. Dr. Petra Högger

Date of Public Defense:

Date of Receipt of Certificates:

The presented work has been carried out as a member of the Graduate School of Life Science under the supervision of Professor Dr. Michael Decker at the Chair of Pharmaceutical and Medicinal Chemistry at the Institute for Pharmacy and Food Chemistry of the Julius Maximilian University of Würzburg between November 2016 und August 2020.

List of Publications

1. **Gunesch, S.**; Soriano-Castell, D.; Lamer, S.; Schlosser, A.; Maher, P.; Decker, M. Development and application of a chemical probe based on a neuroprotective flavonoid hybrid for target identification using activity-based protein profiling. *ACS Chem. Neurosci.* **2020** (in press). DOI: http://dx.doi.org/10.1021/acschemneuro.0c00589

2. **Gunesch, S.**; Hoffmann, M.; Kiermeier, C.; Fischer, W.; Pinto, A. F. M.; Maurice, T.; Maher, P.; Decker, M. 7-*O*-Esters of taxifolin with pronounced and overadditive effects in neuroprotection, anti-neuroinflammation, and amelioration of short-term memory impairment *in vivo*. *Redox Biol.* **2020**, *29* (2020), 101378.

3. Hoffmann, M.; Stiller, C.; Endres, E.; Scheiner, M.; **Gunesch, S.**; Sotriffer, C.; Maurice, T.; Decker, M. Highly selective butyrylcholinesterase inhibitors with tunable duration of action by chemical modification of transferable carbamate units exhibit pronounced neuroprotective effect in an Alzheimer's disease mouse model. *J. Med. Chem.* **2019**, *62* (20), 9116-9140.

4. Scheiner, M.; Dolles, D.; **Gunesch, S**.; Hoffmann, M.; Nabissi, M.; Marinelli, O.; Naldi, M.; Bartolini, M.; Petralla, S.; Poeta, E.; Monti, B.; Falkeis, C.; Vieth, M.; Hübner, H.; Gmeiner, P.; Maitra, R.; Maurice, T.; Decker, M. Dual-acting cholinesterase-human cannabinoid receptor 2 ligands show pronounced neuroprotection *in vitro* and overadditive and disease-modifying neuroprotective effects *in vivo*. *J. Med. Chem.* **2019**, *62* (20), 9078-9102.

5. Schramm, S.; **Gunesch, S.**; Lang, F.; Saedtler, M.; Meinel, L.; Högger, P.; Decker, M. Investigations into neuroprotectivity, stability, and water solubility of 7-*O*-cinnamoylsilibinin, its hemisuccinate and dehydro derivatives. *Arch. Pharm. Chem. Life Sci.* **2018**, *351* (11), e1800206.

6. Schramm, S.; Huang, G.; **Gunesch, S.**; Lang, F.; Roa, J.; Högger, P.; Sabaté, R.; Maher, P.; Decker, M. Regioselective synthesis of 7-*O*-esters of the flavonolignan silibinin and SARs lead to compounds with overadditive neuroprotective effects. *Eur. J. Med. Chem.* **2018**, *146* (2018), 93-107.

7. Dolles, D.; Hoffmann, M.; **Gunesch, S.**; Marinelli, O.; Möller, J.; Santoni, G.; Chatonnet, A.; Lohse, M. J.; Wittmann, H. J.; Strasser, A.; Nabissi, M.; Maurice, T.; Decker, M. Structure-activity relationships and computational investigations into the development of potent and balanced dual-acting butyrylcholinesterase inhibitors and human cannabinoid receptor 2 ligands with pro-cognitive *in vivo* profiles. *J. Med. Chem.* **2018**, *61* (4), 1646-1663.

8. **Gunesch S.**; Schramm, S.; Decker, M. Natural antioxidants in hybrids for the treatment of neurodegenerative diseases: a successful strategy? *Future Med. Chem.* **2017**, *9* (8), 711-713.

Other scientific contributions

Gunesch, S.; Hofmann, J.; Decker, M. Synthesis and characterization of flavonoid-based chemical probes for target identification. EUREKA! Symposium 2019 of the Graduate School of Life Sciences, Würzburg (Germany), October 9th – 10th, 2019 (Poster).

Gunesch S.; Kiermeier, C.; Maher, P.; Decker, M. Hybrids of taxifolin and phenolic acids – *in vitro* assays reveal overadditive neuroprotection. EFMC-ACSMEDI MedChem Frontiers 2019 Symposium, Krakow (Poland), June 10th – 12th, 2019 (Poster).

Gunesch, S.; Schramm, S.; Lang, F.; Roa, J.; Högger, P.; Sabaté, R.; Maher, P.; Decker, M. Novel hybrids of neuroprotective natural products: *in vitro* investigation reveal overadditive effect. MuTaLig & Companies: The multi-targeting drug discovery with implications at industrial level of the MuTaLig COST Action, Valletta (Malta), October 18th – 19th, 2018 (Poster).

Gunesch, S.; Kiermeier, C.; Decker, M. Neuroprotective hybrids of taxifolin – *In vitro* investigations reveal overadditive effect and HO-1 upregulation. EUREKA! Symposium 2018 of the Graduate School of Life Sciences, Würzburg (Germany), October 10th – 11th, 2018 (Poster).

Gunesch S. Natural product hybrids as neuroprotectants. Neuroscience Summer School of the Graduate School of Life Sciences, Marktbreit (Germany), October 5th – 7th, 2018 (Presentation).

Copyrights

Parts of this work have been published previously and are reproduced, adapted, and/or modified with the permission of:

Gunesch, S.; Soriano-Castell, D.; Lamer, S.; Schlosser, A.; Maher, P.; Decker, M. Development and application of a chemical probe based on a neuroprotective flavonoid hybrid for target identification using activity-based protein profiling. *ACS Chem. Neurosci.* **2020** (in press). DOI: http://dx.doi.org/10.1021/acschemneuro.0c00589

Gunesch, S.; Hoffmann, M.; Kiermeier, C.; Fischer, W.; Pinto, A. F. M.; Maurice, T.; Maher, P.; Decker, M. 7-*O*-Esters of taxifolin with pronounced and overadditive effects in neuroprotection, anti-neuroinflammation, and amelioration of short-term memory impairment *in vivo*. *Redox Biol.* **2020**, *29* (2020), 101378.

Gunesch S.; Schramm, S.; Decker, M. Natural antioxidants in hybrids for the treatment of neurodegenerative diseases: a successful strategy? *Future Med. Chem.* **2017**, *9* (8), 711-713.

Declaration of Authorship

Publication (complete reference): **Gunesch, S.**; Soriano-Castell, D.; Lamer, S.; Schlosser, A.; Maher, P.; Decker, M. Development and application of a chemical probe based on a neuroprotective flavonoid hybrid for target identification using activity-based protein profiling. *ACS Chem. Neurosci.* **2020** (in press). DOI: http://dx.doi.org/10.1021/acschemneuro.0c00589					
Participated in	**Author Initials,** Responsibility decreasing from left to right				
Study Design Methods Development	SG/PM/MD	AS	DSC		
Data Collection	SG	PM	DSC	SL/AS	
Data Analysis and Interpretation	SG	PM	SL/AS	DSC	
Manuscript Writing Writing of Introduction Writing of Materials & Methods Writing of Discussion Writing of First Draft	 SG SG SG SG	 PM SL/AS PM/MD PM/MD	 MD PM		

Explanations (if applicable): exclusive first authorship

Publication (complete reference): **Gunesch, S.**; Hoffmann, M.; Kiermeier, C.; Fischer, W.; Pinto, A. F. M.; Maurice, T.; Maher, P.; Decker, M. 7-*O*-Esters of taxifolin with pronounced and overadditive effects in neuroprotection, anti-neuroinflammation, and amelioration of short-term memory impairment *in vivo*. *Redox Biol.* **2020**, *29* (2020), 101378.					
Participated in	**Author Initials,** Responsibility decreasing from left to right				
Study Design Methods Development	SG/MD	PM/TM	WF/AFMP		
Data Collection	SG	MH	CK	WF	
Data Analysis and Interpretation	SG	MD/PM/TM			
Manuscript Writing Writing of Introduction Writing of Materials & Methods Writing of Discussion Writing of First Draft	 SG SG SG SG	 MD MH/WF PM/TM PM/MD	 MD	 MH	

Explanations (if applicable): exclusive first authorship

Affidavit

I hereby confirm that my thesis entitled *Molecular Mode of Action of Flavonoids: From Neuroprotective Hybrids to Molecular Probes for Chemical Proteomics* is the result of my own work. I did not receive any help or support from commercial consultants. All sources and/or materials applied are listed and specified in the thesis.

Furthermore, I confirm that this thesis has not yet been submitted as part of another examination process neither in identical nor in similar form.

Place, Date Signature

Eidesstattliche Erklärung

Hiermit erkläre ich an Eides statt, die Dissertation *Wirkmechanismen von Flavonoiden: Von neuroprotektiven Hybriden zu Sonden für chemische Proteomik* eigenständig, d.h. insbesondere selbstständig und ohne Hilfe eines kommerziellen Promotionsberaters, angefertigt und keine anderen als die von mir angegebenen Quellen und Hilfsmittel verwendet zu haben.

Ich erkläre außerdem, dass die Dissertation weder in gleicher noch in ähnlicher Form bereits in einem anderen Prüfungsverfahren vorgelegen hat.

Ort, Datum Unterschrift

Acknowledgements

The present work would not have been possible without the willingness and support of my supervisors, collaborators, and coworkers.

I want to thank my thesis committee for their support and inspiring discussions. Prof. Dr. Dr. Meinel and Prof. Dr. Högger provided workspace in their labs, which I gratefully acknowledge, and which made the interdisciplinarity of this work possible. I also would like to recognize the effort that I received from the scientists in their labs. Many thanks to Dr. Alexandra Braun, Dr. Valerie Spieler, Dr. Marcus Gutmann, and Niklas Hauptstein from the Meinel lab and Dr. Stoyan Dirimanov and Florian Lang from the Högger lab.

I would like to thank my primary supervisor Prof. Dr. Michael Decker, for providing guidance throughout the project, for the motivation, encouragement, and trust in my abilities.

A very important part of this work wouldn't have been possible without Dr. Pamela Maher from the Salk Institute for Biological Studies. I would like to express my deepest gratitude for her support, thoughtful comments and recommendations, considerate guidance, and scientific inspiration, which led to this fruitful collaboration. The time I spent in her and Prof. Schubert's lab brought my research to a higher level and nurtured my confidence as a scientist. I also want to thank all lab members for the warm welcome and for making my two research stays so memorable. Special thanks to Antonio for inspiring questions and, together with Josh, for introducing me to surfing; Devin, David, and Gamze for fun times in and outside the lab.

Several more people contributed to this work, and I would like to thank all my collaboration partners: Dr. Wolfgang Fischer and Dr. Antonio Pinto from the Salk Institute for support with cellular uptake experiments. Dr. Tangui Maurice from the MMDN at the University of Montpellier and Dr. Matthias Hoffmann from the University of Würzburg for the *in vivo* studies. Prof. Dr. Andreas Schlosser and Stephanie Lamer from the RVZ in Würzburg for the chemical proteomics studies. Matthias Scheiner, Feng He and Florian Lang from the University of Würzburg for antioxidant capacity assays, Julian Hofmann from the University of Würzburg for synthetic support and finally, my master student Carolina Kiermeier and my practical student Alexandra Sink, who both contributed to projects.

Further, I would like to acknowledge the GSLS and their extraordinary program and support. The travel fellowships, attending the mentoring program, several workshops, and the opportunity to organize an international symposium were great experiences that promoted my scientific and personal development.

In the Decker lab, I had the great pleasure of working with Dominik, Simon, Luca, Matthias, Matze, Christian, Julian, Diego, Hubert, Anna, Feng, Antonis, Philipp, and Sophie – I'm more than thankful for the positive and supportive environment. Our group spirit felt unique, and I will definitely miss our fun lunch breaks, always enlightening frustrating days. Special thanks also to Xinyu for inspiring conversations and always valuable advice. I also want to thank Daniela, Tomasz, and Carina for the friendship that arose from our time together at the institute.

In addition, I want to thank my "Reisegruppe"-friends for the happy distractions and the interest in my work, with special thanks to Luis for the support with technical equipment while writing this thesis.

Importantly, I want to express my deepest appreciation to my partner Jens for his patience and endless support, his sympathetic ear, and clear thoughts.

On this special occasion, I would like to thank my dear brother Andreas and my parents Johann and Hannelore, for their unconditional love and support. They set me an example of the impact of hard work and dedication on the possibilities and success in life.

Table of Content

1. Introduction

Humans used plants as medicine already 60 000 years ago.[1] Flower pollens discovered in a Neanderthal grave in northern Iraq were identified as plant species with medicinal properties.[2] Traditional medicine with plants intentionally used in potions and oils as treatment is documented back to 2600 BC.[3] Among the plant-derived medicines depicted on clay tablets from Mesopotamia from that period were oils from *Commiphora* species (myrrh) and *Cupressus sempervirens* (cypress), both still in use today for treatment of coughs and inflammation.[3, 4] Historically, the remedies from nature were applied without any knowledge about the bioactive compounds. The treatment was based on the knowledge of people experimenting for centuries.[4]

Nowadays, drug discovery follows two major approaches: First, the phenotypic screening approach identifies compounds leading to a positive outcome in different cellular or animal models of a disease.[5] Institutional compounds like salicylic acid in white willow bark and morphine from poppies were discovered with this approach in the years 1897 and 1806, respectively.[6] Second, the approach of synthetic chemical libraries that are tested against preselected targets (one-target strategy) in high throughput screenings.[7] Advances in combinatorial chemistry and robotic devices enabled and promoted this method.[7] The one-target strategy dominates the pharmaceutical industry and has led to some successful launches of drugs, mostly in the field of cancer.[7] While both approaches have their advantages and disadvantages, the one-target strategy has failed in drug discovery regarding complex diseases, like Alzheimer's disease (AD).[8]

1.1 Alzheimer's Disease

In 1907, Alois Alzheimer described the course of a disease and the examination of his patient Auguste Deter in the report "On an Unusual Illness of the Cerebral Cortex" (orig. title „Über eine eigenartige Erkrankung der Hirnrinde").[9] More than 100 years later his findings have not lost any clinical significance:

"As the illness progressed, these phenomena which are to be interpreted as complex symptoms appear sometimes stronger, sometimes weaker. ... the imbecility of the patient increased in general. Her death occurred after four and a half years of illness. At the end, the patient was lying in bed in a fetal position completely pathetic, incontinent."[10]

Alzheimer's description of the symptoms displays the striking nature of AD. The disease leads to a progressive decline in memory, with the consequence of a person's inability to perform daily activities. AD has an insidious onset with consecutive loss of brain function.[11] Consequently, relatives of patients, who are often the caregivers, are heavily involved by a diseased person in their private sphere as well.[12]

With 60-75% of the cases, AD is the most common form of dementia affecting around 50 million people worldwide, without taking the patient's social environment into account.[12] With the prognosis of growing incidences due to the demographic changes, the disease gains more attention in society and the economy, due to its severe burden for caregivers and healthcare resources.[12]

There are two forms of AD categorized today, the familial form (fAD) and the sporadic form (sAD) of AD. The familial form is associated with early disease onset and corresponds to less than 1% of the cases. fAD is caused by mutations in one of the three genes coding for the amyloid precursor protein (APP), presenilin 1 (PSEN1) or presenilin 2 (PSEN2).[13-15] Another genetic predisposition for AD is the apolipoprotein E type 4 allele (APOE ε4).[16] APOE ε4 carriers hold a dramatically increased risk to develop AD later in life.[17-19]

The second form, sAD, is the common one and does not necessarily hold genetic risk factors. Its etiology is not resolved, and the causality is not entirely elucidated. Several hypotheses were established in the field, attempting to explain the principles and cascades of disease development. None of them, however, proved exclusively valid.[11] Accordingly, none of them led to the cure of AD so far. Since the discovery of AD,

research has made considerable progress in understanding the pathology and development of symptoms. However, clinical trials have largely failed to provide sufficient treatment due to the innate complexity and heterogeneity in the onset of the disease.

1.1.1 Pathology

Not only the clinical symptoms were well described by Alzheimer in 1907, but also his pathological findings are still valid.[9, 10] The protein abnormalities, β-amyloid peptide aggregation, and neurofibrillary tangles (NFT) reported by Alzheimer continue to be the key elements of research.

β-Amyloid

The most known protein associated with AD is the β-amyloid peptide (Aβ). Aβ is a fragment of the integral membrane protein β-amyloid precursor protein (β-APP).[20] Under physiological conditions, Aβ is a regular secretion product of cells expressing the *APP* gene[21-23] but is rapidly degraded.[24] A miscleaved product of APP and aberrant degradation and clearance lead to aggregation and accumulation of the Aβ plaques.[25] The associated pathology of amyloid deposits is seen in all AD patients. Therefore, Aβ represents a hallmark of the disease[26-28] and serves as a diagnostic biomarker in cerebrospinal fluid analysis.[29, 30]

The main theoretical construct for AD provides the amyloid cascade hypothesis by Hardy and Higgins proposed in 1992.[31] According to the theory, Aβ deposits are designated as the prime pathogenic driver of AD and the origin of a series of events: First, microglia and astrocytes are activated, followed by progressive synaptic injuries. This leads to oxidative damages, altered kinase and phosphatase activities producing neurofibrillary tangles (NFTs), neuronal atrophy, and ultimately dementia.[32] While there is general agreement that the multiple factors stated in the amyloid hypothesis contribute to disease progression, the top-down cascade with Aβ as the ultimate origin of the disease is challenged.[33] The main argument against the theory is that cognitive loss does not necessarily correlate with the amount of Aβ deposits.[34, 35] Further, clinical trials with drugs targeting Aβ have failed.[8, 36] Phase III trials of drugs preventing Aβ aggregation, like tramiprosate,[37] tarenflurbil,[38] and semagacestat,[39] had no significant effects in AD patients randomized to placebo. The humanized monoclonal antibodies against Aβ, which scientists had considered a promising approach, also failed in phase

III clinical trials. Bapineuzumab,[40] Solanezumab,[41] and, more recently, aducanumab,[42, 43] did not achieve the amelioration anticipated.

The one-target strategy for drug development was unsuccessful during the last decades. The pathology and progression of the disease became more complex than only focusing on Aβ.[33, 44] Therefore, therapeutic strategies addressing other pathologies and Aβ in parallel are needed.

Tau-Protein

Abnormal tau protein aggregation is another hallmark, and a significant pathology of AD.[45] Tau is a microtubule-associated protein in neurons, stabilizing the microtubules under physiological conditions, necessary for the growth of neurites and neuron development.[46, 47] Abnormal hyperphosphorylation, as it occurs in tau pathology, decreases tau's microtubule-affinity. Aggregates of soluble and insoluble hyperphosphorylated tau form neurofibrillary tangles (NFTs).[48] Consequently, neurons lose axonal integrity, connectivity, and synapses, which leads to an impairment of cognitive performance.[34, 49]

Neuroinflammation

Tau and Aβ pathology are both critical for the pathogenesis of AD. However, neuroinflammation is recognized as a mechanistic driver and gains more importance in neurodegeneration.[50] Usually, neuroinflammation is a reparative and beneficial process upon acute inflammation. A defensive response of the glial cells to repair tissue damage.[51] In the context of neurodegeneration, however, persistent inflammation leads to a chronic condition and release of pro-inflammatory factors that are harmful to the central nervous system (CNS) and enhance neuronal damage.[52]

It has been shown that the brains of AD patients displayed elevated levels of pro-inflammatory cytokines released by microglia, like tumor necrosis factor-alpha (TNF-α) or interleukin 6 (IL-6), compared to healthy controls.[53-55] This indicates that neuroinflammation plays a role in AD and is already present in the early stage of the disease.[56] Indeed, there is a destructive and self-perpetuating process between Aβ deposits and activated microglia mediating neuroinflammation. Aβ itself can cause local inflammatory responses activating microglia,[57, 58] while activated microglia, in turn, induce more amyloid deposition.[59] Similarly, tau pathology is enhanced by neuroinflammation in a vicious cycle. Activated microglia further promote tau

hyperphosphorylation,[60, 61] and tau aggregates released by dead neurons stimulate microglial cells.[62]

Next to promoting and enhancing AD pathology by the interplay with Aβ and tau, there is evidence that microglia also actively contribute to synapse loss and consequent cognitive decline. Synaptic pruning by phagocytic microglia is part of the physiological brain development. However, it might be reactivated in adult brains in AD, mediating synapse loss by phagocytosis.[63, 64] Therefore, neuroinflammation directly contributes to AD pathology and should be considered in a holistic view on disease origin and progression when searching for effective treatment.

Oxidative Stress

Oxidative stress occurs when the homeostasis of pro-oxidants and antioxidants in cells, or neurons in the context of AD, is out of balance. Reactive oxygen species (ROS) accumulate, eventually resulting in cell death. In AD, oxidative stress has been recognized as an important driver of disease progression and cognitive decline.[65] There are several sources of ROS, with mitochondrial dysfunction being the major contributor. Mitochondrial malfunction leads to increased production and release of ROS.[66] Further, Aβ toxicity in neurons is related to increased ROS production concomitant with oxidative stress, tau phosphorylation, lipid peroxidation, and ultimately synaptic dysfunction.[67] Once again, highlighting the synergy of AD pathologies.

The Cholinergic System

The principal neurotransmitter in the brain, acetylcholine (ACh), is used by all cholinergic neurons for signal transduction.[68] Cholinergic neurons innervate almost all regions of the brain, and therefore, cholinergic neurotransmission plays a crucial role in brain function and is essential for memory, learning, attention, and sensory information.[68-71] ACh is synthesized by the enzyme choline acetyltransferase from choline and acetyl-coenzyme A in the cytoplasm of cholinergic neurons.[72] Upon depolarization, ACh is released into the synaptic cleft from synaptic vesicles, where it activates nicotinic and/or muscarinic receptors on the postsynaptic membrane. The enzyme acetylcholinesterase (AChE) inactivates ACh in the synaptic cleft with a very high kinetic efficiency, releasing choline and acetate.[73, 74]

As ACh is important for cognitive function, the cholinergic system came to the fore early in dementia and AD research.[75] The cholinergic hypothesis was the first causal hypothesis for AD proposed by Bartus et al. in 1982.[76] The theory was based on brains of AD patients showing a loss of cholinergic activity.[77, 78] So far, this is the only hypothesis that brought drugs to approval. AChE inhibitors increase ACh levels in the synaptic cleft and ameliorate AD symptoms.[79, 80] Currently, four drugs are approved for AD patients: The AChE inhibitors donepezil, rivastigmine, and galantamine, and the N-methyl-D-aspartate (NMDA) receptor antagonist memantine (Fig. 1). All of them only ameliorate symptoms and aim to stabilize or slow down progression, but cannot cure the disease or even modify its course.[81] These four drugs result in five medication options as a combination treatment of donepezil and memantine (Namzaric®) was approved by the FDA in 2014.[82]

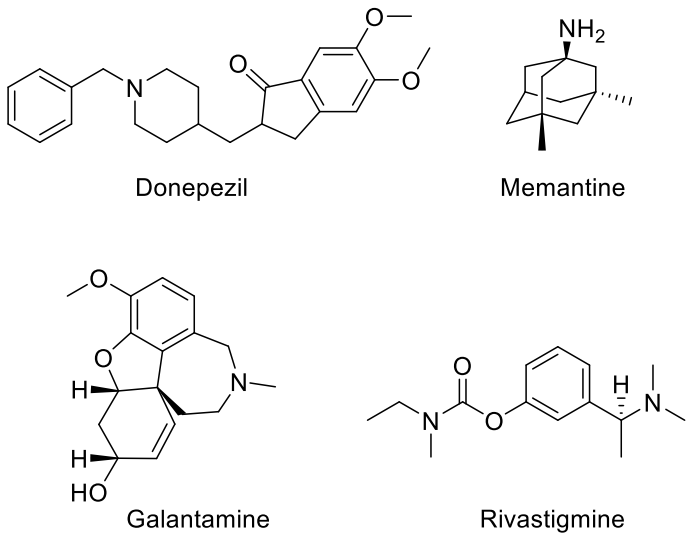

Figure 1: Chemical structures of the drugs approved for the treatment of Alzheimer's disease. Donepezil, galantamine, and rivastigmine are AChE inhibitors, and memantine is an NMDA receptor antagonist.

The treatment with AChE inhibitors provides amelioration for patients only for a short time.[83] One reason for the time-restricted effect of the AChE inhibitors might be the loss of enzymatic activity of AChE and the decrease of AChE levels as AD progresses.[84,85] With the target diminishing, naturally, the therapeutic effect of the drugs cannot be maintained. Butyrylcholinesterase (BChE) is a second choline esterase present in the brain.[86] AChE decrease in AD correlates with increasing levels BChE,[85] suggesting BChE as a potential target for therapeutics.[87]

Due to the limited effect of choline esterase inhibitors, one might say these drugs are not a real success in combating AD. Again, the strategy of addressing a singular symptom of AD failed. The complexity of AD pathology becomes evident, considering that ACh also plays an important role in neuroinflammation. ACh controls glial activation and inhibits the release of pro-inflammatory cytokines.[88] Therefore, cholinergic deficits, as a characteristic of AD brains, attenuate the uncontrolled neuroinflammation due to reduced ACh levels.[56, 88] Further, Aβ oligomers are toxic to cholinergic synapses contributing to the synaptic loss,[89, 90] highlighting once more, how closely intertwined the pathologies of AD are (Fig. 2).

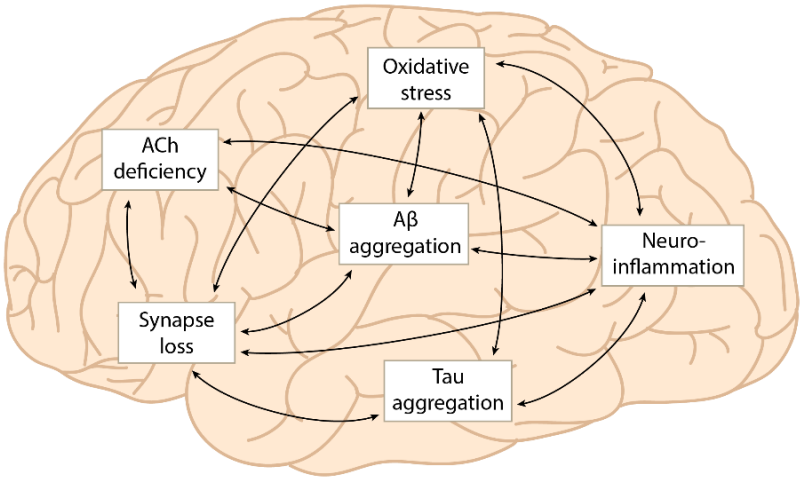

Figure 2: Overview of dependencies and synergies in AD pathology displaying its innate complexity.

Instead of a serial model of disease origin and progression, as described in the amyloid cascade hypothesis or cholinergic hypothesis, a parallel occurrence of the main contributors early before the first symptoms appear is likely to be the cause of AD. The temporal sequence resulting in cognitive decline is unknown and could not be determined or scientifically proven so far. Hence, it is useful to apply a holistic view to combating the disease. Compounds bearing a pleiotropic effect addressing several key elements of AD in parallel are needed to encounter this devastating disease of the human intellect, threatening aging societies and us as we age.

1.1.2 Age as a Risk Factor

The stereotype AD patient is an elderly individual with insidiously progressing problems of memory. Indeed, age is the major risk factor for developing AD[91] if there is no genetic predisposition causing fAD with an early onset.[11] López-Otin et al.[92] defined the nine so-called "hallmarks of aging" in 2013 with the primary hallmarks being genomic instability, telomere attrition, epigenetic alterations, and loss of proteostasis. In AD, genomic instability and loss of proteostasis and the resulting consequences are the most important hallmarks of aging.

As the aggregated proteins tau and Aβ are the main characteristics of AD pathology, loss of proteostasis – the balance between protein synthesis and degradation – is a hallmark of aging and AD. Regarding genomic instability, neurons are particularly predetermined to be affected. As postmitotic cells, they are more susceptible to DNA damage accumulating over time as proliferating cells and thereby more sensitive to aging.[93] The consequences of DNA damage are inflammation and senescence, both contributing to age-related neurodegeneration.[94] The number of senescent cells naturally increases with age, but senescence can also be induced by Aβ or tau pathology, leading to cognitive deficits.[95, 96] Further, nuclear damage leads to mitochondrial dysfunction. Brain mitochondria become impaired with age as a consequence of increased damage and reduced biogenesis accompanied by aging.[94] Due to stress and dysfunction, mitochondria tend to permeabilize and thereby initiate apoptotic signaling.[97] This contributes to neuronal loss but also triggers inflammatory reactions and accumulation of oxidative stress, both drivers of AD pathology.[98]

1.2 Natural Products as Neuroprotectants

As mentioned before, traditional herbal medicines have been used for a long time in the history of humankind. Not only for the treatment of colds and wounds but also to treat dementia and forgetfulness – in East Asian traditional medicine for this use case exists for over 2000 years.[99] The concepts were rather systemic, and herbs applied against forgetfulness were, for example, the ones that nourished the blood and were blood circulation-promoting.[99] While natural products are decried due to their limited stability, often low bioavailability, and restricted passage through the blood-brain barrier,[100] several *in vivo* studies have shown the beneficial effect of plant-based natural products on neuroprotection and amelioration of AD.[101] The most famous

herbal supplement for the treatment of dementia is *Ginkgo biloba* leaf extract. Glycosides of the flavonoids quercetin, kaempferol, and isorhamnetin are with 24% of the total weight the main constituents of the Ginkgo extract, followed by terpene trilactones contributing to 6% of the total weight.[102] Several randomized, placebo-controlled, double-blind clinical trials have shown the clinical efficacy and safety of *G. biloba* extract EGb761 against dementia.[103] More recently, the treatment outcome of ginkgo extract was compared to donepezil in a study with AD patients older than 80 years, showing similar effects on cognitive symptoms with a favorable safety profile.[104]

With oxidative stress being a significant driver of AD and other neurodegenerative disorders, plant-derived polyphenols gained attention as neuroprotectants due to their antioxidant activity.[105] Among them are flavonoids, like taxifolin, quercetin, and fisetin (Fig. 3). These abundant dietary secondary plant metabolites are proposed to ameliorate neurodegeneration via multiple effects.[106] Chemically, the common structure of flavonoids contains two phenyl rings A and B and a heterocyclic ring C, which are then stocked with hydroxyl groups in different positions (Fig. 3).

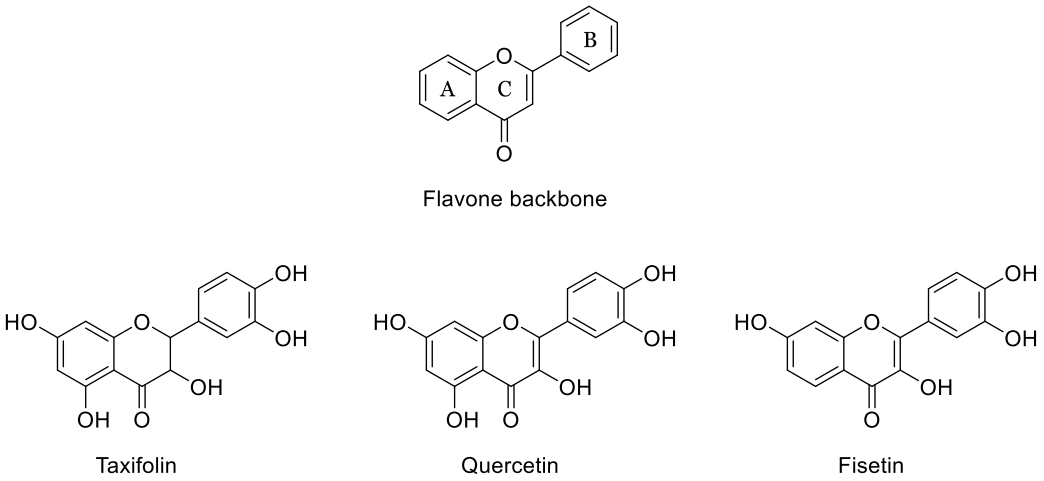

Figure 3: Chemical structures of the general flavone backbone of flavonoids, and the polyphenolic flavonoids taxifolin, quercetin, and fisetin as examples.

Even though the exact mechanism of action and the active metabolic component of this class of compounds are not always precise,[107, 108] flavonoids have been assigned to various beneficial effects in the context of AD.[109] Next to their antioxidant and radical scavenging activity,[110] flavonoids showed to be anti-inflammatory,[111, 112] anti-amyloidogenic,[113, 114] anti-aging,[115] and to improve learning and memory.[116] Therefore, flavonoids are interesting starting points for drug development for complex CNS

diseases where a pleiotropic approach is needed, and treatment might be employed over a long duration.[100]

1.3 Phenotypic Screening

Many of the pathologies described in AD and aging can be reproduced in cell-based assays.[117] These assays can be used as a model to identify compounds whose biological activity is beneficial to several mechanisms relevant to aging and disease.[7, 118] Thereby compounds with pleiotropic effects are revealed, which independently address several pathways in parallel, without the need to inhibit the function of one specific pathway completely. Two advantages for drug development compared to the one-target strategy arise as a result: First, long-term therapy might be accompanied by fewer side effects, as the normal constitutive function of the pathways might not be constrained,[33] and second, identified compounds address multiple centers of the disease in parallel.

The phenotypic screening assays introduced in the following have been used within the scope of this work and are not intended to be exhaustive. Of course, any type of assay displaying pathologies of AD or aging would add on to these phenotypic screening assays. Examples that are already in practice but are not described in detail here are PC12 cell differentiation[119] or intracellular amyloid toxicity using MC65 cells.[120]

Oxytosis

Oxytosis is a specific form of cell death distinct from apoptosis and induced by the inhibition of the cystine/glutamate antiporter system x_c^- with high extracellular concentrations of glutamate.[121] The murine neuronal cell line HT22, a subclone of the hippocampal cell line HT4, lacks ionotropic glutamate receptors and therefore does not die of glutamate-induced excitotoxicity.[122] Glutamate blocks cystine uptake via system x_c^- into nerve cells. The reduced form of cystine is the rate-limiting amino acid cysteine of the tripeptide glutathione (GSH). Therefore, glutamate treatment leads to GSH depletion (Fig. 4). GSH is the major player in the intracellular antioxidant defense, and its decrease leads to a dramatic increase in ROS from complex I of the mitochondrial transport chain. These endogenously generated ROS start a cascade of 12/15 lipoxygenase (LOX) activation, increased intracellular cyclic guanosine monophosphate (cGMP) levels resulting in the opening of calcium channels, and ultimately cell death.[121] Murphy et al.[123] first described the pathway in 1989, and Tan

et al.[121] extensively studied it. Oxytosis gained relevance in neurodegeneration, as the morphological and physiological features relate to nerve cell death observed in AD and

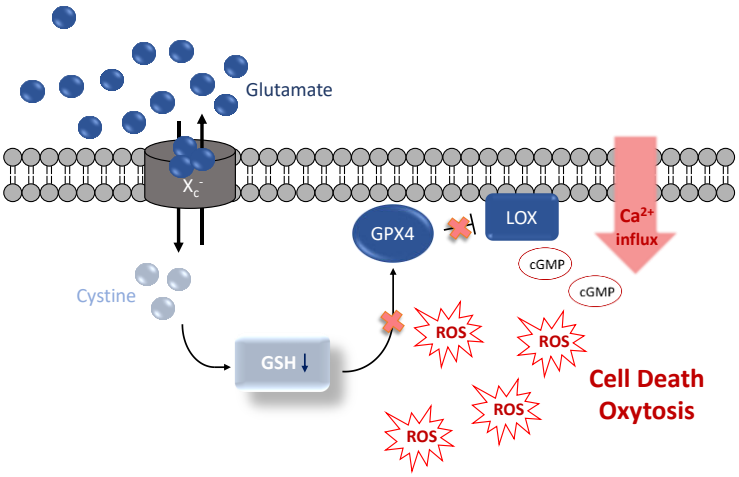

Figure 4: High concentrations of extracellular glutamate block the glutamate/cystine antiporter system x_c^- in HT22 cells and lead to intracellular cystine depletion and thereby GSH depletion. Decreased GSH levels inhibit GPX4, which activates LOX, ROS production, cGMP accumulation, and calcium influx.

stroke.[121]

Ferroptosis

Ferroptosis and oxytosis are closely related forms of cell death in HT22 cells. It is under debate whether they are individual pathways or the same pathways with an insult-dependent variation.[124] Experimentally, ferroptosis is induced by direct inhibition of the enzyme glutathione peroxidase 4 (GPx4) with RSL3. The consequences are very similar to the cellular pathways observed in oxytosis: Upon GPx4 inhibition, ROS levels increase, lipoxygenase is activated, leading to increased cGMP levels, calcium influx, and cell death.[124] Induction of ferroptosis occurs downstream in the cell death pathway of oxytosis (Fig. 5), as GSH depletion occurring in oxytosis also leads to inhibition of GPx4. Hence, the discussion about the distinction of the pathways.[125] Within the phenotypic screening approach, both assays are applied. Thereby, additional information about the compound's mode of action can be gained and some compounds showed differences in the ability to protect against the insults. For example, in HT22 cells, the protein synthesis inhibitor cycloheximide protected against oxytosis. However, it was not protective against RSL3 induced ferroptosis, as protein synthesis was required early in the cell death pathway - upstream of GPx4 inhibition but downstream of system x_c^- inhibition.[124] Within this work, the term ferroptosis is used

when oxidative stress is induced by applying the GPx4 inhibitor RLS3 and oxytosis for the glutamate-induced cell death.

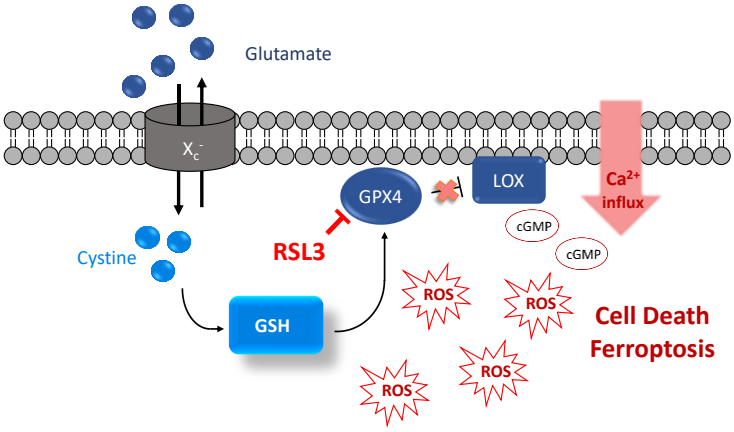

Figure 5: In ferroptosis, RSL3 directly inhibits the enzyme GPX4 and thereby induces the neuronal death cascade.

ATP depletion

As we age, energy metabolism changes. ATP levels in the brain decrease,[126] and also hypoglycemia impairs cerebral function and cognition.[127] A model for ATP depletion and loss of mitochondrial energy metabolism is therefore relevant in the context of AD. Iodoacetic acid (IAA) is used to induce ATP depletion in HT22 cells. IAA irreversibly inhibits the glycolytic enzyme glyceraldehyde 3-phosphate dehydrogenase (GAPDH), which is part of the glycolytic breakdown in cells and therefore required for energy supply.[128] Compounds that maintain ATP levels and counteract IAA-induced neuronal death are of interest for the treatment of neurodegeneration.

BV-2 Activation

Neuroinflammation is a critical contributor to the pathology of AD.[51, 129] Hence, neuroinflammation is an important model of AD when screening for neuroprotective compounds with pleiotropic effects and therapeutic potential. As outlined in the AD pathology section, pro-inflammatory microglia are resident CNS immune cells and key players in AD-related neuroinflammation.[130] Inflammation can be investigated in the murine microglia cell line BV-2. Treatment with bacterial lipopolysaccharide (LPS) leads to the production and release of pro-inflammatory cytokines, free radicals, excitatory neurotransmitters, and other factors contributing to neuroinflammation, neurodegeneration, and cell death.[130]

2. Scope and Objectives

In aging societies, Alzheimer's disease (AD) grows in importance as a global health concern, and available therapies are scarce. As outlined in the introduction, it is of particular importance to gain a more detailed understanding of the disease and its causes. Because the one-target strategy has not been successful in drug development, research needs to incorporate a holistic view of AD. To take account of the complex and multifactorial nature of the disease, this work focuses on natural products, such as secondary plant metabolites. These compounds possess pleiotropic effects exceeding their antioxidant capacity and have been used in traditional medicine to treat disorders related to the nervous system.

The goal of this work was to synthesize derivatives of secondary plant metabolites, characterize their neuroprotective potential, and investigate their mode of action.

Chapters 3 and 4 address the first objective, the examination of 7-*O*-esters of the flavonoid taxifolin as neuroprotectants. Previous studies with taxifolin described neuroprotective effects only at high concentrations of the flavonoid (> 100 µM)[131] and condemned it for therapeutic use. Ester hybrids of the flavonolignan silibinin have been shown to reduce the neuroprotective concentration to the low micromolar range.[132] However, the flavonolignan-based esters suffer from drawbacks regarding the high molecular weight and constrained solubility, which counteract their drugability. To eliminate these disadvantages, 7-*O*-esters of taxifolin with phenolic acids were synthesized and investigated in phenotypic screening assays addressing different aspects of neurodegeneration and aging. Disease-modifying effects of the compounds were examined *in vivo* in an AD mouse model.

Despite the neuroprotective effect of taxifolin and derivatives thereof, specific intracellular targets and the mode of action of this class of compounds remain elusive. Therefore, a chemical probe of 7-*O*-cinnamoyltaxifolin was designed, synthesized, and validated to be used in an activity-based protein profiling approach for target identification. Identified proteins are promising as specific targets of 7-*O*-cinnamoyltaxifolin. They will provide further insights into proteins involved in AD that might serve as potential and innovative targets for drug development in the future.

Chapter 5 addressed the second objective, the examination of synthetic approaches for the chemical modification of the flavonoids taxifolin, quercetin, and fisetin. The

chemistry of flavonoids is particular and rarely described in the literature. To further derivatize the natural products, synthetic strategies for modifying the respective flavonoids are presented and discussed.

Chapter 6 covers the objective to specifically address an established target in AD, namely BChE, with a derivative of the alkaloid dehydroevodiamine (DHED). For other heterocycles, the introduction of a heptyl carbamate led to selective and highly potent inhibition of BChE.[133, 134] However, those lipophilic compounds' physicochemical properties are not optimal. DHED is exceptional in its structure and exists as water-soluble quaternary salt at acidic pH, improving its solubility and was therefore applied in this study. The enzyme inhibition was assessed in a colorimetric assay.

The future perspectives in chapter 7 conclude this thesis and provide research directions extrapolated from the results of this work. The objective was to discuss and inspire future studies on natural product derivatives, exploiting their neuroprotective potential to treat neurodegenerative disorders.

3. 7-*O*-Esters of Taxifolin with Pronounced and Overadditive Effects in Neuroprotection, Anti-Neuroinflammation, and Amelioration of Short-Term Memory Impairment *In Vivo*

Redox Biology 29 (2020) 101378

Contents lists available at ScienceDirect

Redox Biology

journal homepage: www.elsevier.com/locate/redox

Research Paper

7-*O*-Esters of taxifolin with pronounced and overadditive effects in neuroprotection, anti-neuroinflammation, and amelioration of short-term memory impairment *in vivo*

Sandra Gunesch[a], Matthias Hoffmann[a], Carolina Kiermeier[a], Wolfgang Fischer[b], Antonio F.M. Pinto[b], Tangui Maurice[c], Pamela Maher[b,**], Michael Decker[a,*]

[a] *Pharmaceutical and Medicinal Chemistry, Institute of Pharmacy and Food Chemistry, Julius Maximilian University of Würzburg, Am Hubland, 97074, Würzburg, Germany*
[b] *The Salk Institute for Biological Studies, 10010 N Torrey Pines Road, La Jolla, CA, 92037, USA*
[c] *MMDN, University of Montpellier INSERM, EPHE, UMR-S1198, 434095, Montpellier, France*

The content of this chapter was previously published in *Redox Biology* **2020**, *29* and adapted with the permission of Elsevier.

https://doi.org/10.1016/j.redox.2019.101378

Author contributions:

S. Gunesch (under supervision of Prof. Dr. M. Decker) designed and synthesized the compounds and performed all *in vitro* characterization experiments, cell-based assays and cellular uptake experiments (under supervision of Dr. P. Maher).

Dr. M. Hoffmann (under supervision of Dr. T. Maurice) performed *in vivo* studies.

C. Kiermeier (under supervision of S. Gunesch and Prof. Dr. M. Decker) assisted with the synthesis.

Dr. W. Fischer performed HPLC measurements.

Dr. A. F. M. Pinto performed MS measurements.

3.1 Introduction

Natural products have gained increased attention for their potential as neuroprotectants, as by their nature, they show pleiotropic effects instead of addressing a single target.[101, 117] A library of 7-*O*-esters of the flavonolignan silibinin with different phenolic acids showed overadditive neuroprotective features in a set of assays related to neurodegeneration and aging.[132] Position 7 of silibinin was regioselectively esterified in that study,[132] as the 7-OH group, in contrast to the other four hydroxyl groups of silibinin, was attributed a pro-oxidant character.[135] Esterification with a phenolic acid derivative increased the antioxidant capacity and blocked the pro-oxidant effect of the 7-OH group. Structure-activity relationships (SARs) revealed the influence of different numbers of hydroxy- and methoxy-groups as aromatic substituents and the Michael system on the neuroprotective and antioxidant effects. SARs analysis showed that phenolic acids possessing a Michael system are essential for the neuroprotective activity of the compounds.[132] The assays applied were cell-based, avoiding potentially false-positive results due to false-positive readouts as it was shown for pan assay interference compounds (PAINS).[136, 137] The most potent esters of the compound library in that study were 7-*O*-cinnamoylsilibinin and 7-*O*-feruloylsilibinin.[132]

Phenolic acids have been studied in the context of neurodegenerative diseases before due to their antioxidant capacities. Ferulic acid is a free radical scavenger that counteracted intracellular apoptotic pathways induced by oxidative stress[138] and was studied in *in vivo* models of AD. Long-term administration of ferulic acid prevented the neurotoxic effect caused by β-amyloid in mice,[139] and reduced behavioral impairment in a transgenic PSAPP mouse model.[140] Cinnamic acid upregulated the suppressor of cytokine signaling 3 (SOCS3) in BV-2 microglial cells and suppressed the expression of pro-inflammatory cytokines counteracting neuroinflammation.[141]

Flavonolignan-based silibinin-esters with phenolic acids suffer from some drawbacks. The high molecular weight of the compounds and their constrained solubility counteract their drugability.[142] The secondary plant metabolite taxifolin is a flavonoid, structurally closely related to silibinin, but smaller (Fig. 6). The catechol moiety of taxifolin is an important antioxidant group and was shown to site-specifically inhibit aggregation of 42-residue amyloid β-protein (A*β*42) *in vitro*, which is relevant for the pathogenesis of AD.[114] This was confirmed by a computational study analyzing the

reaction mechanism. The covalent adduct was shown to be formed via an aza-Michael addition of the oxidized *o*-quinone species of (+)-taxifolin with a lysine residue of the Aβ42 fibril.[143] Previously, Vrba et al.[144] had esterified taxifolin semisynthetically in position 7 with gallic acid. The compound upregulated the nuclear factor (erythroid-derived 2)-like 2 (Nrf2) pathway in RAW264.7 cells,[144] an important cytoprotective mechanism in response to redox imbalance. It has been shown that orally administered taxifolin exhibits a pleiotropic beneficial effect on intracerebral profiles in a cerebral amyloid angiopathy (CAA) mouse model *in vivo*, a disease often accompanied by AD.[145]

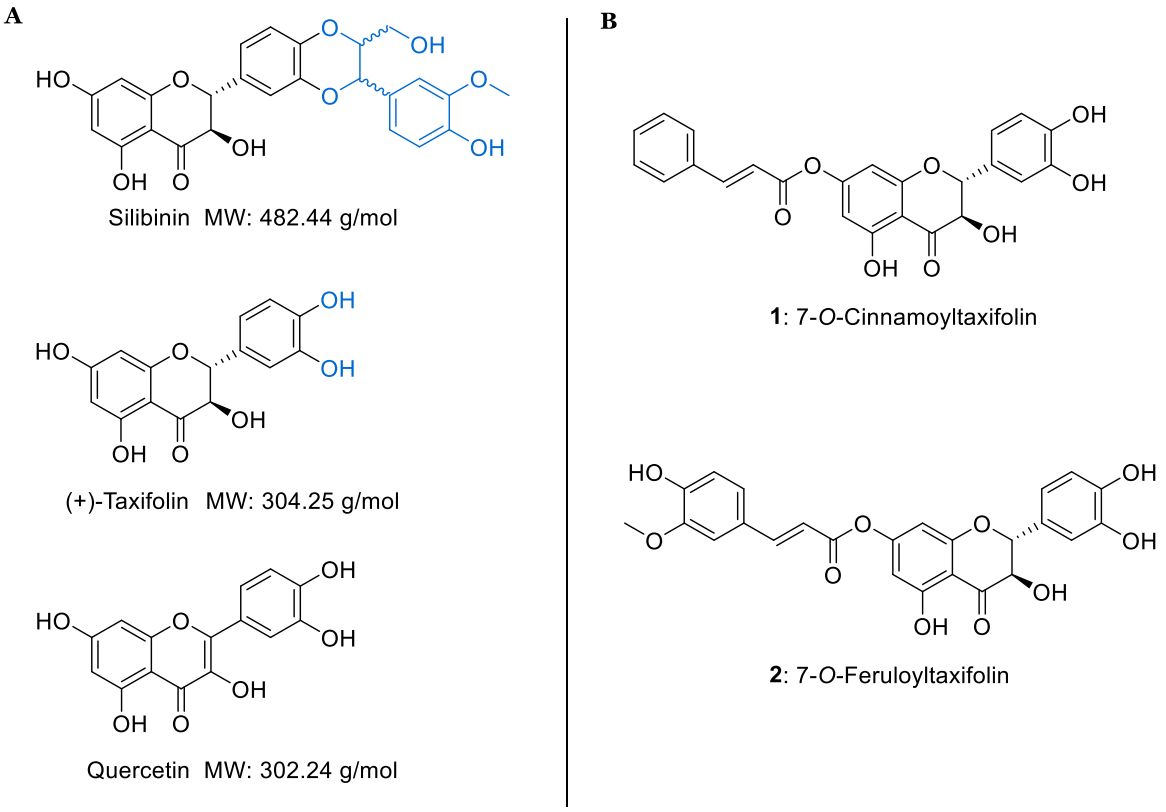

Figure 6: A) Chemical structures of the flavonolignan silibinin and the flavonoids taxifolin and quercetin. Structural differences between the natural products silibinin and taxifolin are highlighted in blue. **B)** Target compounds 7-*O*-cinnamoyltaxifolin (**1**) and 7-*O*-feruloyltaxifolin (**2**).

Highlighting the therapeutic potentials of taxifolin and ferulic and cinnamic acid in the context of neurodegenerative diseases,[131, 146] it was of interest to investigate natural product hybrids of the flavonoid taxifolin and the acids as novel potent neuroprotectants. Therefore, 7-*O*-esters of taxifolin and cinnamic or ferulic acid were synthesized (Fig. 6).

3.2 Chemistry

Despite several hydroxyl groups, 7-*O*-esterification of taxifolin was achieved without using protective groups under optimized reaction conditions. This was possible due to two reasons. First, the reactivity of the five hydroxyl groups of taxifolin is distinct, and position 7 is the most reactive one. Adjusting reaction time and conditions led to the 7-*O*-ester as the main product. Second, optimized gradients in silica gel column chromatography allowed the separation from byproducts esterified in other or multiple positions. Acyl chlorides of ferulic or cinnamic acid were generated with oxalyl chloride and catalytic amounts of DMF and immediately added to taxifolin in basic solution under anhydrous conditions (Scheme 1).[132, 144] Extensive purification by column chromatography after the workup was necessary to remove all byproducts and obtain the pure compounds 7-*O*-cinnamoyltaxifolin **1** and 7-*O*-feruloyltaxifolin **2**.

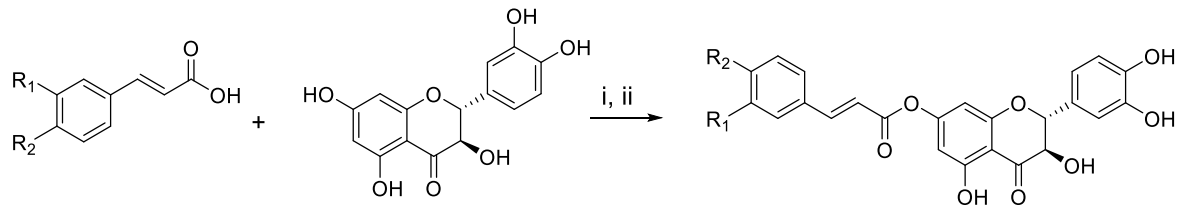

Scheme 1. Synthesis of 7-*O*-cinnamoyltaxifolin (**1**, 43% yield) and 7-*O*-feruloyltaxifolin (**2**, 27% yield). i) Acid, oxalyl chloride, DMF, dry THF, 1 h, room temperature; ii) taxifolin, triethylamine, dry THF, 2 h, room temperature after addition of the respective acyl chloride.

3.3 Biology

A variety of assays was applied to investigate the neuroprotective features of the 7-*O*-esters of taxifolin **1** and **2**, for two reasons. First, with the catechol moiety, the molecules hold a so-called PAINS motif.[137] Even though neither a high-throughput screening nor colorimetric target-based assays were performed where PAINS could lead to misleading data,[147] the results of assays have to be examined carefully, and different methods have to be applied to exclude false-positive results (cf. Appendix III).[136] Second, addressing complex CNS disorders like AD, the single-target approach

was hampering drug development in the past, as mentioned above.[8] Hence, a phenotypic screening approach was followed.

3.3.1 Neuroprotection in HT22 Cells

Oxytosis. Glutamate treatment leads to intracellular GSH depletion resulting in programmed cell death due to oxidative stress.[121, 148] As shown in Figure 7A and C, compounds **1** and **2** were highly protective at a concentration of 5 µM, exceeding the beneficial effect of 25 µM quercetin, which served as a positive control. Taxifolin, the respective acid, and the equimolar mixtures thereof were not neuroprotective at the

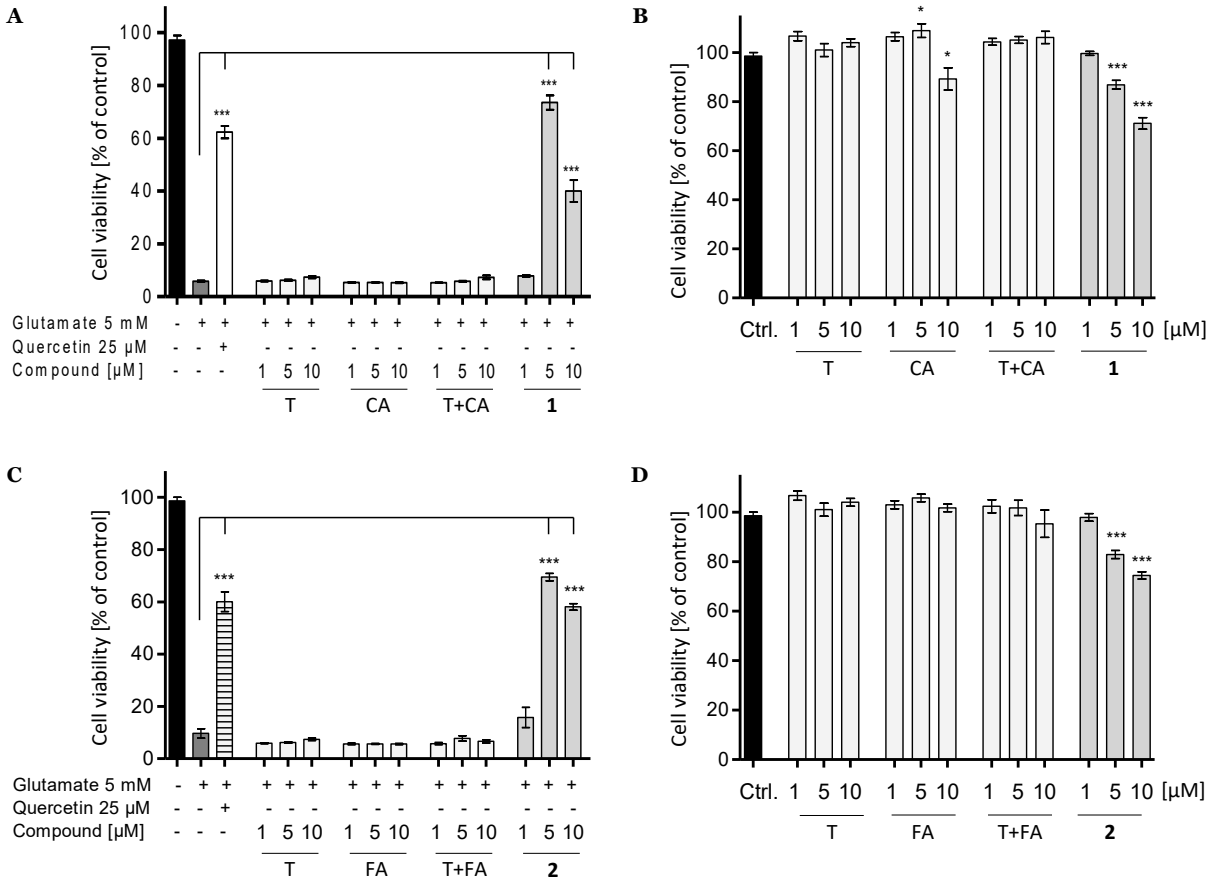

Figure 7. 5 mM glutamate was used to induce toxicity (dark grey) and 25 µM Quercetin served as a positive control (patterned). Neuroprotective effect (**A**) and neurotoxicity (**B**) of 7-*O*-cinnamoyltaxifolin (**1**) and the controls taxifolin (T), cinnamic acid (CA), and the equimolar mixture of taxifolin and cinnamic acid (T+CA). **C)** Neuroprotective effect and neurotoxicity (**D**) of 7-*O*-feruloyltaxifolin (**2**) and the controls taxifolin (T), ferulic acid (FA), and the one-to-one mixture of taxifolin and ferulic acid (T+FA). Data are presented as means ± SEM of three independent experiments, and results refer to untreated control cells (black). Statistical analysis was performed using One-way ANOVA followed by Dunnett's multiple comparison posttest referring to cells treated with 5 mM glutamate only in **A)** and **C)** or to untreated control cells in **B)** and **D)**. Levels of significance: * $p < 0.01$; ***$p < 0.001$.

tested concentrations (Fig. 7A, C). The equimolar mixture is of interest as it represents the hydrolysis products of the ester components and ensures that the effects observed are not based solely on the presence of the two compounds. In investigations towards the compounds' toxicity, the taxifolin esters **1** and **2** were found to exhibit a slight, dose-dependent neurotoxic effect (Fig. 7B, D). However, for both compounds, greater than 70% of the cells survived even at the highest concentration tested (Fig. 7B, D).

Ferroptosis. Ferroptosis is a cell death pathway induced by direct inhibition of GPx4 via covalent interaction of the compound RSL3 with the active site selenocysteine of GPx4.[149] As shown in Figure 8, both 7-*O*-esters of taxifolin, **1** and **2**, were neuroprotective against ferroptosis. In contrast, the individual components and the respective equimolar mixture did not exhibit any protective activity at the tested concentrations.

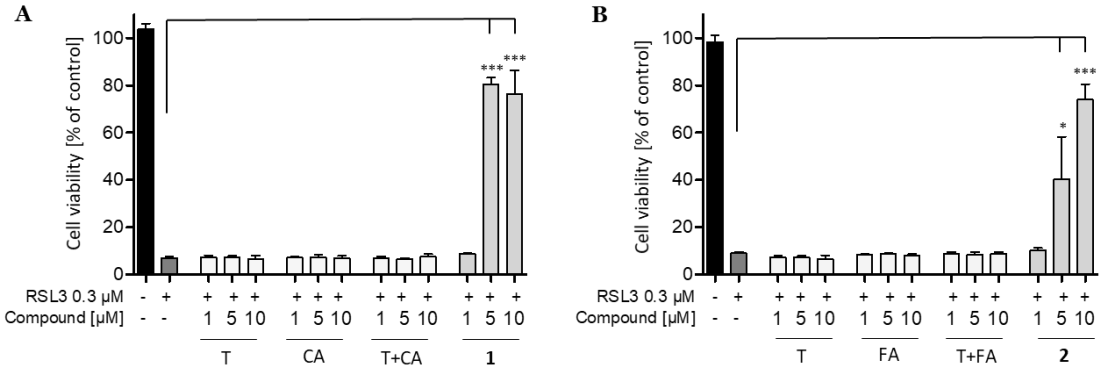

Figure 8. Neuroprotective effect of 7-*O*-cinnamoyltaxifolin **1** (**A**), 7-*O*-feruloyltaxifolin **2** (**B**) and the controls taxifolin (T), cinnamic acid (CA), ferulic acid (FA), and the equimolar mixtures (T+CA), and (T+FA). Data are presented as means ± SEM of three independent experiments, and results refer to untreated control cells (black). Statistical analysis was rendered using One-way ANOVA referring to cells treated with 300 nM RSL3 only (dark grey). Levels of significance: $^{*}p < 0.01$; $^{***}p < 0.001$.

ATP Depletion. Iodoacetic acid (IAA) was used to induce ATP loss in HT22 cells.[128] The overadditive effect in oxytosis and ferroptosis was also observed for ATP depletion (Fig. 9). Compound **1** showed an effect already at 1 µM with 40% cell survival.

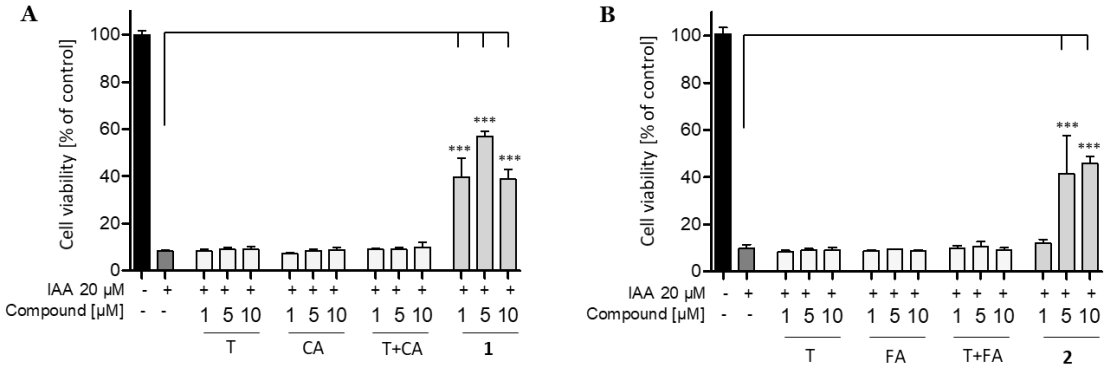

Figure 9. Protective effect of 7-*O*-cinnamoyltaxifolin **1** (**A**) and 7-*O*-feruloyltaxifolin **2** (**B**) with the controls taxifolin (T), cinnamic acid (CA), ferulic acid (FA), the equimolar mixtures (T+CA), and (T+FA). Data are presented as means ± SEM of three independent experiments, refer to untreated control cells (black). Statistical analysis was performed using One-way ANOVA referring to cells treated with 20 µM IAA only (dark grey). Levels of significance: ***$p < 0.001$.

GSH Quantification. As GSH and GSH-dependent enzymes provide the main line of defense in the protection towards oxidative stress in cells and GSH levels decrease with age,[148] it was of interest whether the neuroprotective ester 7-*O*-cinnamoyltaxifolin **1** and 7-*O*-feruloyltaxifolin **2** had an influence on total glutathione levels (tGSH) in HT22

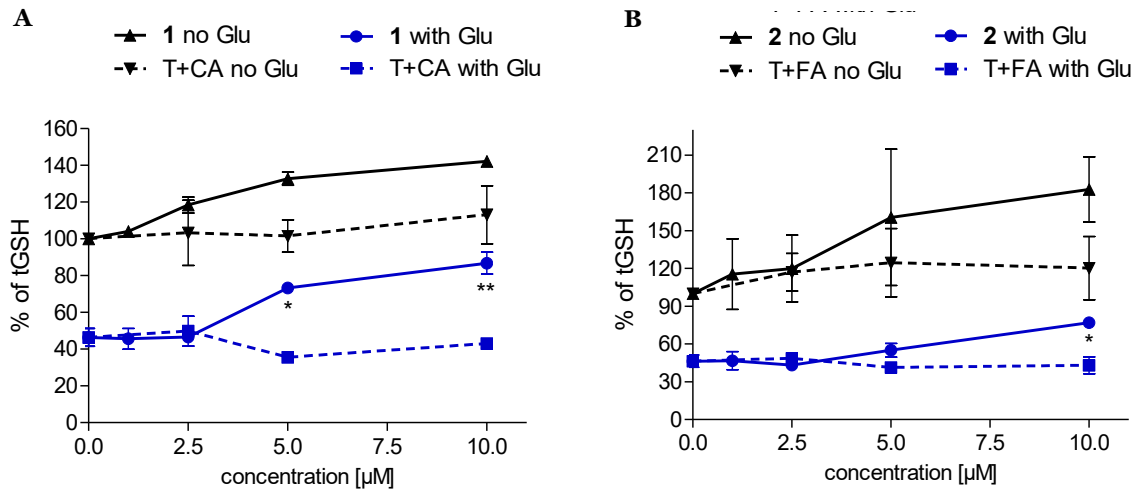

Figure 10. Dose-dependent effects of 7-*O*-cinnamoyltaxifolin **1** (**A**) and 7-*O*-feruloyltaxifolin **2** (**B**) and the equimolar mixtures (T+CA in **A** and T+FA in **B**) on total glutathione (tGSH) levels in HT22 cells in the absence (black lines) or presence (grey lines) of 5 mM glutamate (Glu) to induce oxytosis. Results are given as mean ± SEM and were analyzed by One-way ANOVA followed by Dunnett's multiple comparison posttest using GraphPad Prism 5 referring to cells with no compound added. Levels of significance: *$p < 0.05$, **$p < 0.01$.

cells. Levels of tGSH were determined in the presence of increasing concentrations of **1** and **2** with and without glutamate (Fig. 10). The equimolar mixture of taxifolin and the respective acid served as controls. Figure 10 shows that compounds **1** and **2** had an influence on tGSH levels and increased tGSH under oxidative stress induced by glutamate treatment in HT22 cells.

3.3.2 Anti-Inflammatory Effects in BV-2 Cells

NO and cytokines. BV-2 mouse microglial cells were used to investigate the ability of **1** and **2** to counteract inflammation induced by bacterial lipopolysaccharide (LPS). Both 7-*O*-esters **1** and **2** strongly reduced NO production (Fig. 11A, B), and compound **1** was further examined to affect the cytokines IL6 and TNFα using ELISAs (Fig. 11C). IL6 induction was significantly reduced by **1**. Even though the levels of TNFα were

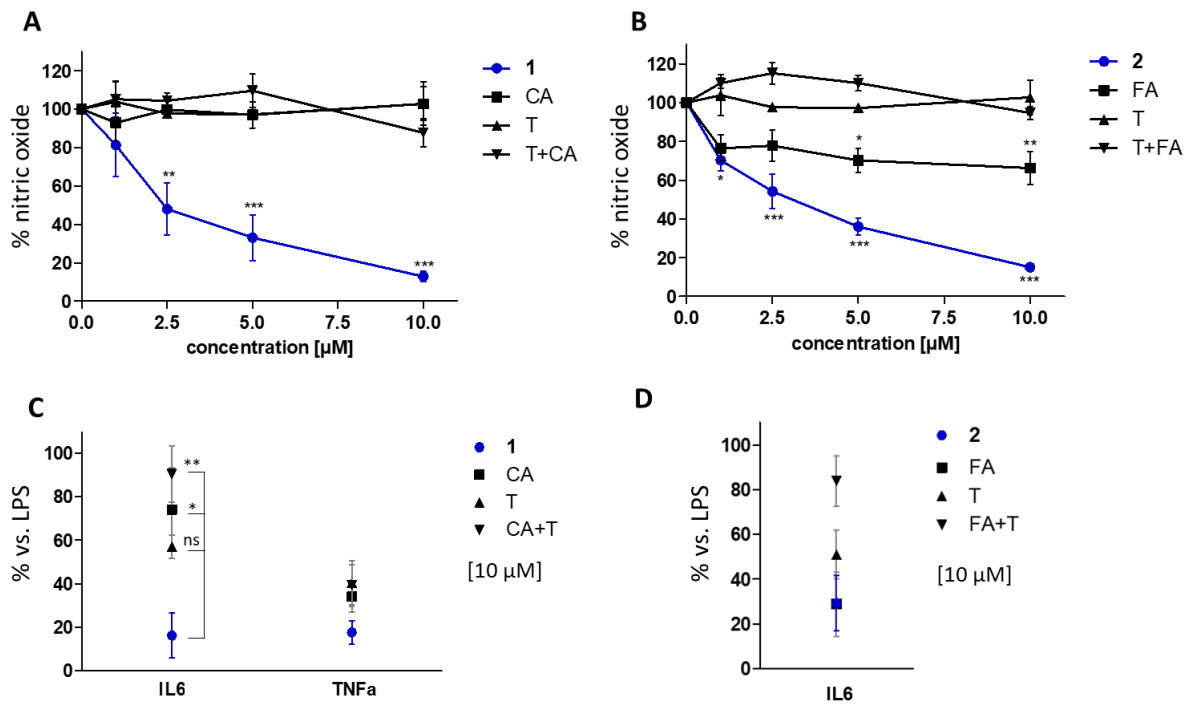

Figure 11. Cells were treated overnight with 50 ng/mL LPS alone or in the presence of compound **1**, cinnamic acid (CA), taxifolin (T), or the one-to-one mixture (T+CA) (**A** and **C**) or with compound **2**, ferulic acid (FA), taxifolin (T), or (T+FA) (**B** and **D**). NO was quantified by the Griess assay. Data in **A** and **B** are given as means ± SEM and relative to BV-2 cells treated with LPS only, set as 100%. One-way ANOVA was used for statistical analysis followed by Dunnett's multiple comparison posttest. **C)** The effect of 10 µM **1** on levels of IL6 and TNFα after LPS-treatment was assessed using ELISAs as was the effect of 10 µM **2** on IL6 (**D**). For **C)** and **D)**, Results are presented as percent (%) of treatment with LPS alone, which was set as 100%. Shown are means ± SEM analyzed by One-way ANOVA followed by Tukey's posttest. Levels of significance: $^{*}p < 0.05$, $^{**}p < 0.01$, $^{***}p < 0.001$

decreased strongest by **1**, the difference to the controls taxifolin, cinnamic acid, and the one-to-one mixture of both was not statistically significant (Fig. 11C).

Nrf2 Upregulation. Previously, taxifolin esterified in position 7 with gallic acid had been shown to upregulate the nuclear factor (erythroid-derived 2)-like 2 (Nrf2) pathway in RAW264.7 cells,[144] a macrophage cell line. Brain microglial cells have many properties similar to peripheral macrophages, and compound **1** was the most potent reducer of neuroinflammation markers in the BV-2 cells. Therefore, it was of interest whether Nrf2 was involved in the compound's mode of action. Nuclear fractions of BV-2 cells treated with the compounds were subjected to Western blot analysis. 7-*O*-cinnamoyltaxifolin **1** dose-dependently increased nuclear Nrf2 levels up to 24-fold at 10 µM after 4 hours of incubation (Fig. 12A).

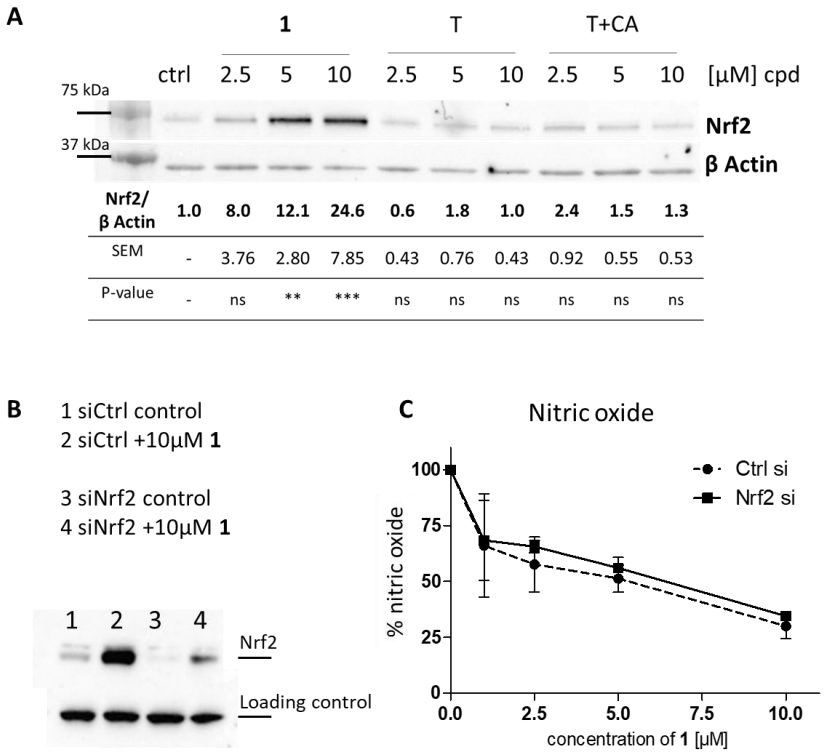

Figure 12. A) Cells were treated for 4 hours with DMSO or increasing concentrations of **1**, taxifolin (T), or the equimolar mixture (T+CA). Nuclear fractions of BV-2 cells were analyzed by Western blot for Nrf2 and normalized to actin. **B)** Transfection of BV-2 cells with control or Nrf2 siRNA. **C)** NO quantification of transfected cells treated with increased concentrations of **1**.

Taxifolin and the equimolar mixture of taxifolin and cinnamic acid did not induce Nrf2 translocation to the nucleus. Next, it was of interest whether Nrf2 was directly involved in the anti-inflammatory effects of **1**, and Nrf2 was downregulated in BV-2 microglia

by transfection using specific siRNA. Figure 12B shows the effective downregulation of Nrf2 in cells treated with siNrf2 (lane 3) even in the presence of the potent inducer **1** (lane 4), compared to the nonspecific control siRNA (lanes 1 and 2). The LPS inflammation assay with siRNA-modified BV-2 cells showed that Nrf2 knockdown did not affect the anti-inflammatory activity of compound **1** (Fig. 12C).

3.3.3 Cellular Uptake Experiments

Vrba et al.[144] had shown that a semisynthetic gallic acid ester of taxifolin was converted to a quercetin derivative in RAW264.7 cells. Therefore, cellular uptake metabolites of the synthetic hybrid 7-*O*-cinnamoyltaxifolin **1** were investigated in murine BV-2 microglial cells.[144] A reference HPLC chromatogram with 50 ng of each compound was recorded to determine their retention times (Fig. 13A). For cellular uptake experiments, BV-2 cells were incubated with 50 µM 7-*O*-cinnamoyltaxifolin **1** for 0, 30, 90, and 240 minutes, and lysates were analyzed by HPLC (Fig. 13B). Next to compound **1**, a second peak was detected at 48.9 minutes of retention time, and the compounds were metabolized over the time course of 4 hours (Fig. 13B). Both compounds were found to be stable with regard to hydrolysis. Figure 13C showed that the conversion of 7-*O*-cinnamoyltaxifolin **1** was dependent on the presence of cells. The two peaks at 43.9 and 48.9 minutes were collected and submitted to MS analysis for identification (Fig. 13D, E). The peak with a retention time of 43.9 minutes was identified as 7-*O*-cinnamoyltaxifolin **1** with $[M+H]^+$ m/z = 435.11 (m/z calc. = 434.10). MS/MS fragmentation resulted in signals at m/z = 305.07 corresponding to taxifolin and at m/z = 131.05 and m/z = 103.05 corresponding to cinnamic acid (minus H_2O and additional loss of CO, respectively). MS analysis of the peak with a retention time of 48.9 minutes gave signals at $[M+H]^+$ m/z = 433.09 corresponding to 7-*O*-cinnamoylquercetin with a calculated m/z = 432.08 (Fig. 13E). The compound was confirmed by MS/MS fragmentation where the masses of cinnamic acid (m/z = 131.05 and m/z = 103.05) and quercetin (m/z = 303.05) were identified.

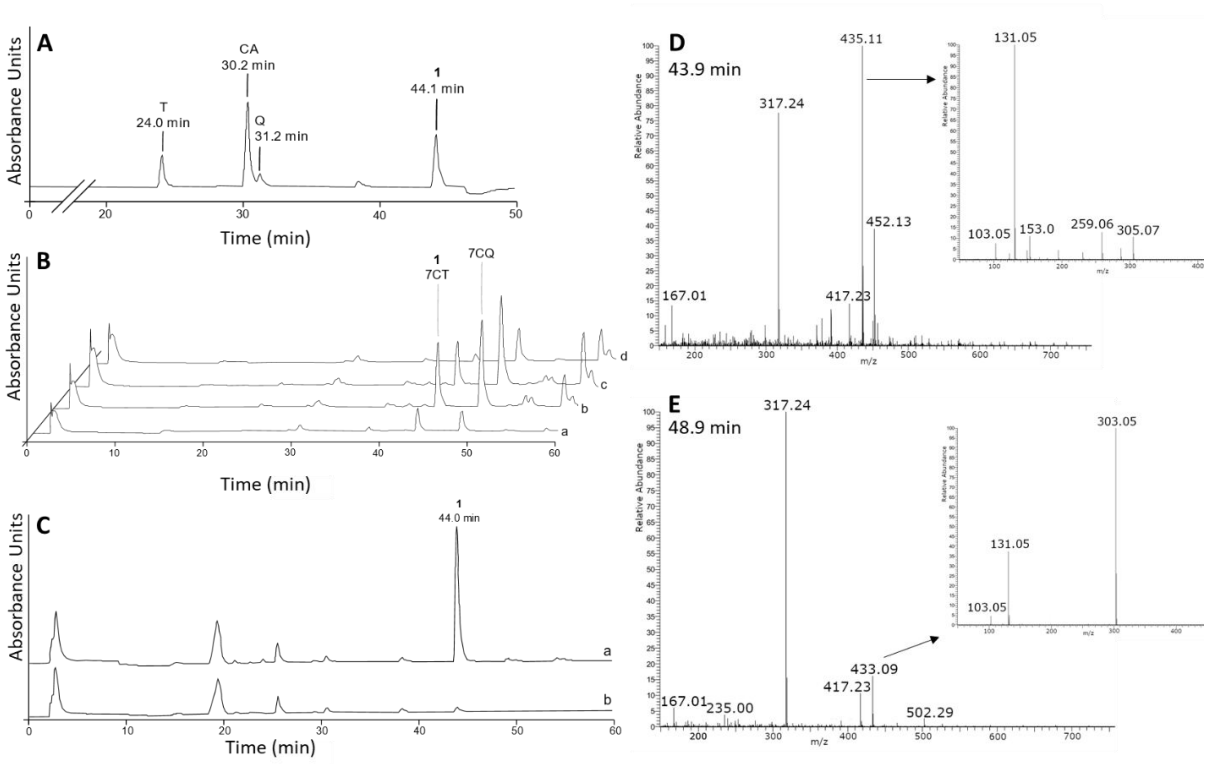

Figure 13. Cellular uptake of compound **1**. **A)** 50 ng of taxifolin (T), cinnamic acid (CA), quercetin (Q), and 7-*O*-cinnamoyltaxifolin (**1**) were submitted to HPLC as reference for the compounds' retention times. **B)** 50 µM **1** was added to BV-2 cells, and cells were immediately lysed (**a**) or incubated for 30 min (**b**), 90 min (**c**), or 4 hours (**d**) before lysis and sample preparation. **C)** Incubation of 50 µM **1** for 30 min in medium only did not lead to compound conversion (**a**). (**b**): blank chromatogram with medium only. **D)** MS spectrum of the first HPLC peak (43.9 min) after incubating **1** for 30 min with BV-2 cells. The signal at *m/z* = 435.11 corresponds to **1** and was isolated for MS/MS fragmentation (inset) where *m/z* = 131.05 and *m/z* = 305.07 were detected corresponding to cinnamic acid and taxifolin, respectively. **E)** MS spectrum of the 48.9 min fraction gave a signal at *m/z* = 433.09, and the MS/MS fragmentation (inset) of the selected ion at *m/z* = 131.05 and *m/z* = 303.05 fit the *m/z* values of cinnamic acid and quercetin.

3.4 *In Vivo* Studies

The esters **1** and **2** were evaluated and compared to the one-to-one mixtures of the respective acids and taxifolin in a mouse model of AD regarding their protective effects against $A\beta_{25\text{-}35}$-induced memory impairment.[150-152] The experiments were performed by Dr. Matthias Hoffmann (Decker lab) under supervision of Dr. Tangui Maurice at the MMDN, University of Montpellier in France.

AD-like cognitive dysfunction was induced by intracerebroventricular (icv) injection of oligomerized $A\beta_{25-35}$ peptide into the mouse brain on day 1. Compounds were injected intraperitoneally (ip) from day 1 to day 7, and spatial working memory was evaluated on day 8 in a Y-maze assay. On days 9 and 10 of the study, a step-through passive-avoidance assay was performed as a measure of long-term memory improvement, followed by sacrifice on day 11 (for detailed experimental procedures cf. Appendix I). Investigating the spatial working memory, compound **2** reduced the $A\beta_{25-35}$–induced spontaneous alternation deficits at all doses tested (Fig. 14A). Compound **1** showed significant prevention of the $A\beta_{25-35}$-induced alternation deficit at 3 and 10 mg/kg (Fig. 14B). The esters **1** and **2** appeared to be significantly more neuroprotective than the mixtures of taxifolin and the respective acids (Fig. 14C, D, E).

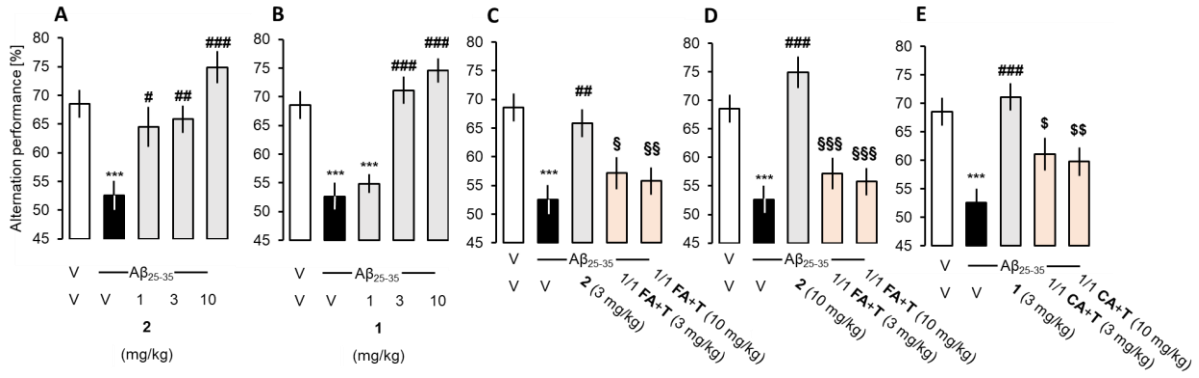

Figure 14. Effect of the compounds on $A\beta_{25-35}$-induced spontaneous alternation deficits in mice. V – vehicle, **2** – 7-*O*-feruloyltaxifolin, **1** – 7-*O*-cinnamoyltaxifolin, FA – ferulic acid, T – taxifolin, CA – cinnamic acid. Data shows mean ± SEM. ANOVA: $F_{(4,59)} = 8.77$, $p < 0.001$, n = 11-12 per group in **A)**; $F_{(4,58)} = 19.97$, $p < 0.001$, n = 11-12 in **B)**; $F_{(7,95)} = 7.35$, $p < 0.001$, n = 11-12 in **C)** and **D)**; $F_{(7,95)} = 8.54$, $p < 0.001$, n = 11-12 in **E)**. *** $p < 0.01$ vs. (V+V)-treated group; # $p < 0.05$, ## $p < 0.01$, ### $p < 0.001$ vs. ($A\beta_{25-35}$+V)-treated group; § $p < 0.05$, §§ $p < 0.01$, §§§ $p < 0.001$ vs. ($A\beta_{25-35}$+**2**)-treated group; $ $p < 0.05$, $$ $p < 0.01$ vs. ($A\beta_{25-35}$+**1**)-treated group; Dunnett's test.

On day 9 of the study, the step-through passive-avoidance training was conducted, followed by assessing the step-through latency on day 10 to examine the effects on long-term memory.[150-152] None of the compounds or mixtures improved the Aβ-induced impairment of long-term memory in prolonging step-through latency (for data cf. Appendix I). A dichotomy between the effects on $A\beta_{25-35}$-induced short-term and long-term memory deficits could, however, be anticipated. Antioxidants like idebenone and α-tocopherol prevented the short-term memory deficits in the Y-maze and water-maze, but not passive avoidance deficits in $A\beta_{1-42}$-treated mice.[153] Furthermore,

taxifolin has a preventive effect on $A\beta_{1-42}$ accumulation and aggregation.[154, 155] It was previously reported that a γ-secretase inhibitor, BMS-299897, attenuated $A\beta_{25-35}$-induced $A\beta_{1-42}$ seeding and toxicity.[156] Importantly, BMS-299897 blocked the $A\beta_{25-35}$-induced deficits in spontaneous alternation or novel object recognition using a 1 h intertrial time interval but failed to affect the passive avoidance impairments or novel object recognition using a 24 h intertrial time interval. Therefore, $A\beta_{25-35}$ injection provoked an accumulation in endogenous $A\beta_{1-42}$, an effect that was blocked by γ-secretase inhibition. This $A\beta_{1-42}$ accumulation marginally contributed to the toxicity or long-term memory deficits, but likely plays a major role in synaptic dysfunction and short-term memory deficits.

3.5 Conclusion

7-*O*-esters of taxifolin and ferulic or cinnamic acid have shown overadditive neuroprotective effects against oxidative stress and neuroinflammation in various cell-based assays, proving a pleiotropic beneficial effect which is desperately needed in the context of multifactorial neurodegenerative diseases like AD. Due to the significant and overadditive *in vivo* effects, it can be assumed that the compounds could cross the blood-brain barrier, and their metabolic stability was sufficient to evoke an amelioration of short-term memory defects in mice, in contrast to the controls. Even though their detailed mechanism of action remains to be determined, several target pathways were identified, including maintenance of GSH under conditions of oxidative stress and Nrf2 signaling. Thus, the natural product hybrids should be considered as a class of neuroprotective compounds with a distinct and specific pharmacological profile.

3.6 Unpublished Results: Antioxidant Capacities

The beneficial effects of flavonoids towards treating several diseases had previously been mainly attributed to their antioxidant capacity. The published work in this chapter showed that 7-*O*-esters of taxifolin modified intracellular pathways and the effect was not solely based on their function as antioxidants. To examine this hypothesis, the antioxidant and radical scavenging capacity of taxifolin and 7-*O*-cinnamoyltaxifolin **1** were investigated in different antioxidant assays, addressing

various aspects of antioxidant activity. The DPPH (diphenyl-1-picrylhydrazyl) assay was performed by Matthias Scheiner (Decker lab, University of Würzburg), Feng He (Decker lab, University of Würzburg) performed the metal chelation and the ORAC (oxygen radical absorbance capacity) assay, and Florian Lang (Högger lab, University of Würzburg) conducted the FRAP (ferric ion reducing antioxidant parameter) assay.

The assays were chosen based on the categories of antioxidant capacity assays according to the chemical reactions involved.[157] The DPPH and FRAP assay are based on hydrogen atom transfer, while the ORAC assay quantifies the antioxidant capacity based on single electron transfer. Metal chelation was investigated as antioxidants can scavenge alkoxyl radicals, which can be formed through metal-catalyzed Fenton-type reactions during the decomposition of peroxides. This aspect is particularly important in AD, as postmortem analysis of AD brains showed the accumulation of redox-active transition metals iron and copper.[158] The results of the DPPH, FRAP, and ORAC assays of compound **1**, taxifolin, and cinnamic acid are shown in Table 1. Cinnamic acid was inactive in all assays and showed no antioxidant capacity. In the DPPH and FRAP assays, comparable values were observed for the antioxidant capacities of **1** and taxifolin. The esterification to cinnamic acid did not significantly impair the antioxidant capacity of taxifolin in the DPPH and FRAP assays, showing that the hydroxyl group in position 7 was not relevant for electron-transfer reactions. The ORAC assay, however, showed the antioxidant capacity involving hydrogen atom transfer reactions was negatively influenced by esterification (Table 1).

Compound	**IC_{50} DPPH assay [µM]**	**FRAP assay [equiv. $FeSO_4$]**	**ORAC [Trolox equiv.]**
Taxifolin	5.0	2.0 ± 0.7	8.4 ± 0.4
7-*O*-Cinnamoyltaxifolin **1**	5.6	1.7 ± 0.7	4.3 ± 0.4
Cinnamic acid	n. a.	n. a.	n. a.

Table 1: Results of the antioxidant capacity assays.

These results show that the overadditive effect observed in cell-based assays cannot be explained by a synergistic effect of taxifolin and cinnamic acid in their antioxidant capacity. Only for the chelation of copper compound **1** was a more potent chelator than taxifolin (Fig. 15A). These findings support that 7-*O*-esters of taxifolin modify

intracellular pathways and hold a distinct mode of action for neuroprotection, exceeding their effects as antioxidants.

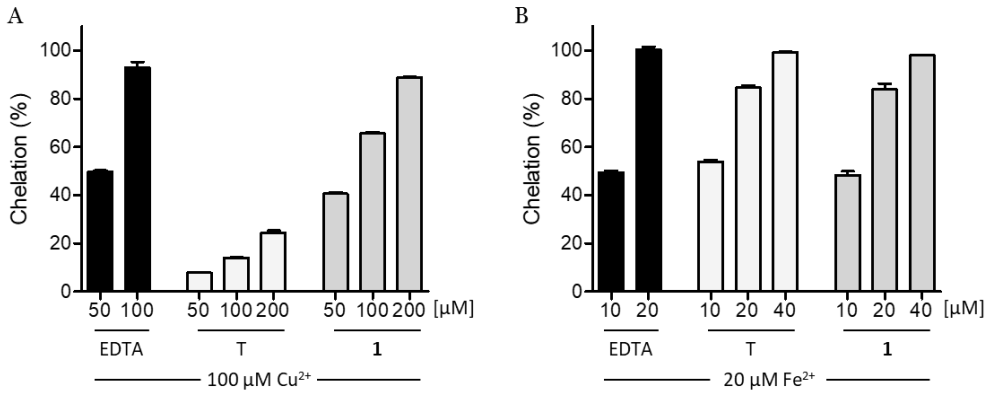

Figure 15: The capacity of taxifolin (T) and 7-*O*-cinnamoyltaxifolin **1** to chelate copper ions (**A**) or ferrous iron (**B**). EDTA served as a positive control. Data are presented as mean ± SEM.

4. Development and Application of a Chemical Probe Based on a Neuroprotective Flavonoid Hybrid for Target Identification Using Activity-Based Protein Profiling

ACS Chemical Neuroscience

pubs.acs.org/chemneuro Research Article

Development and Application of a Chemical Probe Based on a Neuroprotective Flavonoid Hybrid for Target Identification Using Activity-Based Protein Profiling

Sandra Gunesch, David Soriano-Castell, Stephanie Lamer, Andreas Schlosser, Pamela Maher,* and Michael Decker*

The content of this chapter was originally published in *ACS Chemical Neuroscience* **2020** and adapted with permission of the American Chemical Society.

http://dx.doi.org/10.1021/acschemneuro.0c00589

Author contributions:

S. Gunesch (under supervision of Prof. Dr. M. Decker) designed and synthesized the compounds and performed all cell-based assays (under supervision of Dr. P. Maher).

Dr. D. Soriano-Castell performed the microscopic analysis.

S. Lamer (under supervision of Prof. Dr. A. Schlosser) performed MS analysis.

Dr. P. Maher performed the knockdown experiments.

4.1 Introduction

In this follow-up project, the mode of action of the neuroprotectant 7-*O*-cinnamoyltaxifolin (**1**, 7CT) was closer examined on the molecular level by applying activity-based protein profiling (ABPP) to identify intracellular targets of the compound. A bioorthogonal Cu(I)-catalyzed [3+2] azido-alkyne cycloaddition (CuAAC) approach was used.[159-161] Briefly, an alkyne tagged chemical probe of the compound of interest undergoes covalent interactions with its target proteins when incubated with cells. The alkyne probe binds to its native targets and can then be tagged with any azide in a CuAAC reaction (Fig. 16). Depending on the application, tags can either be fluorescent dyes or other markers to visualize and identify target proteins. A widely used tag is biotin as the high affinity for streptavidin is convenient for the enrichment of bound proteins and enables characterization by MS analysis.[160] Within this work, a chemical probe of 7CT suitable for target identification was designed, synthesized, validated, and implemented in ABPP.

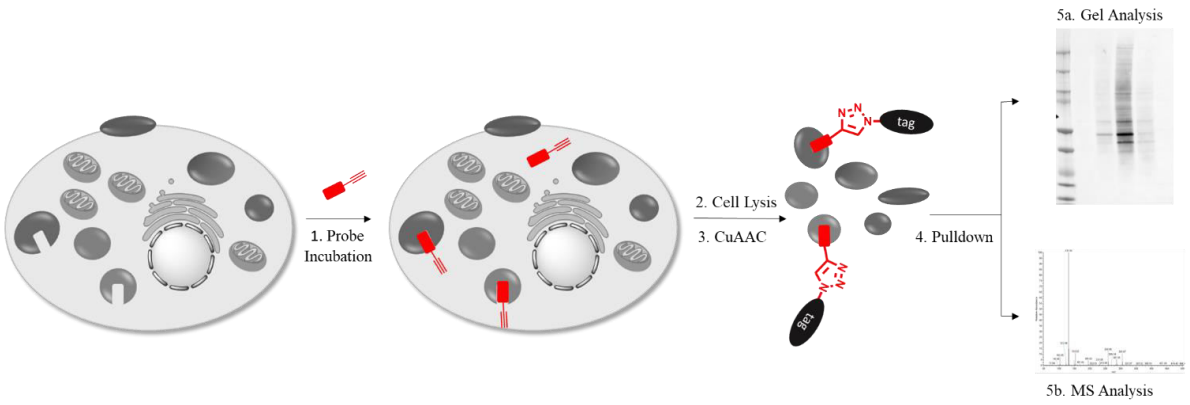

Figure 16: Workflow of the CuAAC approach for target identification. During incubation, the chemical probe binds to its native targets inside the cells. The cells are lysed and submitted to CuAAC reaction to tag the chemical probe, which is covalently bound to its intracellular targets. After pulldown purification, target proteins are analyzed.

4.2 Chemistry

Designing a chemical probe for target identification purposes, it is of utmost importance not to alter the mode of action of the compound. For 7-*O*-cinnamoyltaxifolin, its simultaneous influence on several proteins and signaling pathways could be mediated through the Michael acceptor sites at the cinnamoyl

moiety and the catechol residue, allowing covalent conjugation to proteins (Fig. 17A). Comprehensive SARs on the respective silibinin ester supported this hypothesis.[132]

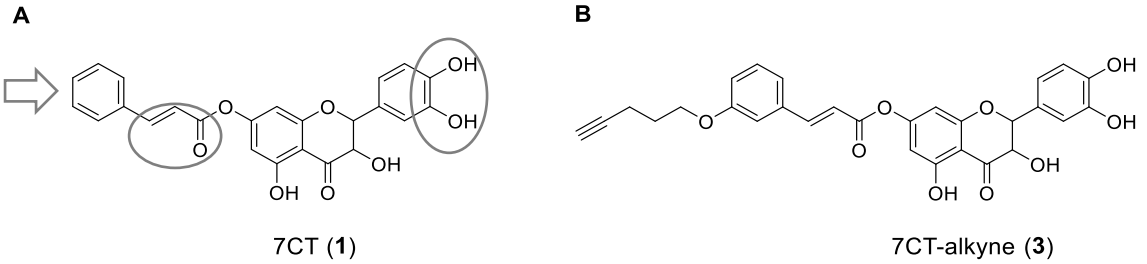

Figure 17: A) Design of the chemical probe without altering electrophilic moieties (encircled) of 7-*O*-cinnamoyltaxifolin; **B)** The chemical structure of 7CT-alkyne (**3**).

The attack of a nucleophilic side chain, of cysteinyl thiolates, for example, to the electrophilic beta-carbon, could be one potential mechanism to form covalent adducts inducing cellular responses.[162] To preserve potential reactive sites of 7CT, the aromatic

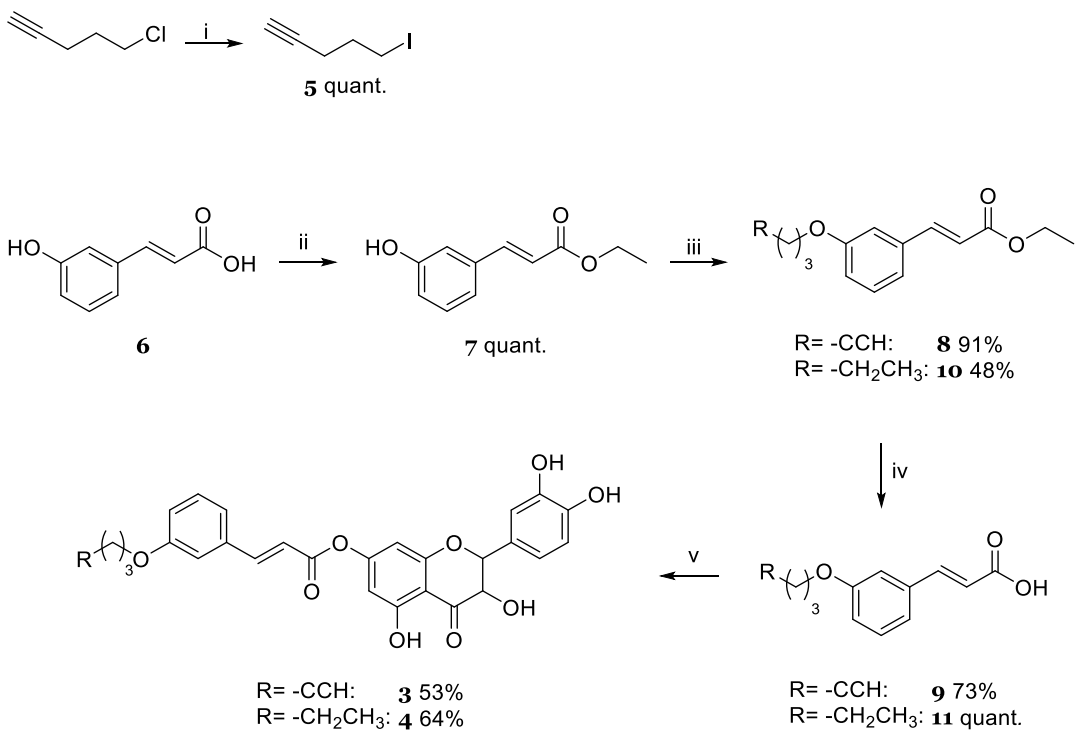

Scheme 2: Synthesis of 7CT-alkyne **3**, a 7-*O*-cinnamoyltaxifolin based chemical probe, and the control compound **4**. i) NaI, dry acetone, reflux, overnight; ii) H_2SO_4, ethanol, reflux, 6 h; iii) **5** or 1-iodopentane, K_2CO_3, dry acetone, 0 °C to reflux, overnight; iv) NaOH, water, ethanol, room temperature; v) 1. Oxalyl chloride, DMF, dry THF, room temperature, 30 min; 2. Taxifolin, triethylamine, room temperature, overnight.

moiety of the phenolic acid was chosen to introduce the alkyne tag necessary for CuAAC. Previous SARs study with phenolic acid esters of silibinin[132] and 7-*O*-feruloyltaxifolin as a potent neuroprotectant[163] showed that this entity tolerated modification without loss of activity. Therefore, 7CT-alkyne (**3**) (Fig. 17B) was synthesized, starting from 3-hydroxy cinnamic acid (**6**). The carboxylic acid moiety was protected using ethanol to selectively react with 5-iodopentyne (**5**), which was synthesized via a Finkelstein reaction, at the aromatic hydroxyl position. Deprotection under basic conditions gave compound **9**. Regioselective esterification with taxifolin without protective groups was achieved by forming the acid chloride of compound **9** with oxalyl chloride. *In situ* esterification under basic conditions with adjusted reaction times and extensive column purification gave the target compound 7CT-alkyne (**3**). The control compound 7CT-alkane (**4**) was synthesized to compare the influence of an aliphatic modification in the aromatic position on the neuroprotective performance of the compound and served as a negative control in the CuAAC reaction. The synthetic route for compound **4** was analogous to compound **3,** replacing 5-iodopentyne (**5**) with 1-iodopentane in step iii (Scheme 2).

4.3 Biology

For validation of the chemical probe, 7CT-alkyne **3** and the control compound 7CT-alkane **4** were subjected to phenotypic screening assays described before. Figure 18 shows the activity of the chemical probe **3** and the control compound **4** compared to the lead compound 7-*O*-cinnamoyltaxifolin (7CT). Even though there was a slight increase in toxicity by introducing the aliphatic moiety (Fig. 18A), compound **3** proved to be neuroprotective throughout all assays, as was the control compound **4**. At a concentration of 5 µM, 7CT-alkyne **3** was as protective as 7CT in the phenotypic screening assays for protection against oxytosis (Fig. 18B), ferroptosis (Fig. 18C), and ATP depletion (Fig. 18D), proving that the compound was active and therefore suitable for use as a chemical probe for target identification.

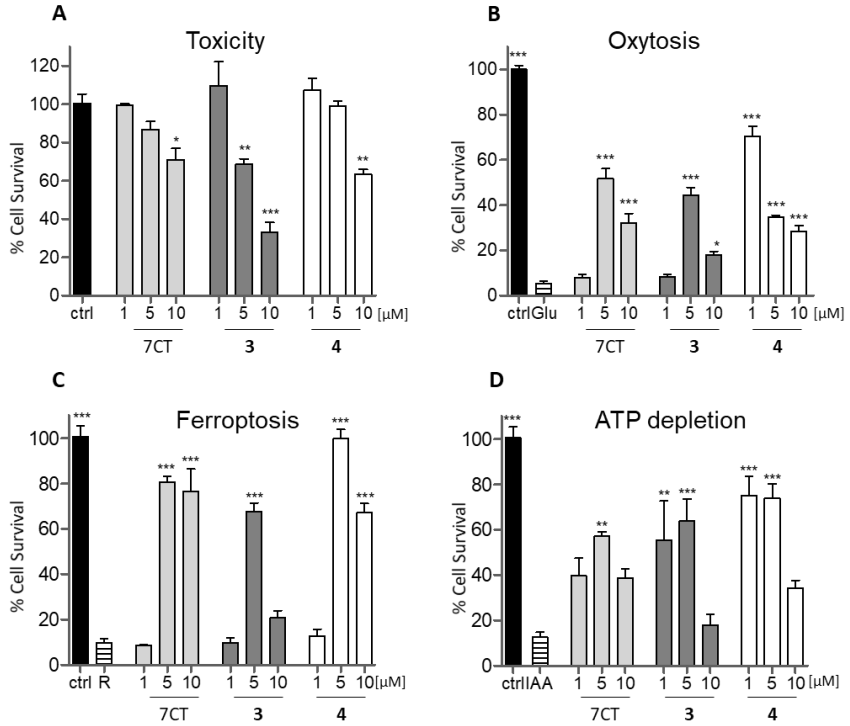

Figure 18: Phenotypic screening assays in HT22 cells. **A)** Toxicity of the compounds 7CT, 7CT-alkyne (**3**), and 7CT-alkane (**4**). **B)** Neuroprotective effects of 7CT, **3**, and **4** against oxytosis induced by 5 mM glutamate (patterned). **C)** Neuroprotection of 7CT, **3**, and **4** against ferroptosis induced by 0.3 µM RSL3 (patterned). **D)** Neuroprotective effects of 7CT, **3**, and **4** against ATP depletion induced by 20 µM iodoacetic acid (IAA, patterned). Means ± SEM of three independent experiments are shown referring to untreated control cells (black). One-way ANOVA followed by Dunnett's multiple comparison posttests was used for analysis referring to untreated controls in A) or cells treated with the respective insult in B), C), and D). Levels of significance: * $p < 0.05$; ** $p < 0.01$; *** $p < 0.001$.

Further validation experiments showed that the probe 7CT-alkye **3** remained active against neuroinflammation and induced Nrf2 upregulation (Fig. 19). Even though 7CT seemed more potent at higher concentrations and led to nearly 6-fold induction of Nrf2 levels at 10 µM, increased Nrf2 levels were significant for both compounds at the same concentration of 5 µM (Fig. 19B).

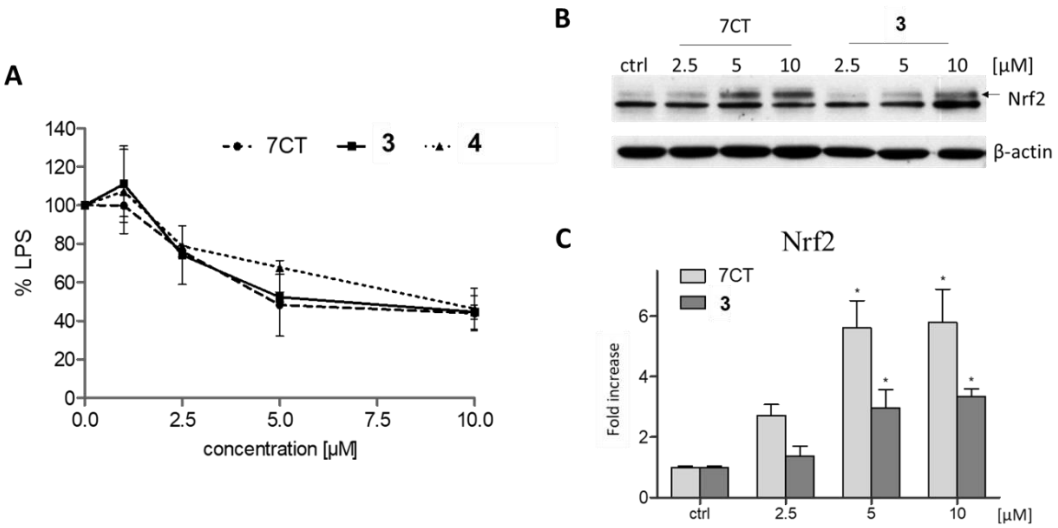

Figure 19: A) Neuroinflammation in BV-2 cells. Effects of 7CT, **3**, and **4** on NO production in LPS-induced inflammation. NO was quantified by the Griess assay. Data are given as means ± SEM and relative cells treated with LPS only set as 100%. **B)** Western blot analysis of Nrf2 induction by 7CT and **3** in nuclear fractions of HT22 cells. DMSO served as a control. Levels of Nrf2 were normalized to actin, and representative blots are shown. **C)** Quantification of the results from three independent experiments, as shown in B). Statistical significance refers to DMSO-treated controls with * $p < 0.05$.

Flavonoids like fisetin have been shown to modulate MAP kinases,[116] and modifications of MAP kinases have not been investigated for 7-*O*-esters of taxifolin before. Therefore, compound 7CT and its chemical probe **3** were analyzed to induce the MAP kinases ERK and p38, both relevant for AD. ERK signaling is involved in cell proliferation, differentiation, and survival or promotion of cell death. It, therefore, can be engaged in neurodegeneration.[164] Postmortem brains of early-stage AD patients showed increased phosphorylation of p38, which is connected to mediating Aβ-induced inflammation and impaired autophagy in neurons leading to neurodegeneration.[165-167] 7CT and compound **3** led to a significant increase in ERK phosphorylation and activation after 5 minutes (Fig. 20B). The effect ceased with increased incubation times, thereby excluding chronic ERK activation, which is correlated with neurodegeneration.[168]

Figure 20C shows that at a concentration of 10 µM, compound **3** and 7CT both reduced p38 phosphorylation. Decreased activation was observed after 5 minutes of incubation and was significantly reduced for the whole time-course of 2 hours. The activation of ERK and deactivation of p38 underlined that 7CT and compound **3** modify MAP kinases. Thus, these results strengthened the reliability of compound **3** as a suitable bait for target identification.

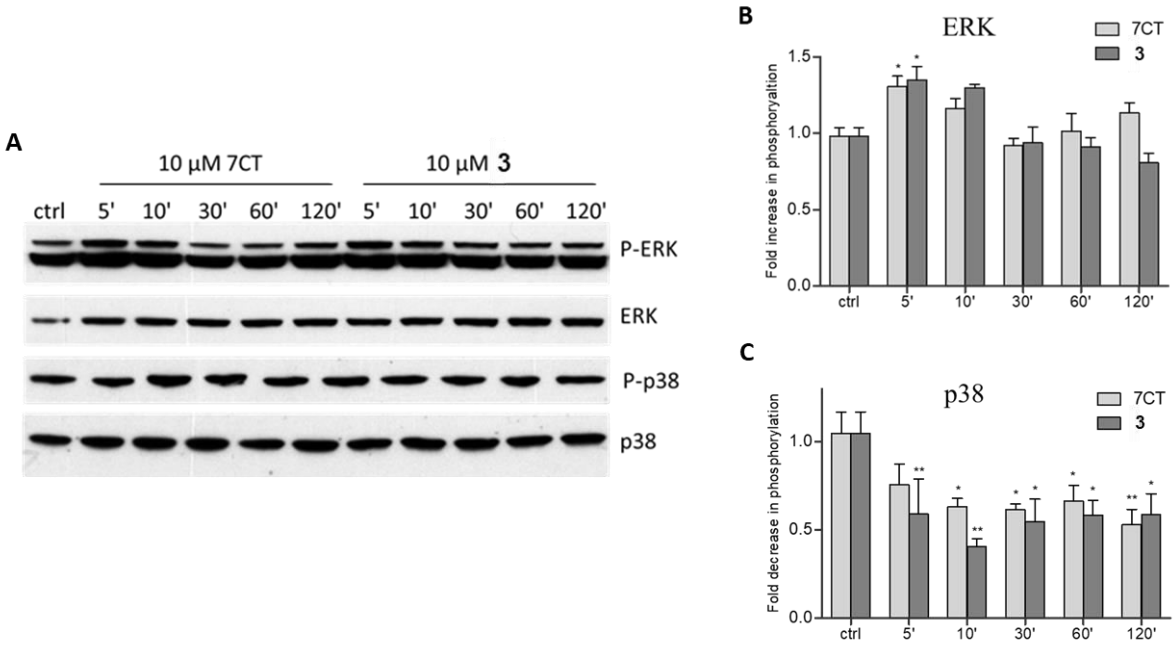

Figure 20: A) Cells were treated for the indicated time points with 10 µM **3** or 7CT. DMSO treatment served as a control. Lysates of HT22 cells were prepared in sample buffer and analyzed by Western blot for phosphorylated ERK (P-ERK), total ERK (ERK), phosphorylated p38 (P-p38), or total p38 (p38). Levels of the phosphorylated protein were normalized to those of the total protein, and representative blots are shown. **B)** and **C)** Quantification of the results from three independent experiments, as shown in **A)**. Statistical significance refers to DMSO-treated controls with * $p < 0.05$, ** $p < 0.01$.

4.4 Microscopic Analysis

As outlined in the introduction of this work, neuronal cell death in AD is associated with mitochondrial dysfunction.[169] To determine whether compound **3** targets mitochondria, high-resolution fluorescence microscopy was used to analyze its intracellular location in an HT22 cell line expressing green fluorescent protein (GFP) in mitochondria (HT22-mitoGFP). HT22-mitoGFP cells were treated with the probe 7CT-alkyne **3** for 30 minutes, permeabilized, and reacted with the fluorescent dye Cy3-azide in a CuAAC reaction (for experimental details cf. Appendix II). Cy3 is then

covalently bound to the probe **3**, and its detection with fluorescence microscopy shows the probe's intracellular localization. As shown in Figure 21, compound **3** was found at several locations, including unknown structures in the perinuclear region. Notably, the fluorescence profiles of mito-GFP and Cy3 indicated that compound **3** was also strongly enriched in mitochondria after 30 minutes of incubation (see graphs on the right of Fig. 21). No significant signal for Cy3 was detected in control cells treated with DMSO. These results suggested that the interaction partners of compound **3** and 7CT might be associated with mitochondria.

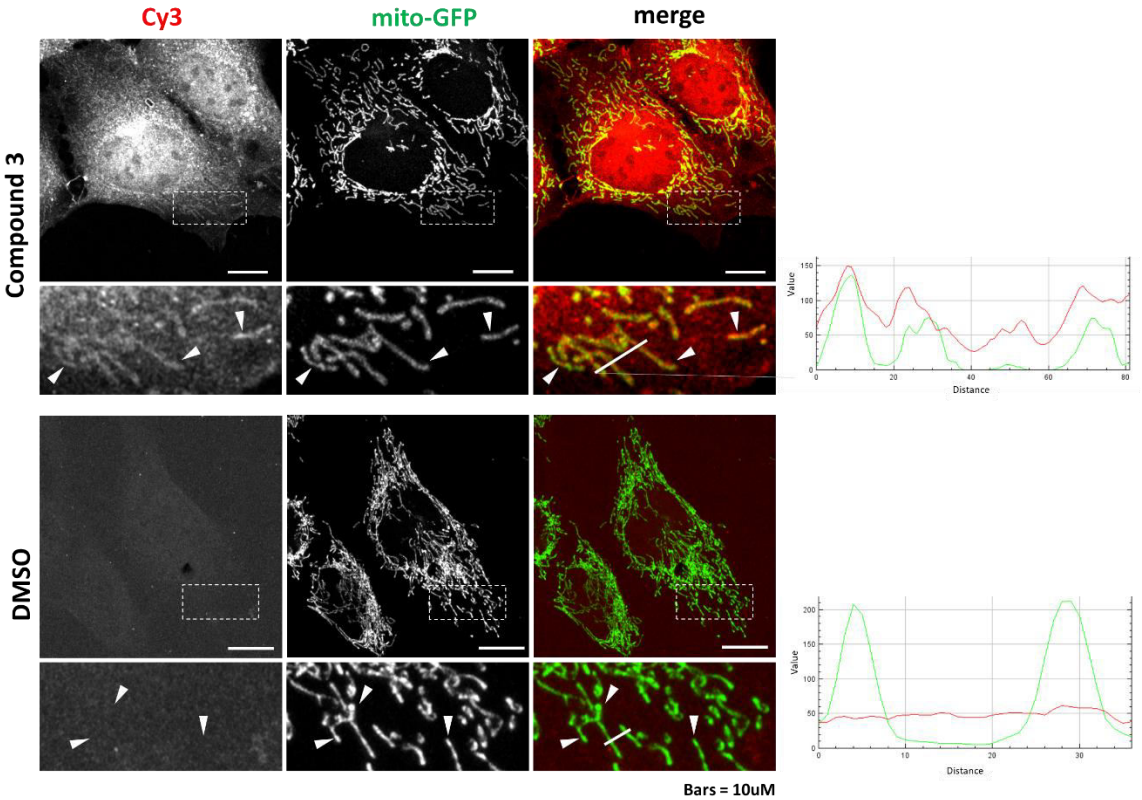

Figure 21: Representative microscopic images of HT22-mitoGFP cells incubated with 5 µM **3** or DMSO for 30 minutes. Red signals derive from Cy3 and correspond to adducted proteins; green signals are mito-targeted GFP. Arrows indicate mitochondrial structures to note the co-localization of Cy3 staining with mitochondria in cells incubated with compound **3** compared to the absence of signal in DMSO-treated cells. Co-localization was visualized by a line plotted in the merged images (magnified images). Charts on the right show quantification of the fluorescence profile along this line for each channel. The X-axis indicates distance, and the Y-axis represents fluorescence intensity in arbitrary units.

4.5 Affinity Pulldown and MS Analysis

For the affinity pulldown, 200 µM of compound **3** were incubated with HT22 cells for 2 hours before lysis and CuAAC reaction with biotin-azide. Proteins bound to **3** were purified on streptavidin magnetic beads, separated by SDS-PAGE, and analyzed by nanoLC-MS/MS after tryptic digestion. MS analysis and quantification were performed by Stephanie Lamer and Prof. Dr. Andreas Schlosser at the RVZ of the University of Würzburg. A total of 708 proteins were identified in a label-free approach and quantified. Seventy of these were significantly enriched in both replicates and thus classified as potential target candidates (summed significance 4; Fig. 22).

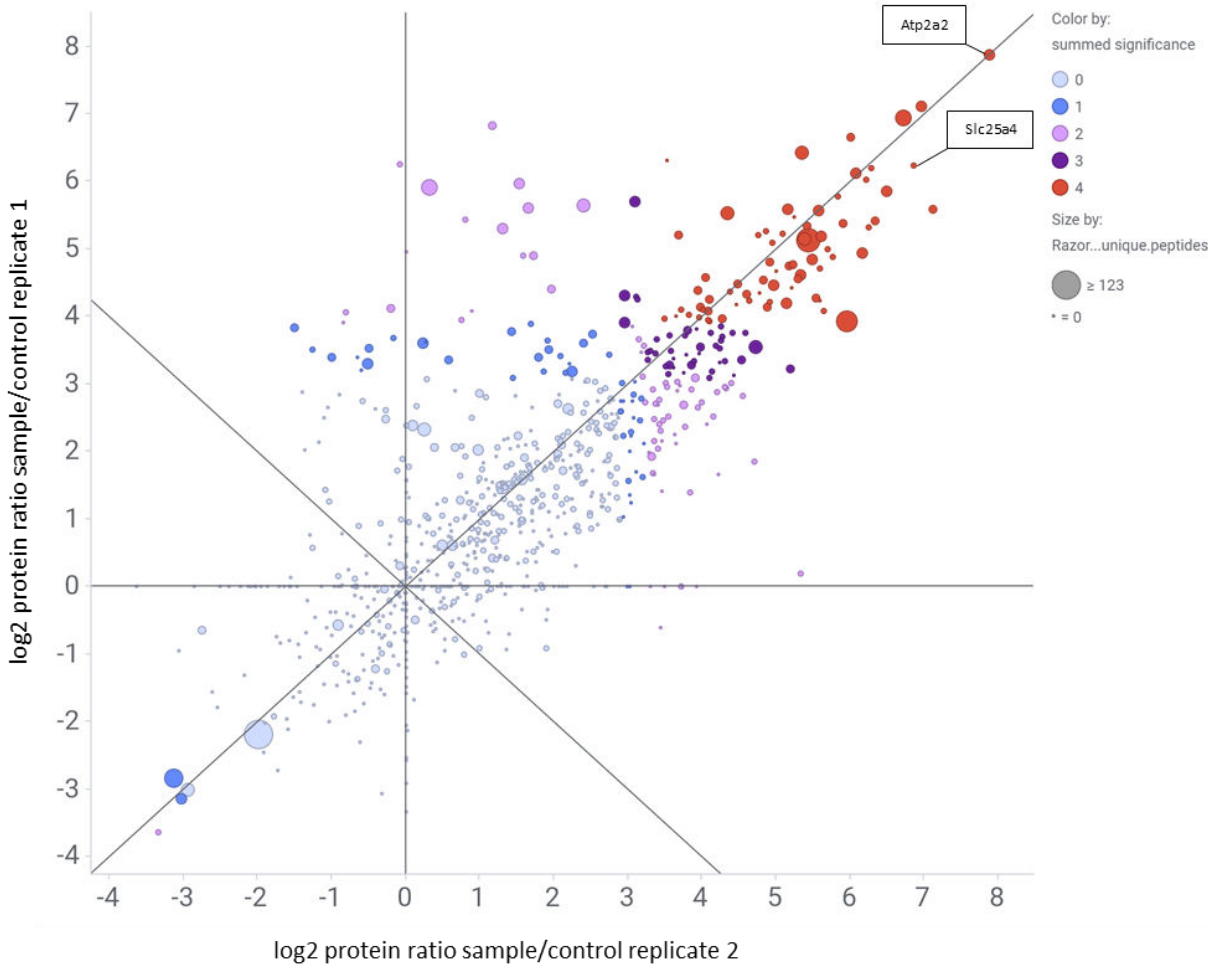

Figure 22: Log2 transformed protein ratios sample/control of two replicates are shown. Summed significance values were used to identify the best target candidates (significance 2 in both replicates = significance 4, marked in red). The size of the dots corresponds to the number of razors and unique peptides of a protein.

Two of the 70 hits were pursued further to investigate the interaction between compound **3** and 7CT and the respective identified proteins. One was the sarco/endoplasmic reticulum Ca^{2+}-ATPase (SERCA, Atp2a2), which was the protein with the highest significance in the log2 protein ratio sample/control and, therefore, the top target identified according to MS analysis (Fig. 22). As the microscopic analysis showed compound **3** in mitochondria, mitochondrial proteins among the targets were of interest. The mitochondrial carrier adenine nucleotide translocase 1 (ANT-1, Slc25a4) was as top 4 the most significant hit of a mitochondrial protein and the only mitochondrial protein among the top 10 of the identified proteins. Therefore, ANT-1 was chosen as a second target for further examination.

4.6 ANT-1 and SERCA as Targets

ANT-1 is an ADP/ATP carrier at the inner mitochondrial membrane and the most abundant protein in mitochondria, contributing to 1-10% of total mitochondrial protein.[170] ANT-1 is relevant as a potential pharmacological target in neurodegenerative disorders, particularly for AD, as mitochondrial dysfunction is proposed to be one of the major hallmarks of the disease.[171, 172] The carrier was characterized as a pro-apoptotic protein, as increased ATP export is essential for apoptosis, and is mediated by enhanced levels of ANT-1 leading to mitochondrial breakdown and the apoptotic cascade.[173-175] Its role in non-apoptotic forms of cell death, like ferroptosis and oxytosis covered in this work, has not been investigated yet. Therefore, HT22 cells transfected with ANT-1 siRNA were tested for effects on oxytosis and ferroptosis. ANT-1 knockdown protected against these insults. Significantly more

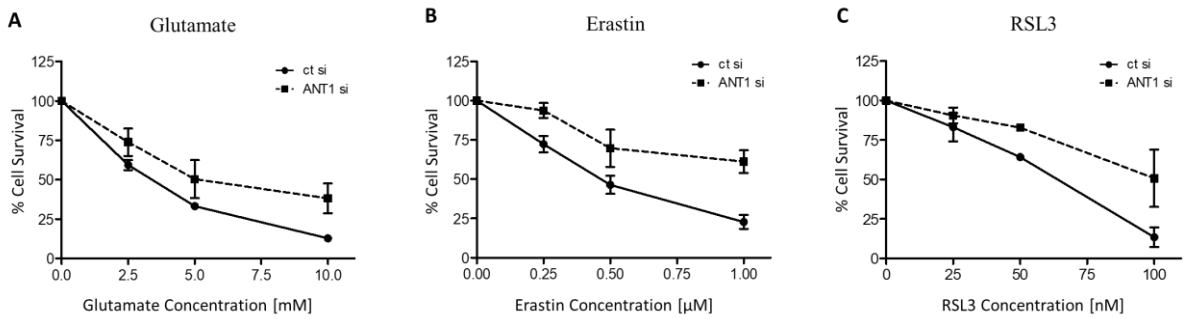

Figure 23: ANT-1 knockdown leads to protection against glutamate as an inducer of oxytosis (**A**), and erastin (**B**) and RSL3 (**C**) as inducers of ferroptosis.

cells survived treatment with glutamate as an inducer of oxytosis (Fig. 23A), or erastin and RSL3 as inducers of ferroptosis (Fig. 23B, C, respectively). These findings strongly supported the implication of ANT-1- inhibition in the protective effect of compound **3** and, consequently, 7CT.

In the absence of 7CT, the knockdown of ANT-1 was protective (Fig. 23). However, under oxytosis conditions and the treatment of 7CT, the control cells were as protected as the ANT-1 knockdown cells. This indicates that ANT-1 was not the exclusive target of 7CT, and other mechanisms are also involved as the compound provided additional protection (Fig. 24B). ROS and oxidative stress lead to increased mitochondrial membrane potential (MMP).[176] Modification of the MMP by 7CT would also be a possible mechanism of action. It was shown that FCCP, a mitochondrial uncoupler dissipating the MMP, also protected cells from oxytosis.[177] Further, a study with quercetin showed that low concentrations of the flavonoid reduced the MMP and inhibited adenine nucleotide exchange by ANT-1.[178] As the concentrations at which neuroprotection was observed in our study were in the low micromolar range, **3** and 7CT could act as mild uncouplers and inhibitors of ANT-1 and thereby protect cells.

The sarco/endoplasmic reticulum Ca^{2+}-ATPase 2 (SERCA), a second interaction partner identified by MS analysis, is located in the endoplasmic reticulum (ER). The pump regulates calcium influx into the ER under ATP consumption. ER-stress concomitant with calcium dysregulation causes neuronal impairment and neuronal

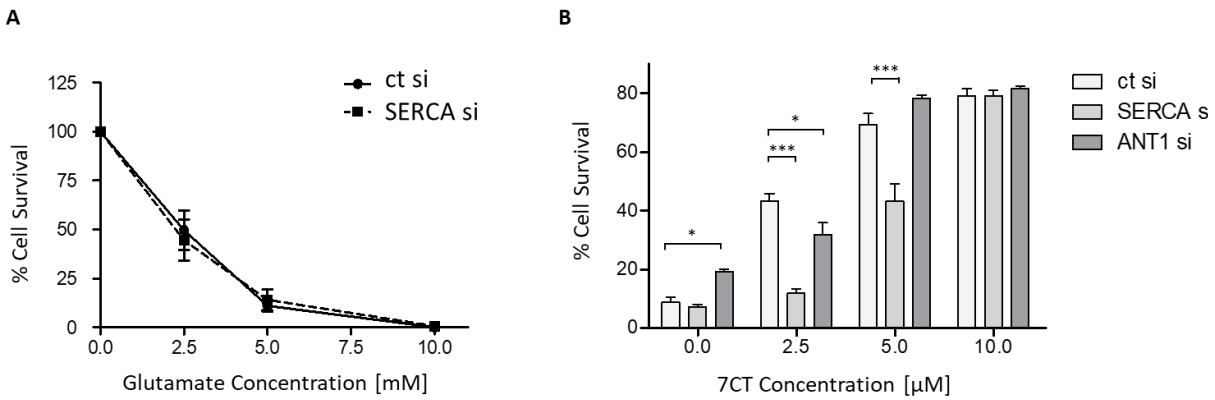

Figure 24: A) The transfection of HT22 cells with SERCA siRNA is not protective against glutamate-induced oxytosis. **B)** ANT-1 (dark grey) and SERCA (light grey) knockdown cells were treated with increasing concentrations of 7CT in the presence of glutamate. Data are presented as means ± SEM of four independent experiments. Statistical analysis was rendered using Two-way ANOVA followed by Bonferroni posttests using GraphPad Prism 5. Levels of significance: * $p < 0.05$; ***$p < 0.001$.

death and is involved in the progressive neurological decline of AD.[179] Krajnak et al.[180] showed that activation of SERCA was neuroprotective and improved memory and cognition in APP/PS1 mice. In this work, SERCA was validated as a target for 7-*O*-esters of taxifolin by knockdown experiments. In contrast to the results with ANT-1, HT22 cells treated with SERCA siRNA were not protected against glutamate-induced oxytosis (Fig. 24A). However, SERCA knockdown significantly impaired the protection by compound 7CT at the lower concentrations of 2.5 and 5 µM (Fig. 24B), suggesting a vital role of SERCA in the protective mechanism of 7CT. At a concentration of 10 µM 7CT, the decrease in protection by the absence of SERCA was no longer seen. Higher concentrations of 7CT likely activate other protective pathways due to the pleiotropic action of the compound and hence compensate for SERCA knockdown.

4.7 Conclusion

In conclusion, the probe **3**, designed and synthesized within this work, proved its suitability as a neuroprotectant in cell-based phenotypic screening assays addressing different aspects of neurodegeneration and aging. On a molecular level, Western blots confirmed that the parent compound 7CT and the probe act on the same pathways. The alkyne-tag was not altering the mechanisms of action. SERCA, the top target candidate of compound **3** in MS analysis, and ANT-1, the top mitochondrial target candidate, were investigated for their relevance for compound **3** and 7CT in knockdown experiments. Both proteins are crucial for cell homeostasis and survival and were, for the first time, shown to be modified by 7-*O*-esters of flavonoids.

5. Studies on Chemical Modifications of Flavonoids

5.1 Chemical Modification of Fisetin

Fisetin (Scheme 3) is a secondary plant metabolite found in fruits and vegetables and enriched in strawberries. The flavonoid is structurally closely related to quercetin, lacking the hydroxyl group in position 5 of the A-ring. Fisetin was shown to be neuroprotective in several *in vitro* assays and proved to be orally active and cognition-enhancing in *in vivo* studies.[181] The natural product entered clinical trials for the treatment of AD.[181] Different intracellular pathways were shown to be modified by fisetin,[115, 116, 182] however, the identification of direct interaction partners is of interest to understand its detailed mode of action. Therefore, within this work, an alkyne moiety should be introduced to fisetin for target identification studies applying the approach established in chapter 4 (details cf. Appendix II). In previous studies with taxifolin and another study with the structural closely related silibinin,[132, 163] position 7 proved suitable and well-tolerated for chemical modifications regarding neuroprotection. Hence, the alkyne tag should be introduced in position 7 of fisetin.

Chemical modifications of fisetin are so far confined to a study aimed to increase its direct radical-scavenging ability by C-methylation[183] and a more extensive study investigating SARs by modifying hydroxyl groups and the flavone scaffold to improve its neuroprotectivity for the treatment of stroke.[184] In both studies, the flavonoid was synthesized by aldol condensation of an aldehyde and acetophenone with the respective modification to a chalcone, which was subsequently reacted to the flavone (Fig. 25).

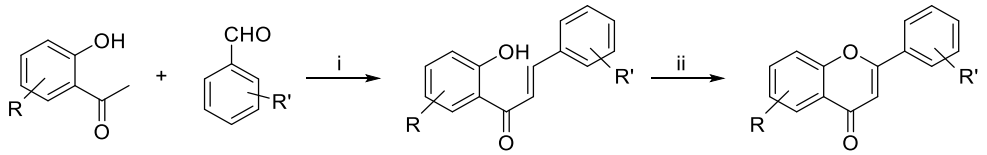

Figure 25: Total synthesis of fisetin derivatives according to Chiruta et al.[184] i) $Ba(OH)_2$, MeOH, 40 °C, overnight; ii) I_2, DMSO, 130 °C, 6 h.

As fisetin is commercially available, the compound was directly used for chemical modification. Direct alkynylation without protective groups failed as an inseparable mixture of 3'-*O*, 4'-*O*, and 7-*O*-alkynated products was obtained and protective groups

were required. Mattarei et al.[185] used protective acetyl groups for the selective methylation of quercetin in an improved synthesis of the natural product rhamnetin (7-*O*-methyl quercetin). Based on that study, protective acetyl groups were introduced into the flavonoid fisetin. The specific reactivity of the hydroxyl groups was utilized for selective deprotection in position 7 with imidazole-assisted deacetylation (Scheme 3). Acetylation of all four hydroxyl groups of fisetin to **12** was achieved with a quantitative reaction. Selective deprotection occurred with detriments in yields, and compound **13** was isolated with a yield of 49%. The reaction was limited by the incomplete conversion of the starting material **12** (Scheme 3).

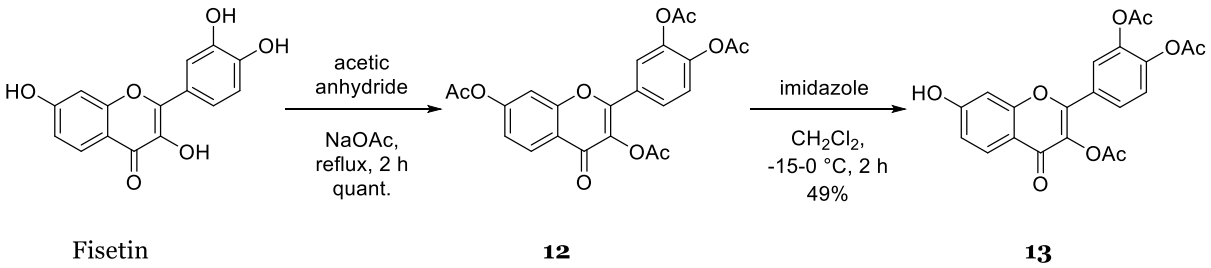

Scheme 3: Protection of fisetin.

To facilitate the reaction, thiophenol was added as acetyl scavenger as proposed by Li et al.[186] However, the conversion was not improved by thiophenol, and also changing the solvent from dichloromethane to *N*-methyl-2-pyrrolidone (NMP) as suggested by Li et al.[186] did not lead to a significant increase of yield, which would justify the use of the toxic chemical or abstain from TLC monitoring, which was hampered using NMP.

Reacting compound **13** with 5-hexynoic acid alkynylation in two positions of the flavonoid was observed. Next to the starting material **13**, LC-MS analysis revealed *m/z* = 503 as the main product corresponding to the proposed structure **14** with $[M+H]^+$

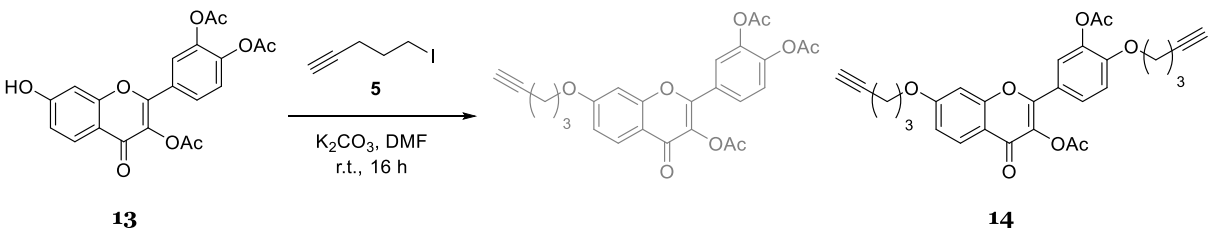

Scheme 4: LC-MS analysis revealed alkyne addition in two different positions of **13**. Shown is a proposed structure. The exact position of the linker was not assigned.

calculated = 502. Hence, for fisetin, not all protective acetyl groups were stable under the reaction conditions for nucleophilic substitution (Scheme 4).

Alternative protective groups used for flavonoids are mainly benzyl protective groups. However, after introducing an alkyne tag, hydrogenolysis cannot be applied for deprotection, limiting the selection of protective groups. As the 3-OH is relatively unreactive due to the hydrogen bond with the carbonyl in position 4 of fisetin, it was assumed that the protection of 3'- and 4'-OH might be sufficient to modify position 7

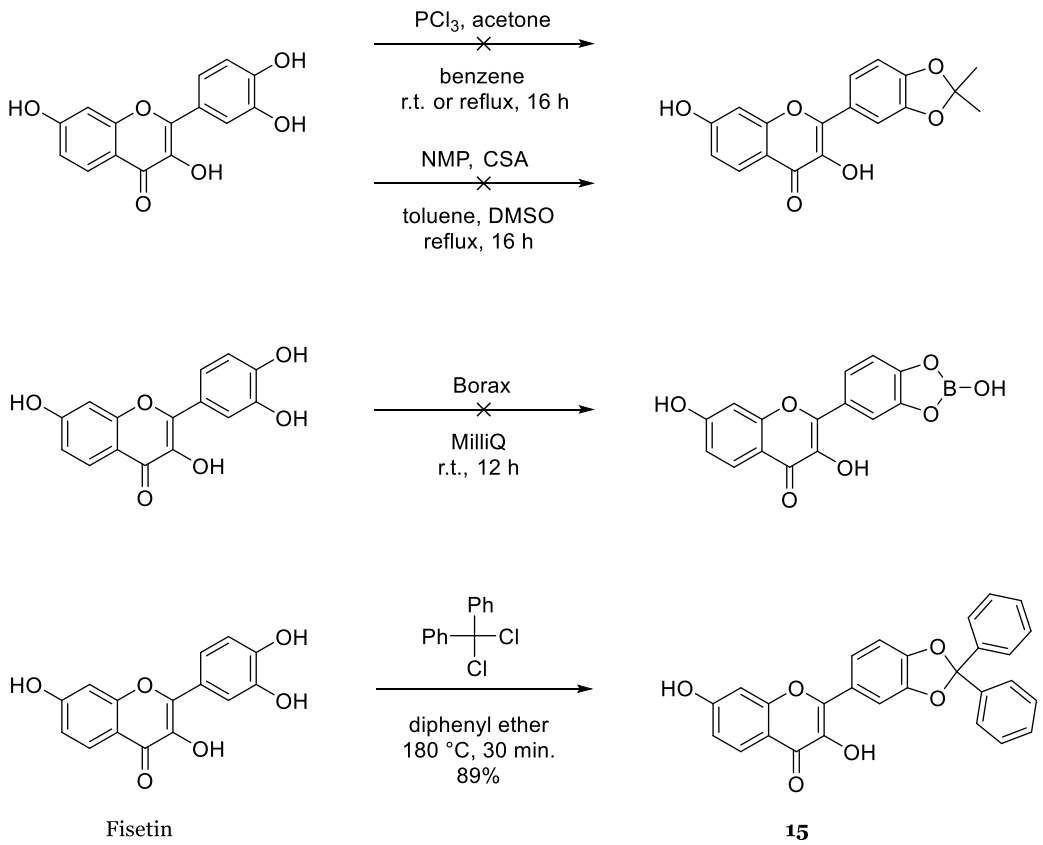

Scheme 5: 3'-4' diol protection approaches of fisetin. No conversion was achieved with the acetonide or borax protective groups.

selectively. Due to the specific reactivity of 3-OH and 7-OH, finetuning of the reaction conditions was expected to give selectively 7-*O*-akynylated fisetin. Hence, 1,2-diol protective groups were applied. Several approaches to introduce acetonide or borate protective groups failed as no reaction occurred, and fisetin was recovered (Scheme 5). Successful diol protection of fisetin was achieved in a microwave-assisted reaction with dichlorodiphenylmethane yielding compound **15** (Scheme 5). The diphenyl protective group could be removed with glacial acetic acid in water in a five to one ratio, which was compatible with the alkyne moiety.

The reaction of compound **15** with 1.0 equivalent of 5-iodopentyne led to the substitution of both positions 7 and 3 as the main product **16**. Shi et al.[187] applied the diphenyl protective group to study *O*-methylation patterns of quercetin as an inhibitor of cancer cell proliferation. In that study, positions 7 and 3 were methylated in parallel using 2.6 equivalents methyl iodine instead of 1.0 equivalent applied in this work.[187] Tight monitoring of the reaction with TLC and LC-MS revealed that the double alkynylated product formed immediately. Decreasing the amount of 5-iodopentyne to 0.5 equivalent did not influence regioselectivity. Therefore, 7-*O*-alkynation of fisetin was not successful using protective groups.

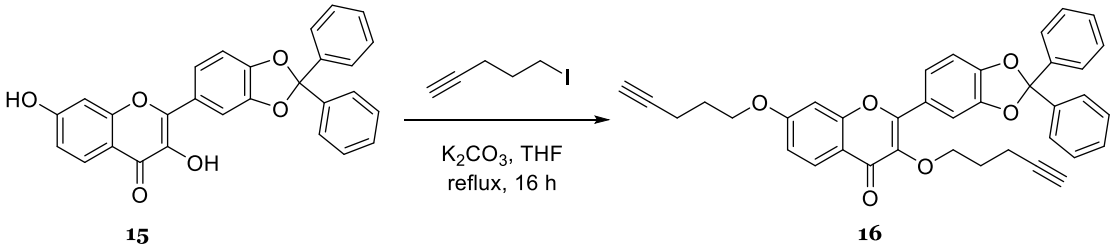

Scheme 6: Alkynation of compound **15**.

5.2 Chemical Probes of Taxifolin and Quercetin

Investigating 7-*O*-esters in chapter 3, taxifolin was not protective in the assays applied. However, it must be noticed that the concentrations studied were in the low micromolar range. Using a >10-fold higher dosage of the flavonoid, several studies had shown neuroprotective effects of taxifolin *in vivo*.[131] However, the detailed mechanisms of action of taxifolin are mostly elusive and not well understood. Therefore, with adapted concentrations, interactions of taxifolin with target proteins should be detected in the pulldown fraction of the ABPP approach. Hence, a chemical probe of taxifolin was synthesized together with Julian Hofmann (Decker lab, University of Würzburg).

The flavonoid quercetin is also a known neuroprotectant with an elusive mode of action.[188] In cellular uptake studies, 7-*O*-cinnamoyltaxifolin was metabolized to 7-*O*-cinnamoylquercetin (Fig. 13, chapter 3). Interestingly, Vrba et al.[144] had shown that incubation of taxifolin alone did not lead to the conversion to quercetin. Therefore, the mode of action of taxifolin and quercetin might vary, and the chemical probe of quercetin was also synthesized. Based on the previous studies with taxifolin and

silibinin,[132, 163] the alkyne tag should be introduced in position 7 of taxifolin and quercetin. The direct reaction of the pentyne halide to the native flavonoid was not regioselective, and protective groups had to be applied for the selective modification in position 7. As the acetyl protective groups described in the synthesis of the chemical modification of fisetin (Scheme 3) were proven stable in the study of Mattarei et al.[185] for the selective methylation of quercetin, the acetyl protective group strategy was applied for taxifolin and quercetin (Scheme 7).

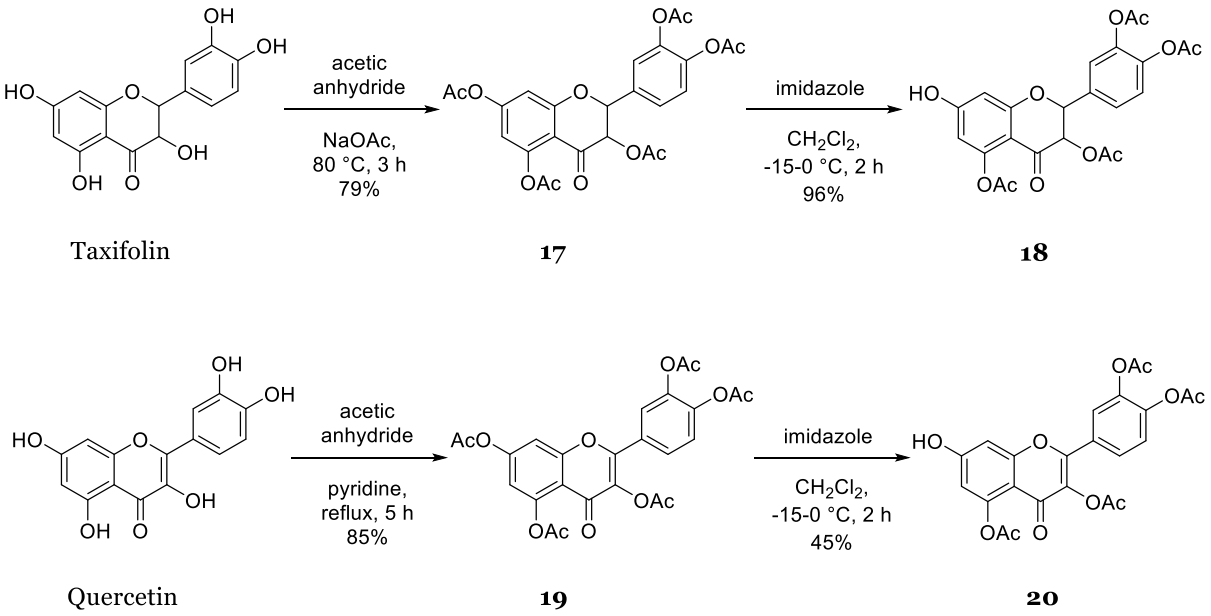

Scheme 7: Protection and selective deprotection of the flavonoids taxifolin and quercetin.

For the two flavonoids taxifolin and quercetin, the protection and selective deprotection reactions proceeded with satisfying yields and compounds **18** and **20** proved to be stable in the following steps of the synthesis route. A Finkelstein reaction with 5-chloropentyne gave 5-iodopentyne **21** as a linker precursor. In a nucleophilic substitution, **21** was reacted with the 7-*O*-deprotected flavonoids **18** and **20**. Acidic removal of protective acetyl groups gave the target compounds **22** and **23**, respectively (Scheme 8).

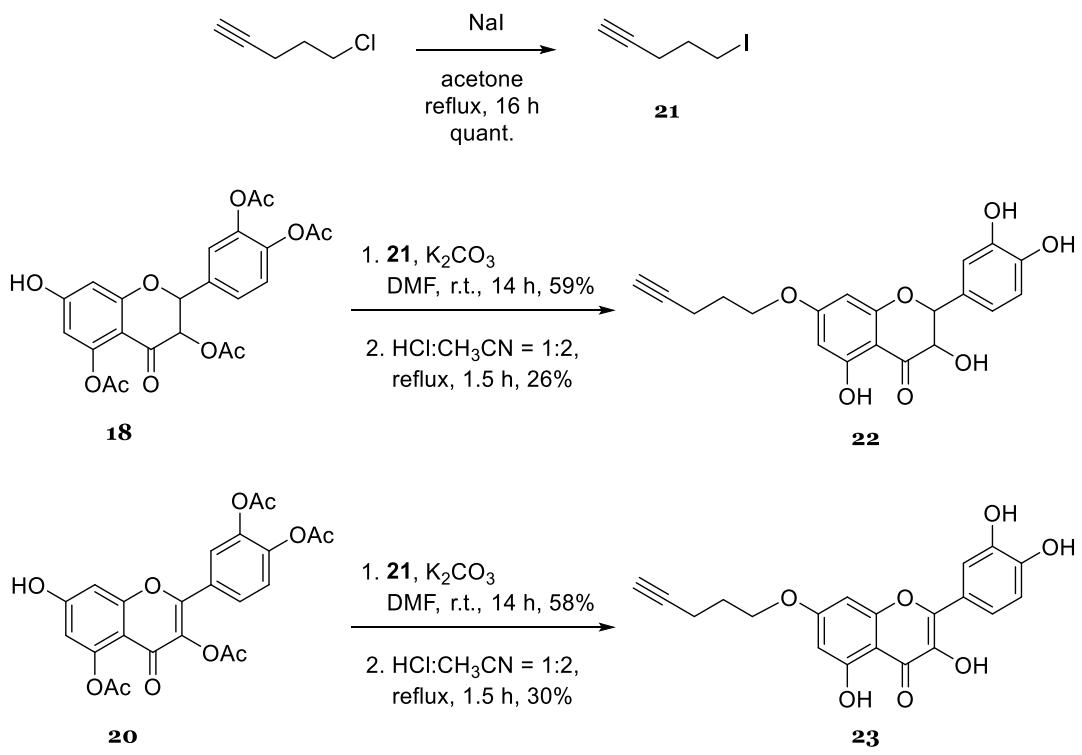

Scheme 8: Alkynylation of taxifolin and quercetin.

In future work, compounds **22** and **23** could be used in an ABPP approach according to the established protocol in chapter 4. A comparative analysis of the resulting lists of targets could give insights about the compounds' mode of actions. Three key hypothetical outcomes would allow the following valuable conclusions:

1. A large intersection of targets between 7CT and quercetin would suggest quercetin as the active metabolite important for the cellular response.
2. If the targets of quercetin and taxifolin are distinct from 7CT, the result would indicate that 7-*O*-esters of taxifolin are a specific class of compounds with a different intracellular mode of action.
3. If the targets identified are mostly overlapping between 7CT and taxifolin, it might indicate that the phenolic acid moiety serves as a sort of carrier, facilitating cellular uptake. A time-course experiment of cellular uptake quantifying and comparing the intracellular amount of taxifolin and 7-*O*-cinnamoyltaxifolin would give hints towards this hypothesis.

5.3 Synthesis of Amine-Functionalized Derivatives of Taxifolin and Quercetin

Hydrolysis represents a common degradation reaction affecting the stability of chemical compounds. Ester bonds are prone to hydrolyze and are therefore preferably used in prodrugs than in the active compound in medicinal chemistry. Even though cellular uptake experiments of the ester 7-*O*-cinnamoyltaxifolin showed that the primary metabolic product is the quercetin derivative, the compound was mostly degraded within 4 hours (Fig. 13, chapter 3).

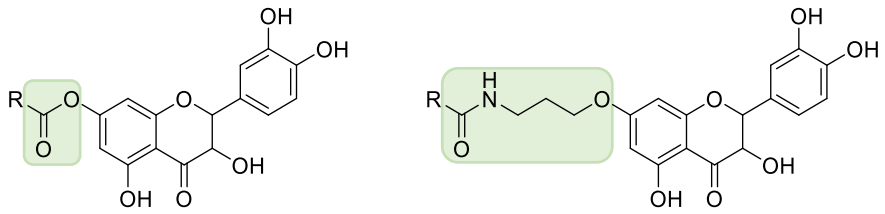

Figure 26: General structure of 7-*O*-esters of taxifolin (left) and the compound with the amide linker (right) for comparison.

To replace the ester group by an amide moiety, which is less readily hydrolyzed, amine-functionalized derivatives of taxifolin and quercetin were synthesized. The introduction of an amine linker connected via an ether to the flavonoid enables the synthesis of another, more stable class of hybrids via an amide bond (Fig. 26).

The linker precursor was synthesized starting with 3-bromopropylamine. The amine group was Boc-protected to compound **24**. In a Finkelstein reaction, the bromine was replaced by iodine, compound **25**, to improve the leaving group in the nucleophilic substitution (Scheme 9).

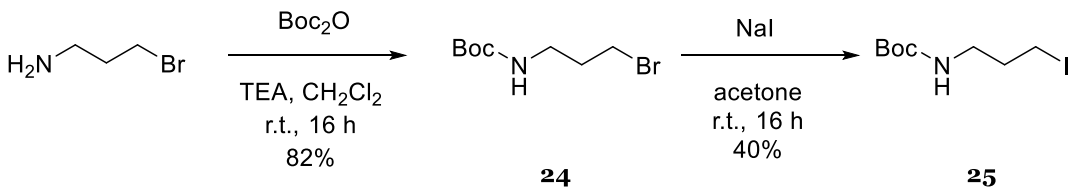

Scheme 9: Synthesis of the linker precursor **25**.

In contrast to the 7-*O*-ester formation, where direct esterification was possible without protective groups, the introduction of the linker via an ether bond was not

regioselective and required the use of protective groups. The acetylated derivatives **18** and **20** described before to synthesize chemical probes (Scheme 8) were applied for the synthesis. For the linker addition, basic conditions in anhydrous DMF were used. Even though sodium hydrate was better soluble in the solvent, potassium carbonate was the base of choice as test reactions revealed fewer side products monitored by TLC. Compounds **18** and **20** were dissolved in dry DMF and reacted with **25**. Compounds **26** and **27** were purified by silica gel column chromatography, isolated, and spectrally characterized. However, yields were low (Scheme 10). Milder conditions with extended reaction time and stirring at ambient temperature did not improve the yield, as shown in Table 2.

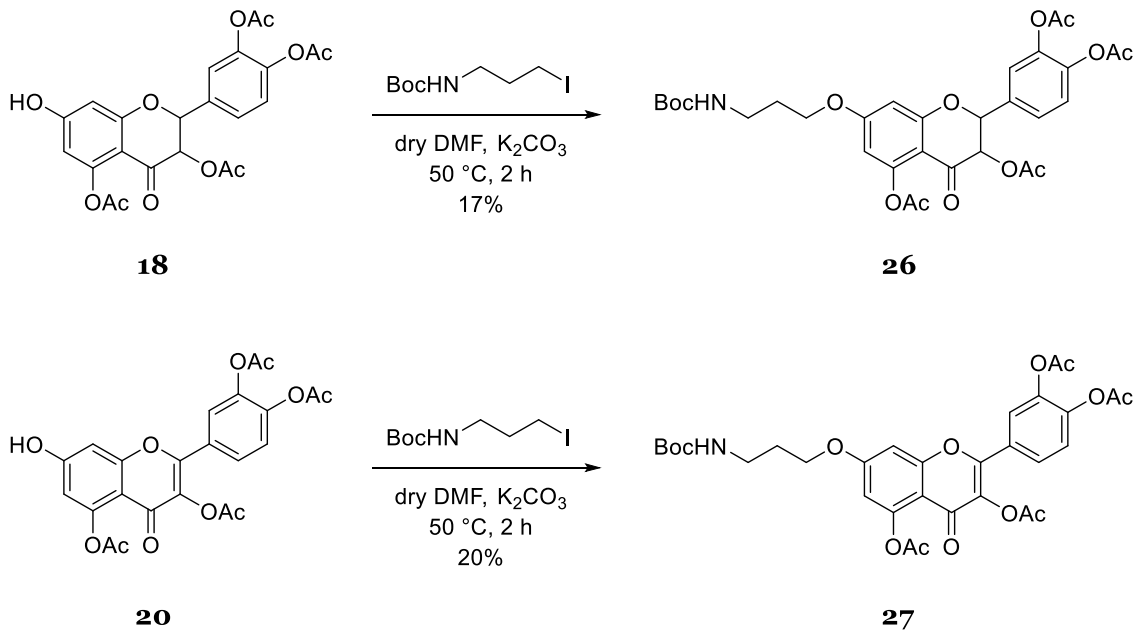

Scheme 10: Nucleophilic substitution to introduce the linker moiety in position 7 of the flavonoids.

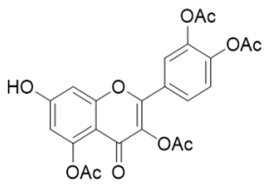

Educt **20**

Base	Reaction time	Temp.	yield
K_2CO_3	overnight	ambient	21%
NaH	overnight	ambient	17%
K_2CO_3	2 h	50 °C	20%

Table 2: Reaction conditions for the linker coupling with 7-*O*-deprotected quercetin.

Examining the multiple side products during the linker addition shown in Scheme 10, the apparent hindrance was the loss of the flavonoid's protective groups during the reaction. LC-MS analysis revealed a mixture of byproducts with different numbers of protective groups and mono- or dialkylated products. Table 3 gives an overview of the most abundant byproducts in the crude reaction mixture of the quercetin derivative.

Retention time	Area	*m/z* found	*m/z* calculated	Proposed corresponding structure *
11.4 min	25%	$[M+H]^+$ 429.10	428.07	Educt **20**
12.1 min	15%	$[M+H]^+$ 544.25	543.17	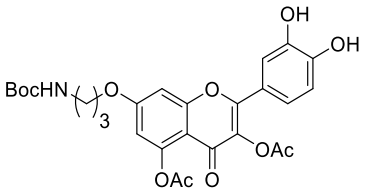
12.6 min	28%	$[M+Na]^+$ 650.50	627.20	Product **27**
13.2 min	13%	$[M+Na]^+$ 765.35	742.29	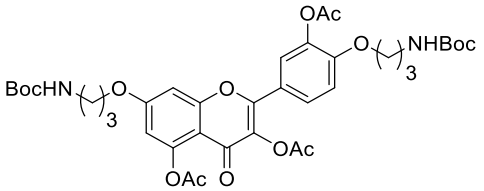

* exact position of the linker and/or acetyl groups was not assigned.

Table 3: LC-MS analysis of the linker coupling to compound **20**.

In the final step synthesizing the amine-functionalized flavonoids taxifolin and quercetin, all protective groups were removed under acidic conditions (Scheme 11). Purification turned out to be difficult due to the amine group in conjunction with the free hydroxyl groups. During extraction, compounds **28** and **29** remained in the aqueous phase, as either the hydroxyl groups were charged under basic conditions or the amine under acidic conditions. Purification using reversed-phase column chromatography led to strong interactions of the compounds with the column material. Compounds **28** and **29** could only be isolated with low yields.

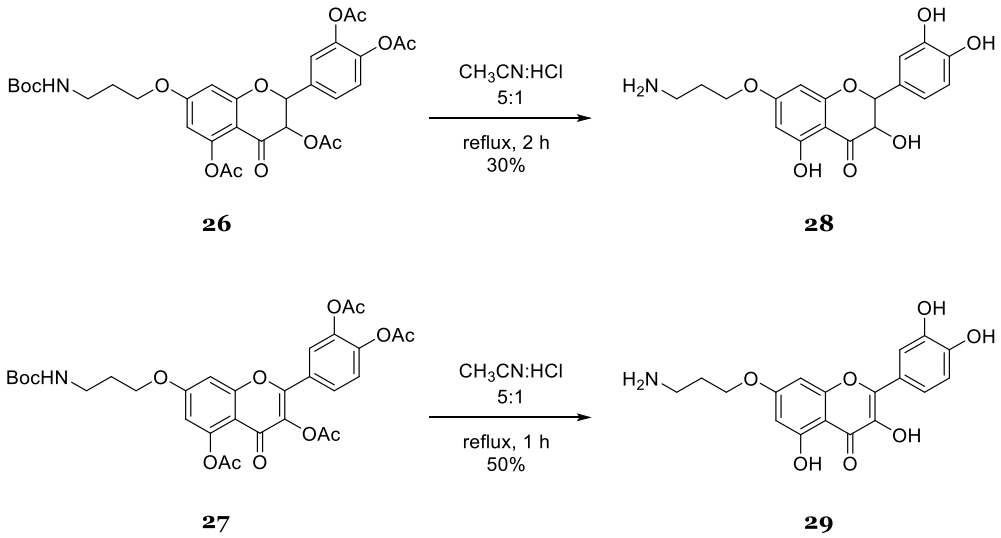

Scheme 11: Deprotection of **26** and **27** obtaining the derivatives of taxifolin **28** and quercetin **29** with a linker in position 7 bearing a free amine.

5.4 Synthetic Groundwork for Amide-Coupled Derivatives

The amine-functionalized compounds **28** and **29** can serve as precursors for different derivatives of taxifolin and quercetin. Via an amide bond, various moieties can be introduced with a more stable chemical connection. Taxifolin amides, with phenolic acids, for example (Fig. 27A), could be investigated in phenotypic screening assays to examine the influence of the ester bond and the presence of a linker on neuroprotective features in SARs.

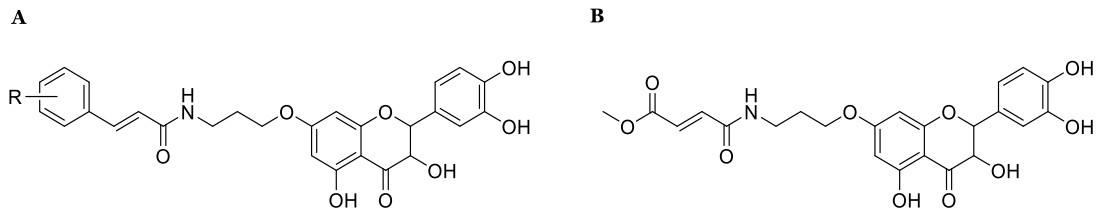

Figure 27: Example structures of compounds resulting from amine-functionalized flavonoids. The taxifolin core is generic. **A)** Amide coupled phenolic acids with R = hydroxy or methoxy groups, depending on the acid. **B)** Amide coupled MMF.

Another exciting group to attach was monomethylfumarate (MMF, Fig. 27B). Dimethyl fumarate, the prodrug of MMF, is an FDA-approved drug to treat relapsing forms of multiple sclerosis.[189] Among the mechanisms of action of MMF is the activation of the Nrf2 pathway to modulate inflammation and oxidative stress,[190] which both play pivotal roles in AD pathology. In the first approach, the direct regioselective

esterification with taxifolin was implemented. The purified product **30**, however, hydrolyzed within hours (Scheme 12), and TLC analysis observed complete degradation overnight. Therefore, the compound was not suitable for *in vitro* investigations. Coupling MMF via an amide bond might stabilize the compound and overcome accelerated hydrolysis (Scheme 12).

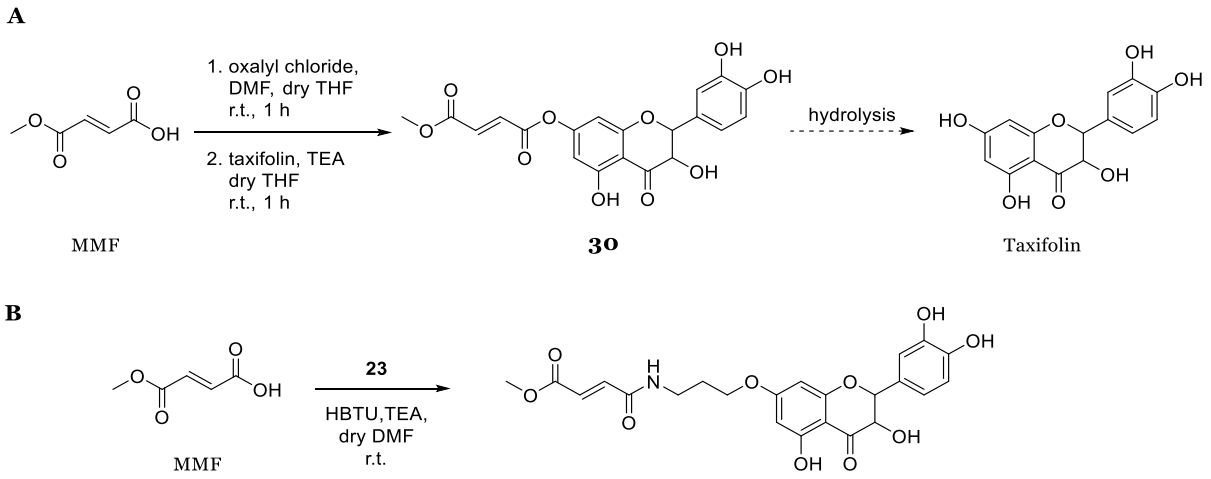

Scheme 12: A) Synthesis of the 7-*O*-ester of taxifolin and MMF **30**. The ester hydrolyzed, and within 24 h, accumulation of taxifolin was observed. Degradation products of MMF are not detectable on TLC and LC-MS. **B)** Synthesis proposal of MMF coupled to taxifolin via an amide linker.

Further, chemical probes were synthesized using the amine derivatives of taxifolin and quercetin. For the amide coupling, the compounds **28** for taxifolin and **29** for quercetin were reacted with 5-hexynoic acid and HBTU as coupling agent under basic conditions to give compound **31** and **32**, respectively (Scheme 13).

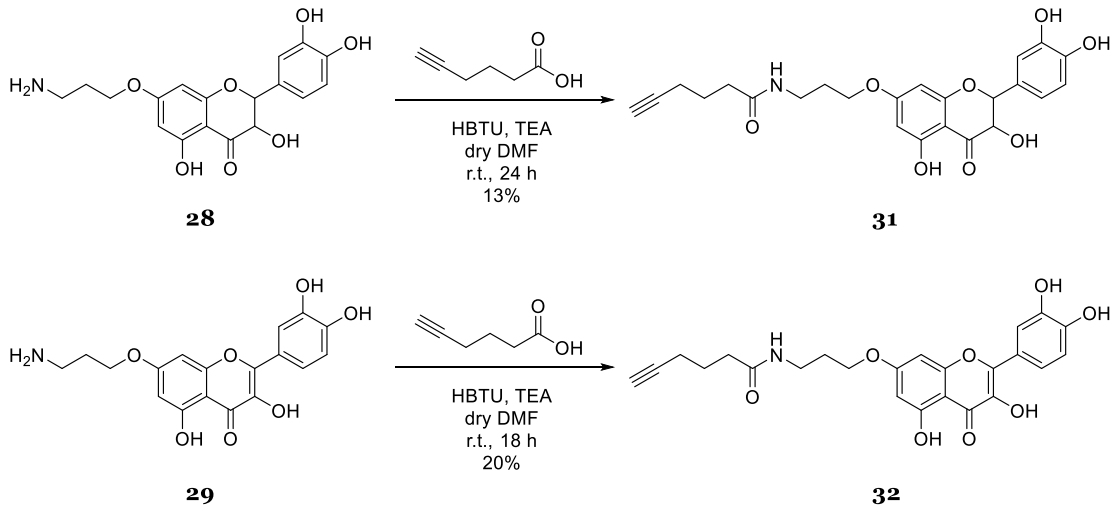

Scheme 13: Amide coupling to obtain compounds **31** and **32** based on taxifolin and quercetin, respectively.

5.5 Conclusion and Outlook

Within this work, essential intermediates for amide-coupled derivatives of taxifolin and quercetin have been synthesized. The synthetic route needs optimization towards work-up and purification methods to improve the yields. A robust synthesis is required as the amine-functionalized compounds **28** and **29** can serve as the basis for a variety of derivatization by introducing phenolic acids, MMF, or other moieties of interest for SARs and pleiotropic molecule design. An option would be to introduce protective groups more stable than acetyl groups. Benzyl and diphenylmethane protective groups, for example, could be used. The diphenyl-protection of quercetin's catechol moiety was successful in a test reaction using microwave-assistance, under conditions used for the reaction of fisetin to compound **15**. Further, treatment of **33** with benzyl bromide and potassium carbonate should give the 3-benzyl protected compound **34,** and presumably, the 3,7-dibenzyl protected derivate as a side product, which should be separated easily. The Boc-protected linker precursor could then be introduced selectively in position 7, and hydrogenation and an acidic workup would remove all protective groups. The suggested route in Scheme 14 for quercetin would also apply to taxifolin.

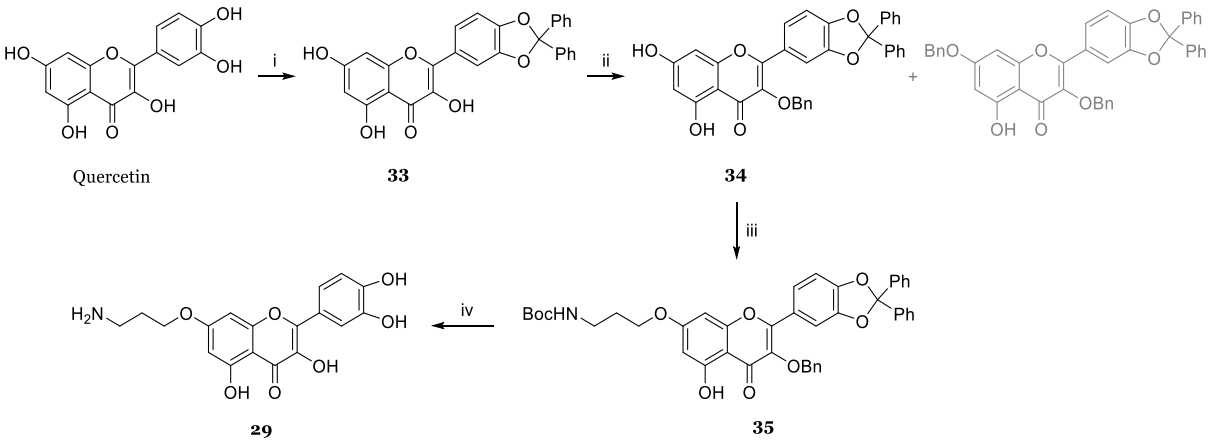

Scheme 14: Synthetic route proposal for aminated flavonoid derivatives using benzyl and diol protective groups. Reagents and conditions: i) dichlorodiphenylmethane, diphenyl ether, 180 °C. ii) BnBr, K_2CO_3, DMF, room temperature iii) **25**, K_2CO_3, DMF, 50 °C. iv) Pd/C, H_2, MeOH, room temperature.

Another approach would be the total synthesis of the flavonoids. According to a synthetic approach applied in our lab (Hofmann et al.),[191] the aminated acetophenone **39** and the aldehyde **41** would be reacted to the chalcone **43** (Scheme 15). Stirring **43** with hydrogen peroxide in methanol under basic conditions according Chiruta et al.[184]

followed by acidic workup should result in ring closure and deprotection and give the respective fisetin **44** or quercetin **45** derivative.

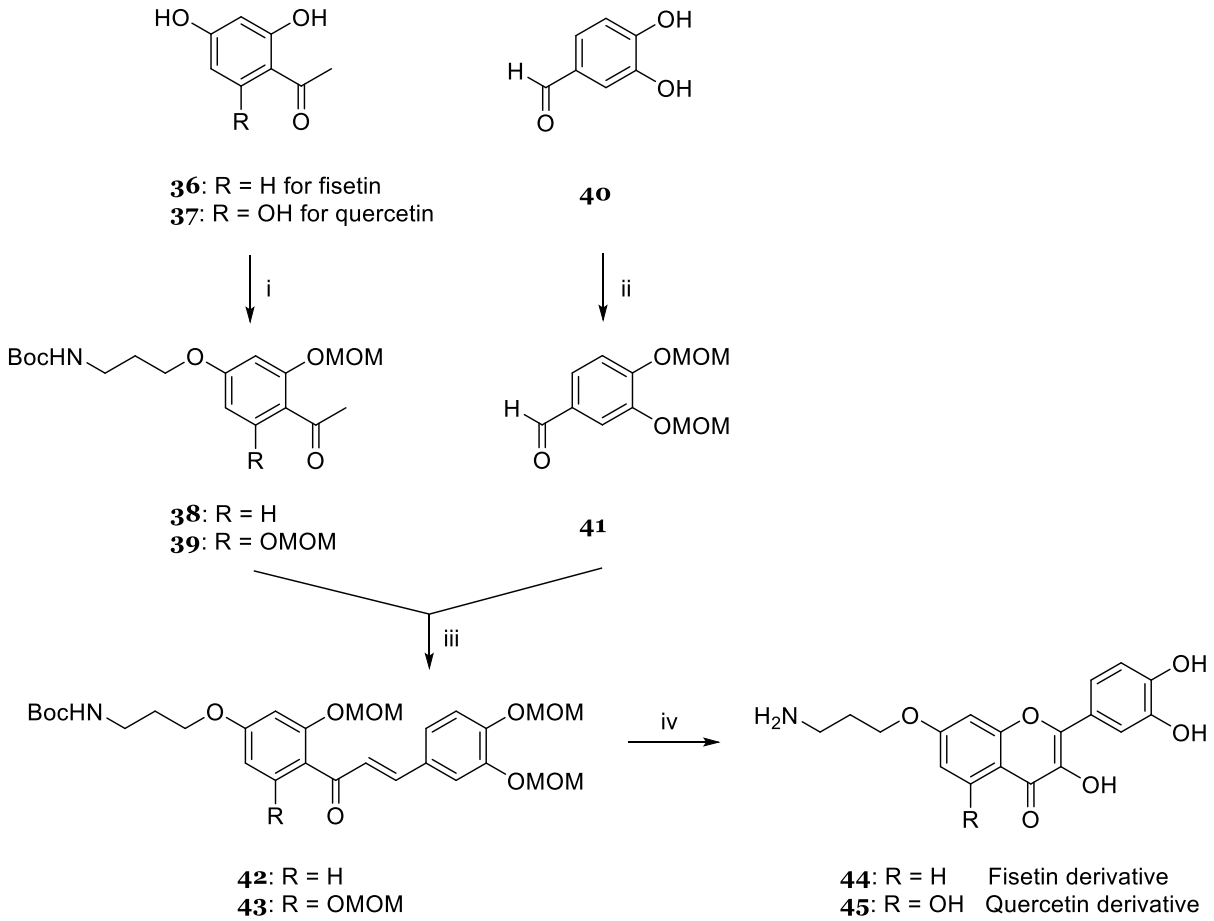

Scheme 15: Proposal for the total synthesis of amine derivates of flavonoids. Reagents and conditions: i) 1. **25**, K_2CO_3, DMF, 50 °C; 2. NaH, MOMCl, DMR, 0 °C to room temperature. ii) NaH, MOMCl, DMR, 0 °C to room temperature. iii) KOH, EtOH, 0 °C to room temperature. iv) 1. NaOH, 30% H_2O_2, MeOH, 0 °C to room temperature; 2. HCl, MeOH, room temperature.

For fisetin, the direct alkynylation was not successful as it was difficult to convert or fragile protective groups hampered the synthesis. The total synthesis of this compound could also be considered as proposed in Scheme 15. Starting from 2,4-dihydroxyacetophenone **36,** MOM-protection in step i is not needed as it was shown by Imai et al.[183] The alkyne linker would be connected to **44** via an amide bond. It needs to be investigated whether the amide moiety interferes with its use as a chemical probe.

6. A DHED-Based Carbamate as *h*BChE Inhibitor

The flavonoid hybrids described in chapters 3 and 4 are neuroprotective due to pleiotropic effects addressing several targets in parallel. However, neuroprotective effects *in vitro* and *in vivo* can also be induced by the targeted inhibition of the enzyme butyrylcholinesterase (BChE).[134, 192, 193] As outlined in the introduction, inhibition of AChE and BChE is an important therapeutic approach to treat AD. Alkaloids are a class of natural products that can serve as ChE inhibitors and have proven relevant to AD.[194] The FDA-approved drug galantamine, for example, is an alkaloid. The natural products dehydroevodiamine, evodiamine, and rutaecarpine are alkaloids and the main components of dried fruits of the medicinal plant *Evodia rutaecarpa (Juss.)* Bentham (Fig. 28). The source of the alkaloids is often stated as "Wu-Chu-Yu," which is the name of the dried fruits of *E. rutaecarpa*.[195] In traditional medicine, *E. rutaecarpa* extracts were used to treat various diseases and conditions like headache, dysmenorrhea, gastro-intestinal discomforts, and abdominal pain. Due to its pharmacological relevance and clinical use, the extract is listed in the Chinese Pharmacopeia 2015 Edition.[196]

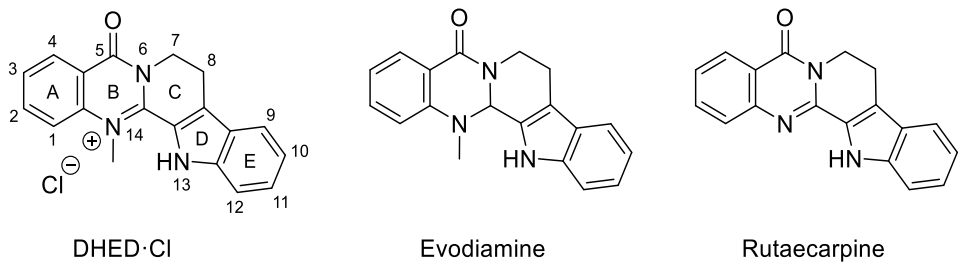

Figure 28: Structures of the alkaloids dehydroevodiamine, evodiamine, and rutaecarpine.

While research on rutaecarpine mainly focused on its benefits in cardiovascular diseases,[195, 196] evodiamine and DHED drew attention in neurodegenerative disorders. Evodiamine was found to significantly alleviate impairments of learning and memory *in vivo* in AD mouse models,[197] showed to be protective against oxidative stress in HT22 cells, and reduced levels of AChE in brains of AD mice.[198] DHED was first mentioned in the context of CNS-related activity in 1996 when Park et al.[199] screened 29 plants to find new compounds with antiamnesic effect. *E. rutaecarpa* was the most potent plant specimen in their amnesia model, and fractionation identified DHED as the active component. DHED was found to be a non-competitive dose-dependent inhibitor of AChE and was able to reverse scopolamine-induced amnesia in an *in vivo*

AD rat model. Further, DHED was shown to improve cognitive impairment and ameliorate learning and memory deficits in an AD rat model.[200] In a study by Wang et al.,[201] DHED also significantly improved $A\beta_{25-35}$-induced amnesia in mice additional to its cholinergic activity, supporting the compound as an exciting candidate for treatment against AD.

As mentioned before, cholinergic dysfunction is one characteristic of AD with increased levels of BChE, as the disease progresses.[87] Therefore, special emphasis was placed on selective BChE inhibitors.[202] Selective BChE inhibitors were previously designed and synthesized by implying evodiamine as a carrier scaffold for carbamates functioning as pseudo-irreversible inhibitors of cholinesterases. Huang et al.[203] revealed the heptyl carbamate of 5-deoxo-3-hydroxyevodiamine **46** as a very potent and highly selective BChE inhibitor with IC_{50} = 77 nM and a selectivity index of >130. Furthermore, the released hydroxyevodiamine derivate **47** after carbamate transfer served as a potent neuroprotectant against oxidative stress (Fig. 29).[203]

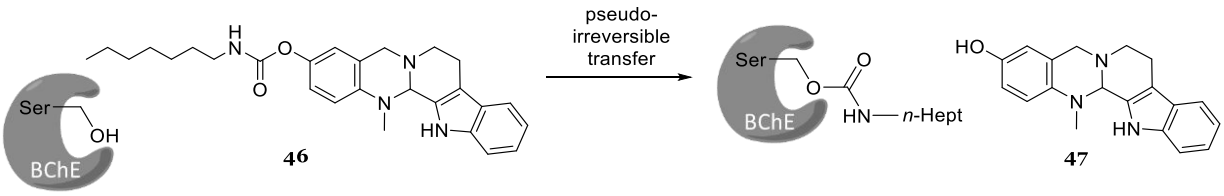

Figure 29: Mode of BChE inhibition by the heptyl carbamate **46**. After the transfer, the neuroprotectant **47** is released.[134]

DHED was shown to improve memory impairments related to AD.[200, 201] Furthermore, the alkaloid has an interesting characteristic of pH-dependent structural conformational changes. At acidic pH, the compound exists a water-soluble quaternary salt and at basic pH the ring open form exists, which is in an equilibrium with the uncharged hydroxy-form (Fig. 30). To utilize these features, the scope of this project was to synthesize the DHED-based heptyl carbamate **48** as a selective BChE inhibitor (Fig. 30). DHED was suitable as a carrier unit addressing cholinesterases as the compound showed to be a micromolar inhibitor of AChE and BChE with 6.3 µM and 8.4 µM, respectively.[204] Introduction of the heptyl carbamate was meant to lead towards selectivity for BChE and increase the inhibitory activity.[192]

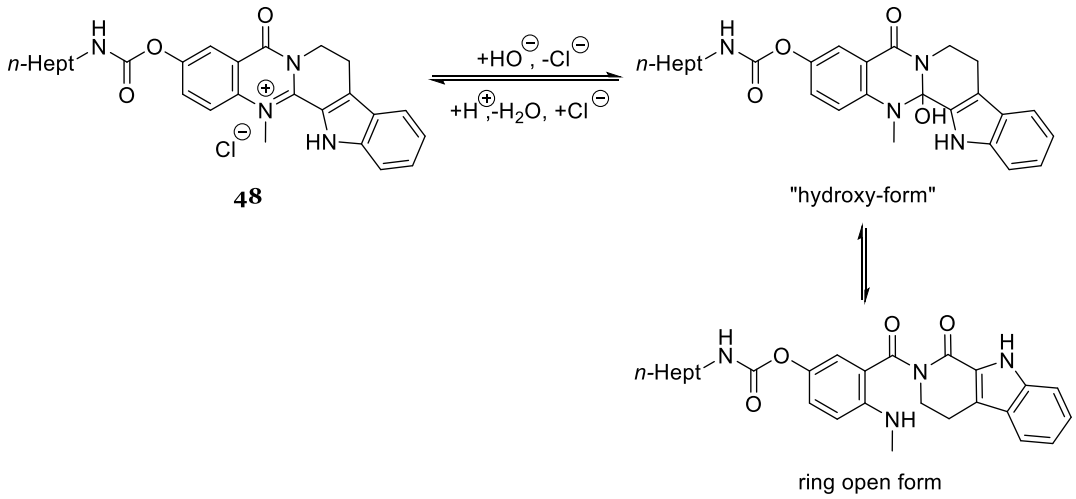

Figure 30: Structures of the target compound **48** and the pH-dependent structural changes towards the hydroxy-form, which is in equilibrium with the ring open form.[206]

6.1 Synthesis

While many reviews discussed the pharmacological profile of DHED and evaluated its biological activity, the literature on the synthesis of DHED was scarce. The most common method described to form the pentacyclic quinazolinium core was via condensation of the anthranilic ester **50** with an activated indolo lactam **49**.[204, 205] Phosphorus(V) oxychloride was used for the activation of the lactam moiety (Fig. 31).

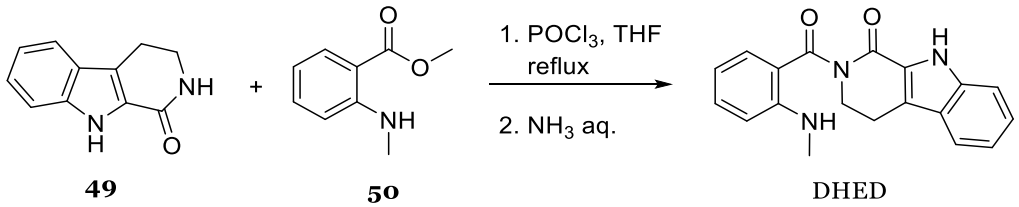

Figure 31: Condensation reaction of the pyrido indol derivate **49** with the anthranilic ester **50** for the synthesis of DHED as described by Nakayama et al.[205]

Alternative synthetic access to quinazolinium-salts of DHED with improved yields was described by Wehle et al.[206] In that approach, the *N*-methylated isatoic anhydride **51** was directly reacted with the pyrido indole **52** without the use of coupling reagents, resulting in evodiamine **53**, which was then oxidized to DHED (Fig. 32). This approach was also adapted for the synthesis of the DHED-heptyl carbamate derivative **48** within this work.

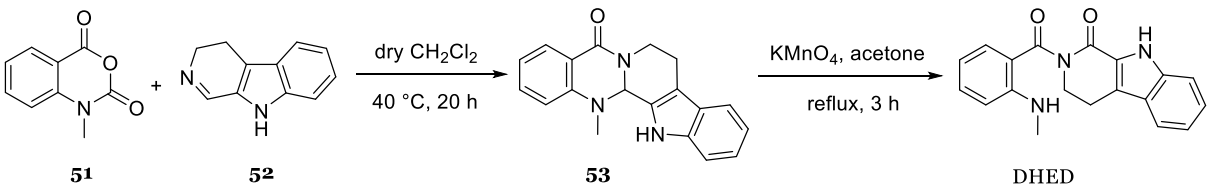

Figure 32: Alternative synthetic route for DHED by Wehle et al.[206] Compounds **51** and **52** were reacted without coupling reagent. Evodiamine **53** was then oxidized to DHED using potassium permanganate.

To introduce the carbamate in para-position to nitrogen 14, a hydroxyl group was needed in position 3 of the isatoic anhydride. The synthesis of the precursor **56** started from 3-methoxy anthranilic acid **54**. The anhydride **55** was formed using triphosgene in dry THF followed by *N*-methylation with methyl iodide to synthesize the isatoic anhydride precursor **56** according to previously described synthetic routes.[192, 207] For the pyrido indole precursor **52**, tryptamine **57** was reacted with ethyl formate to form the amide **58**. A cyclization reaction with phosphorus oxychloride gave compound **52**. The pyrido indole derivate **52** was coupled with the methylated isatoic anhydride **56** refluxing overnight in dichloromethane to give 3-methoxy evodiamine **59**. Oxidation of **59** to 3-methoxy DHED **60** required optimization of reaction conditions. Refluxing for 3 hours, as proposed by Wehle et al.,[206] led to 3-methoxy rutaecarpine as the main product. LC-MS analysis of the reaction revealed 70% demethylated product corresponding to 3-methoxy rutaecarpine, and only 22% of the desired compound. Studies to optimize conditions showed mild conditions stirring at room temperature

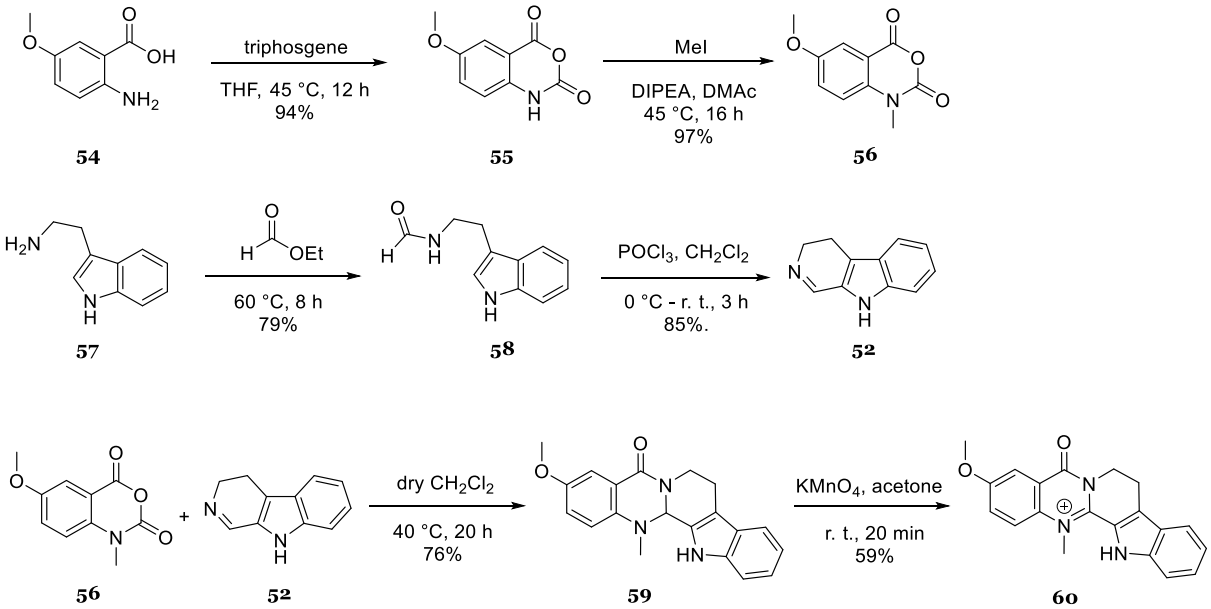

Scheme 16: Synthetic route applied for 3-methoxy DHED **60**.

for 20 minutes are sufficient to oxidize 3-methoxy evodiamine **59** to 3-methoxy DHED **60** (Scheme 16).

For the deprotection of **60**, 47% HBr in water was applied. Milder conditions using aluminum chloride failed to remove the methyl protective group, and the starting material was regained. After refluxing **60** overnight with hydrobromic acid, LC-MS analysis of the crude reaction mixture showed 70% HO-DHED **61**. However, purification of the product turned out to be challenging. Due to the pH-dependent conformational change of the DHED structure, basification of the aqueous phase should shift the equilibrium towards the ring open dicarbonyl form, transferring the compound to the organic layer. For HO-DHED **61**, however, basification also led to deprotonation of the hydroxyl group hampering extraction to the organic phase. Adequate purification was only possible using reversed phase column chromatography resulting in deficits in yield. Carbamoylation of HO-DHED **61** with heptyl isocyanate in dimethylformamide with triethylamine gave the target compound DHED heptyl carbamate **48** (Scheme 17).

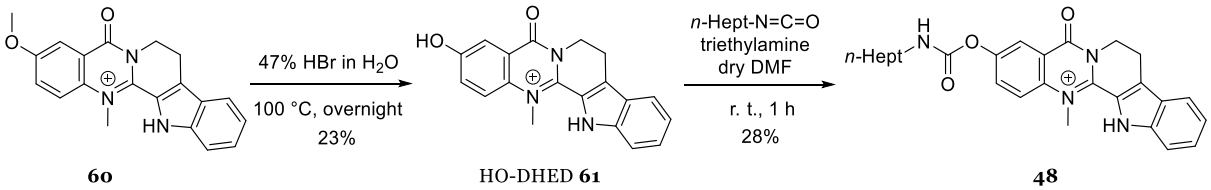

Scheme 17: Synthetic route for HO-DHED **61** and the target compound DHED heptyl carbamate **48**.

6.2 BChE Inhibition

Inhibition of human butyrylcholinesterase (*h*BChE) was assessed in the Ellman's assay.[208, 209] 5,5'-Dithiobis-(2-nitrobenzoic acid) (DTNB), *h*BChE, and the compounds to be tested were incubated for 20 minutes when the synthetic substrate butyrylthiocholine (BTC) was added. Generated thiols by enzymatic conversion reacted with DTNB in a color reaction and were quantified photometrically. DHED and the heptyl carbamate of 5-deoxo-3-hydroxyevodiamine (**46**) inhibited BChE in the low or even sub-micromolar range. As these compounds represent the lead structures, enzyme inhibition was examined with 1 µM of the DHED heptyl carbamate compound **48**. As the introduction of the heptyl carbamate moiety should increase inhibitory capacity at *h*BChE, HO-DHED **61** was assessed for comparison. After 20 minutes incubation of 1 µM **48** and **61**, 20% and 21% inhibition of *h*BChE, respectively, was

observed (Table 4), leading to two unexpected drawbacks. First, the activity of the compounds for enzyme inhibition was comparatively low, and second, no difference for the heptyl carbamate derivative **48** and HO-DHED **61** was observed. The incubation time of 20 minutes was applied as it proved to be the optimal period for complete carbamoylation of BChE.[193, 210] However, an unforeseen different binding mode might need adapted incubation times. Therefore, shorter and longer incubation times than 20 minutes were assessed the Ellman's assay to validate the results (Table 4). Inhibitory activity was determined from 4.5 minutes up to 4 hours, but neither increased activity nor a difference in inhibition capacity was observed at any time points for the heptyl carbamate derivative **48** and HO-DHED **61**.

Incubation time		4.5 min	10 min	15 min	20 min	2.5 h	4 h
% *h*BChE inhibition [1 µM] cpd.	**48**	14 %	25 %	23 %	21 %	40 %	50%
	61	9 %	19 %	18 %	20 %	-	-

Table 4: Results of the Ellman's assay with 1 µM DHED heptyl carbamate **48** and HO-DHED **61**.

6.3 Conclusion

Even though the heptyl-residue proved to be important in previous SARs with other tetracyclic carriers,[134, 203] the introduction of the heptyl carbamate did not improve the inhibitory capacity for DHED. This might be due to the core structure of DHED. In the study of Huang et al.[203] where evodiamine derivatives were investigated, selectivity and inhibition increased with the introduction of the heptyl carbamate only for 5-deoxo derivatives of evodiamine (**46**). Carbamoylation of hydroxy-evodiamine with a heptyl moiety did not alter or improve its effect on BChE. DHED, like evodiamine, bears a carbonyl in position 5, which might explain the lack of improvement of the DHED heptyl carbamate **48** as a selective inhibitor of BChE. To investigate this hypothesis, a 5-deoxo derivate of DHED would be needed. However, this compound is synthetically not accessible. Position 5 of DHED is oxidation sensitive, and the reduced form cannot exist, holding the characteristic oxidation in the B-ring necessary for DHEDs' pH-dependent conformational change.

In conclusion, introducing a heptyl carbamate did not improve DHED's features as a selective inhibitor of *h*BChE. For alkaloids, the absence of the 5-carbonyl moiety seemed to be the more relevant structural feature for enzyme inhibition.

7. Future Perspectives

7.1 Mitochondria as Site of Action

Mitochondrial dysfunction plays a crucial role in early-stage AD and aging, and mitochondria hold a pivotal role in neuronal survival. Due to the findings in microscopic analysis, where the Cy-3 labeled probe of 7-*O*-cinnamoyltaxifolin colocalized with mitochondria (Fig. 21, chapter 4), it might be of interest to further investigate mitochondria as drug targets and site of action for flavonoid-derivatives in AD.

Mitochondria provide an oxidative microenvironment that might influence the compounds' chemical structures, as flavonoids are redox-sensitive. In cellular uptake experiments, it was shown that 7-*O*-cinnamoyltaxifolin is metabolized to 7-*O*-cinnamoylquercetin (Fig. 13, chapter 3). The active metabolite for neuroprotection, however, was unknown. Identifying an active metabolite of 7-*O*-cinnamoyltaxifolin in a mitochondrial environment could be achieved by incubating the compound with isolated mitochondria. MS analysis of the supernatant could be used for the characterization of metabolites. Mitochondria can be isolated by differential centrifugation[211] or ultracentrifugation. Confirming that the isolated mitochondria are intact, cytochrome c should be determined using ELISA or the potential-sensitive fluorescent dye tetramethylrhodamine ethyl ester (TMRE) could be applied using a plate reader.

With the 3',4'-dihydroxy substituent pattern on the B-ring, taxifolin is prone to oxidization by free radicals in the mitochondrial environment. Therefore, taxifolin semiquinone and quinone metabolites would be expected upon incubating the compound with mitochondria (Fig. 33).

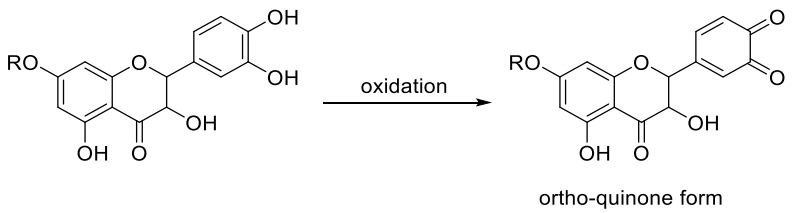

Figure 33: Oxidation of 7-*O*-taxifolin ester in mitochondria might result in quinone-formation in the B-ring.

These quinone-type metabolites may act as electrophiles and serve as Michael acceptors undergoing redox cycling and result in ROS-production. Therefore, high concentrations of the flavonoid could result in a cytotoxic pro-oxidant effect counteracting the compounds' initial use as an antioxidant. The concentrations used in this work, and intended to be used in future work, were in the low micromolar range, and the compounds showed no inherent toxicity in viability assays. More important, it might even be necessary for the flavonoids to be oxidized to quinones to exploit their full potential of action. In cancer therapeutics, for instance, Michael acceptors are gaining importance, and in 2016 Pierce et al.[212] even defined the "quinonome" as intracellular protein targets of quinone reactive intermediate electrophiles. In the context of AD, it has been shown that for taxifolin to interact with Aβ fibrils, the *o*-quinone form of the catechol moiety needed to be present to undergo the aza-Michael addition.[143] Further, the presence of quinones can be important to induce the Nrf2-dependent ARE gene expression, as it has been shown for the transcription factor BTB and CNC homology-1 (Bach1), one of the negative regulators of Nrf2.[162] Quinones suppress Bach1 and therefore activate Nrf2 and the expression of antioxidant enzymes, like HO-1.

Despite the potential structural changes of the compounds upon entering mitochondria, it has been shown that flavonoids can modify mitochondrial activity.[178] To investigate the role of 7-*O*-esters of taxifolin on mitochondrial function, several aspects should be considered and evaluated. Mitochondrial respiration and the mitochondrial membrane potential (MMP) are direct measures of mitochondrial function and can be assessed *in vitro*. Mitochondrial respiration can be determined by quantifying the oxygen consumption of mitochondria using a Clark type electrode or by plate-based fluorescence assays.[213, 214] Oxygen consumption can be measured in the presence or absence of compounds to investigate their influence on mitochondrial respiration. The MMP can be assessed using lipophilic cationic dyes, e.g., saphranine. Changes in absorbance due to the potential-dependent distribution of the dye in the intramitochondrial compartment and the external medium enables MMP calculation.[215] As discussed in chapter 4, it has been shown that mild MMP uncouplers were protective against oxytosis in HT22 cells.[177] Therefore, the effect of the flavonoid-derivatives on the MMP would be of interest to further elucidate their mode of action. Especially as ANT-1 was identified as a target for 7-*O*-cinnamoyltaxifolin (cf. chapter 4

and Appendix II), and plays an important role in the dissipation of the MMP as part of the mitochondrial permeability transition pore (mPTP).

7.2 ANT-1 as Target in Alzheimer's Disease

The mPTP plays a crucial role in apoptosis, as its opening leads to the collapse of mitochondrial integrity and is the point of no return for apoptotic cell death. Several phytochemicals, among them flavonoids, have shown to modify mPTP formation and are thereby neuroprotective.[216] While the role of mitochondria and the mPTP is well understood for apoptosis, its role in ferroptosis remains debatable.[217] ANT-1, a significant component of the mPTP on the inner mitochondrial membrane, was identified as a target of 7-*O*-cinnamoyltaxifolin. In apoptosis, increased oxidative damage led to ANT-1 upregulation.[218] In ferroptosis, its knockdown showed to be neuroprotective (Fig. 23, chapter 4). Hence, it needs to be investigated whether ANT-1 is upregulated in ferroptosis and if protective compounds counteract increased ANT-1 levels. Using an ANT-1 antibody for Western blot analysis of HT22 cells treated with RSL3 or erastin for ferroptotic insult would determine whether ANT-1 levels change during ferroptosis. Co-incubation with compounds of interest would give insights on a contingent direct effect of the compounds on ANT-1 levels. Next to 7CT and its components taxifolin and cinnamic acid, other neuroprotective flavonoids like fisetin and sterubin[181, 219] might be attractive candidates to investigate their influence on ANT-1.

If ANT-1 became crucial for ferroptosis, one could consider expanding its role in drug development approaches. As its knockdown was protective, it might be of interest to modify the flavonoid-hybrids towards more potent ANT-1 inhibition. Classical and robust inhibitors of ANT-1 are carboxyatractyloside (CATR), assumed to bind at the ADP binding site of ANT-1,[220] and bongkrekic acid (BKA), assumed to bind at the ATP site of the carrier.[221] Both compounds are natural products. BKA is secreted by the bacteria *Pseudomonas cocovenenans,* and the Mediterranean thistle *Atractylis gummifera* produces actractylosides like CATR. The chemical structures of BKA and CATR are very different (Fig. 34), and so are their chemical properties. BKA is a membrane-permeable polyunsaturated methoxy tricarboxylic acid polyketide, and CATR a membrane-impermeable diterpene glycoside.

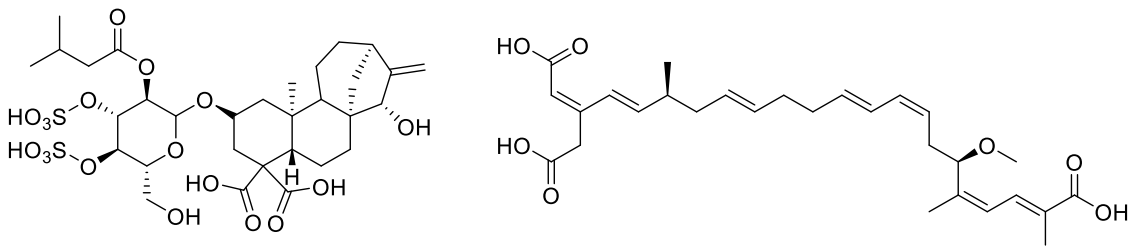

Figure 34: Chemical structures of the ANT-1 inhibitors carboxyatractyloside (CATR) and bongkrekic acid (BKA).

Both inhibitors could be included in a hybrid compound with flavonoids. According to Pebay-Peyroula et al.,[220] the diterpene moiety of CATR bound to the ADP binding site. It was stabilized by various hydrogen bonds, while the glucose moiety with the two sulfate groups was oriented towards the outside. The terminal methyl groups of the butanoic ester residue were important for van der Waals contacts between the inhibitor and the carrier.[220] Assuming that the flavonoid-core can form relevant hydrogen bonds with ANT-1, it might be interesting to introduce an isoalkane residue at the cinnamoyl moiety and investigate the neuroprotective features and ANT-1 inhibition capacity (Fig. 35).

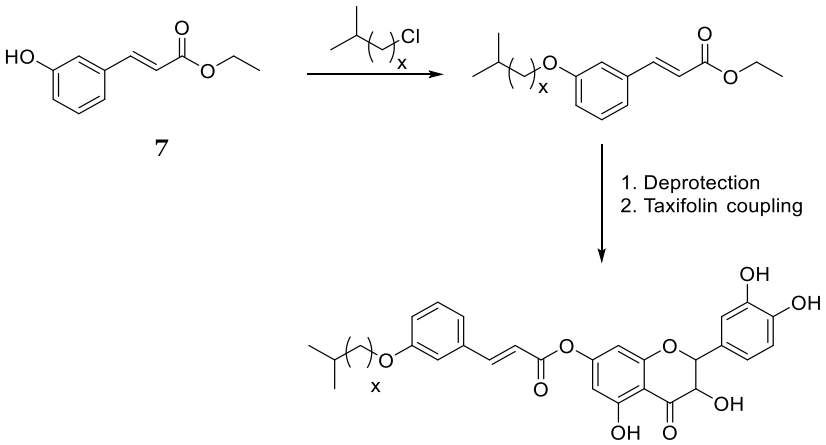

Figure 35: Introduction of an isoalkane residue to 7-*O*-cinnamoyltaxifolin. In a nucleophilic substitution, ethyl protected hydroxy-cinnamic acid (7) reacts with 1-chloro-2-methylpropane or other suitable isoalkanes for SARs. After deprotection, the flavonoid could be coupled as previously described.

With two possible binding sites described, site-directed mutagenesis could be applied to investigate the binding site of 7CT to ANT-1. Pebay-Peyroula et al.[220] proposed tyrosine 186 as an important interaction partner of CATR in the nucleotide-binding site in the c-state. In the m-state bound by BKA, the central substrate-binding site is

formed by the amino acids K30, R88, G192, I193, Y196, S238 and R287.[221] Mutating tyrosine to serine for example would revoke aromatic stacking. The role of the individual amino acids of the binding pockets could be investigated by changing to alanine. Systematic mutations in these regions and transfection of HT22 cells could give information about the binding site of the compounds, if changes in the assays are observed.

7.3 Further Proteins Identified with the Chemical Probe 7CT-Alkyne

Next to ANT-1, 69 other proteins were significantly enriched in MS analysis of pulldown fractions. The proteins identified by alignment with the UniProt mouse database were possible interaction partners and intracellular targets of 7-*O*-cinnamoyltaxifolin. Among the 70 most significant hits, Gene Ontology (GO) terms noticeably often held "nucleotide-binding" as a description of the molecular function of the proteins. Indeed, 12 of the 70 hit genes of the database encoded for proteins directly binding ATP (red in Fig. 36), another 5 were GTP-binding (blue), and a further 15 are DNA or RNA binding proteins (yellow, Fig. 36).

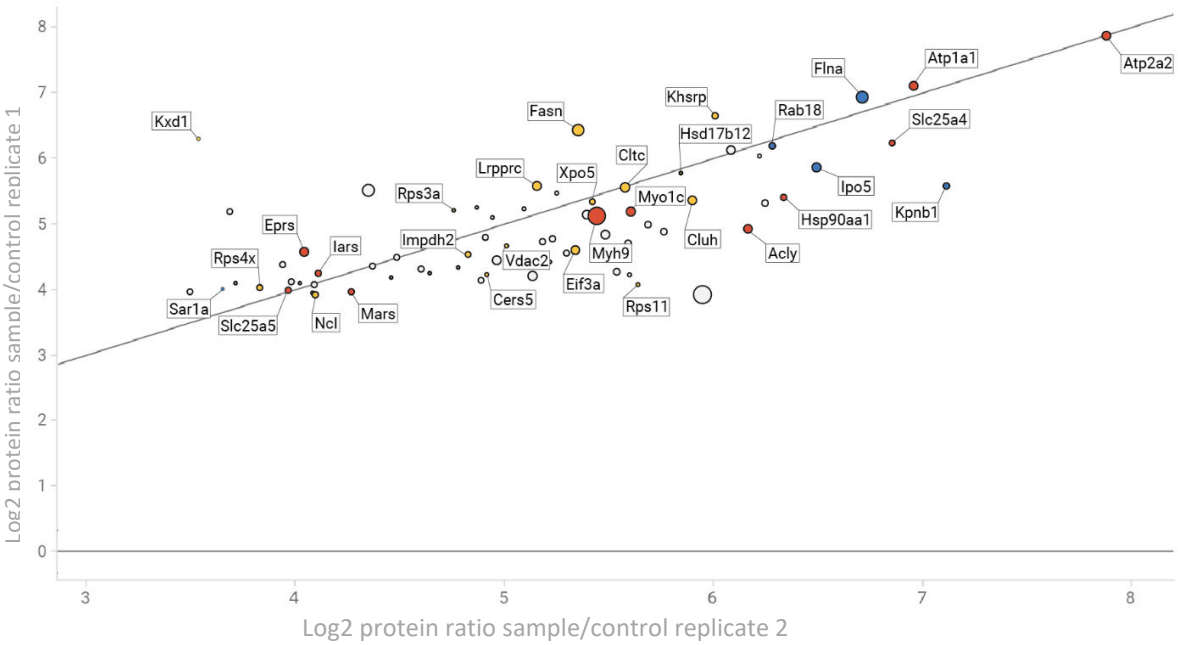

Figure 36: The 70 most significant proteins identified by MS-analysis are depicted. Tags show the gene name according to the UniProt mouse database. Red dots correspond to ATP-binding proteins, blue dots to GTP-binding proteins, and yellow corresponds to proteins binding DNA or RNA.

It has been shown before that flavonoids can interact with ATP binding sites of proteins. For example, quercetin and apigenin showed to bind the ATP binding site of p-glycoprotein.[222] In the ABPP experiment, heat-shock protein 90 α (Hsp90α, Hsp90aa1 in Fig. 36) was among the ten most significant targets identified by MS analysis. Hsp90 holds an ATP binding site and is vital for cell protein homeostasis. As a chaperone, Hsp90 modulates the proper folding of nascent proteins and assists in either refolding of misfolded proteins or ensures their degradation.[223] As the hallmarks of AD are defective protein accumulation of Aβ and tau, it seems reasonable to investigate Hsp90 as a pharmacological target for a neuroprotective effect.

The inhibition of Hsp90 leads to degradation of Hsp90-dependent kinases like glycogen synthase kinase 3 β (GSK3β) and Akt, contributing to tau hyperphosphorylation.[224] Hsp90 inhibition has two beneficial aspects: First, adverse kinases like GSK3β and Akt are diminished, and second, a prosurvival heat shock response is induced.[224] The natural products Epigallocatechin-3-gallate (EGCG) and silibinin have been shown to inhibit Hsp90 and modulate protein degradation.[225] EGCG binds to the C-terminal domain of Hsp90, which also holds an ATP binding site.[226] To investigate the direct interaction of 7-*O*-cinnamoyltaxifolin co-immunoprecipitation of the pulldown with an Hsp90-α antibody could be done. Interestingly, co-IP with an antibody for the Hsp90-β isoform did not give a signal as it has been shown for xanthohumol in a similar target identification approach by Brodziak-Jarosz et al.[227] Xanthohumol is a natural product present in hops bearing a Michael system. Hence, the mechanism of action of 7CT seems to exceed an interaction solely based on electrophilic addition due to the Michael system. To examine whether 7CT binds to the ATP binding site for Hsp90 inhibition, a fluorescence polarization assay could be used.[228]

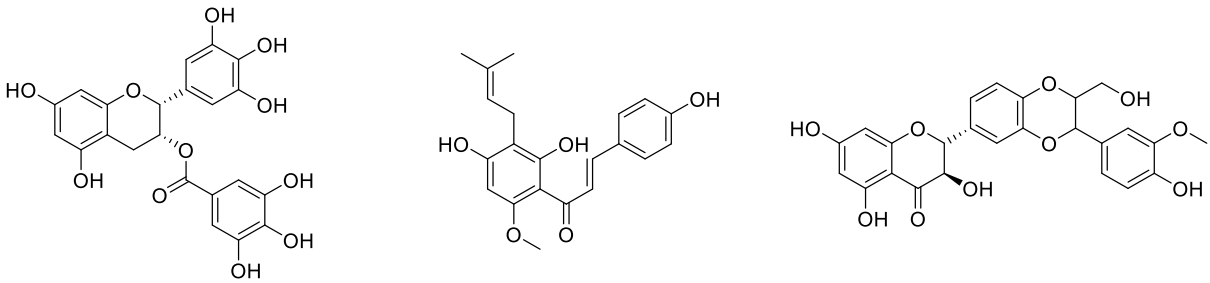

Figure 37: Chemical structures of EGCG, silibinin, and xanthohumol.

Another valuable approach to investigate binding or interaction sites of compounds with distinct protein targets are *in silico* studies. A computational modeling study with silibinin showed the inhibition of Hsp90 at the C-terminal domain overlapping with the binding pocket of the Hsp90 inhibitor novobiocin.[229] Due to the structural similarity between silibinin and 7CT, it would be interesting to perform molecular docking, exploring whether 7CT shows preferences for the nucleotide-binding site or the novobiocin/silibinin binding site of Hsp90.

Other proteins of the list of identified targets might be suitable for docking experiments as well. The crystal structure for SERCA and Heme oxygenase-2 (HO-2), for example, were resolved and could be used in a docking or molecular dynamic (MD) simulation to identify the binding mode of the compound in the enzyme.[230, 231] Especially for SERCA, it would again be interesting to see whether 7CT binds to the nucleotide-binding pocket. The feasibility of *in silico* experiments might be limited due to the subpar resolution of the crystal structure or complex protein dynamics. ANT-1, for example, is a highly dynamic protein hampering molecular docking experiments. Nevertheless, *in silico* studies hold immense value in the elucidation of potential binding sites of flavonoids at proteins identified as potential targets for therapeutic approaches in AD.

8. Summary

Alzheimer's disease is the most common form of dementia, and currently, there is no treatment to cure or halt disease progression. As life expectancy increases and age is the major risk factor for disease development, the number of affected people will increase. Given the severity of the global situation, it is of urgent need that science engages with AD and neurodegeneration to deepen the understanding of cellular processes in disease progression and to identify new approaches for pharmacological intervention.

Because the one-target strategy focusing on amyloid-β has failed to generate successful pharmaceutical treatment for AD, this work studies natural products with pleiotropic effects focusing on oxidative stress and neuroinflammation as key drivers of disease progression.

The central part of this work focused on flavonoids as neuroprotectants. Flavonoids are a class of secondary plant metabolites and, as polyphenolic compounds, inherent antioxidants. Further, flavonoids have been shown to modify intracellular pathways relevant for neuroprotection. 7-*O*-Esters of taxifolin and cinnamic or ferulic acid were synthesized and investigated towards their neuroprotective potential in cell-based phenotypic screening assays addressing relevant pathways in aging and disease (chapter 3). 7-*O*-Feruloyl- and 7-*O*-cinnamoyltaxifolin showed overadditive effects in oxidative stress-induced assays in the mouse hippocampal neuronal cell line HT22 and proved to be protective against neuroinflammation in microglial BV-2 cells. Specifically, the individual components of the ester and their equimolar mixture were not protective at the tested concentrations in any assay, whereas the esterified compounds showed pronounced neuroprotective activity. The overadditive effect translated to animals using an $A\beta_{25-35}$-induced memory-impaired AD mouse model where the compound was able to ameliorate short-term memory defects. While the disease-modifying effects *in vivo* were observed, the detailed mechanisms of action and intracellular targets of the compounds remained unclear. Hence, a chemical probe of the neuroprotective flavonoid ester 7-*O*-cinnamoyltaxifolin was developed and applied in an activity-based protein profiling approach (chapter 4). The probe was validated in cell-based assays and Western blot analyses. MS analysis of the pulldown fraction identified and quantified a total of 708 proteins. Seventy of the identified proteins were significantly enriched, of which two proteins, SERCA and ANT-1, were

further investigated. SERCA was the top target specified in the analysis, and ANT-1 was the top mitochondrial target, which was of interest as microscopic examination showed localization of the probe in mitochondria. Validation experiments with siRNA suggested that 7-*O*-cinnamoyltaxifolin could act as a mild uncoupler of the mitochondrial membrane potential and inhibitor of ANT-1 and that SERCA plays a vital role in the protective mechanism of the compound.

To broaden the set of flavonoid-based compounds, chemical modifications on the flavonoids taxifolin, quercetin, and fisetin were performed (chapter 5). Chemical probes of taxifolin and quercetin were designed and synthesized, and the synthetic groundwork for amide-functionalized derivatives was accomplished by replacing the ester bond with an amine linker. Amide-coupling of, for example, phenolic acids allows to investigate the role of the ester bond in the compounds overadditive effect and enables the establishment of a new class of amide-based flavonoid hybrids.

A further part of this work focused on the cholinergic hypothesis, which is an important consideration regarding AD and its treatment, as three of four currently approved drugs are AChE inhibitors. With BChE gaining importance as a pharmacological target in AD, the biologically active alkaloid DHED should be optimized as a selective BChE inhibitor (chapter 6). To improve the inhibitory activity at the enzyme and increase the selectivity towards BChE over AChE, a heptyl-carbamate was introduced, which proved to be essential for inhibition and selectivity in previous SARs.[134, 203] The introduction of a heptyl carbamate, however, did not improve DHED as a selective inhibitor of *h*BChE. For alkaloids, the absence of the 5-carbonyl moiety seemed to be the more relevant structural feature for enzyme inhibition, as it was shown for evodiamine and 5-deoxo-evodiamine derivates.[203]

The achievements of this work are an important contribution to the use of secondary plant metabolites as neuroprotectants. Chemical modifications increased the neuroprotective effect of the natural products, and distinct intracellular pathways involved in the neuroprotective mechanisms were identified. The beneficial pleiotropic effects of secondary plant metabolites are not exploited as a treatment for complex neurodegenerative diseases, like AD. The results of this work support the use of secondary plant metabolites as potential therapeutics and hint towards new pharmacological targets for the treatment of AD and other neurodegenerative disorders.

9. Zusammenfassung

Morbus Alzheimer ist die häufigste Form der Demenz und derzeit unheilbar. Die therapeutischen Möglichkeiten beschränken sich auf die symptomatische Behandlung der Krankheit und ihrer Folgeerscheinungen. Da sich mit steigendem Alter das Risiko an Alzheimer zu erkranken stark erhöht, wird mit dem demografischen Wandel unserer Gesellschaft auch die Anzahl der betroffenen Personen dramatisch zunehmen. Angesichts des zu erwartenden Anstiegs an Patienten und der fehlenden Behandlungsmöglichkeiten, ist es unabdingbar, dass sich die Wissenschaft intensiver mit Morbus Alzheimer beschäftigt. Durch Ursachenforschung und detailliertem Verständnis der molekularen Mechanismen müssen neue therapeutische Ansätze hervorgebracht werden, um die Krankheit zu heilen.

Der bisherige Fokus der Medikamentenforschung lag auf der Behebung von Aggregationen des Amyloidproteins, einem Hauptmerkmal und Kennzeichen von Morbus Alzheimer. Diese eindimensionale Strategie konnte nicht zu einer erfolgreichen Therapie führen, da hierbei die Komplexität der Krankheit vernachlässigt wurde. Daher sollten andere Forschungsansätze verfolgt und gefördert werden. Diese Arbeit rückt oxidativen Stress und Neuroinflammation als Schlüsselrollen für den Fortschritt der Krankheit in den Mittelpunkt und untersucht Naturstoffe mit pleiotropischer Wirkung, die diesen Pathologien entgegengesetzt werden können.

Der Großteil der Arbeit beschäftigt sich mit Flavonoiden, einer Substanzklasse der Sekundärmetaboliten von Pflanzen, die als Neuroprotektiva eingesetzt werden sollen. Flavonoide waren von Interesse, da sie aufgrund ihrer polyphenolischen Strukturen Antioxidantien sind und darüber hinaus neuroprotektive Eigenschaften aufweisen.

Das Flavonoid Taxifolin wurde selektiv in Position 7 mit den Phenolsäurederivaten Ferula- und Zimtsäure verestert und die Substanzen wurden hinsichtlich ihrer neuroprotektiven Eigenschaften untersucht (Kapitel 3). Hierzu wurde ein sogenanntes phänotypisches Screening durchgeführt. Die Effektivität der Substanzen wurde in verschiedenen Assays mit neuronalen Zelllinien analysiert, wobei die Zellmodelle das Krankheitsbild oder zellphysiologische Prozesse des Alterns abbildeten. Diverse Formen von oxidativem Stress wurden in der hippocampalen Mauszelllinie HT22

analysiert und Untersuchungen neuronaler Entzündungsprozesse wurden an der murinen Mikroglia Zelllinie BV-2 durchgeführt.

Die Zimt- und Ferulasäureester von Taxifolin zeigten überadditive protektive Wirkung in allen Tests. Das bedeutet, dass die einzelnen Komponenten der Esterverbindungen sowie deren äquimolare Mischung in den getesteten Konzentrationen keine protektive Wirkung aufwiesen, während die Ester selbst die Zellen vor den induzierten Schäden schützen konnten. Die überadditive Wirkung der synthetisierten Substanzen ließ sich auch auf ein Tiermodell übertragen. In einem Alzheimer Mausmodell konnten Beeinträchtigungen des Kurzzeitgedächtnisses aufgrund von Amyloid-Ablagerungen im Gehirn durch die Verabreichung der Taxifolin-Zimtsäure- und -Ferulasäureester behoben werden. Obwohl ein krankheitsmodifizierender Effekt *in vivo* beobachtet werden konnte, sind die molekularen Mechanismen der Wirkung und die intrazellulären Zielstrukturen der Substanz weitgehend unbekannt. Um dieses Problem zu adressieren, wurde eine chemische Sonde des Taxifolin-Zimtsäureesters entwickelt und synthetisiert, um Interaktionen der Substanz mit intrazellulären Proteinen mittels der sogenannten Activity Based Protein Profiling Methode aufzuklären (Kapitel 4). Die Sonde wurde in zellbasierten Tests und Western Blot Untersuchungen validiert und die Pulldown-Fraktion nach der Inkubation der Sonde mit Zellen massenspektrometrisch analysiert. In der MS Analyse wurden insgesamt 708 Proteine quantifiziert von denen 70 Proteine signifikant angereichert waren. Zwei der 70 Proteine wurde genauer untersucht: SERCA, welches in der MS Analyse die höchste Signifikanz aufwies, und ANT-1, das relevanteste mitochondriale Protein der Analyse. Letzteres war von besonderem Interesse, da mikroskopische Untersuchungen eine Lokalisierung der Substanz in den Mitochondrien von Zellen zeigten. Für die Validierung der beiden Proteine als Interaktionspartner des Taxifolin-Zimtsäureesters wurden knockdown Experimente mit siRNA durchgeführt. Im Zusammenhang mit ANT-1 konnten Hinweise gefunden werden, dass die Substanzen als mitochondriale Entkoppler und Inhibitoren von ANT-1 wirken könnten. Studien zu SERCA zeigten, dass das Protein eine wichtige Rolle für den protektiven Wirkmechanismus des Esters spielt.

Um Flavonoid-basierte Substanzen weiterzuentwickeln wurden im Rahmen dieser Arbeit verschiedene chemische Modifikationen an den Flavonoiden Taxifolin, Quercetin und Fisetin durchgeführt (Kapitel 5). Chemische Sonden von Taxifolin und Quercetin wurden entwickelt und dargestellt um die intrazellulären Mechanismen

dieser Substanzklasse weiter zu untersuchen. Um die Rolle der Esterbindung für die überadditive Wirkung genauer zu untersuchen, wurde die Esterbindung durch einen Amin Linker ersetzt. Diesen Verbindungen bilden außerdem durch die eingeführte Aminogruppe die Grundlage für eine neue Serie an Amid-gekoppelten Hybriden.

Ein weiterer Teil der Arbeit befasste sich mit der cholinergen Hypothese für die Entstehung von Alzheimer und den daraus resultierenden pharmakologischen Ansätzen der Therapie. Diese Hypothese stellte sich als vielversprechend für die symptomatische Behandlung von Morbus Alzheimer heraus, da vier der fünf verfügbaren Medikamente AChE Inhibitoren sind. Da dem Enzym BChE zunehmend mehr Bedeutung als therapeutischer Ansatzpunkt zukommt, war das Ziel dieser Arbeit mittels chemischer Modifikationen die inhibitorischen Eigenschaften des Alkaloids DHED an der BChE zu verbessern (Kapitel 6). Um die Inhibitionswirkung an der BChE zu erhöhen und gleichzeitig die Selektivität gegenüber der AChE zu steigern, wurde ein Heptylcarbamat an der Substanz Hydroxy-DHED eingeführt. In Struktur-Aktivitäts-Studien mit anderen Alkaloiden erwies sich die Heptylcarbamat-Gruppe als erfolgsbringend um die beiden Anforderungen zu erfüllen.[134, 203] Für DHED allerdings konnte die selektive Inhibition durch das Heptylcarbamat nicht verbessert werden. Stattdessen scheint das Modifizieren anderer Positionen der Verbindung effizienter zu sein. So führte beispielsweise das Entfernen der 5-Carbonylgruppe in einer Studie mit dem strukturell sehr nah verwandten Alkaloid Evodiamin zu einer deutlichen Verbesserung der Inhibition.[203]

Die Erkenntnisse dieser Arbeit leisten einen wichtigen Beitrag zu der Verwendung von pflanzlichen Sekundärmetaboliten als Substanzen mit neuroprotektiven Eigenschaften. Gezielte chemische Veränderungen konnten die Effektivität erhöhen und es konnten Signalwege und bestimmte Proteine identifiziert werden, die mit den Verbindungen und deren Wirkung in Zusammenhang stehen. Das Potential von Naturstoffen als Behandlungsmöglichkeit von Alzheimer und anderen neurodegenerativen Erkrankungen wird derzeit nicht ausgeschöpft. Die Ergebnisse dieser Arbeit unterstützen die Entwicklung naturstoffbasierter Therapeutika, die dringend benötigt werden, um neue Strategien für die Behandlung komplexer multifaktorieller Krankheiten wie Alzheimer hervorzubringen.

10. Experimental Section

General information. All reagents were used without further purification and purchased from common commercial suppliers in reagent grade. For anhydrous reaction conditions, tetrahydrofuran (THF) was distilled from sodium slices, and dichloromethane (CHCl2) was distilled from CaH_2 under an argon atmosphere. Thin-layer chromatography (TLC) was performed on silica gel 60 alumina foils with fluorescent indicator 254nm (Macherey Nagel GmbH & Co. KG, Düren, Germany). UV light (254 and 366 nm) was used for detection. For column chromatography, silica gel 60 (particle size 0.040–0.063 mm from VWR chemicals, Leuven, Belgium) was used. Nuclear magnetic resonance (NMR) spectra were recorded with a Bruker AV-400 NMR instrument (Bruker, Karlsruhe, Germany) in a deuterated solvent. Chemical shifts are expressed in ppm relative to the solvent applied (2.50 ppm for 1H and 39.5 ppm for 13C in DMSO-d6; 7.26 ppm for 1H and 77.2 ppm for 13C for $CDCl_3$; 2.05 ppm for 1H and 206.3 ppm for 13C for acetone-d6; 4.87 ppm for 1H and 49.0 ppm for 13C for MeOD). Abbreviation for data quoted are s – singlet; d – doublet; t – triplet; quart – quartet; quint – quintet; dd – doublet of doublets; dt – doublet of triplets; m - multiplet. The purity of the synthesis products was determined by HPLC (Shimadzu Products), containing a DGU-20A3R degassing unit, an LC20AB liquid chromatograph, and an SPD-20A UV/vis detector. UV detection was measured at 254nm. Mass spectra were obtained by an LCMS 2020 (Shimadzu Products). As a stationary phase, a Synergi 4U fusion-RP (150 mm × 4.6 mm) column was used, and as a mobile phase, a gradient of methanol/water with 0.1% formic acid. Parameters: A = water, B = methanol, V(B)/(V(A)+ V(B)) = from 5% to 90% over 10 min, V(B)/(V(A)+V(B)) = 90% for 5 min, V(B)/(V(A) + V(B)) = from 90% to 5% over 3 min. The method was performed with a flow rate of 1.0 mL/min. Compounds were only used for biological evaluation if the purity was ≥95%. Melting points were determined using an OptiMelt automated melting point system (Scientific Instruments GmbH, Gilching, Germany). Microwave assisted synthesis was performed on a MLS-rotaPREP instrument (Milestone, Leutkirch, Germany) using 8-10 Teflon disks.

10.1 Chemical Synthesis

4-(3,7-Diacetoxy-4-oxo-4*H*-chromen-2-yl)-1,2-phenylene diacetate (12)

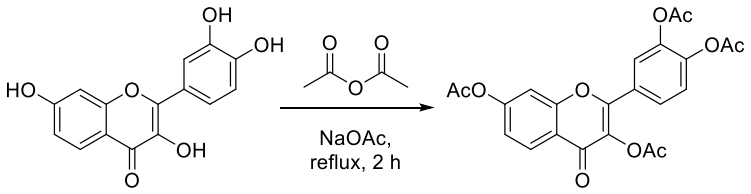

Fisetin (1.00 g, 3.49 mmol, 1.0 equiv.) was suspended in 10 mL acetic anhydride (10.70 g, 100.00 mmol, 30.0 equiv.), sodium acetate (0.57 g, 6.98 mmol, 2.0 equiv.) was added. The solution was heated to reflux, and after 2 hours, a white precipitate formed. The precipitate was filtered off and washed with cold water giving compound **12** as white solid (1.59 g, 3.50 mmol, quantitative).

^{1}H NMR (400 MHz, DMSO-d6) δ 8.13 (d, *J* = 8.7 Hz, 1H), 7.89-7.87 (m, 2H), 7.71 (d, *J* = 2.1 Hz, 1H), 7.54-7.52 (m, 1H), 7.37 (dd, *J* = 8.6 and 2.1 Hz, 1H), 2.35-2.33 (m, 12H) ppm. ^{13}C NMR (101 MHz, DMSO-d6) δ 170.6, 168.6, 168.2, 168.0, 167.8, 155.5, 154.9, 154.2, 146.2, 144.4, 142.2, 127.7, 127.5, 126.7, 126.5, 124.5, 123.8, 120.6, 111.9, 20.9, 20.4, 20.3, 20.2 ppm. ESI-MS: *m/z* calc. for C23H18O10 $[M+H]^+$ 454.09, found $[M+H]^+$ 455.15.

4-(3-Acetoxy-7-hydroxy-4-oxo-4*H*-chromen-2-yl)-1,2-phenylene diacetate (13):

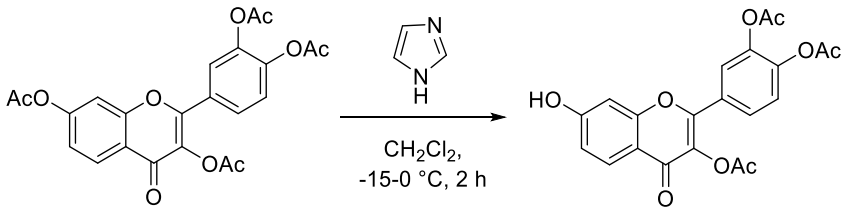

Compound **12** (1.14 g, 2.53 mmol, 1.0 equiv.) was dissolved in dry dichloromethane and cooled to -15 °C in an ice/acetone bath. Imidazole (344 mg, 5.10 mmol, 2.0 equiv.) was dissolved in dry dichloromethane and was added dropwise to the compound solution in the cold. The solution was warmed to room temperature and stirred for 2 hours when the reaction was diluted with dichloromethane and extracted with 1 M HCl. The organic layers were combined, washed with brine, dried over sodium sulfate, and the solvent was evaporated. Flash column chromatography using a gradient of acetone

in dichloromethane (5-30% in 30 mins, 30-100% in 5 mins) gave the compound **13** as yellow solid (511 mg, 1.24 mmol, 49% yield).

^{1}H NMR (400 MHz, DMSO-d6) δ 10.96 (s, 1H), 7.94-7.92 (m, 1H), 7.84-7.82 (m, 2H), 7.52 (d, *J* = 8.2 Hz, 1H), 7.00-6.98 (m, 2H), 2.33 (m, 6H), 2.31 (s, 3H) ppm. ^{13}C NMR (101 MHz, DMSO-d6) δ 170.3, 168.2, 168.0, 167.9, 163.4, 156.9, 153.1, 144.1, 142.1, 132.8, 127.8, 126.8, 126.5, 124.4, 123.6, 115.7, 115.5, 102.5, 20.4, 20.3, 20.2 ppm. ESI-MS: *m/z* calc. for C21H16O9 $[M+H]^+$ 412.08, found $[M+H]^+$ 413.15.

2-(2,2-Diphenylbenzo[*d*][1,3]dioxol-5-yl)-3,7-dihydroxy-4*H*-chromen-4-one (15):

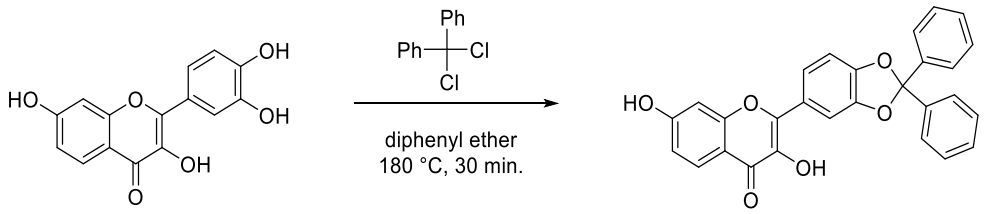

Fisetin (1.00 g, 3.49 mmol, 1.0 equiv.) and dichlorodiphenylmethane (1.24 g, 5.20 mmol, 1.5 equiv.) were suspended in 50 mL diphenyl ether and heated to 180 °C with microwave-assistance for 30 minutes. The reaction mixture was diluted with petroleum ether, and a yellow precipitate formed, which was filtered off. Purification of the solid using column chromatography with a gradient of 25-50% ethyl acetate in petroleum ether gave compound **15** as light brown crystals (1.34 g, 3.10 mmol, 89% yield).

^{1}H NMR (400 MHz, DMSO-d6) δ 10.77 (s, 1H), 9.31 (s, 1H), 7.93 (d, *J* = 8.7 Hz, 1H), 7.89 – 7.76 (m, 2H), 7.58 (d, *J* = 6.5 Hz, 4H), 7.45 (d, *J* = 6.5 Hz, 6H), 7.22 (s, 1H), 6.97 (s, 1H), 6.91 (d, *J* = 8.8 Hz, 1H) ppm. ^{13}C NMR (101 MHz, DMSO-d6) δ 172.1, 162.4, 156.4, 147.3, 146.7, 143.9, 139.5 (s, 2C), 137.8, 129.5 (s, 2C), 128.6 (s, 4C), 126.5, 125.8 (s, 4C), 125.7, 122.7, 116.9, 114.8, 114.2, 108.8, 107.7, 102.0 ppm. ESI-MS: *m/z* calc. for C28H18O6 $[M+H]^+$ 450.11, found $[M+H]^+$ 451.15.

2-(3,4-Diacetoxyphenyl)-4-oxochromane-3,5,7-triyl triacetate (17):

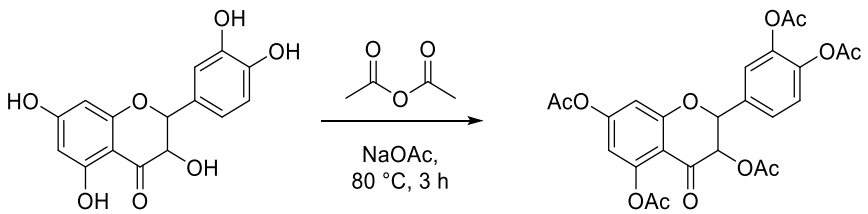

Taxifolin (1.00 g, 3.29 mmol, 1.0 equiv.) was dissolved in acetic anhydride (10.06 g, 98.70 mmol, 30.0 equiv.), and sodium acetate (539 mg, 6.57 mmol, 2.0 equiv.) was added. The solution stirred at 80 °C for three hours when it was diluted with ethyl acetate, extracted twice with water, and washed with brine. The organic layer was dried over sodium sulfate, and the solvent was evaporated. Silica gel column chromatography using 2% acetone in dichloromethane was used for purification, giving compound **17** as an off-white foam (1.33 g, 2.59 mmol, 79% yield).

^{1}H NMR (400 MHz, DMSO-d6) δ 7.55 (dd, *J* = 2.1 Hz and 8.41 Hz, 1H), 7.50 (d, *J* = 2.0 Hz, 1H), 7.37 (d, *J* = 8.31 Hz, 1H), 6.95 (d, *J* = 2.0 Hz, 1H), 6.81 (d, *J* = 2.1 Hz, 1H), 5.95 (d, *J* = 12.3 Hz, 1H), 5.81 (d, *J* = 12.4 Hz), 2.30-2.28 (m, 15H) ppm. ^{13}C NMR (101 MHz, DMSO-d6) δ 185.4, 168.6, 168.5, 168.3, 168.2, 168.1, 162.1, 156.3, 150.8, 142.7, 141.8, 134.0, 126.1, 123.9, 123.3, 111.6, 110.4, 109.3, 79.2, 72.8, 20.9, 20.7, 20.3, 20.3, 20.0 ppm. ESI-MS: *m/z* calc. for C25H22O12 $[M+H]^+$ 514.11, found: 515.15.

4-(3,5-Diacetoxy-7-hydroxy-4-oxochroman-2-yl)-1,2-phenylene diacetate (18):

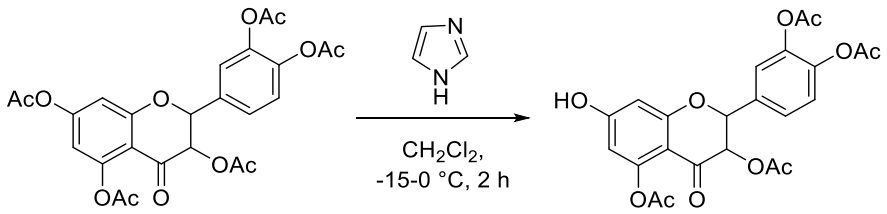

Compound **17** (1.33 g, 2.59 mmol, 1.0 equiv.) was dissolved in dichloromethane and cooled in an ice-acetone bath to -15 °C. Imidazole (352 mg, 5.17 mmol, 2.0 equiv.) was dissolved in dichloromethane and added dropwise to the ice-cold solution. The reaction mixture was warmed to room temperature and stirred at ambient temperature for 2 hours when dichloromethane was added for dilution. The solution was extracted with 1 M HCl, washed with brine, dried over sodium sulfate, and the solvent was evaporated. For purification, silica gel column chromatography was used with a gradient from 3% to 10% acetone in dichloromethane to give **18** as red solid (1.18 g, 2.50 mmol, 96% yield).

^{1}H NMR (400 MHz, DMSO-d6) δ 11.81 (s, 1H), 7.53 (dd, *J* = 8.4, 2.0 Hz, 1H), 7.48 (d, *J* = 2.0 Hz, 1H), 7.35 (d, *J* = 8.3 Hz, 1H), 6.36 (d, *J* = 2.3 Hz, 1H), 6.29 (d, *J* = 2.3 Hz, 1H), 5.76 (d, *J* = 12.2 Hz, 1H), 5.65 (d, *J* = 12.1 Hz, 1H), 2.29 (s, 6H), 2.27 (s, 3H), 1.95 (s, 3H) ppm. ^{13}C NMR (101 MHz, DMSO-d6) δ 184.2, 168.6, 168.5, 168.2, 168.1, 164.9,

163.0, 151.9, 142.6, 141.8, 134.4, 126.0, 123.8, 123.2, 105.9, 105.3, 101.1, 79.0, 72.7, 20.8, 20.4, 20.3, 20.1 ppm. ESI-MS: *m/z* calc. for C23H20O11 $[M+H]^+$ 472.10, found: 473.15.

2-(3,4-Diacetoxyphenyl)-4-oxo-4*H*-chromene-3,5,7-triyl triacetate (19):

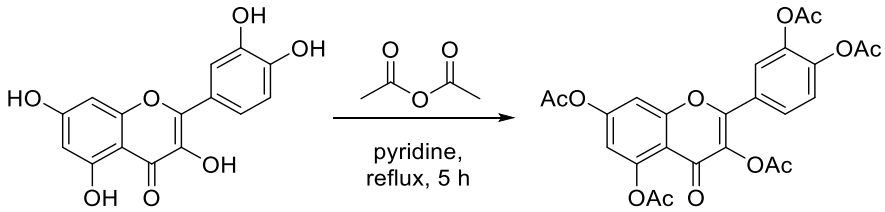

Quercetin (2.00 g, 6.60 mmol, 1.0 equiv.) was dissolved in 30 mL pyridine, acetic anhydride (13.50 g, 132.00 mmol, 20.0 equiv.) was added, and the solution was heated to reflux. After 5 hours, 100 mL ice-water was added to the warm mixture, and the compound precipitated. The precipitate was filtered off and washed with ethyl acetate giving the **19** as off-white solid (2.89 g, 5.65 mmol, 85% yield).

^{1}H NMR (400 MHz, DMSO-d6) δ 7.89-7.87 (m, 2H), 7.56-7.53 (m, 1H), 7.15 (d, *J* = 2.0 Hz, 1H), 6.76 (d, *J* = 2.0 Hz, 1H), 2.36 – 2.31 (m, 15H) ppm. ^{13}C NMR (101 MHz, DMSO-d6) δ 175.6, 168.3, 168.2, 168.0, 167.9, 167.8, 160.3, 156.3, 155.6, 154.8, 144.7, 142.2, 131.6, 127.0, 126.9, 124.6, 123.9, 108.2, 105.7, 102.1, 20.9, 20.4, 20.3, 20.3, 20.1 ppm. ESI-MS: *m/z* calc. for C25H20O12 $[M+H]^+$ 512.10, found: 513.15.

4-(3,5-Diacetoxy-7-hydroxy-4-oxo-4*H*-chromen-2-yl)-1,2-phenylene diacetate (20):

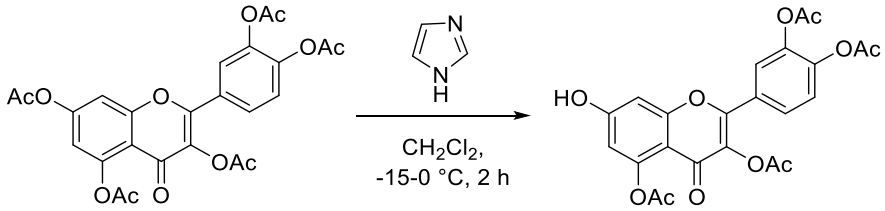

Compound **19** (2.89 g, 5.65 mmol, 1.0 equiv.) was dissolved in dichloromethane and cooled in an ice-acetone bath to -15 °C. Imidazole (769 mg, 11.30 mmol, 2.0 equiv.) was dissolved in dichloromethane and added dropwise to the ice-cold solution. The reaction mixture was warmed to room temperature and stirred at ambient temperature for 2 hours when dichloromethane was added for dilution. The solution was extracted with 1 M HCl, washed with brine, dried over sodium sulfate, and the solvent was evaporated. For purification, silica gel column chromatography was used with a

gradient from 3% to 10% acetone in dichloromethane to give compound **20** as an off-white foam (1.18 g, 2.52 mmol, 45% yield).

^{1}H NMR (400 MHz, DMSO-d6) δ 11.32 (s, 1H), 7.83-7.80 (m, 2H), 7.50 (d, *J* = 8.3 Hz, 1H), 6.94 (d, *J* = 2.2 Hz, 1H), 6.66 (d, *J* = 2.2 Hz, 1H), 2.34 – 2.28 (m, 12H) ppm. ^{13}C NMR (101 MHz, DMSO-d6) δ 169.0, 168.8, 168.2, 168.0, 167.9, 162.8, 157.6, 152.4, 150.3, 144.2, 142.2, 132.8, 127.5, 126.5, 124.4, 123.6, 109.4, 109.1, 101.0, 20.9, 20.4, 20.3, 20.2 ppm. ESI-MS: *m/z* calc. for C23H18O11 $[M+H]^+$ 470.08, found: 471.10.

5-Iodopent-1-yne (21)

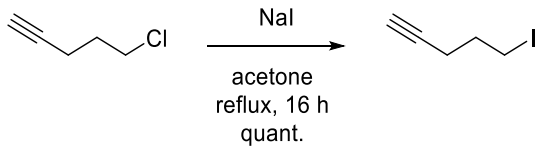

5-Chloropent-1-yne (53 mg, 0.52 mmol, 1.0 equiv.) was dissolved in acetone and sodium iodide (386 mg, 2.58 mmol, 5.0 equiv.) was added. The reaction was refluxed overnight when the solution turned deep yellow, and a white precipitate formed. The solution was diluted with water and extracted with diethyl ether. The organic layer was washed with water, brine, dried over sodium sulfate, and the solvent was evaporated. Compound **21** was obtained as a yellow oil (100 mg, 0.52 mmol, quant.).

^{1}H NMR (400 MHz, $CDCl_3$) δ 3.30 (t, *J* = 6.8 Hz, 2H), 2.33 (dd, *J* = 6.8, 2.7 Hz, 2H), 2.03-1.96 (m, 3H) ppm. ^{13}C NMR (101 MHz, $CDCl_3$) δ 82.4, 69.6, 32.0, 19.6, 5.2 ppm.

2-(3,4-Dihydroxyphenyl)-3,5-dihydroxy-7-(pent-4-yn-1-yloxy)chroman-4-one (22):

1. Linker addition (4-(3,5-diacetoxy-4-oxo-7-(pent-4-yn-1-yloxy)chroman-2-yl)-1,2-phenylene diacetate):

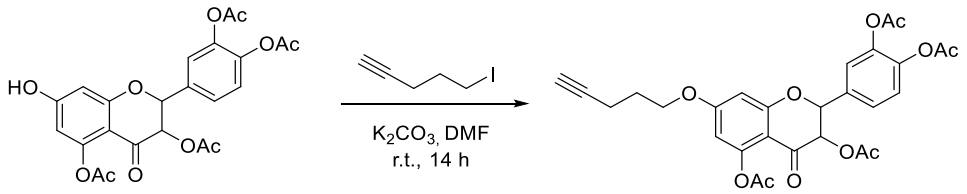

Compound **18** (130 mg, 0.28 mmol, 1.0 equiv.) was dissolved in dry DMF when compound **21** (80 mg, 0.41 mmol, 1.5 equiv.) and potassium carbonate (38 mg, 0.28 mmol, 1.0 equiv.) were added under argon atmosphere. The reaction stirred overnight at room temperature. Dichloromethane was added, and the organic layer was washed

with 5% aqu. HCl, dried over sodium sulfate, and the solvent was evaporated. Purification using silica gel column chromatography with 2.5% methanol in dichloromethane gave the compound as a pale-yellow oil (88 mg, 0.16 mmol, 59% yield).

^{1}H NMR (400 MHz, $CDCl_3$) δ 7.38 (dd, *J* = 8.4, 2.0 Hz, 1H), 7.29 (d, *J* = 2.0 Hz, 1H), 7.26 (d, *J* = 8.4 Hz, 1H), 6.42 (d, *J* = 2.3 Hz, 1H), 6.34 (d, *J* = 2.4 Hz, 1H), 5.63 (d, *J* = 12.1 Hz, 1H), 5.38 (d, *J* = 12.1 Hz, 1H), 4.13 – 4.09 (m, 3H), 2.37 (s, 3H), 2.30 (s, 6H), 2.04 (s, 3H), 2.00 – 1.96 (m, 4H) ppm. ^{13}C NMR (101 MHz, $CDCl_3$) δ 184.5, 169.5, 169.4, 168.1, 165.4, 163.4, 152.2, 143.0, 142.3, 134.1, 125.5, 123.9, 123.0, 106.8, 106.1, 100.2, 84.6, 82.9, 80.4, 73.2, 69.5, 67.1, 27.8, 21.2, 20.8, 20.5, 15.2, 14.3 ppm. ESI-MS: *m/z* calc. for C28H26O11 $[M+H]^+$ 538.15, found: 539.15.

2. Deprotection:

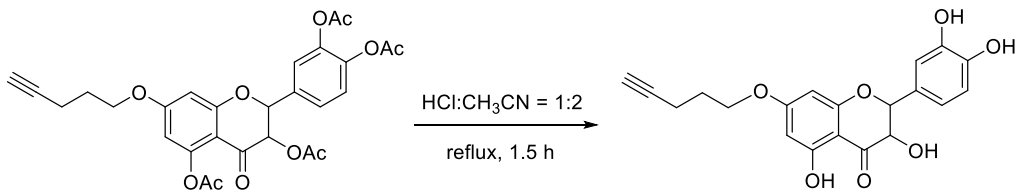

The compound (88 mg, 0.19 mmol, 1.0 equiv.) was dissolved in 6 mL acetonitrile and 3 mL 6 M HCl and refluxed for 1.5 hours. The reaction was cooled to room temperature when ethyl acetate was added, and the mixture was washed with 5% aqu. HCl and brine. The organic layer was dried over sodium sulfate, and the solvent was evaporated. Purification using silica gel column chromatography with 3% methanol in dichloromethane gave compound **22** as white solid (18 mg, 0.04 mmol, 23% yield).

^{1}H NMR (400 MHz, MeOD) δ 7.00 (d, *J* = 1.9 Hz, 1H), 6.88 (d, *J* = 1.9 Hz, 1H), 6.83 (d, *J* = 8.1 Hz, 1H), 6.12 (d, *J* = 2.2 Hz, 1H), 6.08 (d, *J* = 2.1 Hz, 1H), 4.98 (d, *J* = 11.5 Hz, 1H), 4.57 (d, *J* = 11.5 Hz, 1H), 4.14 (t, *J* = 6.1 Hz, 2H), 2.39 (dt, *J* = 6.9, 2.6 Hz, 2H), 2.29 (d, *J* = 2.6 Hz, 1H), 2.02-1.95 (m, 2H) ppm. ESI-MS: *m/z* calc. for C20H18O7 $[M+H]^+$ 370.10, found: 371.10.

2-(3,4-Dihydroxyphenyl)-3,5-dihydroxy-7-(pent-4-yn-1-yloxy)-4*H*-chromen-4-one (23):

1. Linker addition (4-(3,5-diacetoxy-4-oxo-7-(pent-4-yn-1-yloxy)-4*H*-chromen-2-yl)-1,2-phenylene diacetate):

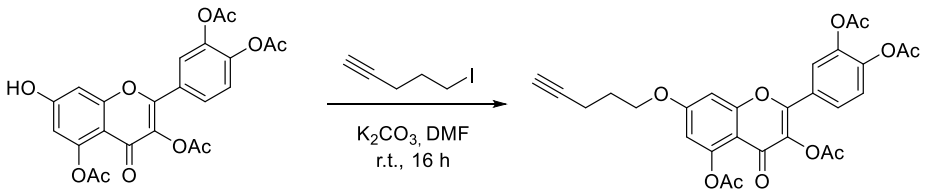

Compound **20** (130 mg, 0.28 mmol, 1.0 equiv.) was dissolved in dry DMF when **21** (80 mg, 0.41 mmol, 1.5 equiv.) and potassium carbonate (38 mg, 0.28 mmol, 1.0 equiv.) were added under argon atmosphere. The reaction stirred overnight at room temperature. Dichloromethane was added, and the organic layer was washed with 5% aqu. HCl, dried over sodium sulfate, and the solvent was evaporated. Purification using silica gel column chromatography with 2.5% methanol in dichloromethane gave the compound as a pale-yellow oil (86 mg, 0.16 mmol, 58% yield).

^{1}H NMR (400 MHz, $CDCl_3$) δ 7.72 – 7.67 (m, 2H), 7.33 (d, *J* = 8.5 Hz, 1H), 6.84 (d, *J* = 2.3 Hz, 1H), 6.63 (d, *J* = 2.2 Hz, 1H), 4.17 (t, *J* = 6.1 Hz, 2H), 2.43 – 2.39 (m, 5H), 2.33 (s, 3H), 2.32 (s, 6H), 2.07-2.02 (m, 2H), 2.00 (t, *J* = 2.6 Hz, 1H) ppm. ^{13}C NMR (101 MHz, $CDCl_3$) δ 170.1, 169.6, 168.1, 168.0, 167.8, 163.3, 158.2, 153.2, 150.8, 144.3, 142.3, 134.0, 128.2, 126.5, 123.9, 123.8, 111.2, 109.2, 99.4, 82.9, 69.6, 67.2, 27.8, 21.2, 20.8, 20.7, 20.6, 15.1 ppm. ESI-MS: *m/z* calc. for C28H24O11 $[M+H]^+$ 536.13, found: 537.15.

2. Deprotection:

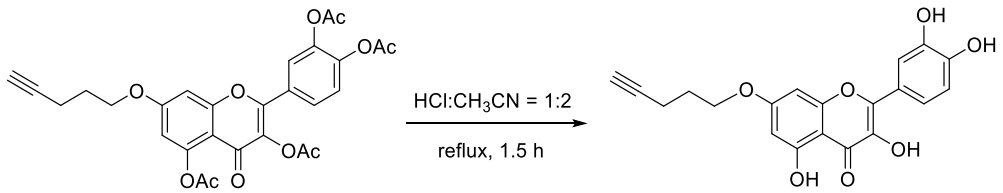

The compound (88 mg, 0.16 mmol, 1.0 equiv.) was dissolved in 6 mL acetonitrile and 3 mL 6 M HCl and refluxed for 1.5 hours. The reaction was cooled to room temperature when ethyl acetate was added, and the mixture was washed with 5% aqu. HCl and brine. The organic layer was dried over sodium sulfate, and the solvent was evaporated. Purification using silica gel column chromatography with 3% methanol in dichloromethane gave **23** as a yellow solid (18 mg, 0.05 mmol, 30% yield).

^{1}H NMR (400 MHz, MeOD) δ 7.90 (s, 1H), 7.79 (d, *J* = 8.4 Hz, 1H), 7.04 (d, *J* = 8.5 Hz, 1H), 6.70 (s, 1H), 6.42 (s, 1H), 4.30 (t , *J* = 6.0 Hz, 2H), 2.53 (dt, *J* = 6.9, 2.3 Hz, 2H), 2.43 (t , *J* = 2.4 Hz, 1H), 2.16-2.10 (m, 2H) ppm. ESI-MS: *m/z* calc. for C20H16O7 $[M+H]^+$ 368.10, found: 369.10.

***tert*-Butyl (3-bromopropyl)carbamate (24):**

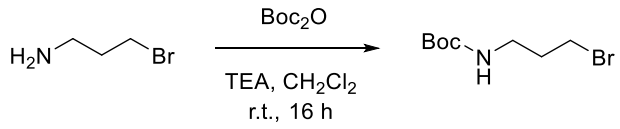

3-Bromopropylamine (1.00 g, 4.57 mmol, 1.0 equiv.) was dissolved in 30 mL dry dichloromethane, triethylamine (1.84 g, 18.27 mmol, 4.0 equiv.) was added, and the solution was stirred at room temperature for 30 minutes when di-tert-butyl dicarbonate (1.49 g, 6.85 mmol, 1.5 equiv.) was added. The reaction mixture was stirred at ambient temperature overnight when water was added, and the solution was extracted with ethyl acetate. Organic layers were combined, washed with brine, and dried over sodium sulfate. Silica gel column chromatography with petroleum ether and ethyl acetate 2:1 gave the compound **24** as a yellow oil (894 mg, 3.75 mmol, 82% yield).

^{1}H NMR (400 MHz, $CDCl_3$) δ 3.41-3.37 (m, 2H), 3.24-3.20 (m, 2H), 2.02-1.98 (m, 2H), 1.40 (m, 9H) ppm. ^{13}C NMR (101 MHz, $CDCl_3$) δ 146.9, 85.3, 39.2, 32.9, 30.9, 28.5 (3x Boc-*C*H_3) ppm.

***tert*-Butyl (3-iodopropyl)carbamate (25):**

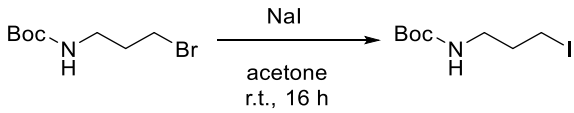

Compound **24** (700 mg, 2.94 mmol, 1.0 equiv.) was dissolved in dry acetone, and sodium iodide (499 mg, 3.33 mmol, 1.2 equiv.) was added. The mixture was refluxed overnight when a precipitate formed. Water was added, and the reaction was extracted with ethyl acetate three times to give compound **25** as a brown oil (314 mg, 1.15 mmol, 40% yield).

^{1}H NMR (400 MHz, $CDCl_3$) δ 4.67 (s, 1H, N*H*), 3.20-3.16 (m, 4H), 2.02-1.96 (m, 2H), 1.42 (m, 9H) ppm. ^{13}C NMR (101 MHz, $CDCl_3$) δ 156.1, 79.5, 41.2, 33.5, 28.5 (3x Boc-*C*H_3), 3.2 ppm.

7-(3-((*tert*-Butoxycarbonyl)amino)propoxy)-2-(3,4-diacetoxyphenyl)-4-oxochromane-3,5-diyl diacetate (26):

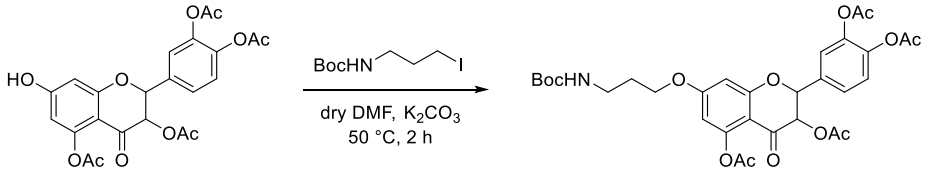

Compound **18** (411 mg, 0.87 mmol, 1.0 equiv.) was dissolved in dry DMF. Compound **25** (372 mg, 1.30 mmol, 1.5 equiv.) and potassium carbonate (179 mg, 1.30 mmol, 1.5 equiv.) were added, and the solution was stirred at 50 °C for two hours. The reaction was diluted with dichloromethane, extracted with 1 M HCl, and washed with brine. The organic layer was dried over sodium sulfate, and the solvent was evaporated. The crude product was purified using silica gel column chromatography with 3-10% acetone in dichloromethane, giving compound **26** as dark brown oil (95 mg, 0.15 mmol, 17% yield).

^{1}H NMR (400 MHz, DMSO-d6) δ 7.54 (dd, *J* = 8.4, 2.0 Hz, 1H), 7.49 (d, *J* = 2.0 Hz, 1H), 7.35 (d, *J* = 8.3 Hz, 1H), 6.63 (d, *J* = 2.4 Hz, 1H), 6.49 (d, *J* = 2.3 Hz, 1H), 5.83 (d, *J* = 12.2 Hz, 1H), 5.71 (d, *J* = 12.2 Hz, 1H), 4.08 (t, *J* = 6.2 Hz, 2H), 3.05 (q, *J* = 6.1 Hz, 2H), 2.30 – 2.28 (m, 9H), 1.96 (s, 3H), 1.85 – 1.78 (m, 2H), 1.36 (s, 10H) ppm. ^{13}C NMR (101 MHz, DMSO-d6) δ 185.0, 169.0, 168.9, 168.7, 168.6, 165.5, 163.5, 156.1, 152.0, 149.2, 143.1, 142.3, 134.7, 126.6, 124.3, 123.7, 106.7, 106.0, 100.5, 79.6, 78.0, 73.1, 67.0, 37.1, 30.0, 29.2, 28.7, 21.3, 20.8, 20.7, 20.6 ppm. ESI-MS: *m/z* calc. for C31H35NO13 $[M+H]^+$ 629.21, found $[M+Na]^+$ 652.25.

7-(3-((*tert*-Butoxycarbonyl)amino)propoxy)-2-(3,4-diacetoxyphenyl)-4-oxo-4*H*-chromene-3,5-diyl diacetate (27):

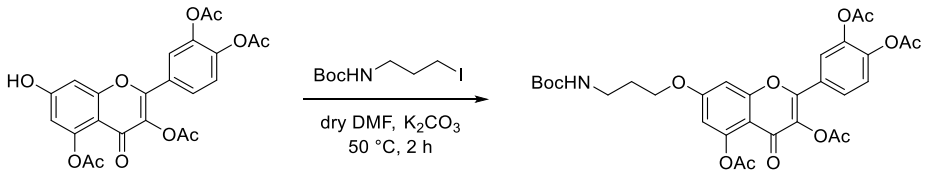

Compound **20** (400 mg, 0.85 mmol, 1.0 equiv.) was dissolved in dry DMF. Compound **25** (290 mg, 1.02 mmol, 1.2 equiv.) and potassium carbonate (151 mg, 1.02 mmol, 1.2 equiv.) were added, and the mixture was stirred for two hours at 50 °C. The reaction was diluted with dichloromethane and extracted with 1 M HCl and washed with brine. The organic layer was dried over sodium sulfate, and the solvent was evaporated.

Purification with silica gel column chromatography using 5% acetone in dichloromethane gave the compound **27** as a yellow oil (105 mg, 0.17 mmol, 20% yield).

^{1}H NMR (400 MHz, DMSO-d6) δ 7.86-7.84 (m, 2H), 7.53-7.51 (m, 1H), 7.25 (d, *J* = 2.2 Hz, 1H), 6.93-6.91 (m, 1H), 6.83 (d, *J* = 2.2 Hz, 1H), 4.17 (t, *J* = 6.1 Hz, 2H), 3.13-3.08 (m, 2H), 2.32-2.30 (m, 12H), 1.92-1.86 (m, 2H), 1.37 (s, 9H) ppm. ^{13}C NMR (101 MHz, DMSO-d6) δ 169.0, 168.7, 168.2, 168.0, 167.8, 163.1, 157.6, 155.7, 152.5, 149.9, 144.3, 142.2, 133.0, 127.4, 126.5, 124.5, 123.5, 110.1, 109.2, 99.9, 77.6, 66.8, 36.7, 28.8, 28.2 (3C Boc), 20.8, 20.4, 20.3, 20.2 ppm. ESI-MS: *m/z* calc. for C31H33NO13 $[M+H]^+$ 627.20, found $[M+Na]^+$ 650.25.

7-(3-Aminopropoxy)-2-(3,4-dihydroxyphenyl)-3,5-dihydroxychroman-4-one (28):

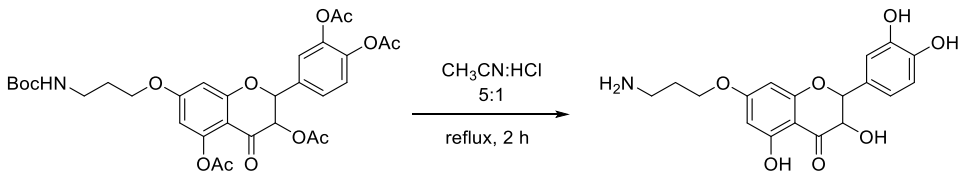

Compound **26** (40 mg, 0.06 mmol) was dissolved in 5 mL acetonitrile and 1 mL conc. HCl was added. The solution was refluxed for 2 hours when a precipitate formed. The solid was filtered and purified by reversed phase flash column chromatography with water and acetonitrile supplemented with 0.1% formic acid to give compound **28** as off-white oil (7 mg, 0.02 mmol, 30%).

ESI-MS: *m/z* calc. for C18H19NO7 $[M+H]^+$ 361.12, found $[M+H]^+$ 362.10, HPLC Purity: 83%.

7-(3-Aminopropoxy)-2-(3,4-dihydroxyphenyl)-3,5-dihydroxy-4*H*-chromen-4-one (29):

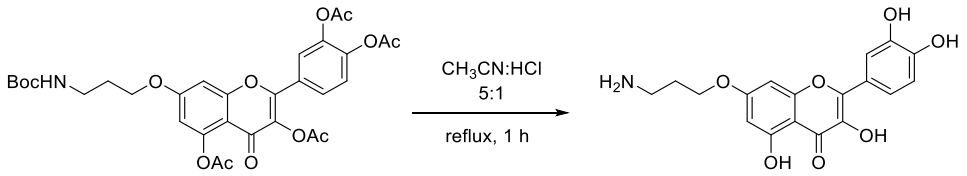

Compound **27** (60 mg, 0.10 mmol) was dissolved in 5 mL acetonitrile and 1 mL conc. HCl was added. The solution was refluxed for 1 hour when a precipitate formed. The solid was filtered and purified by reversed phase flash column chromatography with

water and acetonitrile supplemented with 0.1% formic acid to give compound **29** as off-white oil (16 mg, 0.05 mmol, 50%).

ESI-MS: *m/z* calc. for C18H17NO7 $[M+H]^+$ 359.10, found $[M+H]^+$ 360.10; HPLC purity: 98%.

N-(3-((2-(3,4-Dihydroxyphenyl)-3,5-dihydroxy-4-oxochroman-7-yl)oxy)propyl)hex-5-ynamide (31):

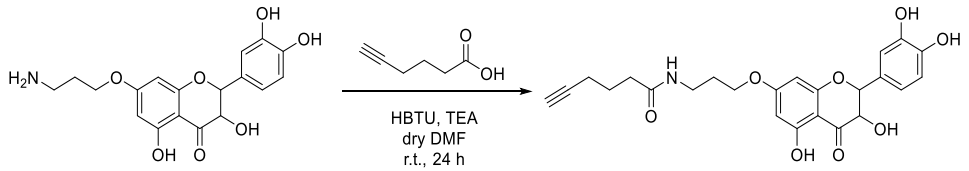

Compound **28** (18 mg, 0.05 mmol, 1.0 equiv.) was dissolved in dry DMF and 5-hexynoic acid (9 mg, 0.08 mmol, 1.5 equiv.), HBTU (28 mg, 0.08 mmol, 1.5 equiv.) and triethylamine (10 mg, 0.10 mmol, 2.0 equiv.) were added. The reaction stirred under an argon atmosphere at room temperature for 24 hours when the solution was diluted with ethyl acetate and rinsed with saturated $NaHCO_3$, water, and brine. The organic layer was dried over sodium sulfate, and the solvent was evaporated. Reversed phase flash column chromatography with water and acetonitrile with 0.1% formic acid was used for purification, and **31** was obtained as a pale-yellow oil (3 mg, 0.007 mmol, 13% yield).

^{1}H NMR (400 MHz, DMSO-d6) δ 11.85 (s, 1H), 9.02 (s, 1H), 8.96 (s, 1H), 7.87 (s, 1H), 6.88 (d, *J* = 1.5 Hz, 1H), 6.75 – 6.71 (m, 2H), 6.07 (dd, *J* = 11.0, 2.2 Hz, 2H), 5.02 (d, *J* = 11.2 Hz, 1H), 4.54 (d, , *J* = 11.3 Hz, 1H), 4.04 (t, *J* = 6.1 Hz, 2H), 3.15 (quart., *J* = 6.5 Hz, 2H), 2.75 (t, *J* = 2.6 Hz, 1H), 2.17 – 2.11 (m, 4H), 1.81 (quint., *J* = 6.5 Hz, 2H), 1.65 (quint., *J* = 7.2 Hz, 2H) ppm. ^{13}C NMR (101 MHz, DMSO-d6) δ 198.3, 171.4, 166.8, 163.0, 162.5, 145.8, 144.9, 127.9, 119.4, 115.4, 115.1, 101.3, 95.2, 94.1, 84.1, 83.2, 71.6, 71.4, 66.1, 35.3, 34.1, 28.6, 24.2, 17.4 ppm. ESI-MS: *m/z* calc. for C24H25NO8 $[M+H]^+$ 455.16, found $[M+H]^+$ 456.20. HPLC purity: 83%.

N-(3-((2-(3,4-Dihydroxyphenyl)-3,5-dihydroxy-4-oxo-4*H*-chromen-7-yl)oxy)propyl)hex-5-ynamide (32):

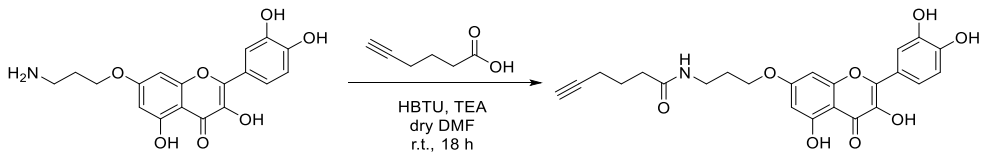

Compound **29** (16 mg, 0.05 mmol, 1.1 equiv.) was dissolved in dry DMF and 5-hexynoic acid (5 mg, 0.04 mmol, 1.0 equiv.), HBTU (17 mg, 0.05 mmol, 1.1 equiv.) and triethylamine (6 mg, 0.06 mmol, 1.5 equiv.) were added. The reaction stirred under an argon atmosphere at room temperature for 18 hours when the solution was diluted with ethyl acetate and rinsed with saturated $NaHCO_3$, water, and brine. The organic layer was dried over sodium sulfate, and the solvent was evaporated. Reversed phase flash column chromatography with water and acetonitrile with 0.1% formic acid was used for purification, and **32** was obtained as a pale-yellow oil (4 mg, 0.008 mmol, 20% yield).

^{1}H NMR (400 MHz, DMSO-d6) δ 12.47 (s, 1H), 9.62 (s, 1H), 9.45 (s, 1H), 9.27 (s, 1H), 7.72 (d, *J* = 2.2 Hz, 1H), 7.56 (dd, *J* = 8.5, 2.2 Hz 1H), 6.89 (d, *J* = 8.5 Hz, 1H), 6.68 (d, *J* = 2.1 Hz, 1H), 6.33 (d, *J* = 2.1 Hz, 1H), 4.10 (t, *J* = 6.2 Hz, 2H), 3.22 – 3.18 (m, 2H), 2.76 (t, *J* = 2.7 Hz, 1H), 2.19 – 2.14 (m, 4H), 1.87 (quint, *J* = 6.2 Hz, 2H), 1.66 (quint, *J* = 7.2 Hz, 2H) ppm. ^{13}C NMR (101 MHz, DMSO-d6) δ 171.5, 165.5, 164.2, 160.4, 156.0, 147.8, 147.3, 145.1, 136.0, 121.9, 120.0, 115.6, 115.3, 97.8, 92.3, 84.1, 71.4, 66.2, 57.8, 35.3, 34.1, 28.6, 24.2, 17.4 ppm. ESI-MS: *m/z* calc. for C24H23NO8 $[M+H]^+$ 453.14, found $[M+H]^+$ 454.20, HPLC purity: 91%.

3-((Heptylcarbamoyl)oxy)-14-methyl-5-oxo-5,7,8,13-tetrahydroindolo[2',3':3,4]pyrido[2,1-*b*]quinazolin-14-ium (48)

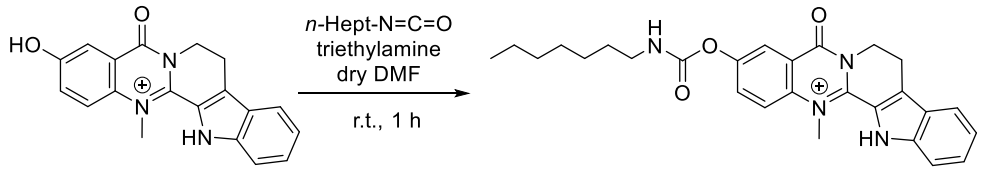

Compound **61** (59 mg, 0.18 mmol, 1.0 equiv.) was dissolved in dry DMF, and triethylamine (21 mg, 0.21 mmol, 1.2 equiv.) was added. The solution stirred for 5 minutes at room temperature when heptyl isocyanate (30 mg, 0.21 mmol, 1.2 equiv.) was added. After 1 hour, 200 µL 1 M HCl was added, and the reaction was quenched with water. The solvent was evaporated, and the crude mixture was first purified by preparative HPLC with a gradient of methanol in water with 0.1% formic acid giving a mixture of 44% **48** and 34% HO-DHED **61**. Purification with reversed phase column chromatography with methanol/water without acid increased purity to 86% **48**. However, 13% of HO-DHED **61** could not be removed.

^{1}H NMR (400 MHz, MeOD) δ 8.14 (d, *J* = 2.7 Hz, 1H), 8.10-7.94 (m, 1H), 7.88-7.83 (m, 2H), 7.72-7.64 (m, 1H), 7.58-7.50 (m, 1H), 7.33 (m, 1H), 4.62-4.57 (m, 2H), 4.44 (s, 3H), 3.41 (t, *J* = 7.1 Hz, 2H), 1.64-1-57 (m, 2H), 1.39-1.29 (m, 10H), 0.94-0.90 (m, 3H) ppm. ESI-MS: *m/z* calc. for C27H31N4O3+ $[M+H]^+$ 459.24, found: 459.25.

4,9-Dihydro-3*H*-pyrido[3,4-*b*]indole (52)

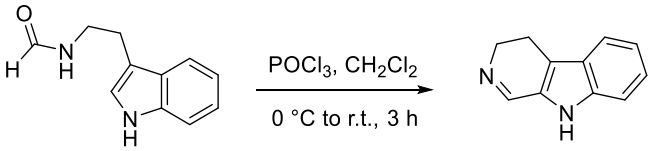

Compound **58** (1.80 g, 9.6 mmol, 1.0 equiv.) was dissolved in 6 mL dry dichloromethane and cooled to 0°C in an ice bath. $POCl_3$ (3.66 g, 23.9 mmol, 2.5 equiv.) was added dropwise within 5 minutes. The reaction stirred for 1 hour at 0°C and for additional 2 hours at room temperature when the solvent was evaporated. The residue was dissolved in ethyl acetate and extracted six times with 10% acetic acid in water. The water phases were combined and basified to pH 10 with aqueous ammonia before extraction with dichloromethane. The organic layers were combined, washed with brine, dried over sodium sulfate, and the solvent was evaporated to give compound **52** as an orange foam (1.39 g, 8.17 mmol, 85%).

^{1}H NMR (400 MHz, $CDCl_3$) δ 8.48 (s, 1H), 8.39 (m, 1H), 7.60 (d, *J* = 8.0 Hz, 1H), 7.39-7.37 (m, 1H), 7.30-7.28 (m, 1H), 7.18 – 7.14 (m, 1H), 3.98 – 3.93 (m, 2H), 2.94 – 2.89 (m, 2H) ppm. ^{13}C NMR (101 MHz, $CDCl_3$) δ 151.7, 137.0, 128.3, 125.5, 124.8, 120.6, 120.2, 116.4, 112.2, 48.7, 19.2 ppm. ESI-MS: *m/z* calc. for C11H10N2 $[M+H]^+$ 170.08, found: 171.10.

6-Methoxy-2*H*-benzo[*d*][1,3]oxazine-2,4(1*H*)-dione (55):

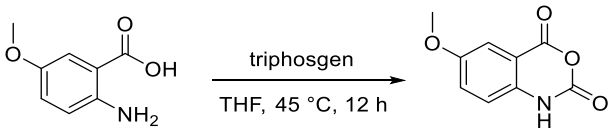

3-methoxy anthranilic acid **54** (5.20 g, 31.1 mmol, 1.0 equiv.) was dissolved in 30 mL dry THF, and triphosgene (3.14 g, 10.6 mmol, 0.34 equiv.) was added. The reaction stirred at 45°C overnight when precipitation formed. The solid was filtered and washed with hexane to give the first product batch. The solvent of the filtrate was evaporated, and the residue was washed with hexane to give the second product batch. The batched

were combined, and compound **55** was obtained as off-white solid (5.63 g, 29.1 mmol, 94%).

^{1}H NMR (400 MHz, DMSO-d6) δ 11.60 (s, 1H), 7.40 – 7.37 (dd, *J* = 3.0 Hz, 8.9 Hz, 1H), 7.34 (d, *J* = 3.0 Hz, 1H), 7.11 (d, *J* = 8.9 Hz, 1H), 3.81 (s, 3H) ppm. ^{13}C NMR (101 MHz, DMSO-d6) δ 155.2, 146.9, 135.5, 125.7, 116.9, 114.6, 110.7, 109.9, 55.7 ppm.

6-Methoxy-1-methyl-2*H*-benzo[*d*][1,3]oxazine-2,4(1*H*)-dione (56)

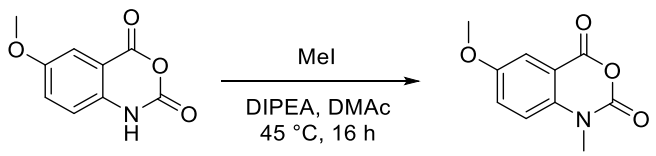

Compound **55** (5.50 g, 28.5 mmol, 1.0 equiv.) was dissolved in 40 mL DMAc. DIPEA (7.73 g, 59.8 mmol, 2.1 equiv.) was added, and the solution stirred for 10 minutes at room temperature when methyl iodide (10.50 g, 74.0 mmol, 2.6 equiv.) was added, and the reaction was heated to 40°C. After stirring overnight, the reaction was cooled to room temperature. Upon addition of water with vigorous stirring, an off-white precipitate formed. The solid was filtered and washed with hexane to obtain compound **56** (5.61 g, 27.1 mmol, 97%).

^{1}H NMR (400 MHz, DMSO-d6) δ 7.45 (m, 3H), 3.84 (s, 3H), 3.45 (s, 3H) ppm. ^{13}C NMR (101 MHz, DMSO-d6) δ 158.9, 155.2, 147.6, 136.3, 125.0, 116.6, 112.2, 110.8, 55.8, 31.7 ppm. ESI-MS: *m/z* calc. for C10H9NO4 $[M+H]^+$ 207.05, found: 208.10.

N-(2-(1*H*-Indol-3-yl)ethyl)formamide (58)

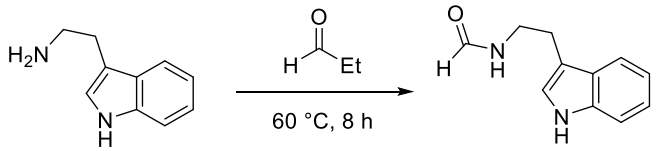

Tryptamine **57** (3.00 g, 18.7 mmol, 1.0 equiv.) was suspended in ethyl formate (11.01 g, 149.6 mmol, 8.0 equiv.) and heated to reflux for 8 hours. The solvent was evaporated, and the crude product was purified using silica gel column chromatography with 1.3% methanol in dichloromethane (conforms a 75:1 ratio) to give compound **58** as a brown oil (2.76 g, 14.7 mmol, 79%).

^{1}H NMR (400 MHz, $CDCl_3$) δ 8.79 (s, 1H), 7.94 (s, 1H), 7.58 – 7.56 (m, 1H), 7.34 – 7.32 (m, 1H), 7.23 – 7.18 (m, 1H), 7.14 – 7.10 (m, 1H), 6.92 (d, *J* = 2.1 Hz, 1H), 6.04 (s, 1H),

3.56 (quart., J = 6.7 Hz, 2H), 2.93 (t, J = 6.9 Hz, 2H) ppm. ^{13}C NMR (101 MHz, $CDCl_3$) δ 161.6, 136.5, 127.2, 122.4, 122.0, 119.4, 119.3, 118.5, 111.5, 38.4, 25.0 ppm. ESI-MS: *m/z* calc. for C11H12N2O $[M+H]^+$ 188.09, found: 189.15.

3-Methoxy-14-methyl-8,13,13*b*,14-tetrahydroindolo[2',3':3,4]pyrido[2,1-*b*]quinazolin-5(7*H*)-one (59)

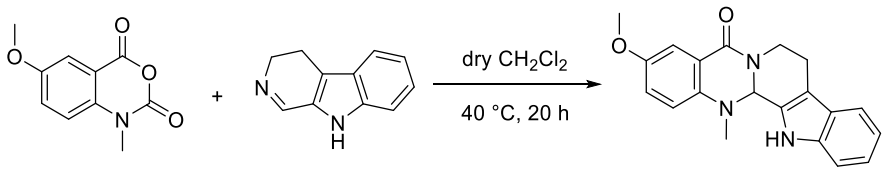

Compound **56** (400 mg, 1.93 mmol, 1.0 equiv.) and **52** (335 mg, 1.97 mmol, 1.02 equiv.) were dissolved in dry dichloromethane and heated to reflux. After 20 hours, the total consumption of the anhydride derivate **56** was observed, and the solvent was evaporated. The crude product was washed with diethyl ether and purified by column chromatography with 50% ethyl acetate in petroleum ether. Compound **59** was obtained as beige solid (489 mg, 1.46 mmol, 76%).

^{1}H-NMR (400 MHz, $CDCl_3$) δ 9.05 (s, 1H), 7.51 – 7.47 (m, 2H), 7.35 – 7.32 (m, 1H), 7.15 – 7.11 (m, 1H), 7.07 – 7.03 (m, 1H), 6.96 – 6.95 (m, 2H), 5.77 (s, 1H), 4.81 – 4.76 (m, 1H), 3.74 (s, 3H), 3.22 – 3.15 (m, 1H), 2.92 – 2.79 (m, 2H), 2.28 (s, 3H) ppm. ^{13}C NMR (101 MHz, $CDCl_3$) δ 163.6, 154.9, 143.7, 136.7, 129.4, 125.7, 123.0, 122.8, 121.9, 120.6, 118.8, 118.3, 111.6, 111.5, 110.7, 69.0, 55.4, 39.7, 36.8, 19.7 ppm. ESI-MS: *m/z* calc. for C20H19N3O2 $[M+H]^+$ 333.15, found: 334.15.

3-Hydroxy-14-methyl-5-oxo-5,7,8,13-tetrahydroindolo[2',3':3,4]pyrido[2,1-*b*]quinazolin-14-ium (60)

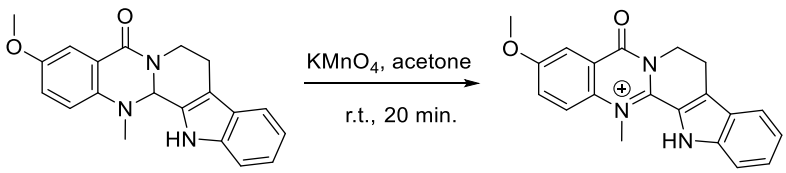

Compound **59** (500 mg, 1.50 mmol, 1.0 equiv.) was dissolved in acetone, and potassium permanganate was added (355 mg, 2.25 mmol, 1.5 equiv.). The reaction stirred at room temperature for 20 minutes and was then poured over celite to filter off the formed MnO_2. The filter was washed with acetone, and the solvent was removed to give compound **60** as an orange oil (296 mg, 0.89 mmol, 59%).

^{1}H NMR (400 MHz, MeOD) δ 8.42 (s, 1H), 8.02 (d, *J* = 9.3 Hz, 1H), 7.84 – 7.82 (m, 2H), 7.66 (dd, *J* = 9.3, 3.2 Hz, 2H), 7.53-7.49 (m, 1H), 7.30 – 7.26 (m, 1H), 4.59 (t, *J* = 7.0 Hz, 2H), 4.44 (s, 3H), 3.99 (s, 3H), 3.38 (t, *J* = 7.0 Hz, 2H) ppm. ^{13}C NMR (101 MHz, MeOD) δ 161.2, 159.4, 150.0, 143.4, 135.1, 132.1, 130.3, 126.2, 125.2, 123.2, 122.4, 121.8, 121.3, 121.1, 114.4, 110.3, 56.8, 43.7, 41.4, 20.0 ppm. ESI-MS: *m/z* calc. for C20H18N3O2+ $[M+H]^+$ 332.14, found: 332.20.

3-Hydroxy-14-methyl-5-oxo-5,7,8,13-tetrahydroindolo[2',3':3,4]pyrido[2,1-*b*]quinazolin-14-ium (61)

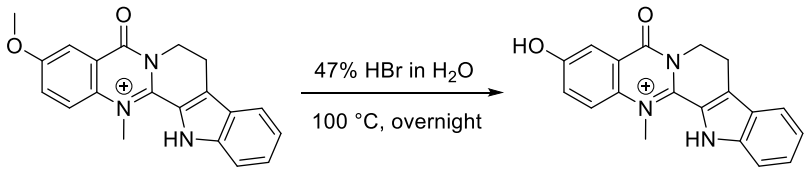

Compound **60** (320 mg, 0.96 mmol, 1.0 equiv.) was dissolved in 25 mL 47% HBr in water and stirred overnight at 100°C. The precipitate was filtered off, and the solvent was evaporated. The crude product was purified using reversed phase column chromatography with a gradient from 15% to 50% methanol in water over 30 minutes. HO-DHED **61** was obtained as a yellow oil (72 mg, 0.22 mmol, 23%).

^{1}H NMR (400 MHz, MeOD) δ 8.49 (s, 1H), 7.96 (d, *J* = 9.2 Hz, 1H), 7.85 (d, *J* = 8.1 Hz, 1H), 7.75 (m, 1H), 7.68 (d, *J* = 8.3 Hz, 1H), 7.57 – 7.53 (m, 2H), 7.35 – 7.33 (m, 1H), 4.61 (t, *J* = 7.1 Hz, 2H), 4.44 (s, 3H), 3.41 (t, *J* = 7.1 Hz, 2H) ppm. ESI-MS**:** *m/z* calc. for C19H16N3O2+ $[M+H]^+$ 318.12, found: 318.15.

10.2 *In Vitro* Assays

DPPH Assay

Stock solutions [3 mM] of the compounds were prepared in DMSO, ascorbic acid in *dd*H_2O. All compounds were further diluted in a 96-well plate using methanol, and blank absorption was measured at 517 nm. Methanol replacing the compound dilution served as a negative control. To 100 µL compound dilution, 33.3 µL [200 µM] freshly prepared methanolic DPPH solution were added. The plate was shaken for 5 seconds and incubated at room temperature for 30 min. After incubation, the absorbance was

measured at 517 nm. The percentage of DPPH radical scavenging activity (SCV) was calculated by the following equation:

$$\% \, SCV = \frac{(A_{neg.control} - A_{blank1}) - (A_{sampel} - A_{blank2})}{(A_{neg.control} - A_{blank1})} * 100$$

Concentration-dependent SCV curves were calculated using a non-linear fit, and IC_{50} values were then determined graphically using GraphPad Prism 5 software.

FRAP Assay

The FRAP reagent was prepared by mixing 300 mmol/L sodium acetate buffer (pH 3.6), 10 mmol/L TPTZ (2,4,6-tripyridyl-s-triazine, Sigma Aldrich, Munich, Germany) solution in 40 mmol/L HCl and 20 mmol/L FeCl3·6H2O solution at a 10:1:1 ratio. The freshly prepared FRAP reagent and the SpectraMax 250 plate reader were warmed to 37 °C. 0.1, 0.2, 0.4, 0.6, 0.8 and 1 mM methanolic solutions (10% DMSO) of the compounds were prepared. FeSO4 was used for calibration. Ascorbic acid and Trolox (Sigma Aldrich, Munich, Germany) served as reference compounds and displayed the antioxidant capacity of 2.0 and 1.8 equivalents of $FeSO_4$, respectively.

In every well of a 96-well-plate, 220.6 µL of FRAP reagent, 22 µL of distilled water, and 7.4 µL of sample or standard were mixed, and the absorbance changes were determined at 593 nm versus the FRAP reagent with methanol. DMSO alone served as a blank. The final dilution of the test samples in the reaction mixture was 1/34. The reaction started immediately and was monitored every 15 s for 4 min with a multiwell plate photometer (Tecan e SpectraMax 250). Experiments were performed in triplicates.

The analysis was accomplished using GraphPad Prism 5 Software applying Oneway ANOVA followed by subsequent Tukey test. Significance was defined as $*p < .05$.

Metal chelation

The assessment of Fe^{2+} and Cu^{2+} chelation was carried out as described by Santos et al.[232] with partial modifications. To assess the chelation of Fe^{2+} a colorimetric approach was used. Ferrous iron in ferrous sulfate readily reacts with ferrozine (3-(2-Pyridyl)-5,6-diphenyl-1,2,4-triazine-*p,p'*-disulfonic acid monosodium salt hydrate) to form a purple Fe^{2+}-ferrozine complex. To start the reaction, 50 µL of Fe^{2+} aq. (80 µM in sodium acetate buffer (50 mM, pH 6.0)) were added to 100 µL diluted compound in methanol solution, or pure methanol as a negative control. The 96-well plate was incubated at room temperature for 2 minutes and 50 µL ferrozine aq. (250 µM in

buffer) were added to each well. After 10 minutes of incubation at room temperature, the absorbance at 562 nm was determined with a microplate reader. The experiments were performed in duplicates. The dilution series of the respective compound in methanol and Fe^{2+} aq. served as a blank which the results were normalized to. EDTA·2Na served as a reference.

The method for Cu^{2+}-chelation was modified by using pyrocatechol violet (PV) as the chromogen agent with slightly acidic sodium acetate buffer (pH 6.0). In each well, 50 µL Cu^{2+} aq. (400 µM in buffer) were added to 100 µL diluted compound in methanol solution or pure methanol as a negative control. The 96-well plate was incubated at room temperature for 2 minutes when 50 µL PV aq. (400 µM in buffer) were added. After incubation at room temperature for 10 min, the absorbance at 632 nm was determined using a microplate reader. The experiments were performed in duplicates. Again, EDTA·2Na served as a reference.

ORAC Assay

The assay was applied according to Ou et al.[233] and partially modified according to Dávalos et al.[234] by using fluorescein (FL) as a fluorescent probe, (±)-6-Hydroxy-2,5,7,8-tetramethylchromane-2-carboxylic acid (Trolox) as a reference, and 2,2'-azobis(amidinopropane) dihydrochloride (AAPH) as a free radical generator. Reactions were performed in 75 mM PBS (pH 7.4), and the final reaction volume was 200 µL at 37 °C. Compounds at indicated concentrations (20 µL) and FL (120 µL, 70 nM) solutions were mixed in a black 96-well microplate (SARSTEDT) and pre-incubated for 15 min at 37 °C. Subsequently, AAPH solution (60 µL, 12 mM) was added rapidly, and the plate was placed in a TECAN microplate reader to measure the fluorescence intensity (485 nm excitation and 510 nm emission filters) every two min for 90 min. Samples were measured at two different concentrations (2 and 4 µM). A blank (FL + AAPH in PBS) and a calibration curve of Trolox (1, 2, 4, 6, 8, 10, 12, and 15 µM) were included in each experiment. All samples were prepared in duplicates, and three independent assays were performed for each compound. The area under the fluorescence decay curve (fluorescence vs. time) (AUC) was calculated as

$$AUC = 1 + \sum_{i=1}^{i=45} f_i / f_0$$

where f_0 is the initial fluorescence reading at 0 min, and f_i is the fluorescence reading at time 2i. The net AUC corresponding to a sample was calculated by subtracting the AUC corresponding to the blank (Net AUC = $AUC_{antioxidant} - AUC_{blank}$). Linear regression equations were calculated by plotting the net AUC against the Trolox antioxidant standard concentration (R^2>0.99). ORAC-FL values were expressed as Trolox equivalents.

Ellman's assay for BChE inhibition studies

*h*BChE (E.C. 3.1.1.8, from human plasma) was kindly donated by Dr. Oksana Lockridge, Nebraska Medical Center. 3.33 mM stock solutions (100 µM final conc. in the assay) of the compounds in ethanol were prepared and stepwise diluted to 3.33 nM (0.1 nM in the assay). A 10 mM DTNB (Sigma-Aldrich, Steinheim, Germany) solution in buffer (3.12 g potassium dihydrogen phosphate in 500 mL MilliQ, pH 8.0) was prepared. 75 mM BTC (Sigma-Aldrich, Steinheim, Germany) stocks in buffer were stored frozen until use. The assay was carried out at 25°C.

In a cuvette, 900 µL buffer and 30 µL *h*BChE stock (2.5 units/mL in buffer stabilized with 1 mg/mL BSA (Sigma-Aldrich)) were mixed. 30 µL compound solution (3.33 mM stock in ethanol) in different concentrations was added, mixed thoroughly, and incubated for indicated incubation times. 6 µL BTC (75 mM stock in buffer) was added, and after 2.5 min incubation, the absorbance at 412 nm was measured. Each concentration was assessed in triplicates and referred to a blank sample of buffer and ethanol and full enzyme activity without the addition of compound. 10% ethanol did not affect enzyme activity. The enzyme activity in percent was plotted against the logarithmic inhibitor concentration from which IC_{50} values were calculated using the GraphPad Prism 5 software.

References

1. Solecki, R. S. Shanidar IV, a Neanderthal Flower Burial in Northern Iraq. *Science* **1975**, *190* (4217), 880-881.

2. Lietava, J. Medicinal Plant in a Middle Paleolithic Grave Shanidar IV? *J. Ethnopharmacol.* **1992**, *35* (3), 263-266.

3. Cragg, G. M.; Newman, D. J. Biodiversity: A Continuing Source of Novel Drug Leads. *Pure Appl. Chem.* **2005**, *77* (1), 7-24.

4. Bernardini, S.; Tiezzi, A.; Laghezza Masci, V.; Ovidi, E. Natural Products for Human Health: An Historical Overview of the Drug Discovery Approaches. *Nat. Prod. Res.* **2018**, *32* (16), 1926-1950.

5. Prior, M.; Chiruta, C.; Currais, A.; Goldberg, J.; Ramsey, J.; Dargusch, R.; Maher, P. A.; Schubert, D. Back to the Future with Phenotypic Screening. *ACS Chem. Neurosci.* **2014**, *5* (7), 503-513.

6. Rishton, G. M. Natural Products as a Robust Source of New Drugs and Drug Leads: Past Successes and Present Day Issues. *Am. J. Cardiol.* **2008**, *101* (10), 43-49.

7. Swinney, D. C.; Anthony, J. How Were New Medicines Discovered? *Nat. Rev. Drug. Discov.* **2011**, *10* (7), 507-519.

8. Doig, A. J.; Del Castillo-Frias, M. P.; Berthoumieu, O.; Tarus, B.; Nasica-Labouze, J.; Sterpone, F.; Nguyen, P. H.; Hooper, N. M.; Faller, P.; Derreumaux, P. Why Is Research on Amyloid-β Failing to Give New Drugs for Alzheimer's Disease? *ACS Chem. Neurosci.* **2017**, *8* (7), 1435-1437.

9. Alzheimer, A. Über eine Eigenartige Erkrankung der Hirnrinde. *Allg. Z. Psychiat.* **1907**, *64*, 146-148.

10. Alzheimer, A.; Stelzmann, R. A.; Schnitzlein, H. N.; Murtagh, F. R. An English Translation of Alzheimer's 1907 Paper, "Über eine Eigenartige Erkankung der Hirnrinde". *Clin. Anat.* **1995**, *8* (6), 429-431.

11. Lane, C. A.; Hardy, J.; Schott, J. M. Alzheimer's Disease. *Eur. J. Neurol.* **2018**, *25* (1), 59-70.

12. Patterson, C. World Alzheimer Report 2018 - The State of the Art of Dementia Research: New Frontiers. *London: Alzheimer's Disease International* **2018**.

13. Goate, A.; Chartier-Harlin, M. C.; Mullan, M.; Brown, J.; Crawford, F.; Fidani, L.; Giuffra, L.; Haynes, A.; Irving, N.; James, L. Segregation of a Missense Mutation in the Amyloid Precursor Protein Gene with Familial Alzheimer's Disease. *Nature* **1991**, *349* (6311), 704-706.

14. Sherrington, R.; Rogaev, E. I.; Liang, Y.; Rogaeva, E. A.; Levesque, G.; Ikeda, M.; Chi, H.; Lin, C.; Li, G.; Holman, K.; Tsuda, T.; Mar, L.; Foncin, J. F.; Bruni, A. C.; Montesi, M. P.; Sorbi, S.; Rainero, I.; Pinessi, L.; Nee, L.; Chumakov, I.; Pollen, D.; Brookes, A.; Sanseau, P.; Polinsky, R. J.; Wasco, W.; Da Silva, H. A.; Haines, J. L.; Perkicak-Vance, M. A.; Tanzi, R. E.; Roses, A. D.; Fraser, P. E.; Rommens, J. M.; St George-Hyslop, P. H. Cloning of a Gene Bearing Missense Mutations in Early-Onset Familial Alzheimer's Disease. *Nature* **1995**, *375* (6534), 754-760.

15. Bateman, R. J.; Aisen, P. S.; De Strooper, B.; Fox, N. C.; Lemere, C. A.; Ringman, J. M.; Salloway, S.; Sperling, R. A.; Windisch, M.; Xiong, C. Autosomal-Dominant Alzheimer's Disease: A Review and Proposal for the Prevention of Alzheimer's Disease. *Alzheimers Res. Ther.* **2011**, *3* (1), 1-13.

16. Corder, E. H.; Saunders, A. M.; Strittmatter, W. J.; Schmechel, D. E.; Gaskell, P. C.; Small, G. W.; Roses, A. D.; Haines, J. L.; Pericak-Vance, M. A. Gene Dose of Apolipoprotein E Type 4 Allele and the Risk of Alzheimer's Disease in Late Onset Families. *Science* **1993**, *261* (5123), 921-923.

17. Saunders, A. M.; Strittmatter, W. J.; Schmechel, D.; George-Hyslop, P. H.; Pericak-Vance, M. A.; Joo, S. H.; Rosi, B. L.; Gusella, J. F.; Crapper-MacLachlan, D. R.; Alberts, M. J. Association of Apolipoprotein E Allele Epsilon 4 with Late-Onset Familial and Sporadic Alzheimer's Disease. *Neurology* **1993**, *43* (8), 1467-1472.

18. Petersen, R. C.; Waring, S. C.; Smith, G. E.; Tangalos, E. G.; Thibodeau, S. N. Predictive Value of ApoE Genotyping in Incipient Alzheimer's Disease. *Ann. N. Y. Acad. Sci.* **1996**, *802* (1), 58-69.

19. Filippini, N.; Zarei, M.; Beckmann, C. F.; Galluzzi, S.; Borsci, G.; Testa, C.; Bonetti, M.; Beltramello, A.; Ghidoni, R.; Benussi, L.; Binetti, G.; Frisoni, G. B. Regional Atrophy of Transcallosal Prefrontal Connections in Cognitively Normal ApoE ε4 Carriers. *Magn. Reson. Imaging* **2009**, *29* (5), 1021-1026.

20. Selkoe, D. J.; Yamazaki, T.; Citron, M.; Podlisny, M. B.; Koo, E. H.; Teplow, D. B.; Haass, C. The Role of APP Processing and Trafficking Pathways in the Formation of Amyloid-β protein. *Ann. N. Y. Acad. Sci.* **1996**, *777* (1), 57-64.

21. Haass, C.; Schlossmacher, M. G.; Hung, A. Y.; Vigo-Pelfrey, C.; Mellon, A.; Ostaszewski, B. L.; Lieberburg, I.; Koo, E. H.; Schenk, D.; Teplow, D. B. Amyloid-β Peptide Is Produced by Cultured Cells During Normal Metabolism. *Nature* **1992**, *359* (6393), 322-325.

22. Seubert, P.; Vigo-Pelfrey, C.; Esch, F.; Lee, M.; Dovey, H.; Davis, D.; Sinha, S.; Schlossmacher, M.; Whaley, J.; Swindlehurst, C. Isolation and Quantification of Soluble Alzheimer's β-Peptide from Biological Fluids. *Nature* **1992**, *359* (6393), 325-327.

23. Shoji, M.; Golde, T. E.; Ghiso, J.; Cheung, T. T.; Estus, S.; Shaffer, L. M.; Cai, X. D.; McKay, D. M.; Tintner, R.; Frangione, B. Production of the Alzheimer Amyloid-β Protein by Normal Proteolytic Processing. *Science* **1992**, *258* (5079), 126-129.

24. Baranello, R. J.; Bharani, K. L.; Padmaraju, V.; Chopra, N.; Lahiri, D. K.; Greig, N. H.; Pappolla, M. A.; Sambamurti, K. Amyloid-β Protein Clearance and Degradation (ABCD) Pathways and Their Role in Alzheimer's Disease. *Curr. Alzheimer Res.* **2015**, *12* (1), 32-46.

25. Glenner, G. G.; Wong, C. W. Alzheimer's Disease: Initial Report of the Purification and Characterization of a Novel Cerebrovascular Amyloid Protein. 1984. *Biochem. Biophys. Res. Commun.* **2012**, *425* (3), 534-539.

26. Thal, D. R.; Walter, J.; Saido, T. C.; Fändrich, M. Neuropathology and Biochemistry of Aβ and Its Aggregates in Alzheimer's Disease. *Acta Neuropathol.* **2015**, *129* (2), 167-182.

27. Kayed, R.; Head, E.; Thompson, J. L.; McIntire, T. M.; Milton, S. C.; Cotman, C. W.; Glabe, C. G. Common Structure of Soluble Amyloid Oligomers Implies Common Mechanism of Pathogenesis. *Science* **2003**, *300* (5618), 486-489.

28. Lesné, S.; Koh, M. T.; Kotilinek, L.; Kayed, R.; Glabe, C. G.; Yang, A.; Gallagher, M.; Ashe, K. H. A Specific Amyloid-β Protein Assembly in the Brain Impairs Memory. *Nature* **2006**, *440* (7082), 352-357.

29. Blennow, K.; Zetterberg, H. Biomarkers for Alzheimer's Disease: Current Status and Prospects for the Future. *J. Intern. Med.* **2018**, *284* (6), 643-663.

30. Olsson, B.; Lautner, R.; Andreasson, U.; Öhrfelt, A.; Portelius, E.; Bjerke, M.; Hölttä, M.; Rosén, C.; Olsson, C.; Strobel, G.; Wu, E.; Dakin, K.; Petzold, M.; Blennow, K.; Zetterberg, H. Csf and Blood Biomarkers for the Diagnosis of Alzheimer's Disease: A Systematic Review and Meta-Analysis. *Lancet Neurol.* **2016**, *15* (7), 673-684.

31. Hardy, J. A.; Higgins, G. A. Alzheimer's Disease: The Amyloid Cascade Hypothesis. *Science* **1992**, *256* (5054), 184-185.

32. Hardy, J.; Selkoe, D. J. The Amyloid Hypothesis of Alzheimer's Disease: Progress and Problems on the Road to Therapeutics. *Science* **2002**, *297* (5580), 353-356.

33. Frautschy, S. A.; Cole, G. M. Why Pleiotropic Interventions Are Needed for Alzheimer's Disease. *Mol. Neurobiol.* **2010**, *41* (2), 392-409.

34. Terry, R. D.; Masliah, E.; Salmon, D. P.; Butters, N.; DeTeresa, R.; Hill, R.; Hansen, L. A.; Katzman, R. Physical Basis of Cognitive Alterations in Alzheimer's Disease: Synapse Loss Is the Major Correlate of Cognitive Impairment. *Ann. Neurol.* **1991**, *30* (4), 572-580.

35. Mortimer, J. A. The Nun Study: Risk Factors for Pathology and Clinical-Pathologic Correlations. *Curr. Alzheimer Res.* **2012**, *9* (6), 621-627.

36. Karran, E.; De Strooper, B. The Amyloid Cascade Hypothesis: Are We Poised for Success or Failure? *J. Neurochem.* **2016**, *139* (2), 237-252.

37. Aisen, P. S.; Gauthier, S.; Ferris, S. H.; Saumier, D.; Haine, D.; Garceau, D.; Duong, A.; Suhy, J.; Oh, J.; Lau, W. C.; Sampalis, J. Tramiprosate in Mild-to-Moderate Alzheimer's Disease - a Randomized, Double-Blind, Placebo-Controlled, Multi-Centre Study (the Alphase Study). *Arch. Med. Sci.* **2011**, *7* (1), 102-111.

38. Green, R. C.; Schneider, L. S.; Amato, D. A.; Beelen, A. P.; Wilcock, G.; Swabb, E. A.; Zavitz, K. H. Effect of Tarenflurbil on Cognitive Decline and Activities of Daily Living in Patients with Mild Alzheimer Disease: A Randomized Controlled Trial. *Jama* **2009**, *302* (23), 2557-2564.

39. Doody, R. S.; Raman, R.; Farlow, M.; Iwatsubo, T.; Vellas, B.; Joffe, S.; Kieburtz, K.; He, F.; Sun, X.; Thomas, R. G.; Aisen, P. S.; Siemers, E.; Sethuraman, G.; Mohs, R. A Phase 3 Trial of Semagacestat for Treatment of Alzheimer's Disease. *N. Engl. J. Med.* **2013**, *369* (4), 341-351.

40. Salloway, S.; Sperling, R.; Fox, N. C.; Blennow, K.; Klunk, W.; Raskind, M.; Sabbagh, M.; Honig, L. S.; Porsteinsson, A. P.; Ferris, S.; Reichert, M.; Ketter, N.; Nejadnik, B.; Guenzler, V.; Miloslavsky, M.; Wang, D.; Lu, Y.; Lull, J.; Tudor, I. C.; Liu, E.; Grundman, M.; Yuen, E.; Black, R.; Brashear, H. R. Two Phase 3 Trials of Bapineuzumab in Mild-to-Moderate Alzheimer's Disease. *N. Engl. J. Med.* **2014**, *370* (4), 322-333.

41. Doody, R. S.; Farlow, M.; Aisen, P. S. Phase 3 Trials of Solanezumab and Bapineuzumab for Alzheimer's Disease. *N. Engl. J. Med.* **2014**, *370* (15), 1459-1460.

42. Selkoe, D. J. Alzheimer Disease and Aducanumab: Adjusting Our Approach. *Nat. Rev. Neurol.* **2019**, *15* (7), 365-366.

43. Budd Haeberlein, S.; O'Gorman, J.; Chiao, P.; Bussière, T.; von Rosenstiel, P.; Tian, Y.; Zhu, Y.; von Hehn, C.; Gheuens, S.; Skordos, L.; Chen, T.; Sandrock, A. Clinical Development of Aducanumab, an Anti-Aβ Human Monoclonal Antibody Being Investigated for the Treatment of Early Alzheimer's Disease. *J. Prev. Alzheimers Dis.* **2017**, *4* (4), 255-263.

44. De Strooper, B.; Karran, E. The Cellular Phase of Alzheimer's Disease. *Cell* **2016**, *164* (4), 603-615.

45. Gao, Y.; Tan, L.; Yu, J. T.; Tan, L. Tau in Alzheimer's Disease: Mechanisms and Therapeutic Strategies. *Curr. Alzheimer Res.* **2018**, *15* (3), 283-300.

46. Binder, L. I.; Frankfurter, A.; Rebhun, L. I. The Distribution of Tau in the Mammalian Central Nervous System. *J. Cell Biol.* **1985**, *101* (4), 1371-1378.

47. Avila, J.; Lucas, J. J.; Perez, M.; Hernandez, F. Role of Tau Protein in Both Physiological and Pathological Conditions. *Physiol. Rev.* **2004**, *84* (2), 361-384.

48. Barron, M.; Gartlon, J.; Dawson, L. A.; Atkinson, P. J.; Pardon, M. C. A State of Delirium: Deciphering the Effect of Inflammation on Tau Pathology in Alzheimer's Disease. *Exp. Gerontol.* **2017**, *94* (2017), 103-107.

49. DeKosky, S. T.; Scheff, S. W. Synapse Loss in Frontal Cortex Biopsies in Alzheimer's Disease: Correlation with Cognitive Severity. *Ann. Neurol.* **1990**, *27* (5), 457-464.

50. Calsolaro, V.; Edison, P. Neuroinflammation in Alzheimer's Disease: Current Evidence and Future directions. *Alzheimers. Dement.* **2016**, *12* (6), 719-732.

51. Streit, W. J.; Mrak, R. E.; Griffin, W. S. Microglia and Neuroinflammation: A Pathological Perspective. *J. Neuroinflammation* **2004**, *1* (1), 1-14.

52. Varnum, M. M.; Ikezu, T. The Classification of Microglial Activation Phenotypes on Neurodegeneration and Regeneration in Alzheimer's Disease Brain. *Arch. Immunol. Ther. Exp.* **2012**, *60* (4), 251-266.

53. Fillit, H.; Ding, W. H.; Buee, L.; Kalman, J.; Altstiel, L.; Lawlor, B.; Wolf-Klein, G. Elevated Circulating Tumor Necrosis Factor Levels in Alzheimer's Disease. *Neurosci. Lett.* **1991**, *129* (2), 318-320.

54. Strauss, S.; Bauer, J.; Ganter, U.; Jonas, U.; Berger, M.; Volk, B. Detection of Interleukin-6 and Alpha 2-Macroglobulin Immunoreactivity in Cortex and Hippocampus of Alzheimer's Disease Patients. *Lab. Invest.* **1992**, *66* (2), 223-230.

55. Hansen, D. V.; Hanson, J. E.; Sheng, M. Microglia in Alzheimer's Disease. *J. Cell. Biol.* **2018**, *217* (2), 459-472.

56. Eikelenboom, P.; Hoozemans, J. J.; Veerhuis, R.; van Exel, E.; Rozemuller, A. J.; van Gool, W. A. Whether, When and How Chronic Inflammation Increases the Risk of Developing Late-Onset Alzheimer's Disease. *Alzheimers Res. Ther.* **2012**, *4* (3), 15-24.

57. Bradt, B. M.; Kolb, W. P.; Cooper, N. R. Complement-Dependent Proinflammatory Properties of the Alzheimer's Disease β-Peptide. *J. Exp. Med.* **1998**, *188* (3), 431-438.

58. Cotman, C. W.; Tenner, A. J.; Cummings, B. J. β-Amyloid Converts an Acute Phase Injury Response to Chronic Injury Responses. *Neurobiol. Aging* **1996**, *17* (5), 723-731.

59. Guo, J. T.; Yu, J.; Grass, D.; de Beer, F. C.; Kindy, M. S. Inflammation-Dependent Cerebral Deposition of Serum Amyloid a Protein in a Mouse Model of Amyloidosis. *J. Neurosci.* **2002**, *22* (14), 5900-5909.

60. Maphis, N.; Xu, G.; Kokiko-Cochran, O. N.; Jiang, S.; Cardona, A.; Ransohoff, R. M.; Lamb, B. T.; Bhaskar, K. Reactive Microglia Drive Tau Pathology and Contribute to the Spreading of Pathological Tau in the Brain. *Brain* **2015**, *138* (6), 1738-1755.

61. Li, Y.; Liu, L.; Barger, S. W.; Griffin, W. S. Interleukin-1 Mediates Pathological Effects of Microglia on Tau Phosphorylation and on Synaptophysin Synthesis in Cortical Neurons through a P38-MAPK Pathway. *J. Neurosci.* **2003**, *23* (5), 1605-1611.

62. Morales, I.; Jiménez, J. M.; Mancilla, M.; Maccioni, R. B. Tau Oligomers and Fibrils Induce Activation of Microglial Cells. *J. Alzheimers Dis.* **2013**, *37* (4), 849-856.

63. Hong, S.; Beja-Glasser, V. F.; Nfonoyim, B. M.; Frouin, A.; Li, S.; Ramakrishnan, S.; Merry, K. M.; Shi, Q.; Rosenthal, A.; Barres, B. A.; Lemere, C. A.; Selkoe, D. J.; Stevens, B. Complement and Microglia Mediate Early Synapse Loss in Alzheimer Mouse Models. *Science* **2016**, *352* (6286), 712-716.

64. Rajendran, L.; Paolicelli, R. C. Microglia-Mediated Synapse Loss in Alzheimer's Disease. *J. Neurosci.* **2018**, *38* (12), 2911-2919.

65. Tonnies, E.; Trushina, E. Oxidative Stress, Synaptic Dysfunction, and Alzheimer's Disease. *J. Alzheimers Dis.* **2017**, *57* (4), 1105-1121.

66. Johri, A.; Beal, M. F. Mitochondrial Dysfunction in Neurodegenerative Diseases. *J. Pharmacol. Exp. Ther.* **2012**, *342* (3), 619-630.

67. De Felice, F. G.; Velasco, P. T.; Lambert, M. P.; Viola, K.; Fernandez, S. J.; Ferreira, S. T.; Klein, W. L. Aβ Oligomers Induce Neuronal Oxidative Stress through an N-Methyl-D-Aspartate Receptor-Dependent Mechanism That Is Blocked by the Alzheimer Drug Memantine. *J. Biol. Chem.* **2007**, *282* (15), 11590-11601.

68. Ferreira-Vieira, T. H.; Guimaraes, I. M.; Silva, F. R.; Ribeiro, F. M. Alzheimer's Disease: Targeting the Cholinergic System. *Curr. Neuropharmacol.* **2016**, *14* (1), 101-115.

69. Armstrong, D. M.; Saper, C. B.; Levey, A. I.; Wainer, B. H.; Terry, R. D. Distribution of Cholinergic Neurons in Rat Brain: Demonstrated by the Immunocytochemical Localization of Choline Acetyltransferase. *J. Comp. Neurol.* **1983**, *216* (1), 53-68.

70. Woolf, N. J.; Butcher, L. L. Cholinergic Systems Mediate Action from Movement to Higher Consciousness. *Behav. Brain Res.* **2011**, *221* (2), 488-498.

71. Gold, P. E. Acetylcholine Modulation of Neural Systems Involved in Learning and Memory. *Neurobiol. Learn. Mem.* **2003**, *80* (3), 194-210.

72. Potter, L. T. Synthesis, Storage and Release of [14C]Acetylcholine in Isolated Rat Diaphragm Muscles. *J. Physiol.* **1970**, *206* (1), 145-166.

73. Potter, P. E.; Hadjiconstantinou, M.; Meek, J. L.; Neff, N. H. Measurement of Acetylcholine Turnover Rate in Brain: An Adjunct to a Simple HPLC Method for Choline and Acetylcholine. *J. Neurochem.* **1984**, *43* (1), 288-290.

74. Augustinsson, K. B.; Nachmansohn, D. Distinction between Acetylcholine-Esterase and Other Choline Ester-Splitting Enzymes. *Science* **1949**, *110* (2847), 98-99.

75. Wilcock, G. K.; Esiri, M. M.; Bowen, D. M.; Smith, C. C. Alzheimer's Disease. Correlation of Cortical Choline Acetyltransferase Activity with the Severity of Dementia and Histological Abnormalities. *J. Neurol. Sci.* **1982**, *57* (2), 407-417.

76. Bartus, R. T.; Dean, R. L., 3rd; Beer, B.; Lippa, A. S. The Cholinergic Hypothesis of Geriatric Memory Dysfunction. *Science* **1982**, *217* (4558), 408-414.

77. Davies, P.; Maloney, A. J. Selective Loss of Central Cholinergic Neurons in Alzheimer's Disease. *Lancet* **1976**, *2* (8000), 1403.

78. Perry, E. K.; Tomlinson, B. E.; Blessed, G.; Perry, R. H.; Cross, A. J.; Crow, T. T. Noradrenergic and Cholinergic Systems in Senile Dementia of Alzheimer Type. *Lancet* **1981**, *2* (8238), 140-149.

79. Raina, P.; Santaguida, P.; Ismaila, A.; Patterson, C.; Cowan, D.; Levine, M.; Booker, L.; Oremus, M. Effectiveness of Cholinesterase Inhibitors and Memantine for Treating Dementia: Evidence Review for a Clinical Practice Guideline. *Ann. Intern. Med.* **2008**, *148* (5), 379-397.

80. Rountree, S. D.; Chan, W.; Pavlik, V. N.; Darby, E. J.; Siddiqui, S.; Doody, R. S. Persistent Treatment with Cholinesterase Inhibitors and/or Memantine Slows Clinical Progression of Alzheimer Disease. *Alzheimers Res. Ther.* **2009**, *1* (2), 7.

81. Tan, C. C.; Yu, J. T.; Wang, H. F.; Tan, M. S.; Meng, X. F.; Wang, C.; Jiang, T.; Zhu, X. C.; Tan, L. Efficacy and Safety of Donepezil, Galantamine, Rivastigmine, and Memantine for the Treatment of Alzheimer's Disease: A Systematic Review and Meta-Analysis. *J. Alzheimers Dis.* **2014**, *41* (2), 615-631.

82. FDA, U.S. Food & Drug Administration. Namzaric (Memantine Hydrochloride Extended Release/Donepezil Hydrochloride) Capsules. Application No.: 206439, Approval Date: 12/23/14.

83. Sun, Y.; Lai, M. S.; Lu, C. J.; Chen, R. C. How Long Can Patients with Mild or Moderate Alzheimer's Dementia Maintain Both the Cognition and the Therapy of Cholinesterase Inhibitors: A National Population-Based Study. *Eur. J. Neurol.* **2008**, *15* (3), 278-283.

84. Campanari, M. L.; Navarrete, F.; Ginsberg, S. D.; Manzanares, J.; Sáez-Valero, J.; García-Ayllón, M. S. Increased Expression of Readthrough Acetylcholinesterase Variants in the Brains of Alzheimer's Disease Patients. *J. Alzheimers Dis.* **2016**, *53* (3), 831-841.

85. Giacobini, E. Cholinergic Function and Alzheimer's Disease. *Int. J. Geriatr. Psychiatry* **2003**, *18* (1), 1-5.

86. Mesulam, M.; Guillozet, A.; Shaw, P.; Quinn, B. Widely Spread Butyrylcholinesterase Can Hydrolyze Acetylcholine in the Normal and Alzheimer Brain. *Neurobiol. Dis.* **2002**, *9* (1), 88-93.

87. Darvesh, S. Butyrylcholinesterase as a Diagnostic and Therapeutic Target for Alzheimer's Disease. *Curr. Alzheimer Res.* **2016**, *13* (10), 1173-1177.

88. Carnevale, D.; De Simone, R.; Minghetti, L. Microglia-Neuron Interaction in Inflammatory and Degenerative Diseases: Role of Cholinergic and Noradrenergic Systems. *CNS Neurol. Disord. Drug Targets* **2007**, *6* (6), 388-397.

89. Wong, T. P.; Debeir, T.; Duff, K.; Cuello, A. C. Reorganization of Cholinergic Terminals in the Cerebral Cortex and Hippocampus in Transgenic Mice Carrying Mutated Presenilin-1 and Amyloid Precursor Protein Transgenes. *J. Neurosci.* **1999**, *19* (7), 2706-2716.

90. Bell, K. F.; Ducatenzeiler, A.; Ribeiro-da-Silva, A.; Duff, K.; Bennett, D. A.; Cuello, A. C. The Amyloid Pathology Progresses in a Neurotransmitter-Specific Manner. *Neurobiol. Aging* **2006**, *27* (11), 1644-1657.

91. Wyss-Coray, T. Ageing, Neurodegeneration and Brain Rejuvenation. *Nature* **2016**, *539* (7628), 180-186.

92. López-Otín, C.; Blasco, M. A.; Partridge, L.; Serrano, M.; Kroemer, G. The Hallmarks of Aging. *Cell* **2013**, *153* (6), 1194-1217.

93. Madabhushi, R.; Pan, L.; Tsai, L. H. DNA Damage and Its Links to Neurodegeneration. *Neuron* **2014**, *83* (2), 266-282.

94. Hou, Y.; Dan, X.; Babbar, M.; Wei, Y.; Hasselbalch, S. G.; Croteau, D. L.; Bohr, V. A. Ageing as a Risk Factor for Neurodegenerative Disease. *Nat. Rev. Neurol.* **2019**, *15* (10), 565-581.

95. He, N.; Jin, W. L.; Lok, K. H.; Wang, Y.; Yin, M.; Wang, Z. J. Amyloid-β(1-42) Oligomer Accelerates Senescence in Adult Hippocampal Neural Stem/Progenitor Cells Via Formylpeptide Receptor 2. *Cell Death Dis.* **2013**, *4* (11), 924-934.

96. Musi, N.; Valentine, J. M.; Sickora, K. R.; Baeuerle, E.; Thompson, C. S.; Shen, Q.; Orr, M. E. Tau Protein Aggregation Is Associated with Cellular Senescence in the Brain. *Aging cell* **2018**, *17* (6), e12840.

97. Kroemer, G.; Galluzzi, L.; Brenner, C. Mitochondrial Membrane Permeabilization in Cell Death. *Physiol. Rev.* **2007**, *87* (1), 99-163.

98. Green, D. R.; Galluzzi, L.; Kroemer, G. Mitochondria and the Autophagy-Inflammation-Cell Death Axis in Organismal Aging. *Science* **2011**, *333* (6046), 1109-1112.

99. Kim, H. G.; Oh, M. S. Herbal Medicines for the Prevention and Treatment of Alzheimer's Disease. *Curr. Pharm. Des.* **2012**, *18* (1), 57-75.

100. Di Paolo, M.; Papi, L.; Gori, F.; Turillazzi, E. Natural Products in Neurodegenerative Diseases: A Great Promise but an Ethical Challenge. *Int. J. Mol. Sci.* **2019**, *20* (20), 5170.

101. Pohl, F.; Kong Thoo Lin, P. The Potential Use of Plant Natural Products and Plant Extracts with Antioxidant Properties for the Prevention/Treatment of Neurodegenerative Diseases: In Vitro, in Vivo and Clinical Trials. *Molecules* **2018**, *23* (12), 3283-3313.

102. Xie, H.; Wang, J. R.; Yau, L. F.; Liu, Y.; Liu, L.; Han, Q. B.; Zhao, Z.; Jiang, Z. H. Quantitative Analysis of the Flavonoid Glycosides and Terpene Trilactones in the Extract of Ginkgo Biloba and Evaluation of Their Inhibitory Activity Towards Fibril Formation of β-Amyloid Peptide. *Molecules* **2014**, *19* (4), 4466-4478.

103. Tan, M. S.; Yu, J. T.; Tan, C. C.; Wang, H. F.; Meng, X. F.; Wang, C.; Jiang, T.; Zhu, X. C.; Tan, L. Efficacy and Adverse Effects of Ginkgo Biloba for Cognitive Impairment and Dementia: A Systematic Review and Meta-Analysis. *J. Alzheimers Dis.* **2015**, *43* (2), 589-603.

104. Rapp, M.; Burkart, M.; Kohlmann, T.; Bohlken, J. Similar Treatment Outcomes with Ginkgo Biloba Extract Egb 761 and Donepezil in Alzheimer's Dementia in Very Old Age: A Retrospective Observational Study. *Int. J. Clin. Pharmacol. Ther.* **2018**, *56* (3), 130-133.

105. Kelsey, N. A.; Wilkins, H. M.; Linsemann, D. A. Nutraceuticals Antioxidants as Novel Neuroprotective Agents. *Molecules* **2010**, *15* (11), 7792-7814.

106. Grosso, C.; Valentão, P.; Ferreres, F.; Andrade, P. B. The Use of Flavonoids in Central Nervous System Disorders. *Curr. Med. Chem.* **2013**, *20* (37), 4694-4719.

107. Spencer, J. P.; Abd el Mohsen, M. M.; Rice-Evans, C. Cellular Uptake and Metabolism of Flavonoids and Their Metabolites: Implications for Their Bioactivity. *Arch. Biochem. Biophys.* **2004**, *423* (1), 148-161.

108. Cassidy, A.; Minihane, A. M. The Role of Metabolism (and the Microbiome) in Defining the Clinical Efficacy of Dietary Flavonoids. *Am. J. Clin. Nutr.* **2017**, *105* (1), 10-22.

109. de Andrade Teles, R. B.; Diniz, T. C.; Costa Pinto, T. C.; de Oliveira Junior, R. G.; Gama, E. S. M.; de Lavor, E. M.; Fernandes, A. W. C.; de Oliveira, A. P.; de Almeida Ribeiro, F. P. R.; da Silva, A. A. M.; Cavalcante, T. C. F.; Quintans Junior, L. J.; da Silva Almeida, J. R. G. Flavonoids as Therapeutic Agents in Alzheimer's and Parkinson's Diseases: A Systematic Review of Preclinical Evidences. *Oxid. Med. Cell. Longevity* **2018**, *2018* (1), 7043213.

110. Ishige, K.; Schubert, D.; Sagara, Y. Flavonoids Protect Neuronal Cells from Oxidative Stress by Three Distinct Mechanisms. *Free Radic. Biol. Med.* **2001**, *30* (4), 433-446.

111. Chen, L.; Teng, H.; Jia, Z.; Battino, M.; Miron, A.; Yu, Z.; Cao, H.; Xiao, J. Intracellular Signaling Pathways of Inflammation Modulated by Dietary Flavonoids: The Most Recent Evidence. *Crit. Rev. Food Sci. Nutr.* **2018**, *58* (17), 2908-2924.

112. Spencer, J. P.; Vafeiadou, K.; Williams, R. J.; Vauzour, D. Neuroinflammation: Modulation by Flavonoids and Mechanisms of Action. *Mol. Aspects Med.* **2012**, *33* (1), 83-97.

113. Ben Hmidene, A.; Hanaki, M.; Murakami, K.; Irie, K.; Isoda, H.; Shigemori, H. Inhibitory Activities of Antioxidant Flavonoids from Tamarix Gallica on Amyloid Aggregation Related to Alzheimer's and Type 2 Diabetes Diseases. *Biol. Pharm. Bull.* **2017**, *40* (2), 238-241.

114. Sato, M.; Murakami, K.; Uno, M.; Nakagawa, Y.; Katayama, S.; Akagi, K.; Masuda, Y.; Takegoshi, K.; Irie, K. Site-Specific Inhibitory Mechanism for Amyloid β42 Aggregation by Catechol-Type Flavonoids Targeting the Lys Residues. *J. Biol. Chem.* **2013**, *288* (32), 23212-23224.

115. Currais, A.; Farrokhi, C.; Dargusch, R.; Armando, A.; Quehenberger, O.; Schubert, D.; Maher P. Fisetin Reduces the Impact of Aging on Behavior and Physiology in the Rapid Aging Samp8 Mouse. *J. Gerontol.* **2018**, *73* (3), 299-307.

116. Maher, P.; Akaishi, T.; Abe, K. Flavonoid Fisetin Promotes Erk-Dependent Long-Term Potentiation and Enhances Memory. *Proc. Natl. Acad. Sci. U.S.A.* **2006**, *103* (44), 16568-16573.

117. Currais, A.; Chiruta, C.; Goujon-Svrzic, M.; Costa, G.; Santos, T.; Batista, M. T.; Paiva, J.; do Ceu Madureira, M.; Maher, P. Screening and Identification of Neuroprotective Compounds Relevant to Alzheimers Disease from Medicinal Plants of S. Tome E Principe. *J. Ethnopharmacol.* **2014**, *155* (1), 830-840.

118. Schubert, D.; Maher, P. An Alternative Approach to Drug Discovery for Alzheimer's Disease Dementia. *Future Med. Chem.* **2012**, *4* (13), 1681-1688.

119. Sagara, Y.; Vanhnasy, J.; Maher, P. Induction of PC12 Cell Differentiation by Flavonoids Is Dependent Upon Extracellular Signal-Regulated Kinase Activation. *J. Neurochem.* **2004**, *90* (5), 1144-1155.

120. Sopher, B. L.; Fukuchi, K.; Smith, A. C.; Leppig, K. A.; Furlong, C. E.; Martin, G. M. Cytotoxicity Mediated by Conditional Expression of a Carboxyl-Terminal Derivative of the β-Amyloid Precursor Protein. *Mol. Brain. Res.* **1994**, *26* (1), 207-217.

121. Tan, S.; Schubert, D.; Maher, P. Oxytosis: A Novel Form of Programmed Cell Death. *Curr. Top. Med. Chem.* **2001**, *1* (6), 497-506.

122. Davis, J. B.; Maher, P. Protein Kinase C Activation Inhibits Glutamate-Induced Cytotoxicity in a Neuronal Cell Line. *Brain Res.* **1994**, *652* (1), 169-173.

123. Murphy, T. H.; Miyamoto, M.; Sastre, A.; Schnaar, R. L.; Coyle, J. T. Glutamate Toxicity in a Neuronal Cell Line Involves Inhibition of Cystine Transport Leading to Oxidative Stress. *Neuron* **1989**, *2* (6), 1547-1558.

124. Lewerenz, J.; Ates, G.; Methner, A.; Conrad, M.; Maher, P. Oxytosis/Ferroptosis-(Re-) Emerging Roles for Oxidative Stress-Dependent Non-Apoptotic Cell Death in Diseases of the Central Nervous System. *Front. Neurosci.* **2018**, *2018* (12), 214.

125. Maher, P.; van Leyen, K.; Dey, P. N.; Honrath, B.; Dolga, A.; Methner, A. The Role of Ca(2+) in Cell Death Caused by Oxidative Glutamate Toxicity and Ferroptosis. *Cell Calcium* **2018**, *70* (2018), 47-55.

126. Saxena, U. Bioenergetics Failure in Neurodegenerative Diseases: Back to the Future. *Expert Opin. Ther. Targets* **2012**, *16* (4), 351-354.

127. Warren, R. E.; Frier, B. M. Hypoglycaemia and Cognitive Function. *Diabetes Obes. Metab.* **2005**, *7* (5), 493-503.

128. Maher, P.; Salgado, K. F.; Zivin, J. A.; Lapchak, P. A. A Novel Approach to Screening for New Neuroprotective Compounds for the Treatment of Stroke. *Brain Res.* **2007**, *1173* (2007), 117-125.

129. Schain, M.; Kreisl, W. C. Neuroinflammation in Neurodegenerative Disorders - a Review. *Curr. Neurol. Neurosci. Rep.* **2017**, *17* (3), 25-37.

130. Wyss-Coray, T.; Rogers, J. Inflammation in Alzheimer Disease - a Brief Review of the Basic Science and Clinical Literature. *Cold Spring Harbor Perspect. Med.* **2012**, *2* (1), 6346-6369.

131. Tanaka, M.; Saito, S.; Inoue, T.; Satoh-Asahara, N.; Ihara, M. Novel Therapeutic Potentials of Taxifolin for Amyloid-β-Associated Neurodegenerative Diseases and Other Diseases: Recent Advances and Future Perspectives. *Int. J. Mol. Sci.* **2019**, *20* (9), 2139.

132. Schramm, S.; Huang, G.; Gunesch, S.; Lang, F.; Roa, J.; Högger, P.; Sabaté, R.; Maher, P.; Decker, M. Regioselective Synthesis of 7-*O*-Esters of the Flavonolignan Silibinin and SARs

Lead to Compounds with Overadditive Neuroprotective Effects. *Eur. J. Med. Chem.* **2018**, *146* (2018), 93-107.

133. Darras, F. H.; Kling, B.; Sawatzky, E.; Heilmann, J.; Decker, M. Cyclic Acyl Guanidines Bearing Carbamate Moieties Allow Potent and Dirigible Cholinesterase Inhibition of Either Acetyl- or Butyrylcholinesterase. *Bioorg. Med. Chem.* **2014**, *22* (17), 5020-5034.

134. Sawatzky, E.; Wehle, S.; Kling, B.; Wendrich, J.; Bringmann, G.; Sotriffer, C. A.; Heilmann, J.; Decker, M. Discovery of Highly Selective and Nanomolar Carbamate-Based Butyrylcholinesterase Inhibitors by Rational Investigation into Their Inhibition Mode. *J. Med. Chem.* **2016**, *59* (5), 2067-2082.

135. Gazak, R.; Sedmera, P.; Vrbacky, M.; Vostalova, J.; Drahota, Z.; Marhol, P.; Walterova, D.; Kren, V. Molecular Mechanisms of Silybin and 2,3-Dehydrosilybin Antiradical Activity - Role of Individual Hydroxyl Groups. *Free Radic. Biol. Med.* **2009**, *46* (6), 745-758.

136. Gunesch, S.; Schramm, S.; Decker, M. Natural Antioxidants in Hybrids for the Treatment of Neurodegenerative Diseases: A Successful Strategy? *Future Med. Chem.* **2017**, *9* (8), 711-713.

137. Baell, J. B. Feeling Nature's Pains: Natural Products, Natural Product Drugs, and Pan Assay Interference Compounds (PAINS). *J. Nat. Prod.* **2016**, *79* (3), 616-628.

138. Gay, N. H.; Phopin, K.; Suwanjang, W.; Songtawee, N.; Ruankham, W.; Wongchitrat, P.; Prachayasittikul, S.; Prachayasittikul, V. Neuroprotective Effects of Phenolic and Carboxylic Acids on Oxidative Stress-Induced Toxicity in Human Neuroblastoma SH-SY5Y Cells. *Neurochem. Res.* **2018**, *43* (3), 619-636.

139. Yan, J. J.; Cho, J. Y.; Kim, H. S.; Kim, K. L.; Jung, J. S.; Huh, S. O.; Suh, H. W.; Kim, Y. H.; Song, D. K. Protection against β-Amyloid Peptide Toxicity in Vivo with Long-Term Administration of Ferulic Acid. *Br. J. Pharmacol.* **2001**, *133* (1), 89-96.

140. Mori, T.; Koyama, N.; Guillot-Sestier, M. V.; Tan, J.; Town, T. Ferulic Acid Is a Nutraceutical β-Secretase Modulator That Improves Behavioral Impairment and Alzheimer-Like Pathology in Transgenic Mice. *PloS One* **2013**, *8* (2), e55774.

141. Chakrabarti, S.; Jana, M.; Roy, A.; Pahan, K. Upregulation of Suppressor of Cytokine Signaling 3 in Microglia by Cinnamic Acid. *Curr. Alzheimer Res.* **2018**, *15* (10), 894-904.

142. Schramm, S.; Gunesch, S.; Lang, F.; Saedtler, M.; Meinel, L.; Högger, P.; Decker, M. Investigations into Neuroprotectivity, Stability, and Water Solubility of 7-*O*-Cinnamoylsilibinin, Its Hemisuccinate and Dehydro Derivatives. *Arch. Pharm.* **2018**, *351* (11), e1800206.

143. Ginex, T.; Trius, M.; Luque, F. J. Computational Study of the Aza-Michael Addition of the Flavonoid (+)-Taxifolin in the Inhibition of β-Amyloid Fibril Aggregation. *Chem. Eur. J.* **2018**, *24* (22), 5813-5824.

144. Vrba, J.; Gazak, R.; Kuzma, M.; Papouskova, B.; Vacek, J.; Weiszenstein, M.; Kren, V.; Ulrichova, J. A Novel Semisynthetic Flavonoid 7-*O*-Galloyltaxifolin Upregulates Heme Oxygenase-1 in Raw264.7 Cells Via MAPK/Nrf2 Pathway. *J. Med. Chem.* **2013**, *56* (3), 856-866.

145. Inoue, T.; Saito, S.; Tanaka, M.; Yamakage, H.; Kusakabe, T.; Shimatsu, A.; Ihara, M.; Satoh-Asahara, N. Pleiotropic Neuroprotective Effects of Taxifolin in Cerebral Amyloid Angiopathy. *Proc. Natl. Acad. Sci. U.S.A.* **2019**, *116* (20), 10031-10038.

146. Sgarbossa, A.; Giacomazza, D.; di Carlo, M. Ferulic Acid: A Hope for Alzheimer's Disease Therapy from Plants. *Nutrients* **2015**, *7* (7), 5764-5782.

147. Dahlin, J. L.; Nissink, J. W.; Strasser, J. M.; Francis, S.; Higgins, L.; Zhou, H.; Zhang, Z.; Walters, M. A. Pains in the Assay: Chemical Mechanisms of Assay Interference and

Promiscuous Enzymatic Inhibition Observed During a Sulfhydryl-Scavenging HTS. *J. Med. Chem.* **2015**, *58* (5), 2091-2113.

148. Currais, A.; Maher, P. Functional Consequences of Age-Dependent Changes in Glutathione Status in the Brain. *Antioxid. Redox Signal* **2013**, *19* (8), 813-822.

149. Yang, W. S.; Kim, K. J.; Gaschler, M. M.; Patel, M.; Shchepinov, M. S.; Stockwell, B. R. Peroxidation of Polyunsaturated Fatty Acids by Lipoxygenases Drives Ferroptosis. *Proc. Natl. Acad. Sci. U.S.A.* **2016**, *113* (34), 4966-4975.

150. Dolles, D.; Hoffmann, M.; Gunesch, S.; Marinelli, O.; Moller, J.; Santoni, G.; Chatonnet, A.; Lohse, M. J.; Wittmann, H. J.; Strasser, A.; Nabissi, M.; Maurice, T.; Decker, M. Structure-Activity Relationships and Computational Investigations into the Development of Potent and Balanced Dual-Acting Butyrylcholinesterase Inhibitors and Human Cannabinoid Receptor 2 Ligands with Pro-Cognitive in Vivo Profiles. *J. Med. Chem.* **2018**, *61* (4), 1646-1663.

151. Lahmy, V.; Meunier, J.; Malmstrom, S.; Naert, G.; Givalois, L.; Kim, S. H.; Villard, V.; Vamvakides, A.; Maurice, T. Blockade of Tau Hyperphosphorylation and Aβ1-42 Generation by the Aminotetrahydrofuran Derivative Anavex2-73, a Mixed Muscarinic and Sigma1 Receptor Agonist, in a Nontransgenic Mouse Model of Alzheimer's Disease. *Neuropsychopharmacol.* **2013**, *38* (9), 1706-1723.

152. Maurice, T.; Lockhart, B. P.; Privat, A. Amnesia Induced in Mice by Centrally Administered β-Amyloid Peptides Involves Cholinergic Dysfunction. *Brain Res.* **1996**, *706* (2), 181-193.

153. Yamada, K.; Tanaka, T.; Han, D.; Senzaki, K.; Kameyama, T.; Nabeshima, T. Protective Effects of Idebenone and Alpha-Tocopherol on β-Amyloid-(1-42)-Induced Learning and Memory Deficits in Rats: Implication of Oxidative Stress in β-Amyloid-Induced Neurotoxicity in Vivo. *Eur. J. Neurosci.* **1999**, *11* (1), 83-90.

154. Wang, Y.; Wang, Q.; Bao, X.; Ding, Y.; Shentu, J.; Cui, W.; Chen, X.; Wei, X.; Xu, S. Taxifolin Prevents β-Amyloid-Induced Impairments of Synaptic Formation and Deficits of Memory Via the Inhibition of Cytosolic Phospholipase A2/Prostaglandin E2 Content. *Metab. Brain Dis.* **2018**, *33* (4), 1069-1079.

155. Park, S. Y.; Kim, H. Y.; Park, H. J.; Shin, H. K.; Hong, K. W.; Kim, C. D. Concurrent Treatment with Taxifolin and Cilostazol on the Lowering of β-Amyloid Accumulation and Neurotoxicity Via the Suppression of P-Jak2/P-Stat3/Nf-KappaB/Bace1 Signaling Pathways. *PloS One* **2016**, *11* (12), e0168286.

156. Meunier, J.; Villard, V.; Givalois, L.; Maurice, T. The Gamma-Secretase Inhibitor 2-[(1*R*)-1-[(4-Chlorophenyl)Sulfonyl](2,5-Difluorophenyl) Amino]Ethyl-5-Fluorobenzenebutanoic Acid (Bms-299897) Alleviates Aβ1-42 Seeding and Short-Term Memory Deficits in the Aβ25-35 Mouse Model of Alzheimer's Disease. *Eur. J. Pharmacol.* **2013**, *698* (3), 193-199.

157. Huang, D.; Ou, B.; Prior, R. L. The Chemistry Behind Antioxidant Capacity Assays. *J. Agric. Food Chem.* **2005**, *53* (6), 1841-1856.

158. Liu, Y.; Nguyen, M.; Robert, A.; Meunier, B. Metal Ions in Alzheimer's Disease: A Key Role or Not? *Acc. Chem. Res.* **2019**, *52* (7), 2026-2035.

159. Speers, A. E.; Adam, G. C.; Cravatt, B. F. Activity-Based Protein Profiling in Vivo Using a Copper(I)-Catalyzed Azide-Alkyne [3 + 2] Cycloaddition. *J. Am. Chem. Soc.* **2003**, *125* (16), 4686-4687.

160. Böttcher, T.; Pitscheider, M.; Sieber, S. A. Natural Products and Their Biological Targets: Proteomic and Metabolomic Labeling Strategies. *Angew. Chem. Int. Ed.* **2010**, *49* (15), 2680-2698.

161. Chen, X.; Wong, Y. K.; Wang, J.; Zhang, J.; Lee, Y. M.; Shen, H. M.; Lin, Q.; Hua, Z. C. Target Identification with Quantitative Activity Based Protein Profiling (ABPP). *Proteomics*. **2017**, *17* (3), 1600212.

162. Su, C.; Liu, Z.; Wang, Y.; Wang, Y.; Song, E.; Song, Y. The Electrophilic Character of Quinones Is Essential for the Suppression of Bach1. *Toxicology* **2017**, *387* (2017), 17-26.

163. Gunesch, S.; Hoffmann, M.; Kiermeier, C.; Fischer, W.; Pinto, A. F. M.; Maurice, T.; Maher, P.; Decker, M. 7-*O*-Esters of Taxifolin with Pronounced and Overadditive Effects in Neuroprotection, Anti-Neuroinflammation, and Amelioration of Short-Term Memory Impairment in Vivo. *Redox Biol.* **2020**, *29* (2020), 101378.

164. Rai, S. N.; Dilnashin, H.; Birla, H.; Singh, S. S.; Zahra, W.; Rathore, A. S.; Singh, B. K.; Singh, S. P. The Role of PI3K/Akt and Erk in Neurodegenerative Disorders. *Neurotox. Res.* **2019**, *35* (3), 775-795.

165. Hensley, K.; Floyd, R. A.; Zheng, N. Y.; Nael, R.; Robinson, K. A.; Nguyen, X.; Pye, Q. N.; Stewart, C. A.; Geddes, J.; Markesbery, W. R.; Patel, E.; Johnson, G. V.; Bing, G. P38 Kinase Is Activated in the Alzheimer's Disease Brain. *J. Neurochem.* **1999**, *72* (5), 2053-2058.

166. Sun, A.; Liu, M.; Nguyen, X. V.; Bing, G. P38 MAP Kinase Is Activated at Early Stages in Alzheimer's Disease Brain. *Exp. Neurol.* **2003**, *183* (2), 394-405.

167. Schnoder, L.; Hao, W.; Qin, Y.; Liu, S.; Tomic, I.; Liu, X.; Fassbender, K.; Liu, Y. Deficiency of Neuronal P38α MAPK Attenuates Amyloid Pathology in Alzheimer Disease Mouse and Cell Models through Facilitating Lysosomal Degradation of Bace1. *J. Biol.* **2016**, *291* (5), 2067-2079.

168. Colucci-D'Amato, L.; Perrone-Capano, C.; di Porzio, U. Chronic Activation of Erk and Neurodegenerative Diseases. *BioEssays* **2003**, *25* (11), 1085-1095.

169. Jeong, S. Molecular and Cellular Basis of Neurodegeneration in Alzheimer's Disease. *Mol. Cells* **2017**, *40* (9), 613-620.

170. Brand, M. D.; Pakay, J. L.; Ocloo, A.; Kokoszka, J.; Wallace, D. C.; Brookes, P. S.; Cornwall, E. J. The Basal Proton Conductance of Mitochondria Depends on Adenine Nucleotide Translocase Content. *Biochem. J.* **2005**, *392* (2), 353-362.

171. Wang, W.; Zhao, F.; Ma, X.; Perry, G.; Zhu, X. Mitochondria Dysfunction in the Pathogenesis of Alzheimer's Disease: Recent Advances. *Mol. Neurodegen.* **2020**, *15* (30), 1-22.

172. Cadonic, C.; Sabbir, M. G.; Albensi, B. C. Mechanisms of Mitochondrial Dysfunction in Alzheimer's Disease. *Mol. Neurobiol.* **2016**, *53* (9), 6078-6090.

173. Bobba, A.; Amadoro, G.; Azzariti, A.; Pizzuto, R.; Atlante, A. Extracellular ADP Prevents Neuronal Apoptosis Via Activation of Cell Antioxidant Enzymes and Protection of Mitochondrial ANT-1. *Biochim. Biophys. Acta* **2014**, *1837* (8), 1338-1349.

174. Bauer, M. K.; Schubert, A.; Rocks, O.; Grimm, S. Adenine Nucleotide Translocase-1, a Component of the Permeability Transition Pore, Can Dominantly Induce Apoptosis. *J. Cell Biol.* **1999**, *147* (7), 1493-1502.

175. Chevrollier, A.; Loiseau, D.; Reynier, P.; Stepien, G. Adenine Nucleotide Translocase 2 Is a Key Mitochondrial Protein in Cancer Metabolism. *Biochim. Biophys. Acta* **2011**, *1807* (6), 562-567.

176. Liu, Y.; Schubert, D. The Specificity of Neuroprotection by Antioxidants. *J. Biomed. Sci.* **2009**, *16* (98), 1-14.

177. Tan, S.; Sagara, Y.; Liu, Y.; Maher, P.; Schubert, D. The Regulation of Reactive Oxygen Species Production During Programmed Cell Death. *J. Cell Biol.* **1998**, *141* (6), 1423-1432.

178. Ortega, R.; García, N. The Flavonoid Quercetin Induces Changes in Mitochondrial Permeability by Inhibiting Adenine Nucleotide Translocase. *J. Bioenerg. Biomembr.* **2009**, *41* (1), 41-47.

179. Unterberger, U.; Höftberger, R.; Gelpi, E.; Flicker, H.; Budka, H.; Voigtländer, T. Endoplasmic Reticulum Stress Features Are Prominent in Alzheimer Disease but Not in Prion Diseases in Vivo. *J. Neuropathol. Exp. Neurol.* **2006**, *65* (4), 348-357.

180. Krajnak, K.; Dahl, R. A New Target for Alzheimer's Disease: A Small Molecule SERCA Activator Is Neuroprotective in Vitro and Improves Memory and Cognition in APP/PS1 Mice. *Bioorg. Med. Chem. Lett.* **2018**, *28* (9), 1591-1594.

181. Maher, P. How Fisetin Reduces the Impact of Age and Disease on CNS Function. *Front. Biosci.* **2015**, *7* (2015), 58-82.

182. Currais, A.; Prior, M.; Dargusch, R.; Armando, A.; Ehren, J.; Schubert, D.; Quehenberger, O.; Maher, P. Modulation of p25 and Inflammatory Pathways by Fisetin Maintains Cognitive Function in Alzheimer's Disease Transgenic Mice. *Aging Cell* **2014**, *13* (2), 379-390.

183. Imai, K.; Nakanishi, I.; Ohkubo, K.; Ohno, A.; Mizuno, M.; Fukuzumi, S.; Matsumoto, K. I.; Fukuhara, K. Synthesis and Radical-Scavenging Activity of C-Methylated Fisetin Analogues. *Bioorg. Med. Chem.* **2019**, *27* (8), 1720-1727.

184. Chiruta, C.; Schubert, D.; Dargusch, R.; Maher, P. Chemical Modification of the Multitarget Neuroprotective Compound Fisetin. *J. Med. Chem.* **2012**, *55* (1), 378-389.

185. Mattarei, A.; Biasutto, L.; Rastrelli, F.; Garbisa, S.; Marotta, E.; Zoratti, M.; Paradisi, C. Regioselective *O*-Derivatization of Quercetin Via Ester Intermediates. An Improved Synthesis of Rhamnetin and Development of a New Mitochondriotropic Derivative. *Molecules* **2010**, *15* (7), 4722-4736.

186. Li, M.; Han, X.; Yu, B. Facile Synthesis of Flavonoid 7-*O*-Glycosides. *J. Org. Chem.* **2003**, *68* (17), 6842-6845.

187. Shi, Z. H.; Li, N. G.; Tang, Y. P.; Shi, Q. P.; Tang, H.; Li, W.; Zhang, X.; Fu, H. A.; Duan, J. A. Biological Evaluation and SAR Analysis of *O*-Methylated Analogs of Quercetin as Inhibitors of Cancer Cell Proliferation. *Drug Dev. Res.* **2014**, *75* (7), 455-462.

188. Costa, L. G.; Garrick, J. M.; Roque, P. J.; Pellacani, C. Mechanisms of Neuroprotection by Quercetin: Counteracting Oxidative Stress and More. *Oxid. Med. Cell. Longevity* **2016**, *2016* (1), 2986796.

189. Bomprezzi, R. Dimethyl Fumarate in the Treatment of Relapsing-Remitting Multiple Sclerosis: An Overview. *Ther. Adv. Neurol. Disord.* **2015**, *8* (1), 20-30.

190. Campolo, M.; Casili, G.; Lanza, M.; Filippone, A.; Paterniti, I.; Cuzzocrea, S.; Esposito, E. Multiple Mechanisms of Dimethyl Fumarate in Amyloid-β-Induced Neurotoxicity in Human Neuronal Cells. *J. Cell. Mol. Med.* **2018**, *22* (2), 1081-1094.

191. Hofmann, J.; Fayez, S.; Scheiner, M.; Hoffmann, M.; Oerter, S.; Appelt-Menzel, A.; Maher, P.; Maurice, T.; Bringmann, G.; Decker, M. Sterubin: Enantioresolution and Configurational Stability, Enantiomeric Purity in Nature, and Neuroprotective Activity in Vitro and in Vivo. *Chem. Eur. J.* **2020**, *26* (32), 7299-7308.

192. Darras, F. H.; Kling, B.; Heilmann, J.; Decker, M. Neuroprotective Tri- and Tetracyclic BChE Inhibitors Releasing Reversible Inhibitors Upon Carbamate Transfer. *ACS Med. Chem. Lett.* **2012**, *3* (11), 914-919.

193. Hoffmann, M.; Stiller, C.; Endres, E.; Scheiner, M.; Gunesch, S.; Sotriffer, C.; Maurice, T.; Decker, M. Highly Selective Butyrylcholinesterase Inhibitors with Tunable Duration of Action by Chemical Modification of Transferable Carbamate Units Exhibit Pronounced

Neuroprotective Effect in an Alzheimer's Disease Mouse Model. *J. Med. Chem.* **2019**, *62* (20), 9116-9140.

194. Ng, Y. P.; Or, T. C.; Ip, N. Y. Plant Alkaloids as Drug Leads for Alzheimer's Disease. *Neurochem. Int.* **2015**, *89* (2015), 260-270.

195. Jia, S.; Hu, C. Pharmacological Effects of Rutaecarpine as a Cardiovascular Protective Agent. *Molecules* **2010**, *15* (3), 1873-1881.

196. Tian, K. M.; Li, J. J.; Xu, S. W. Rutaecarpine: A Promising Cardiovascular Protective Alkaloid from Evodia Rutaecarpa (Wu Zhu Yu). *Pharmacol. Res.* **2019**, *141* (2019), 541-550.

197. Yuan, S. M.; Gao, K.; Wang, D. M.; Quan, X. Z.; Liu, J. N.; Ma, C. M.; Qin, C.; Zhang, L. F. Evodiamine Improves Congnitive Abilities in SAMP8 and APPswe/PS1ΔE9 Transgenic Mouse Models of Alzheimer's Disease. *Acta Pharmacol. Sin.* **2011**, *32* (3), 295-302.

198. Zhang, Y.; Wang, J.; Wang, C.; Li, Z.; Liu, X.; Zhang, J.; Lu, J.; Wang, D. Pharmacological Basis for the Use of Evodiamine in Alzheimer's Disease: Antioxidation and Antiapoptosis. *Int. J. Mol. Sci.* **2018**, *19* (5), 1527.

199. Park, C. H.; Kim, S. H.; Choi, W.; Lee, Y. J.; Kim, J. S.; Kang, S. S.; Suh, Y. H. Novel Anticholinesterase and Antiamnesic Activities of Dehydroevodiamine, a Constituent of Evodia Rutaecarpa. *Planta Med.* **1996**, *62* (5), 405-409.

200. Park, C. H.; Lee, Y.-J.; Lee, S. H.; Choi, S. H.; Kim, H.-S.; Jeong, S.-J.; Kim, S. S.; Suh, Y.-H. Dehydroevodiamine HCl Prevents Impairment of Learning and Memory and Neuronal Loss in Rat Models of Cognitive Disturbance. *J. Neurochem.* **2000**, *74* (1), 244-253.

201. Wang, H. H.; Chou, C. J.; Liao, J. F.; Chen, C. F. Dehydroevodiamine Attenuates β-Amyloid Peptide-Induced Amnesia in Mice. *Eur. J. Pharmacol.* **2001**, *413* (2), 221-225.

202. Li, Q.; Yang, H.; Chen, Y.; Sun, H. Recent Progress in the Identification of Selective Butyrylcholinesterase Inhibitors for Alzheimer's Disease. *Eur. J. Med. Chem.* **2017**, *132* (2017), 294-309.

203. Huang, G.; Kling, B.; Darras, F. H.; Heilmann, J.; Decker, M. Identification of a Neuroprotective and Selective Butyrylcholinesterase Inhibitor Derived from the Natural Alkaloid Evodiamine. *Eur. J. Med. Chem.* **2014**, *81* (2014), 15-21.

204. Decker, M. Novel Inhibitors of Acetyl- and Butyrylcholinesterase Derived from the Alkaloids Dehydroevodiamine and Rutaecarpine. *Eur. J. Med. Chem.* **2005**, *40* (3), 305-313.

205. Nakayama, A.; Kogure, N.; Kitajima, M.; Takayama H. Straightforward Asymmetric Total Synthesis of (+)-Evodiamine, a Major Indole Alkaloid in Herbal Medicine "Wu Zhu Yu". *Heterocycles* **2008**, *76* (1), 861-865.

206. Wehle, S.; Espargaró, A.; Sabaté, R.; Decker, M. Investigation into the Stability and Reactivity of the Pentacyclic Alkaloid Dehydroevodiamine and the Benz-Analog Thereof. *Tetrahedron* **2016**, *72* (20), 2535-2543.

207. Beutner, G. L.; Kuethe, J. T.; Yasuda, N. A Practical Method for Preparation of 4-Hydroxyquinolinone Esters. *J. Org. Chem.* **2007**, *72* (18), 7058-7061.

208. Ellman, G. L. A Colorimetric Method for Determining Low Concentrations of Mercaptans. *Arch. Biochem. Biophys.* **1958**, *74* (2), 443-450.

209. Ellman, G. L.; Courtney, K. D.; Andres, V.; Feather-Stone, R. M. A New and Rapid Colorimetric Determination of Acetylcholinesterase Activity. *Biochem. Pharmacol.* **1961**, *7* (2), 88-95.

210. Montanari, S.; Scalvini, L.; Bartolini, M.; Belluti, F.; Gobbi, S.; Andrisano, V.; Ligresti, A.; Di Marzo, V.; Rivara, S.; Mor, M.; Bisi, A.; Rampa, A. Fatty Acid Amide Hydrolase (FAAH),

Acetylcholinesterase (AChE), and Butyrylcholinesterase (BuChE): Networked Targets for the Development of Carbamates as Potential Anti-Alzheimer's Disease Agents. *J. Med. Chem.* **2016**, *59* (13), 6387-6406.

211. Lampl, T.; Crum, J. A.; Davis, T. A.; Milligan, C.; Del Gaizo Moore, V. Isolation and Functional Analysis of Mitochondria from Cultured Cells and Mouse Tissue. *J. Vis. Exp.* **2015**, *97* (2015), 52076.

212. Pierce, E. N.; Piyankarage, S. C.; Dunlap, T.; Litosh, V.; Siklos, M. I.; Wang, Y. T.; Thatcher, G. R. Prodrugs Bioactivated to Quinones Target NF-KB and Multiple Protein Networks: Identification of the Quinonome. *Chem. Res. Toxicol.* **2016**, *29* (7), 1151-1159.

213. Chance, B.; Williams, G. R. Respiratory Enzymes in Oxidative Phosphorylation. I. Kinetics of Oxygen Utilization. *J. Biol. Chem.* **1955**, *217* (1), 383-393.

214. Gerencser, A. A.; Neilson, A.; Choi, S. W.; Edman, U.; Yadava, N.; Oh, R. J.; Ferrick, D. A.; Nicholls, D. G.; Brand, M. D. Quantitative Microplate-Based Respirometry with Correction for Oxygen Diffusion. *Anal. Chem.* **2009**, *81* (16), 6868-6878.

215. Figueira, T. R.; Melo, D. R.; Vercesi, A. E.; Castilho, R. F. Safranine as a Fluorescent Probe for the Evaluation of Mitochondrial Membrane Potential in Isolated Organelles and Permeabilized Cells. *Methods Mol. Biol.* **2012**, *810* (1), 103-117.

216. Naoi, M.; Wu, Y.; Shamoto-Nagai, M.; Maruyama, W. Mitochondria in Neuroprotection by Phytochemicals: Bioactive Polyphenols Modulate Mitochondrial Apoptosis System, Function and Structure. *Int. J. Mol. Sci.* **2019**, *20* (10), 2451.

217. Gao, M.; Yi, J.; Zhu, J.; Minikes, A. M.; Monian, P.; Thompson, C. B.; Jiang, X. Role of Mitochondria in Ferroptosis. *Mol. Cell* **2019**, *73* (2), 354-363.

218. Amadoro, G.; Corsetti, V.; Atlante, A.; Florenzano, F.; Capsoni, S.; Bussani, R.; Mercanti, D.; Calissano, P. Interaction between NH2-Tau Fragment and Aβ in Alzheimer's Disease Mitochondria Contributes to the Synaptic Deterioration. *Neurobiol. Aging* **2012**, *33* (2012), 833-858.

219. Fischer, W.; Currais, A.; Liang, Z.; Pinto, A.; Maher, P. Old Age-Associated Phenotypic Screening for Alzheimer's Disease Drug Candidates Identifies Sterubin as a Potent Neuroprotective Compound from Yerba Santa. *Redox Biol.* **2019**, *21* (2019), 101089.

220. Pebay-Peyroula, E.; Dahout-Gonzales, C.; Kahn, R.; Trézéguet, V.; Lauquin, G. J. M.; Brandolin, G. Structure of Mitochondrial ADP/ATP Carrier in Complex with Carboxyatractyloside. *Nature* **2003**, *426* (6962), 39-44.

221. Ruprecht, J. J.; King, M. S.; Zögg, T.; Aleksandrova, A. A.; Pardon, E.; Crichton, P. G.; Steyaert, J.; Kunji, E. R. S. The Molecular Mechanism of Transport by the Mitochondrial ADP/ATP Carrier. *Cell* **2019**, *176* (3), 435-447.

222. Conseil, G.; Baubichon-Cortay, H.; Dayan, G.; Jault, J. M.; Barron, D.; Di Pietro, A. Flavonoids: A Class of Modulators with Bifunctional Interactions at Vicinal ATP- and Steroid-Binding Sites on Mouse p-Glycoprotein. *Proc. Natl. Acad. Sci. U.S.A.* **1998**, *95* (17), 9831-9836.

223. Schopf, F. H.; Biebl, M. M.; Buchner, J. The Hsp90 Chaperone Machinery. *Nat. Rev. Mol. Cell Biol.* **2017**, *18* (6), 345-360.

224. Zhao, H.; Michaelis, M. L.; Blagg, B. S. Hsp90 Modulation for the Treatment of Alzheimer's Disease. *Adv. Pharmacol.* **2012**, *64* (2012), 1-25.

225. Zhao, H.; Brandt, G. E.; Galam, L.; Matts, R. L.; Blagg, B. S. Identification and Initial SAR of Silybin: An Hsp90 Inhibitor. *Bioorg. Med. Chem. Lett.* **2011**, *21* (9), 2659-2664.

226. Yin, Z.; Henry, E. C.; Gasiewicz, T. A. (-)-Epigallocatechin-3-Gallate Is a Novel Hsp90 Inhibitor. *Biochemistry* **2009**, *48* (2), 336-345.

227. Brodziak-Jarosz, L.; Fujikawa, Y.; Pastor-Flores, D.; Kasikci, S.; Jirasek, P.; Pitzl, S.; Owen, R. W.; Klika, K. D.; Gerhauser, C.; Amslinger, S.; Dick, T. P. A Click Chemistry Approach Identifies Target Proteins of Xanthohumol. *Mol. Nutr. Food Res.* **2016**, *60* (4), 737-748.

228. Howes, R.; Barril, X.; Dymock, B. W.; Grant, K.; Northfield, C. J.; Robertson, A. G.; Surgenor, A.; Wayne, J.; Wright, L.; James, K.; Matthews, T.; Cheung, K. M.; McDonald, E.; Workman, P.; Drysdale, M. J. A Fluorescence Polarization Assay for Inhibitors of Hsp90. *Anal. Biochem.* **2006**, *350* (2), 202-213.

229. Cuyàs, E.; Verdura, S.; Micol, V.; Joven, J.; Bosch-Barrera, J.; Encinar, J. A.; Menendez, J. A. Revisiting Silibinin as a Novobiocin-Like Hsp90 C-Terminal Inhibitor: Computational Modeling and Experimental Validation. *Food Chem. Toxicol.* **2019**, *132* (2019), 110645.

230. Bianchetti, C. M.; Yi, L.; Ragsdale, S. W.; Phillips, G. N., Comparison of Apo- and Heme-Bound Crystal Structures of a Truncated Human Heme Oxygenase-2. *J. Biol. Chem.* **2007**, *282* (52), 37624-37631.

231. Sacchetto, R.; Bertipaglia, I.; Giannetti, S.; Cendron, L.; Mascarello, F.; Damiani, E.; Carafoli, E.; Zanotti, G. Crystal Structure of Sarcoplasmic Reticulum Ca2+-ATPase (SERCA) from Bovine Muscle. *J. Struct. Biol.* **2012**, *178* (1), 38-44.

232. Santos, J. S.; Alvarenga Brizola, V. R.; Granato, D. High-Throughput Assay Comparison and Standardization for Metal Chelating Capacity Screening: A Proposal and Application. *Food Chem.* **2017**, *214* (1), 515-522.

233. Ou, B.; Hampsch-Woodill, M.; Prior, R. L. Development and Validation of an Improved Oxygen Radical Absorbance Capacity Assay Using Fluorescein as the Fluorescent Probe. *J. Agric. Food Chem.* **2001**, *49* (10), 4619-4626.

234. Dávalos, A.; Gómez-Cordovés, C.; Bartolomé, B. Extending Applicability of the Oxygen Radical Absorbance Capacity (ORAC-Fluorescein) Assay. *J. Agric. Food Chem.* **2004**, *52* (1), 48-54.

Abbreviations

7CT	7-*O*-cinnamoyltaxifolin
Aβ	β-amyloid peptide
ABPP	activity-based protein profiling
ACh	acetylcholine
AChE	acetylcholinesterase
AD	Alzheimer's disease
ANOVA	analysis of variance
ANT	adenine nucleotide translocase
APP	amyloid precursor protein
ARE	antioxidant response element
ATP	adenosine triphosphate
Bach1	BTB and CNC homology-1
BChE	butyrylcholinesterase
BKA	bongkrekic acid
Boc_2O	di-*tert*-butyl decarbonate
BSA	bovine serum albumin
BTB	broad complex, tramtrack, bric-a-brac
BTC	butyrylthiocholine
CAA	cerebral amyloid angiopathy
CATR	carboxyatractyloside
cGMP	cyclic guanosine monophosphate
CNC	cap'n'collar
CNS	central nervous system
cpd.	compound
CSA	camphor sulfonic acid
CuAAC	Cu(I)-catalyzed [3+2] azido-alkyne cycloaddition
DHED	dehydroevodiamine chloride
DIPEA	*N,N*-diisopropylethylamine
DMAc	*N,N*-dimethylacetamide
DMF	dimethylformamide
DMSO	dimethylsulfoxide

DPPH	diphenyl-1-picrylhydrazyl
DTNB	5,5'-dithiobis-(2-nitrobenzoic acid)
EGCG	Epigallocatechin-3-gallate
ELISA	enzyme-linked immunosorbent assay
ER	endoplasmic reticulum
ETC	electron transport chain
fAD	familial Alzheimer's disease
FRAP	ferric ion reducing antioxidant parameter
GFP	green fluorescent protein
GPx4	Glutathione peroxidase 4
GSH	glutathione
GSK3β	glycogen synthase kinase 3 β
h	human
HBTU	2-(1*H*-benzotriazol-1-yl)-1,1,3,3-tetramethyluronium hexafluorophosphate
HO-1/-2	heme oxygenase 1/2
Hsp90	heat shock protein 90
IAA	iodoacetic acid
icv	intracerebroventricular
IL6	interleukin-6
ip	intraperitoneal
LOX	lipoxygenase
LPS	bacterial lipopolysaccharide
MD	molecular dynamics
MMF	monomethylfumarate
MMP	mitochondrial membrane potential
mPTP	mitochondrial permeability transition pore
MS	mass spectrometry
NFT	neurofibrillary tangles
MeOH	methanol
NMDA	*N*-methyl-D-aspartate
NMP	*N*-methyl-2-pyrrolidone
NMR	nuclear magnetic resonance

NO	nitric oxide
Nrf2	nuclear factor (erythroid-derived 2)-like 2
ORAC	oxygen radical absorbance capacity
PAINS	pan-assay interference compounds
ROS	reactive oxygen species
r. t.	room temperature
sAD	sporadic Alzheimer's disease
SARs	structure-activity relationships
SERCA	sarco-/endoplasmic reticulum Ca^{2+}-ATPase
SEM	standard error of means
SOCS3	suppressor of cytokine signaling 3
tGSH	total glutathione levels
THF	tetrahydrofuran
TLC	thin layer chromatography
TNFα	tumor necrosis factor α
TMRE	tetramethylrhodamine ethyl ester
v	vehicle

Appendix

Appendix I:

- **Gunesch, S.**; Hoffmann, M.; Kiermeier, C.; Fischer, W.; Pinto, A. F. M.; Maurice, T.; Maher, P.; Decker, M. 7-*O*-Esters of taxifolin with pronounced and overadditive effects in neuroprotection, anti-neuroinflammation, and amelioration of short-term memory impairment *in vivo*. *Redox Biol.* **2020**, *29* (2020), 101378.
- Supporting Information

Appendix II:

- **Gunesch, S.**; Soriano-Castell, D.; Lamer, S.; Schlosser, A.; Maher, P.; Decker, M. Development and application of a chemical probe based on a neuroprotective flavonoid hybrid for target identification using activity-based protein profiling. *ACS Chem. Neurosci.* **2020** (in press).
  DOI: http://dx.doi.org/10.1021/acschemneuro.0c00589
- Supporting Information

Appendix III:

- **Gunesch S.**; Schramm, S.; Decker, M. Natural antioxidants in hybrids for the treatment of neurodegenerative diseases: a successful strategy? *Future Med. Chem.* **2017**, *9* (8), 711-713.

Appendix I:

Gunesch, S.; Hoffmann, M.; Kiermeier, C.; Fischer, W.; Pinto, A. F. M.; Maurice, T.; Maher, P.; Decker, M. 7-*O*-Esters of taxifolin with pronounced and overadditive effects in neuroprotection, anti-neuroinflammation, and amelioration of short-term memory impairment *in vivo*. *Redox Biol.* **2020**, *29* (2020), 101378.

https://doi.org/10.1016/j.redox.2019.101378

Redox Biology 29 (2020) 101378

Contents lists available at ScienceDirect

Redox Biology

journal homepage: www.elsevier.com/locate/redox

Research Paper

7-*O*-Esters of taxifolin with pronounced and overadditive effects in neuroprotection, anti-neuroinflammation, and amelioration of short-term memory impairment *in vivo*

Sandra Gunesch[a], Matthias Hoffmann[a], Carolina Kiermeier[a], Wolfgang Fischer[b], Antonio F.M. Pinto[b], Tangui Maurice[c], Pamela Maher[b,**], Michael Decker[a,*]

[a] *Pharmaceutical and Medicinal Chemistry, Institute of Pharmacy and Food Chemistry, Julius Maximilian University of Würzburg, Am Hubland, 97074, Würzburg, Germany*
[b] *The Salk Institute for Biological Studies, 10010 N Torrey Pines Road, La Jolla, CA, 92037, USA*
[c] *MMDN, University of Montpellier INSERM, EPHE, UMR-S1198, 434095, Montpellier, France*

ARTICLE INFO

Keywords:
Alzheimer's disease
Natural product hybrids
Flavonoids
Phenolic acids
Microglia
In vivo studies

ABSTRACT

Alzheimer's disease (AD) is a multifactorial disease and the most common form of dementia. There are no treatments to cure, prevent or slow down the progression of the disease. Natural products hold considerable interest for the development of preventive neuroprotectants to treat neurodegenerative disorders like AD, due to their low toxicity and general beneficial effects on human health with their anti-inflammatory and antioxidant features. In this work we describe regioselective synthesis of 7-*O*-ester hybrids of the flavonoid taxifolin with the phenolic acids cinnamic and ferulic acid, namely 7-*O*-cinnamoyltaxifolin and 7-*O*-feruloyltaxifolin. The compounds show pronounced overadditive neuroprotective effects against oxytosis, ferroptosis and ATP depletion in the murine hippocampal neuron HT22 cell model. Furthermore, 7-*O*-cinnamoyltaxifolin and 7-*O*-feruloyltaxifolin reduced LPS-induced neuroinflammation in BV-2 microglia cells as assessed by effects on the levels of NO, IL6 and TNFα. In all *in vitro* assays the 7-*O*-esters of taxifolin and ferulic or cinnamic acid showed strong overadditive activity, significantly exceeding the effects of the individual components and the equimolar mixtures thereof, which were almost inactive in all of the assays at the tested concentrations. *In vivo* studies confirmed this overadditive effect. Treatment of an AD mouse model based on the injection of oligomerized $A\beta_{25\text{-}35}$ peptide into the brain to cause neurotoxicity and subsequently memory deficits with 7-*O*-cinnamoyltaxifolin or 7-*O*-feruloyltaxifolin resulted in improved performance in an assay for short-term memory as compared to vehicle and mice treated with the respective equimolar mixtures. These results highlight the benefits of natural product hybrids as a novel compound class with potential use for drug discovery in neurodegenerative diseases due to their pharmacological profile that is distinct from the individual natural components.

1. Introduction

Currently, 50 million people live with dementia and about two thirds of them suffer from Alzheimer's disease (AD), making AD the most common form of dementia with numbers expected to increase dramatically due to our aging society [1]. So far, only 4 of more than 100 attempts to develop a drug against AD have resulted in a product on the market. Moreover, the available drugs only alleviate symptoms and are not able to stop neurodegeneration or cure the disease [1]. Advances in AD drug development have been hampered for several reasons with most of the researchers focused on amyloid β as the main perpetrator for AD [2]. Abnormal protein aggregation of amyloid β accumulating as extracellular plaques in the brain, and hyperphosphorylated tau protein forming neurofibrillary tangles are the main characteristics of AD, but neuroinflammation and oxidative stress are just as important as hallmarks of the disease and contribute dramatically to its progression [3]. Due to the multifactorial nature of AD, the one-target strategy to fight the disease needs to be replaced by a more general approach using pleiotropic compounds to deal with its complexity.

Natural products such as flavonoids are used as active components of natural remedies for the treatment of various diseases in traditional

* Corresponding author.
** Corresponding author.
E-mail addresses: pmaher@salk.edu (P. Maher), michael.decker@uni-wuerzburg.de (M. Decker).

https://doi.org/10.1016/j.redox.2019.101378
Received 20 September 2019; Accepted 7 November 2019
Available online 09 November 2019

medicine. Their well-established antioxidant features proved to be beneficial for general human health and natural products have gained increased attention with respect to their potential as neuroprotectants, as by their nature they show pleiotropic effects instead of addressing a single target [4,5].

In previous work we used the natural product silibinin to synthesize a library of 7-*O*-esters of this flavonolignan with different phenolic acids and investigated their neuroprotective features in a set of assays related to neurodegeneration and aging [6]. The library of esters of silibinin with derivatives of ferulic acid, using substituted and unsubstituted cinnamic, dihydro cinnamic and benzoic acids was investigated for structure-activity relationships (SARs) to reveal the influence of different numbers of hydroxy- and methoxy-groups as aromatic substituents as well as the Michael system on the neuroprotective and antioxidant effects. In all cases, we used natural products or simple derivatives thereof. SARs analysis showed that phenolic acids possessing a Michael system are important for the neuroprotective activity of the compounds [6]. The assays applied were cell-based, avoiding potentially false positive results due to false positive readouts as it was shown for pan assay interference compounds (PAINS) [7,8]. The most potent esters of the compound library in that study were 7-*O*-cinnamoylsilibinin and 7-*O*-feruloylsilibinin. Phenolic acids have been studied in the context of neurodegenerative diseases before due to their antioxidant capacities. Ferulic acid is a free radical scavenger which can counteract apoptotic intracellular pathways induced by oxidative stress [9], and has been studied in *in vivo* models of AD. Long-term administration of ferulic acid counteracted the neurotoxic effect induced by amyloid *β* in mice [10] and reduced behavioral impairment in a transgenic PSAPP mouse model [11]. Cinnamic acid upregulated the suppressor of cytokine signaling 3 (SOCS3) in BV-2 microglial cells and suppressed the expression of pro-inflammatory cytokines counteracting neuroinflammation [12].

Flavonolignan-based silibinin-esters with phenolic acids suffer from some drawbacks. The high molecular weight of the compounds and their constrained solubility counteract their drugability [13]. The secondary plant metabolite taxifolin is a flavonoid, structurally closely related to silibinin, but smaller in size (Fig. 1). In addition, the catechol moiety in taxifolin is an important antioxidant group itself and it has been shown to site-specifically inhibit aggregation of 42-residue amyloid *β*-protein (A*β*42) *in vitro*, which is relevant for the pathogenesis of AD. [14] This was confirmed by a computational study analyzing the reaction mechanism. The covalent adduct is formed via an aza-Michael addition of the oxidized *o*-quinone species of (+)-taxifolin with a lysine residue of the A*β*42 fibril [15]. Previously, taxifolin was semi-synthetically esterified in position 7 with gallic acid by Vrba et al. and shown to upregulate the nuclear factor (erythroid-derived 2)-like 2 (Nrf2) pathway in RAW264.7 cells [16], an important cytoprotective mechanism in response to redox imbalance. Recently, it has been shown that orally administered taxifolin exhibits a pleiotropic beneficial effect on intracerebral profiles in a cerebral amyloid angiopathy (CAA) mouse model *in vivo*, a disease often accompanied by AD [17]. By highlighting the therapeutic potentials of taxifolin and the phenolic acids ferulic and cinnamic acid in the context of neurodegenerative diseases [18,19], these findings inspired us to investigate natural product hybrids based on the flavonoid taxifolin and phenolic acids as novel potent neuroprotectants.

Thus, we present in this paper studies on the 7-*O*-esters of taxifolin with the phenolic acids cinnamic and ferulic acid (Fig. 1B). The latter had proven to be the most effective acids in a comprehensive medicinal chemical structure-activity relationships (SARs) study with silibinin besides their individual neuroprotective features as outlined above. The 7-*O*-taxifolin esters were regioselectively synthesized without the need of protective groups using acyl chlorides [6,16]. To target AD as a multi-factorial disease with age being the highest risk factor, the compounds need to have a broad pharmacological profile. We assessed the compounds' neuroprotective effects using different cellular models reflecting neurodegeneration and the biology of the aging brain [20]. The hybrids 7-*O*-cinnamoyltaxifolin **1** and 7-*O*-feruloyltaxifolin **2** were investigated using the mouse hippocampal neuronal cell line HT22 in different assays of oxidative stress-induced cell death and mouse BV-2 microglia cells for the protection against neuroinflammation. Cellular uptake experiments demonstrated the stability of the compounds under cell culture conditions. Additionally, **1** and **2** were investigated *in vivo* in an AD mouse model which showed their protective effects towards $A\beta_{25\text{-}35}$-induced memory impairment [21].

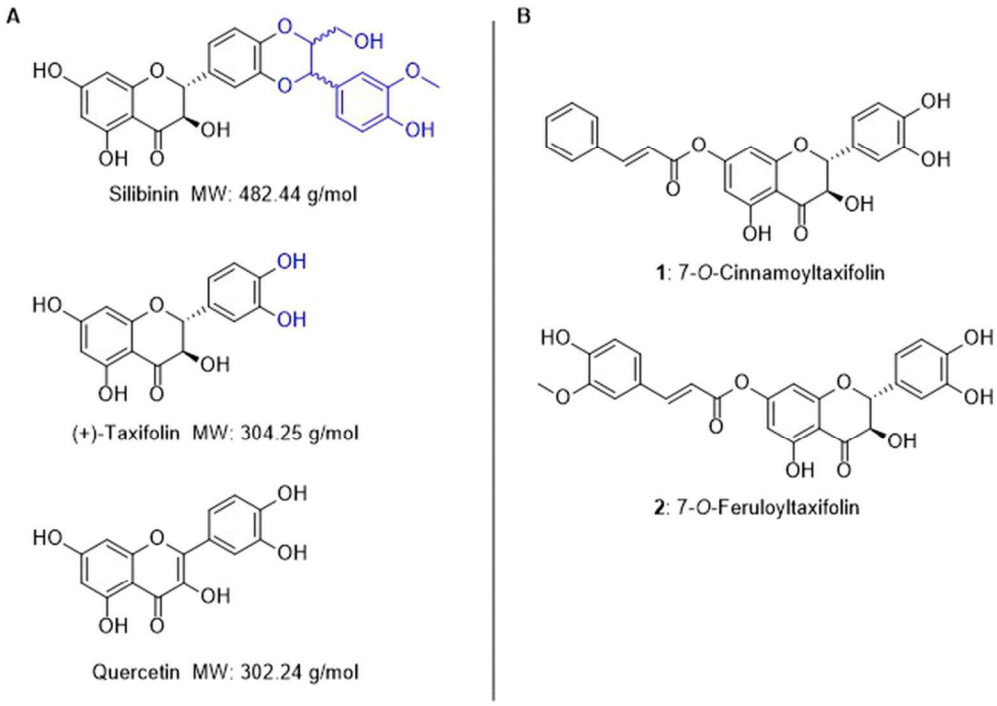

Fig. 1. A) Chemical structures of the flavonolignan silibinin and the flavonoids taxifolin and quercetin. Structural differences between the natural products silibinin and taxifolin are highlighted in blue. **B**) Target compounds 7-*O*-cinnamoyltaxifolin (**1**) and 7-*O*-feruloyltaxifolin (**2**). (For interpretation of the references to color in this figure legend, the reader is referred to the Web version of this article.)

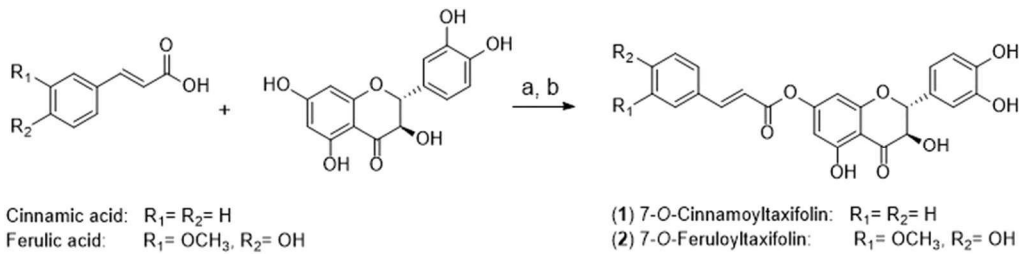

Scheme 1. Synthesis of 7-*O*-cinnamoyltaxifolin (**1**, 43% yield) and 7-*O*-feruloyltaxifolin (**2**, 27% yield). a) acid, oxalyl chloride, DMF, dry THF, 1 h, room temperature; b) taxifolin, triethylamine, dry THF, 2 h, room temperature after addition of the respective acyl chloride.

2. Results

Chemistry. Despite the presence of several hydroxyl groups, 7-*O*-esterification of taxifolin was achieved without the use of protective groups under optimized reaction conditions. Acyl chlorides of ferulic or cinnamic acid were generated with oxalyl chloride and catalytic amounts of DMF, and immediately added under anhydrous conditions to taxifolin in basic solution (Scheme 1) [6,16]. Extensive purification by column chromatography after the workup was necessary to remove all byproducts and obtain the pure compounds 7-*O*-cinnamoyltaxifolin **1** and 7-*O*-feruloyltaxifolin **2**.

2.1. Biological activity

2.1.1. Neuroprotection in HT22 cells

Oxytosis. Glutamate treatment of murine hippocampal HT22 cells leads to intracellular glutathione (GSH) depletion resulting in a form of programmed cell death due to oxidative stress [22]. This assay, also called oxidative glutamate toxicity, has a mechanistic association with aging and AD as GSH reduction is seen in the aging brain and is accelerated in AD [23]. Due to the generality of this toxicity pathway, oxytosis was used to investigate the ability of 7-*O*-cinnamoyltaxifolin **1** and 7-*O*-feruloyltaxifolin **2** to protect against oxidative stress in HT22 cells. As shown in Fig. 2A and C, **1** and **2** were highly protective against glutamate-induced oxidative stress, exceeding the beneficial effect of 25 μM quercetin, which served as a positive control. Compound **1** showed the highest neuroprotective activity at a concentration of 5 μM rescuing 74% of the cells (Fig. 2A). Taxifolin, cinnamic acid and the equimolar mixture of both were not neuroprotective at the tested concentrations of 1, 5 and 10 μM (Fig. 2A). The same neuroprotective pattern was observed for **2** and the respective controls taxifolin, ferulic acid and the one-to-one mixture of taxifolin and ferulic acid. None of the individual compounds nor the equimolar mixture showed any neuroprotective activity at the concentrations tested, but the ester hybrid **2** was highly protective at 5 μM with 70% cell viability compared to cells treated with glutamate only (Fig. 2C). The compounds were also investigated with regard to their toxicity in the absence of glutamate and both **1** and **2** were found to exhibit a slight, dose-dependent neurotoxic effect (Fig. 2B and D). However, for both **1** and **2**, greater than 70% of the cells survived even at the highest concentration tested (Fig. 2B and D).

Ferroptosis. Ferroptosis is a cell death pathway closely related if not identical to oxytosis [24]. Both forms of programmed cell death due to oxidative stress are consequences of GSH depletion, accumulation of reactive oxygen species (ROS) including lipid peroxides, mitochondrial dysfunction and a final influx of Ca^{2+} from the extracellular space [25]. Distinct from oxytosis which is induced by glutamate inhibiting cystine import by blocking system x_c^-, oxidative stress in the ferroptosis assay can be induced downstream in the cascade by inhibition of glutathione peroxidase 4 (GPx4). GPx4 is a GSH-dependent antioxidant enzyme which loses activity under GSH depletion, but can also be inhibited directly via covalent interaction of the compound RSL3 with the active site selenocysteine of GPx4 [26]. As shown in Fig. 3, both 7-*O*-esters of taxifolin, **1** and **2**, were neuroprotective against ferroptosis whereas the individual components and the respective equimolar mixture did not exhibit any protective activity at the tested concentrations. At 5 μM, compound **1** rescued 80% of the cells and its effect remained at the higher concentration (Fig. 3A). The effect of compound **2** was weaker at 5 μM compared to compound **1** with around 40% cell survival (Fig. 3B), but at 10 μM both compounds were equally potent neuroprotectants, exceeding by far the effect of the controls.

ATP depletion. Energy metabolism and ATP levels in the brain decrease with age, as a consequence of a breakdown in neuronal energy production, and are associated with nerve cell damage and death in AD [27]. Iodoacetic acid (IAA), an irreversible inhibitor of the glycolytic enzyme glyceraldehyde 3-phosphate dehydrogenase, was used to induce ATP loss in HT22 cells [28]. 7-*O*-Cinnamoyltaxifolin **1** and 7-*O*-feruloyltaxifolin **2** were investigated towards their ability to protect against ATP loss and found to significantly increase cell survival in contrast to taxifolin, the respective phenolic acid and the mixture of both (Fig. 4). Compound **1** showed an effect already at 1 μM with 40% cell survival. The effect was lost at lower concentrations (data not shown). As observed in the assays described above, the esters **1** and **2** remarkably outshown the effects of the individual components and the one-to-one mixture of the flavonoid and the phenolic acid as potential hydrolysis products.

GSH quantification. As GSH and GSH-dependent enzymes provide the major line of defense in the protection towards oxidative stress in cells and GSH levels decrease with age [23], we were interested in whether the neuroprotective esters 7-*O*-cinnamoyltaxifolin **1** and 7-*O*-feruloyltaxifolin **2** had an influence on total glutathione levels (tGSH) in HT22 cells. Therefore, tGSH levels were determined in the presence of increasing concentrations of **1** and **2**. The equimolar mixture of taxifolin and the respective acid served as controls (Fig. 5). In cells treated only with the compounds, GSH levels were maintained by both compound **1** and the one-to-one mixture (Fig. 5A, black lines). Even though the GSH concentrations of **1-**treated cells were higher than the control starting from 2.5 μM and increased dose-dependently, the difference observed was not statistically significant. However, when HT22 cells were treated with 5 mM glutamate to induce oxytosis, tGSH levels were significantly increased by **1** whereas the presence of the equimolar mixture of taxifolin and cinnamic acid had no effect on the loss of tGSH seen in the presence of glutamate (Fig. 5A, blue lines). As shown in Fig. 5B, the one-to-one mixture of taxifolin and ferulic acid had no influence on tGSH in the absence of glutamate, while compound **2** increased tGSH levels even though the effect was not statistically significant (black lines). The decreased levels of tGSH in the presence of glutamate were significantly elevated by compound **2** at 10 μM where the equimolar mixture of taxifolin and ferulic acid had no effect (Fig. 5B, blue lines). Thus, compounds **1** and **2** both influence tGSH levels and increase tGSH under oxidative stress induced by glutamate treatment in HT22 cells although **1** shows a larger effect at lower concentrations than **2**.

2.1.2. Anti-inflammatory effects in BV-2 cells

NO and cytokines. Microglial cells are the resident immune cells of the CNS. Their activation to the pro-inflammatory phenotype

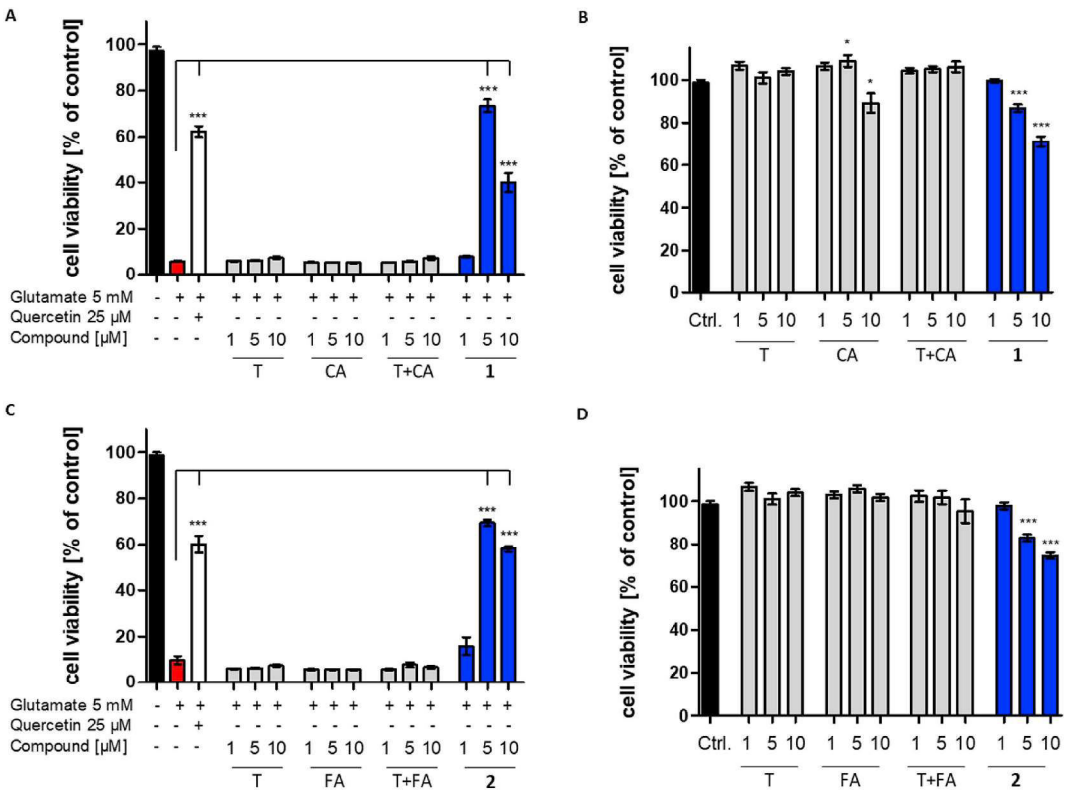

Fig. 2. Oxytosis assay in HT22 hippocampal nerve cells. 25 µM Quercetin served as a positive control (white) while 5 mM glutamate was used to induce toxicity (red). **A)** Neuroprotective effect of 7-*O*-cinnamoyltaxifolin (**1**) and the controls taxifolin (T), cinnamic acid (CA) and the equimolar mixture of taxifolin and cinnamic acid (T + CA). **B)** Neurotoxicity of the compounds taxifolin (T), cinnamic acid (CA), the one-to-one mixture (T + CA) and compound **1. C)** Neuroprotective effect of 7-*O*-feruloyltaxifolin (**2**) and the controls taxifolin (T), ferulic acid (FA) and the one-to-one mixture of taxifolin and ferulic acid (T + FA). **D)** Neurotoxic effect of the compounds taxifolin (T), ferulic acid (FA), the equimolar mixture (T + FA) and compound **2.** Data is presented as means ± SEM of three independent experiments and results refer to untreated control cells (black). Statistical analysis was rendered using One-way ANOVA followed by Dunnett's multiple comparison posttest using GraphPad Prism 5 referring to cells treated with 5 mM glutamate only in **A)** and **C)** or to untreated control cells in **B)** and **D)**. Levels of significance: $*p < 0.01$; $***p < 0.001$. (For interpretation of the references to color in this figure legend, the reader is referred to the Web version of this article.)

contributes to neuroinflammation, a major hallmark of AD [29]. Uncontrolled activation of microglia can lead to production of various pro-inflammatory and cytotoxic factors, like cytokines, free radicals, excitatory neurotransmitters and eicosanoids contributing to neuronal injury and neurodegeneration [29]. Thus, inhibition of pro-inflammatory microglia activation is another important target in the context of AD. BV-2 mouse microglial cells were used to investigate the ability of **1** and **2** to counteract inflammation induced by bacterial lipopolysaccharide (LPS). We were first interested in the effect of the compounds on nitric oxide (NO) production as a pro-inflammatory mediator (Fig. 6A and B). Both 7-*O*-esters **1** and **2** strongly reduced NO production. The levels were decreased dose-dependently in an over-additive manner with a significant effect already at 2.5 µM. As with the neuroprotective effects in the HT22 cells, this again exceeded the effect of the individual components and the equimolar mixture, where only ferulic acid displayed weak activity at higher concentrations. At a concentration of 10 µM, 7-*O*-cinnamoyltaxifolin **1** decreased NO production to only 13% compared to cells treated only with LPS (Figure 6A) and 7-*O*-feruloyltaxifolin **2** decreased the production to 16% NO (Fig. 6B). Compound **1** was further examined towards its effect on the cytokines IL6 and TNFα (Fig. 6C) using ELISAs. At 10 µM, taxifolin, cinnamic acid, the one-to-one mixture and **1** reduced induction of TNFα to less than 40%. Even though the levels of TNFα were decreased strongest by **1**, the difference to the controls taxifolin and cinnamic acid as well as the one-to-one mixture of both was not statistically significant (Fig. 6C). A stronger difference was seen with IL6 induction which was significantly reduced by compound **1** compared to cinnamic acid and the equimolar mixture of taxifolin and cinnamic acid (Fig. 6C). As compound **1** did not show an enhanced effect on TNFα levels as compared to the respective controls, compound **2** was only assessed for its effect on IL6 levels using an ELISA. Although IL6 levels were decreased by compound **2** (Fig. 6D), the difference from the controls was not statistically significant.

Nrf2 upregulation. Previously, taxifolin esterified in position 7 with gallic acid was shown to upregulate the nuclear factor (erythroid-derived 2)-like 2 (Nrf2) pathway in RAW264.7 cells [16], a macrophage cell line. Since brain microglial cells have many properties similar to peripheral macrophages and, of the two compounds, compound **1** was the strongest reducer of neuroinflammation markers in the BV-2 cells, we asked whether Nrf2 was involved in its mode of action. Nuclear fractions of BV-2 cells treated with the compounds were subjected to Western blot analysis. As shown in Fig. 7A, 7-*O*-cinnamoyltaxifolin **1** dose-dependently increased nuclear Nrf2 levels up to 24-fold at 10 µM after 4 h of incubation. Taxifolin and the equimolar mixture of taxifolin and cinnamic acid did not induce Nrf2 translocation to the nucleus. Next, we were interested in whether Nrf2 was directly involved in the anti-inflammatory effects of **1** and so downregulated Nrf2 in BV-2 microglia by transfection using specific siRNA. Fig. 7B shows the effective downregulation of Nrf2 in cells treated with siNrf2 (lane 3) even in the presence of the strong inducer **1** (lane 4), compared to the nonspecific control siRNA (lanes 1 and 2). The siRNA modified BV-2 cells were then used for the LPS inflammation assay. As shown in Fig. 7C, no shift in the dose-response curve for NO reduction was observed between Nrf2 knockdown cells and the control, therefore Nrf2 knockdown had no effect on the anti-inflammatory activity of **1**.

Cellular uptake experiments. Semisynthetic gallic acid esters of

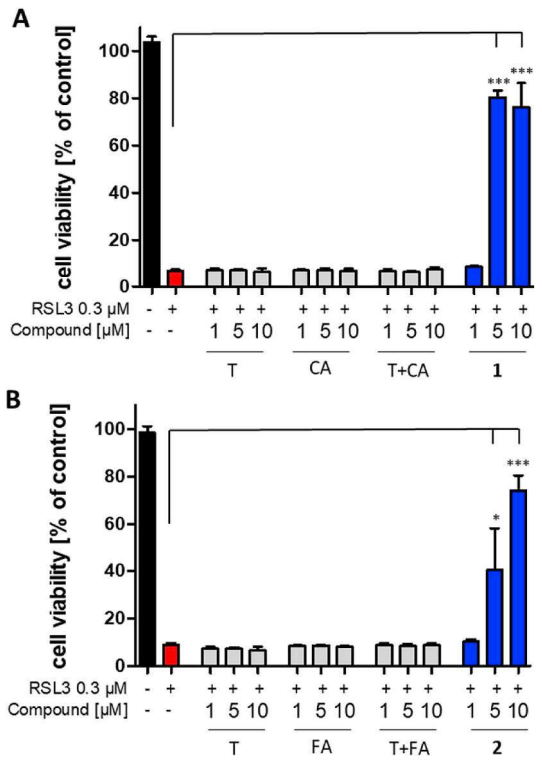

Fig. 3. Ferroptosis was induced in HT22 cells with 300 nM RSL3. **A)** Neuroprotective effect of 7-*O*-cinnamoyltaxifolin (**1**) and the controls taxifolin (T), cinnamic acid (CA) and the equimolar mixture of taxifolin and cinnamic acid (T + CA). **B)** Neuroprotective effect of 7-*O*-feruloyltaxifolin (**2**) and the controls taxifolin (T), ferulic acid (FA) and the one-to-one mixture of taxifolin and ferulic acid (T + FA). For both **A)** and **B)**, data is presented as means ± SEM of three independent experiments and results refer to untreated control cells (black). Statistical analysis was rendered using One-way ANOVA followed by Dunnett's multiple comparison posttest using GraphPad Prism 5 referring to cells treated with 300 nM RSL3 only (red). Levels of significance: $*p < 0.01$; $***p < 0.001$. (For interpretation of the references to color in this figure legend, the reader is referred to the Web version of this article.)

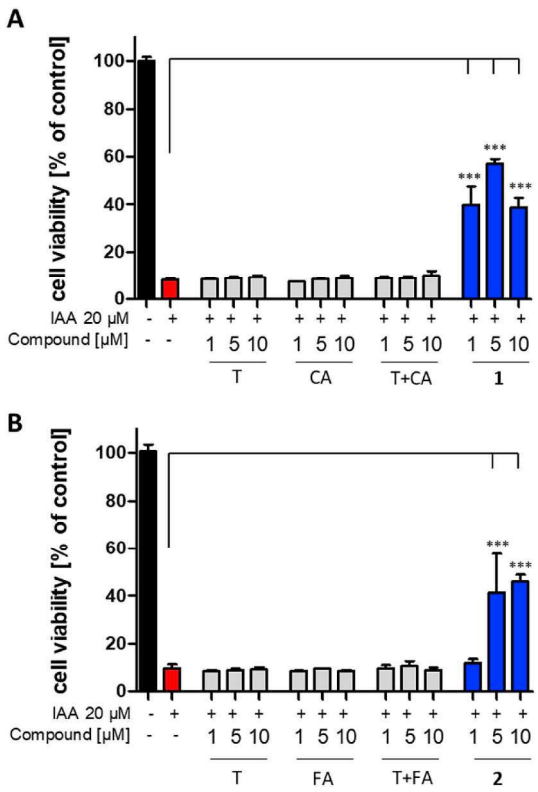

Fig. 4. HT22 cells were treated with 20 µM iodoacetic acid (IAA) to induce ATP depletion in the absence or presence of the compounds. **A)** Protective effect of 7-*O*-cinnamoyltaxifolin (**1**) and the controls taxifolin (T), cinnamic acid (CA) and the equimolar mixture of taxifolin and cinnamic acid (T + CA). **B)** Protective effect of 7-*O*-feruloyltaxifolin (**2**) and the controls taxifolin (T), ferulic acid (FA) and the one-to-one mixture of taxifolin and ferulic acid (T + FA). For both **A)** and **B)**, data is presented as means ± SEM of three independent experiments and results refer to untreated control cells (black). Statistical analysis was rendered using One-way ANOVA followed by Dunnett's multiple comparison posttest using GraphPad Prism 5 referring to cells treated with 20 µM IAA only (red). Levels of significance: $***p < 0.001$. (For interpretation of the references to color in this figure legend, the reader is referred to the Web version of this article.)

taxifolin have been shown to be converted to quercetin derivatives in RAW264.7 cells by Vrba et al. [16]. Therefore, we were interested if we could detect cellular uptake of our synthetic hybrid 7-*O*-cinnamoyltaxifolin **1** in murine BV-2 microglia cells, and if the compound was hydrolyzed or was converted to the respective 7-*O*-quercetin ester, as described before [16]. We first recorded a reference HPLC chromatogram with 50 ng of each compound to determine their retention times (Fig. 8A). For cellular uptake experiments, BV-2 cells were incubated with 50 µM 7-*O*-cinnamoyltaxifolin **1** for 0, 30, 90 and 240 min and lysates were analyzed by HPLC (Fig. 8B). Fig. 8B–a shows that already for time point 0, where cells were lysed immediately after the addition of the compound, next to the peak for **1** at 43.9 min, a second peak was detected with a retention time of 48.9 min. After 30 min both peaks increased in intensity (Fig. 8B–b) and a shift towards the second peak was observed after 90 min incubation (Fig. 8B-c), indicating that the compound was metabolized. After 4 h, compound **1** was only detected in trace amounts and also the second peak decreased (Fig. 8B–d). Both compounds were found to be stable towards their potential hydrolysis products as no additional peaks were detected at lower retention times that would correspond to the reference compounds in Fig. 8A. To ensure that conversion of 7-*O*-cinnamoyltaxifolin was indeed dependent on the presence of cells, 50 µM **1** were incubated for 30 min in culture medium only. HPLC analysis gave one distinct peak with a retention time of 44.0 min and no further compounds were detected (Fig. 8C). To confirm the identity of the detected compounds, the two peaks at 43.9 and 48.9 min were collected and submitted to MS analysis respectively. In Fig. 8D the peak with a retention time of 43.9 min was identified as 7-*O*-cinnamoyltaxifolin with $m/z = 435.11$ ($[M+H]^+$ calc. = 435.11). MS/MS fragmentation resulted in signals at $m/z = 305.07$ corresponding to taxifolin and at $m/z = 131.05$ and $m/z = 103.05$ corresponding to cinnamic acid (minus H_2O and additional loss of CO, respectively). MS analysis of peak 2 with a retention time of 48.9 min gave signals at $m/z = 433.09$ corresponding to 7-*O*-cinnamoylquercetin with a calculated $[M+H]^+$ $m/z = 433.09$ (Fig. 8E). The compound was confirmed by MS/MS fragmentation where the masses of cinnamic acid ($m/z = 131.05$ and $m/z = 103.05$) and quercetin ($m/z = 303.05$) were identified.

***In vivo* studies.** To extend the *in vitro* studies, the esters **1** and **2** were evaluated and compared to the one-to-one mixtures of the respective acids and taxifolin regarding their protective effects against $A\beta_{25\text{-}35}$-induced memory impairment in a mouse model of AD, which has been described in detail before [21,30,31]. AD-like cognitive dysfunction was induced by intracerebroventricular (icv) injection of oligomerized $A\beta_{25\text{-}35}$ peptide into the mouse brain on day 1. Compounds were injected intraperitoneally (ip) from day 1 to day 7, and spatial working memory was evaluated on day 8 in a Y-maze assay. On days 9 and 10 of the study, a step-through passive-avoidance assay was performed as a measure of long-term memory improvement, followed by

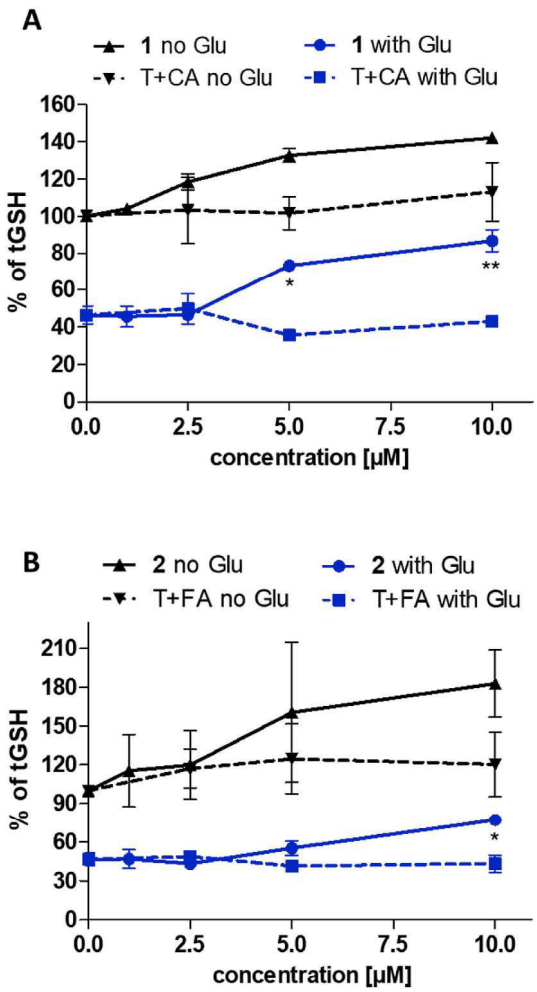

Fig. 5. Dose dependent effects of 7-*O*-cinnamoyltaxifolin **1** (**A**) and 7-*O*-feruloyltaxifolin **2** (**B**) and the equimolar mixtures (T + CA in **A** and T + FA in **B**) on total glutathione (tGSH) levels in HT22 cells in the absence (black lines) or presence (blue lines) of 5 mM glutamate (Glu) to induce oxytosis. GSH levels were measured in a chemical assay after 24 h and normalized to total protein. Results are given as mean ± SEM and were analyzed by One-way ANOVA followed by Dunnett's multiple comparison posttest using GraphPad Prism 5 referring to cells with no compound added. Levels of significance: $*p < 0.05$, $**p < 0.01$. (For interpretation of the references to color in this figure legend, the reader is referred to the Web version of this article.)

sacrifice on day 11. Solutions of compounds in 60% DMSO +40% saline (0.9%) were prepared directly before injection and injected ip once per day to achieve a dose of 1, 3, and 10 mg/kg, respectively. 60% DMSO +40% saline (0.9%) were used as vehicle (V) for control groups. The treatments did not affect the mouse body weight gain significantly during the week of therapy showing good tolerability (Fig. 11). Animals recovered quickly (within 10 min) from the icv injection stress after day 1.

Spatial working memory. Compound **2** reduced the $A\beta_{25\text{-}35}$–induced spontaneous alternation deficits at all doses tested (Fig. 9A). Compound **1** showed significant prevention of the $A\beta_{25\text{-}35}$-induced alternation deficit at 3 and 10 mg/kg (Fig. 9B). The esters **1** and **2** appeared to be significantly more neuroprotective than the mixtures of taxifolin and the respective acids (Fig. 9C,D,E).

Long-term memory. On day 9 of the study, the step-through passive-avoidance training was conducted, followed by the assessment of the step-through latency on day 10 as described earlier [21,30,31]. None of the compounds or mixtures improved the Aβ-induced impairment of long-term memory in prolongation of step-through (Fig. 10).

3. Discussion

In this work we present the synthesis and detailed *in vitro* and *in vivo* evaluation of two natural product hybrids, 7-*O*-cinnamoyltaxifolin **1** and 7-*O*-feruloyltaxifolin **2**, with overadditive neuroprotective effects. The compounds' design was based on interesting results of a SAR study for silibinin esters [6] and the beneficial pleiotropic effects of taxifolin and the phenolic acids as neuroprotectants [32,33] to address multifactorial neurodegenerative diseases like AD. For silibinin, the influence of the individual hydroxyl groups was investigated and position 7 was assigned with a rather pro-oxidant character [34] and therefore was protected by esterification with the antioxidant phenolic acid [6]. As the catechol moiety of the flavonoid taxifolin is a strong antioxidant group itself and modifications on the A-Ring are well tolerated, taxifolin was chemically connected via an ester bond in position 7 to the phenolic acids cinnamic and ferulic acid, which were the superior phenolic acids in the SARs of silibinin esters [6] and counteract pathways of neurodegeneration as described above.

Due to multiple hydroxyl groups, selective esterification of flavonoids is a challenging task and often requires the use of protective groups [35]. Vrba et al. synthesized taxifolin and quercetin esters with gallic acid by using benzyl-protected gallic acid, or benzyl-protected quercetin for esterification in position 3 of the flavonoid [16]. Protection and deprotection steps enlarge the synthetic route and might narrow the yield of target compounds. Similar to the conditions applied before for the synthesis of silibinin esters [6,36] we synthesized the 7-*O*-esters of taxifolin by direct acylation without the use of protective groups. Acyl chlorides of cinnamic or ferulic acid were prepared using oxalyl chloride and catalytic amounts of DMF in tetrahydrofuran (THF) and were added to a solution of taxifolin in THF basified with triethylamine. Optimized reaction conditions even allowed the generation of the feruloyl chloride *in situ* for esterification without protecting the free hydroxyl group.

As the single-target approach has not proven successful for the development of effective drugs against AD up to now, our approach was to characterize the compounds in a broad range of assays developed to reflect the biology of aging and neurodegeneration [37]. This approach is also an asset from a medicinal chemists point of view, as for molecules bearing a Michael system like cinnamic and ferulic acid, it is important to choose a variety of assays estimating the biological activity to avoid false-positive readouts (PAINS) [7]. Here, we used two different cell lines for the biological characterization. HT22 hippocampal nerve cells to study the neuroprotective effects of 7-*O*-cinnamoyltaxifolin **1** and 7-*O*-feruloyltaxifolin **2** against different types of oxidative stress, and mouse BV-2 microglia cells to examine the esters' anti-neuroinflammatory activity. In all cell-based assays, the compounds **1** and **2** showed strong and pronounced overadditive effects. The individual ester components taxifolin and the respective phenolic acids were not neuroprotective in any of our assays, neither was their equimolar mixture representing the potential hydrolysis products. In the rather low concentration range investigated, only the 7-*O*-esters were able to rescue cells from oxytosis, ferroptosis and ATP depletion in HT22 cells and LPS-induced neuroinflammation in BV-2 cells. These findings indicate a specific intracellular mode of action of 7-*O*-cinnamoyltaxifolin **1** and 7-*O*-feruloyltaxifolin **2** with the chemical connection contributing to the biological activity. Flavonoids have been shown to influence GSH levels as part of their antioxidant effect [38] and GSH is developing into an therapeutic objective for the treatment of oxidative stress-related diseases [39]. Compound **1** and **2**, but not the one-to-one mixture of taxifolin and the respective phenolic acid, were able to significantly increase GSH levels in HT22 cells under glutamate-induced oxidative stress.

Nrf2 is an important transcription factor that acts on the antioxidant response element (ARE) and has been shown to be induced by flavonoids [40]. As Nrf2 also has anti-inflammatory effects [41], we investigated the role of Nrf2 in the anti-inflammatory action of 7-*O*-

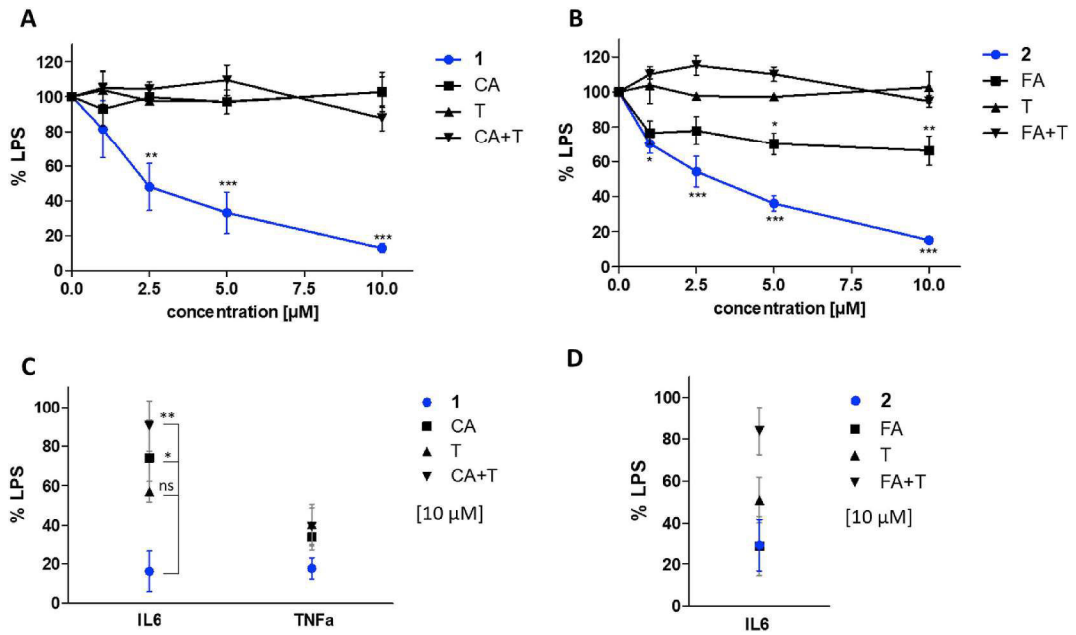

Fig. 6. Effects of **1** and **2** and the respective controls on the production of NO and pro-inflammatory cytokines IL6 and TNFα by LPS-treated BV-2 microglia cells. Cells were treated overnight with 50 ng/mL LPS alone or in the presence of 7-*O*-cinnamoyltaxifolin (**1**), cinnamic acid (CA), taxifolin (T) and the one-to-one mixture of both (T + CA) (**A** and **C**) or with 7-*O*-feruloyltaxifolin (**2**), ferulic acid (FA), taxifolin (T) and the equimolar mixture of the individual components (T + FA) (**B** and **D**). Supernatants were cleared and NO was quantified by the Griess assay. Data in in **A** and **B** are given as means ± SEM and relative to BV-2 cells treated with LPS only, which were set as 100%. One-way ANOVA was used for statistical analysis followed by Dunnett's multiple comparison posttest. Levels of significance: $*p < 0.05$, $**p < 0.01$, $***p < 0.001$. **C**) The effect of 10 µM **1** on levels of the pro-inflammatory cytokines IL6 and TNFα after LPS-treatment was assessed using ELISAs as was the effect of 10 µM **2** on IL6 (**D**). For **C**) and **D**) Results are presented as percent (%) of the values obtained for treatment with LPS alone, which were set as 100% and are shown means ± SEM. Levels of significance: $*p < 0.05$, $**p < 0.01$ of One-way ANOVA followed by Tukey's posttest.

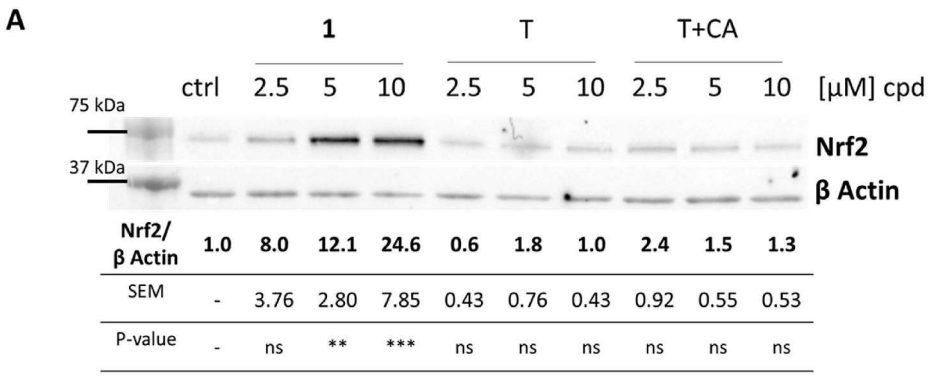

	ctrl	1 2.5	1 5	1 10	T 2.5	T 5	T 10	T+CA 2.5	T+CA 5	T+CA 10
Nrf2/ β Actin	1.0	8.0	12.1	24.6	0.6	1.8	1.0	2.4	1.5	1.3
SEM	-	3.76	2.80	7.85	0.43	0.76	0.43	0.92	0.55	0.53
P-value	-	ns	**	***	ns	ns	ns	ns	ns	ns

Fig. 7. Correlation of 7-*O*-cinnamoyltaxifolin **1** and Nrf2 in BV-2 microglia cells. **A)** Cells were treated for 4 h with DMSO as control or with increasing concentrations of **1**, taxifolin (T) or the equimolar mixture of taxifolin and cinnamic acid (T + CA). Nuclear fractions of BV-2 cells were prepared and analyzed by Western blot for Nrf2 using a specific antibody. Levels of Nrf2 were normalized to actin and a representative blot is shown. **B)** Transfection of BV-2 cells with control siRNA or Nrf2 siRNA. Nuclei of cells incubated with **1** or vehicle (DMSO control) for 4 h were analyzed by Western blots for Nrf2. **C)** Griess assay for NO quantification of transfected cells treated with increased concentrations of 7-*O*-cinnamoyltaxifolin **1**.

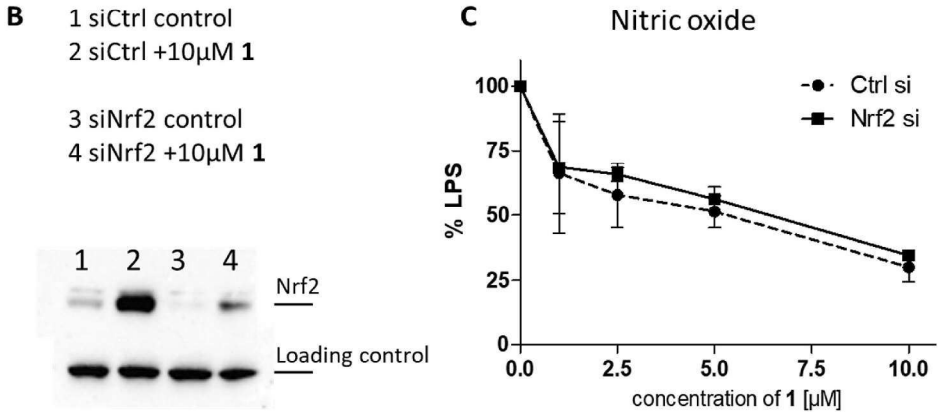

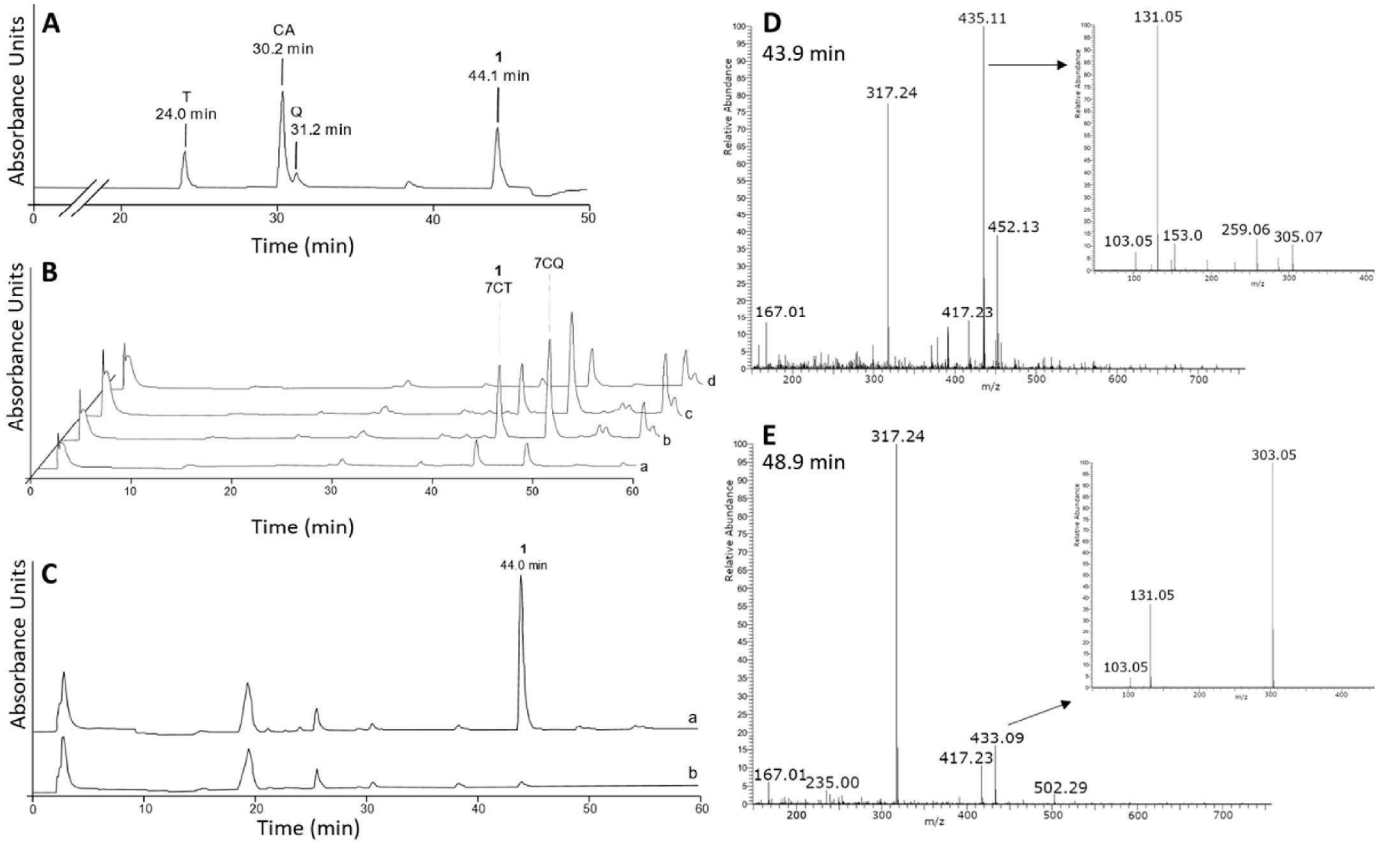

Fig. 8. Cellular uptake of compound **1**. **A)** 50 ng of taxifolin (T), cinnamic acid (CA), quercetin (Q) and 7-*O*-cinnamoyltaxifolin (**1**) were submitted to HPLC as reference for the compounds' retention times. **B)** 50 μM **1** were added to BV-2 cells and cells were immediately lysed (**a**), or incubated for 30 min (**b**), 90 min (**c**) or 4 h (**d**) prior to lysis and sample preparation. **C)** Incubation of 50 μM **1** for 30 min in medium only did not lead to compound conversion (**a**). (**b**): blank chromatogram with medium only. **D)** MS spectrum of the first HPLC peak (43.9 min) after incubating **1** for 30 min with BV-2 cells. The signal at $m/z = 435.11$ corresponds to **1** and was isolated for MS/MS fragmentation (inset) where $m/z = 131.05$ and $m/z = 305.07$ were detected corresponding to cinnamic acid and taxifolin, respectively. **E)** MS spectrum of the 48.9 min fraction gave a signal at $m/z = 433.09$ and the MS/MS fragmentation (inset) of the selected ion at $m/z = 131.05$ and $m/z = 303.05$ fit the m/z values of cinnamic acid and quercetin.

cinnamoyltaxifolin **1**. Compound **1** was a strong inducer of Nrf2 in BV-2 cells with more than a 20-fold increase in Nrf2 levels in the nuclear fraction, again in an overadditive manner. However, the anti-inflammatory effect of **1** was not dependent on Nrf2. BV-2 cells transfected with Nrf2 siRNA still showed reduced levels of NO as an inflammation marker upon treatment with **1** in a concentration dependent manner. Therefore, the exact pathways mediating the anti-inflammatory effects of **1** remain unclear and in future investigations proteins of the NFKB pathway, like pIKBα, or MAP kinases could be considered [40].

The BV-2 cell line was also used for cellular uptake experiments to study the intracellular behavior of the compound. Instead of hydrolysis of the ester bond, we observed the conversion of 7-*O*-cinnamoyltaxifolin **1** to its oxidized quercetin derivative, in accordance to what Vrba et al. had shown for galloyl ester of taxifolin in RAW264.7 cells [16]. The oxidation product 7-*O*-cinnamoylquercetin was detectable right

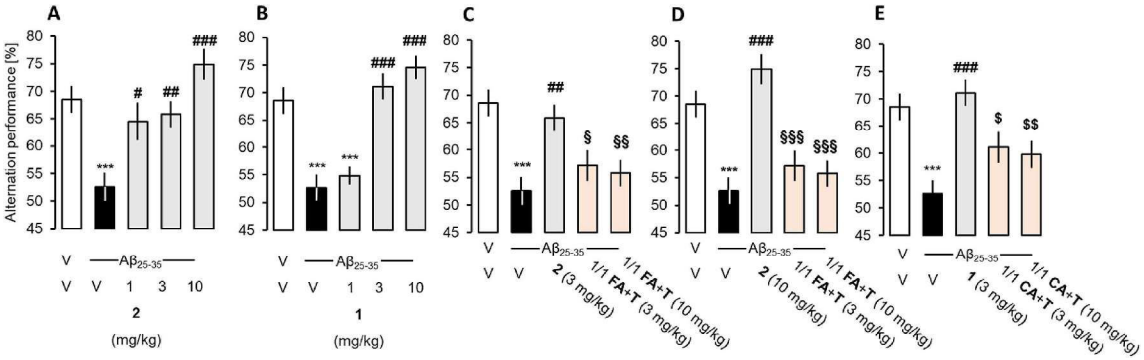

Fig. 9. Effect of the compounds on $A\beta_{25\text{-}35}$-induced spontaneous alternation deficits in mice. V – vehicle, **2** – 7-*O*-feruloyltaxifolin, **1** – 7-*O*-cinnamoyltaxifolin, FA – ferulic acid, T – taxifolin, CA – cinnamic acid. Data shows mean ± SEM. ANOVA: $F_{(4,59)} = 8.77$, $p < 0.001$, n = 11–12 per group in **A)**; $F_{(4,58)} = 19.97$, $p < 0.001$, n = 11–12 in **B)**; $F_{(7,95)} = 7.35$, $p < 0.001$, n = 11–12 in **C)** and **D)**; $F_{(7,95)} = 8.54$, $p < 0.001$, n = 11–12 in **E)**. ***$p < 0.01$ vs. (V + V)-treated group; #$p < 0.05$, ##$p < 0.01$, ###$p < 0.001$ vs. ($A\beta_{25\text{-}35}$ + V)-treated group; §$p < 0.05$, §§$p < 0.01$, §§§$p < 0.001$ vs. ($A\beta_{25\text{-}35}$ + **2**)-treated group; $ $p < 0.05$, $$ $p < 0.01$ vs. ($A\beta_{25\text{-}35}$ + **1**)-treated group; Dunnett's test.

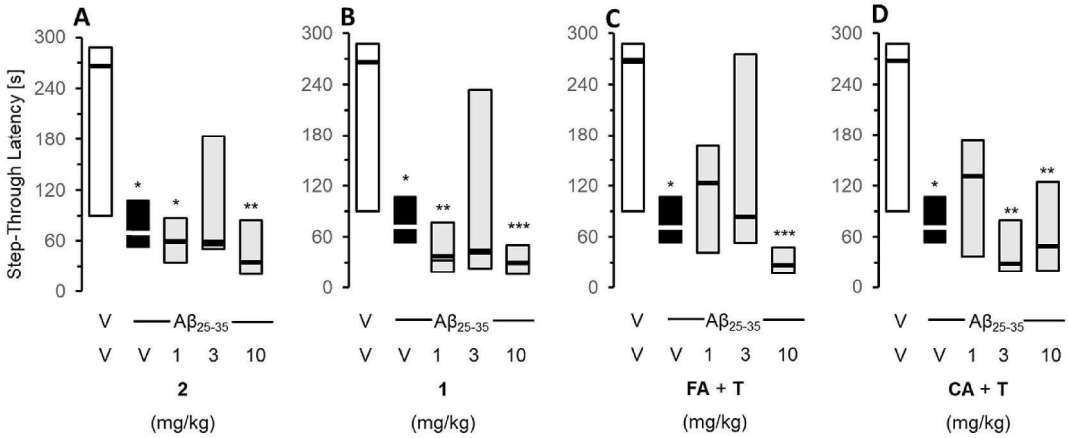

Fig. 10. Effect of the compounds on $A\beta_{25\text{-}35}$-induced passive avoidance impairments in mice. Data shows median and interquartile range. Kruskal-Wallis ANOVA: $H = 9.04$, $p < 0.1$, n = 12 per group in (**A**); $H = 15.0$, $p < 0.05$, n = 12 in (**B**); $H = 13.8$, $p < 0.05$, n = 12 in (**C**); $H = 12.0$, $p < 0.05$, n = 12 in (**D**). $^{*}p < 0.05$, $^{**}p < 0.01$, $^{***}p < 0.001$ vs. (V + V)-treated group; Dunn's test.

after addition of **1**, thus the intracellular oxidation occurred rapidly after cellular uptake and we were unable to determine which derivative contributes to what extent to the biological activity. However, the presence of cells was necessary for the conversion of the compound, as incubation of **1** in medium alone did not produce any metabolic by-product. Remarkably, even after 4 h incubation, none of the potential hydrolysis products expected were detected, proving the stability of the ester bond.

In vivo experiments with both compounds 7-*O*-cinnamoyltaxifolin **1** and 7-*O*-feruloyltaxifolin **2** showed their pharmacological relevance in an $A\beta_{25\text{-}35}$-induced memory impaired AD mouse model. The 7-*O*-esters of taxifolin, **1** and **2**, both showed significant improvement of spatial working memory in the Y-maze assay, although only moderate effects were seen in the non-spatial long-term memory passive avoidance test. A dichotomy between the resulting effects on $A\beta_{25\text{-}35}$-induced short-term and long-term memory deficits could however be predicted. Although silibinin ameliorated $A\beta_{25\text{-}35}$-induced memory deficits and oxidative stress, notably by mobilizing nitric-oxide synthase and TNFα [42,43], antioxidants including idebenone and α-tocopherol prevented the short-term memory deficits in the Y-maze and water-maze, but not passive avoidance deficits in $A\beta_{1\text{-}42}$-treated mice [44]. Another point is that taxifolin has a positive effect on $A\beta_{1\text{-}42}$ accumulation and aggregation [45,46]. We previously reported that a γ-secretase inhibitor, BMS-299897, attenuated $A\beta_{25\text{-}35}$-induced $A\beta_{1\text{-}42}$ seeding and toxicity [47]. Importantly, BMS-299897 blocked the $A\beta_{25\text{-}35}$-induced deficits in spontaneous alternation or novel object recognition, using a 1 h intertrial time interval, but failed to affect the passive avoidance impairments or novel object recognition, using a 24 h intertrial time interval. $A\beta_{25\text{-}35}$ injection therefore provoked an accumulation in endogenous $A\beta_{1\text{-}42}$, an effect that was blocked by γ-secretase inhibition. This $A\beta_{1\text{-}42}$ accumulation marginally contributed to the toxicity or long-term memory deficits but likely plays a major role in synaptic dysfunction and short-term memory deficits. Thus, through this mechanism, taxifolin, and the related compounds **1** and **2**, may be particularly effective in alleviating these changes.

The effect of both 7-*O*-cinnamoyltaxifolin **1** and 7-*O*-feruloyltaxifolin **2** on short-term memory was remarkably superior to the effect evoked by the mixtures of taxifolin and the acids. Thereby, much greater effects on oxidative stress and protection from ATP depletion in the HT22 cells and the anti-neuroinflammatory effect in the BV-2 cells *in vitro* translates into an improved memory rescue *in vivo*, when neuroinflammation and neurotoxicity were induced by $A\beta_{25\text{-}35}$. Of note, both compounds **1** and **2** outperformed the symptomatic memory improvement of taxifolin which had been shown before [45,48]. These findings provide strong support for the general concept of 7-*O*-esterification to improve the neuroprotective effects of taxifolin and show that this might also apply to other natural products with polyphenolic structures.

4. Conclusion

We showed that 7-*O*-esters of taxifolin and ferulic or cinnamic acid have pronounced neuroprotective effects against oxidative stress and neuroinflammation in a variety of assays in HT22 and BV-2 cell models, proving a pleiotropic beneficial effect which is desperately needed in the context of multifactorial neurodegenerative diseases like AD. Since the effects of 7-*O*-cinnamoyltaxifolin and 7-*O*-feruloyltaxifolin were overadditive in each of the assays used, one can conclude a specific cellular interaction distinct from the hybrids' building blocks. Due to the significant and overadditive *in vivo* effects in the $A\beta_{25\text{-}35}$-induced memory impaired AD mouse model, it can be assumed that the compounds were able to cross the blood-brain barrier and their metabolic stability was sufficient to evoke an amelioration of short-term memory defects in mice, in contrast to the controls. Even though their detailed mechanisms of action remains to be determined, several target pathways were identified including maintenance of GSH under conditions of stress and Nrf2 signaling. Thus, the natural product hybrids should be considered as a class of neuroprotective compounds with a distinct and specific pharmacological profile. This might also be true for other polyphenolic hybrids in addition to taxifolin-based esters. Future research aims to further develop the compounds as a potential starting point for drug development to treat neurodegenerative diseases, as their origin as dietary natural products provides medical value due to reduced toxicity and side effects with a pleiotropic pharmacological effect.

5. Experimental section

5.1. Chemical synthesis

General information. All reagents were used without further purification and bought from common commercial suppliers. For anhydrous reaction conditions, THF was dried prior to use by refluxing over sodium slices for at least 2 days under an argon atmosphere. Thin-layer chromatography was performed on silica gel 60 (alumina foils with fluorescent indicator 254 nm). UV light (254 and 366 nm) was used for detection. For column chromatography, silica gel 60 (particle size 0.040–0.063 mm) was used. Nuclear magnetic resonance (NMR) spectra were recorded with a Bruker AV-400 NMR instrument (Bruker, Karlsruhe, Germany) in DMSO-d6, and chemical shifts are expressed in

ppm relative to DMSO-d6 (2.50 ppm for 1H and 39.5 ppm for 13C). Purity of the synthesis products was determined by HPLC (Shimadzu Products), containing a DGU-20A3R degassing unit, a LC20AB liquid chromatograph, and an SPD-20A UV/vis detector. UV detection was measured at 254 nm. Mass spectra were obtained by a LCMS 2020 (Shimadzu Products). As a stationary phase, a Synergi 4U fusion-RP (150 mm × 4.6 mm) column was used, and as a mobile phase, a gradient of methanol/water with 0.1% formic acid. Parameters: A = water, B = methanol, V(B)/(V(A) + V(B)) = from 5% to 90% over 10 min, V(B)/(V(A)+V(B)) = 90% for 5 min, V(B)/(V(A) + V(B)) = from 90% to 5% over 3 min. The method was performed with a flow rate of 1.0 mL/min. Compounds were only used for biological evaluation if the purity was ≥95%. Melting points were determined using an OptiMelt automated melting point system (Scientific Instruments GmbH, Gilching, Germany).

5.2. General procedure for the synthesis of 7-O-ester of taxifolin

The respective phenolic acid (1.5 equiv.) was dissolved in dry THF. 3 μL DMF and oxalyl chloride (1.5 equiv.) were added and the solution stirred at room temperature until TLC indicated complete conversion of the acid. Taxifolin (1.0 equiv.) was dissolved in dry THF and NEt_3 (2.0 equiv.) was added. The freshly prepared acid chloride was added dropwise to the taxifolin solution and the mixture stirred at room temperature for 2 h. The reaction was quenched by the addition of water and extracted with ethyl acetate. The organic layer was washed with 1 M HCl, brine and dried over $NaSO_4$ when the solvent was evaporated. The product was purified twice by column chromatography using 1.5%–3% methanol in CH_2Cl_2 with 1% formic acid.

7-*O*-Cinnamoyltaxifolin ((2R,3R)-2-(3,4-dihydroxyphenyl)-3,5-dihydroxy-4-oxochroman-7-yl cinnamate) **1**: Cinnamic acid (146 mg, 0.98 mmol, 1.5 equiv.) was dissolved in 5 mL dry THF. 3 μL DMF and oxalyl chloride (87.4 μL, 1.02 mmol, 1.5 equiv.) were added and stirred for 30 min when conversion of cinnamic acid into the acid chloride was complete. Taxifolin (200 mg, 657 μmol, 1.0 equiv.) was dissolved in 15 mL dry THF and NEt_3 (182.2 μl, 1.31 mmol, 2.0 equiv.) was added. Following the general procedure, compound **1** was purified twice by column chromatography to obtain the product as an off-white solid (125 mg, 0.28 mmol, 43%).

^{1}H NMR (400 MHz, DMSO-d_6) δ = 11.73 (s, 1H), 9.01 (s, 2H), 7.86 (d, J = 16.0, 1H), 7.80 (dd, J = 7.2, 2.3, 2H), 7.47 (d, J = 1.7, 3H), 6.92 (d, J = 1.8, 1H), 6.86 (d, J = 16.0, 1H), 6.81–6.73 (m, 2H), 6.45 (d, J = 2.1, 1H), 6.42 (d, J = 2.1, 1H), 5.96–5.85 (m, 1H), 5.15 (d, J = 11.5, 1H), 4.69 (dd, J = 11.5, 5.6, 1H) ppm; **^{13}C NMR** (101 MHz, DMSO-d_6) δ = 199.6, 164.0, 162.0, 161.9, 158.0, 147.2, 145.9, 145.0, 133.7, 131.1, 129.0 (2C), 128.8 (2C), 127.6, 119.5, 116.7, 115.5, 115.1, 104.8, 102.8, 101.7, 83.3, 71.9 ppm.

ESI: *m/z* calculated for $C_{24}H_{18}O_8$ $[M+H]^+$ 435.10, found: 435.15; HPLC purity: 98% (retention time: 12.7 min); mp: 189 °C.

7-*O*-Feruloyltaxifolin ((2R,3R)-2-(3,4-dihydroxyphenyl)-3,5-dihydroxy-4-oxochroman-7-yl (E)-3-(4-hydroxy-3-methoxyphenyl)acrylate) **2**: Ferulic acid (268 mg, 1.38 mmol, 1.1 equiv.) was dissolved in dry THF, 3 μL DMF and oxalyl chloride (224 μL, 2.62 mmol, 2.0 equiv.) were added and stirred until the acid chloride formation was complete. Taxifolin (400 mg, 1.31 mmol, 1.0 equiv.) was dissolved in dry THF and NEt_3 (726 μL, 5.24 mmol, 4.5 equiv.) was added. Following the general procedure, compound **2** was obtained as light-yellow foam (168 mg, 0.35 mmol, 27%).

^{1}H NMR (400 MHz, DMSO) δ = 11.72 (s, 1H), 9.74 (s, 1H), 9.01 (m, 2H), 7.77 (d, J = 15.9 Hz, 1H), 7.42 (d, J = 1.9 Hz, 1H), 7.22 (dd, J = 1.9 Hz and 8.3 Hz, 1H), 6.91 (d, J = 1.9 Hz, 1H), 6.83 (d, J = 8.1 Hz, 1H), 6.78 (d, J = 1.9 Hz, 1H), 6.76 (d, J = 8.0 Hz, 1H), 6.70 (d, J = 15.9 Hz, 1H), 6.42 (d, J = 2.1 Hz, 1H), 6.38 (d, J = 2.1 Hz, 1H), 5.87 (d, J = 6.2 Hz, 1H), 5.13 (d, J = 11.5 Hz, 1H), 4.68 (dd, J = 6.1 Hz and J = 11.5 Hz, 1H), 3.83 (s, 3H) ppm. **^{13}C NMR** (101 MHz, DMSO) δ = 199.6, 164.3, 162.0, 161.9, 158.2, 150.0, 148.0, 147.9, 145.9, 145.0, 127.6, 125.3, 123.9, 119.5, 115.6, 115.4, 115.1, 112.8, 111.5, 104.7, 102.8, 101.6, 83.3, 71.9, 55.7 ppm.

ESI: *m/z* calculated for $C_{25}H_{20}O_{10}$ $[M+H]^+$ 481.11; found 481.15; HPLC purity: 96% (retention time: 11.7 min); mp: 191 °C.

5.3. Cell culture general procedures

HT22 cells were grown in Dulbecco's Modified Eagle Medium (DMEM, Sigma Aldrich, Munich Germany) supplemented with 10% (v/v) fetal calf serum (FCS) and 1% (v/v) penicillin-streptomycin. BV-2 cells were grown in low glucose DMEM (Invitrogen, Carlsbad, CA, USA) supplemented with 10% FCS and 1% (v/v) penicillin-streptomycin. Cells were subcultured every two days and incubated at 37°C with 10% CO_2 in a humidified incubator.

Compounds were dissolved in dimethyl sulfoxide (DMSO, Sigma Aldrich, Munich, Germany) as stock solutions and diluted further into 1x phosphate-buffered saline (PBS).

For determination of cell viability, a colorimetric 3-(4,5-dimethylthiazol-2-yl)-2,5- diphenyl tetrazolium bromide (MTT, Sigma Aldrich, Munich, Germany) assay was used. MTT solution (5 mg/mL in PBS) was diluted 1:10 with medium and added to the wells after removal of the old medium. Cells were incubated for 3 h and then lysis buffer (10% SDS) was applied. The next day, absorbance at 560 nm was determined with a multiwell plate photometer (Tecan, SpectraMax 250).

Neurotoxicity and oxytosis in HT22 cells. 5×10^3 cells per well were seeded into sterile 96-well plates and incubated overnight. For the neurotoxicity assay, medium was removed and 1, 5, 10 or 25 μM of the compound diluted with medium from a 0.1 M stock solution was added to the wells. 0.05% DMSO in DMEM served as a control. Cells were incubated for 24 h when neurotoxicity was determined using a colorimetric MTT assay.

For the oxytosis assay, 5 mM glutamate (monosodium-*L*-glutamate, Sigma Aldrich, Munich, Germany) together with 1, 5 or 10 μM of the respective compound were added to the cells and incubated for 24 h. 25 μM quercetin (Sigma Aldrich, Munich, Germany) together with 5 mM glutamate served as a positive control. After 24 h incubation, cell viability was determined using a colorimetric MTT assay as described above. Results are presented as percentage of untreated control cells. Data is expressed as means ± SEM of three independent experiments. Analysis was accomplished using GraphPad Prism 5 Software applying Oneway ANOVA followed by Dunnett's multiple comparison posttest. Levels of significance: *$p < 0.05$; **$p < 0.01$; ***$p < 0.001$.

Ferroptosis in HT22 cells. 3×10^3 cells per well were seeded into sterile 96-well plates and incubated overnight. The next day medium was exchanged with fresh medium and 300 nM RSL3 was added with vehicle (DMSO) to induce oxidative stress, or together with 1, 5 or 10 μM of the respective compound for protection. After 24 h cell viability was determined using a colorimetric MTT assay. Results are presented as percentage of untreated control cells. Data are expressed as means ± SEM of three independent experiments. Analysis was accomplished using GraphPad Prism 5 Software applying Oneway ANOVA followed by Dunnett's multiple comparison posttest. Levels of significance: *$p < 0.05$; **$p < 0.01$; ***$p < 0.001$.

ATP depletion in HT22 cells. 3×10^3 cells per well were seeded into sterile 96-well plates and incubated overnight. The next day medium was exchanged with fresh medium. 20 μM iodoacetic acid (IAA) was added with vehicle (DMSO) as negative control, or together with 1, 5 or 10 μM of the respective compound for protection. After 2 h incubation at 37°C in the incubator, medium was aspirated, and fresh medium was applied and only the compounds at the same respective concentrations were added without IAA. After 24 h cell viability was determined using a colorimetric MTT assay. Results are presented as percentage of untreated control cells. Data are expressed as means ± SEM of three independent experiments. Analysis was accomplished using GraphPad Prism 5 Software applying Oneway

ANOVA followed by Dunnett's multiple comparison posttest. Levels of significance: *$p < 0.05$; **$p < 0.01$; ***$p < 0.001$.

GSH quantification in HT22 cells. 3×10^5 cells per plate were seeded in sterile 60 mm cell culture dishes. After 24 h incubation medium was exchanged with fresh medium and the respective concentrations of compounds in the presence or absence of 5 mM glutamate were added. After 24 h incubation cells were scraped into ice-cold PBS and 10% sulfosalicylic acid was added at a final concentration of 3.3%. tGSH was measured by a recycling assay based on the reduction of 5,5-dithiobis(2-nitrobenzoic acid) with glutathione reductase and NADPH [49]. Results were normalized to protein recovered from the acid-precipitated pellet by treatment with 0.2 N NaOH at 37°C overnight. Protein levels were determined by the bicinchoninic acid assay (Pierce, Rockford, IL, USA).

Anti-inflammatory activity in BV-2 cells. 5×10^5 cells per plate were seeded in sterile 35 mm cell culture dishes. After overnight incubation medium was exchanged with fresh medium. The cells were pretreated with the respective compounds at the indicated concentrations for 30 min when 50 μg/mL bacterial lipopolysaccharide (LPS) was added. After 24 h incubation, the medium was collected, spun briefly to remove floating cells and 100 μL of the supernatant were assayed for nitrite using 100 μL of the Griess Reagent in a 96 well plate. After incubation for 10 min at room temperature the absorbance at 550 nm was read on a microplate reader. The levels of IL6 and TNFα in the supernatants were determined using ELISAs (R&D Systems, Minneapolis, MN, USA) according to the manufacturer's instruction. Results are normalized to cell number as assessed by the MTT assay as described above.

5.4. Western blots

Sample preparation. 3×10^5 BV-2 cells per 60 mm dish were grown for 24 h before treatment with the respective compounds at the indicated concentrations were. After 4 h incubation nuclear fractions were prepared. Cells were rinsed twice in ice-cold Tris-buffered saline (TBS), scraped into ice-cold nuclear fractionation buffer (10 mM HEPES pH 7.9, 10 mM KCl, 0.1 mM EDTA, 0.1 mM EGTA, 1 mM DTT, 1 mM Na_3VO_4, 1x protease inhibitor cocktail and 1 x phosphatase inhibitor cocktail) and incubated on ice for 15 min. NP40 at a final concentration of 0.6% was added, cells were vortexed and the nuclei were pelleted by centrifugation. Nuclear proteins were extracted by sonication of the nuclear pellet in nuclear fractionation buffer and the extracts were cleared by additional centrifugation. Protein concentrations were quantified by the bicinchoninic acid assay (Pierce, Rockford, IL, USA) and adjusted to equal concentrations. 5x Western blot sample buffer (74 mM Tris-HCl pH 8.0, 6.25% SDS, 10% β-mercaptoethanol, 20% glycerol) was added to a final concentration of 2.5x and samples were boiled for 5 min.

Western blotting. Equal amounts of protein (10–20 μg) per lane were used for SDS-PAGE. All samples were separated using 4–12% Criterion XT Precast Bis-Tris Gels (Biorad, Herculs, CA, USA). Proteins were transferred to nitrocellulose membranes and the quality of protein measurement, electrophoresis and transfer were checked by Ponceau S staining. Membranes were blocked with 5% skim milk in TBS-T (20 mM Tris buffer pH 7.5, 0.5 M NaCl, 0.1% Tween 20) for 1 h at room temperature and incubated overnight at 4 °C with the primary antibody diluted in 5% BSA in TBS/0.05% Tween 20. HRP-conjugated rabbit anti-actin (#5125, 1/20 000) from Cell Signaling (Danvers, MA, USA) and rabbit anti-Nrf2 (#sc-13032, 1/500) were used as primary antibody. Subsequently, blots were washed in TBS/0.05% Tween 20 and incubated for 1 h at room temperature in horseradish peroxidase goat ant-rabbit (Biorad) diluted 1/5000 in 5% skim milk in TBS-T. After additional washing, protein bands were detected by chemiluminescence using the ChemiDoc™ MP Imaging System (Biorad).

Transfection. BV-2 cells were plated with 5×10^5 cells per dish in 60 mm tissue culture dishes and 166 pmol Nrf2 siRNA (#sc-37049) or control siRNA (#sc-37007) (Santa Cruz Biotechnology) were used along with RNAi max (Invitrogen) according to the manufacturer's instructions.

Cellular uptake experiments. 5×10^5 BV-2 cells were grown in 35 mm dishes overnight and then 50 μM **1** was added. Cells were incubated for the indicated time periods after which they were scraped and transferred to Eppendorf tubes. Samples were centrifuged, washed twice with ice-cold PBS and resuspended in 200 μL methanol with 5% acetic acid (v/v). After sonication, cell debris was pelleted by centrifugation and the supernatant was collected for HPLC and MS analysis. The reaction mixture was fractionated by reversed-phase HPLC employing a linear gradient (0–80% acetonitrile in 0.1% trifluoroacetic acid within 40–60 min). A Vydac C-18 column was used (1.2 × 150 mm) and absorbance was monitored at a wavelength of 330 nm.

Mass Spectrometry was performed using a ThermoFisher Q Exactive Hybrid Quadrupole Orbitrap mass spectrometer. Samples were introduced by direct electrospray infusion of the HPLC fractions diluted with a one-to-one mixture of methanol and water containing 0.1% formic acid. Full MS scans were recorded for the 150–750 *m/z* range. MS/MS fragmentation was performed on the major peaks which did not correspond with background signals. Fragmentation was achieved by higher-energy collisional dissociation (HCD) at normalized collision energy settings between 10 and 30%.

5.5. In vivo experiments

Protocols for the behavioral experiments were established and described previously [21,30,31,50]. The compounds **1**, **2**, and the mixtures of taxifolin and ferulic or cinnamic acid were tested for their neuroprotective properties against the toxicity of intracerebroventricular (icv) injection of the oligomerized $A\beta_{25\text{-}35}$ peptide in an *in vivo* pharmacological mouse model of AD [21]. All compounds were dissolved in 60% DMSO in saline (0.9%) and injected intraperitoneally (ip) once per day on days 1–7 of the study. The oligomerized $A\beta_{25\text{-}35}$ peptide was injected icv on the first day of the study. Behavioral evaluation of memory was performed between day 8 and 10, followed by sacrifice on day 11. Brain samples were collected and stored at −80°C awaiting further biochemical analysis.

Animals. For *in vivo* experiments, male Swiss mice (6 weeks old, weighing 31–36 g, from JANVIER (Saint Berthevin, France)) were used. Housing and experiments were conducted in the animal facility building of the University of Montpellier (CECEMA, Office of Veterinary Services agreement # B-34-172-23). Animals were randomly assigned to the different treatment groups and housed with access to food and water *ad libitum*, except during behavioral experiments. Temperature and humidity were controlled in the animal facility providing a 12 h/12 h light/dark cycle (lights off at 07:00 p.m.). All animal procedures were conducted in strict adherence to the European Union directive of September 22, 2010 (2010/63/UE) and the ARRIVE guidelines. The project was authorized by the French National Ethic Committee (APAFIS #1485–15034).

Preparation of compounds for injection. Compounds were weighed every day directly before injection, and dissolved in pure DMSO at a concentration of 3.33 mg/mL. The obtained stock solutions were diluted with saline (0.9%) to the test concentration with a final percentage of DMSO in saline of 60% for all compounds. 60% DMSO in saline was used as vehicle. Behavior of the mice in the home cages was checked visually after all injections, including the control of weight gain. As shown in Fig. 11, weight gain was not altered significantly indicating good compound and vehicle solution tolerability. Animals were tested in behavioral tests 24 h after the last compound/vehicle administration.

Amyloid peptides preparation and icv injection. Methods were described previously [21,30,50]. Briefly, mice were anesthetized with isoflurane 2.5% and $A\beta_{25\text{-}35}$ peptide (9 nmol in 3 μL/mouse) was injected icv. $A\beta_{25\text{-}35}$ peptide was prepared and injected according to

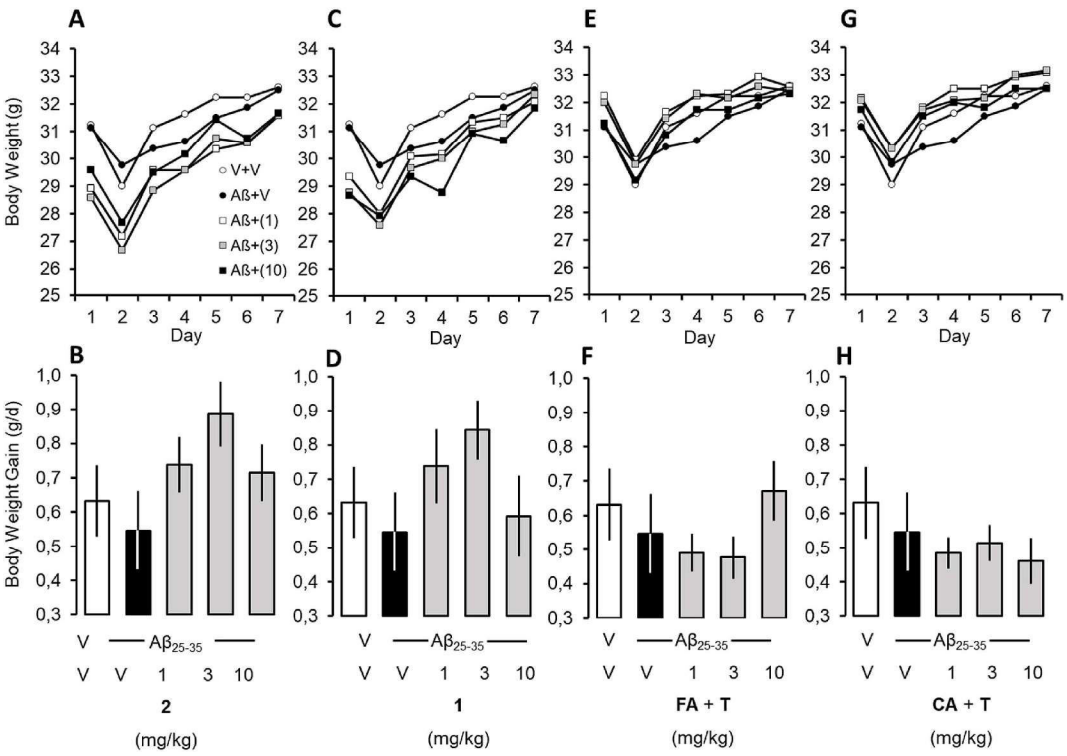

Fig. 11. Upper panel: development of the body weight; lower panel: average of weight gain from day 2–7. Data show mean (upper panel) or mean ± SEM (lower panel). Icv injection provoked a stress-induced acute weight loss, but animals recovered during the following days. ANOVA: $F_{(4,51)} = 1.73$, $p > 0.05$, n = 12 in (**B**); $F_{(4,51)} = 1.25$, $p > 0.05$, n = 12 in (**D**); $F_{(4,51)} = 1.20$, $p > 0.05$, n = 12 in (**F**); $F_{(4,51)} = 0.73$, $p > 0.05$, n = 12 in (**H**).

Maurice et al. [21] Icv injections of bidistilled water served as vehicle.

Spontaneous alternation performances in Y-maze. On day 8, spatial working memory of all mice was evaluated in the Y-maze [21,30,50]. The Y-maze consists of grey polyvinylchloride and 3 arms (40 cm long, 13 cm high, 3 cm wide at the bottom, 10 cm wide at the top, and converging at an equal angle). Every mouse is placed at the end of one arm and allowed to explore the maze freely for 8 min on its own. All entries into an arm (including returns into the same arm) were counted. From this, the number of arm entries and spontaneous alternations (mouse enters all three arms on consecutive occasion) were calculated (alternations/(arm entries-2) x 100).

Passive avoidance test. A passive avoidance test was performed on days 9 (training) and 10 (measurement of retention) to evaluate non-spatial long-term memory, as described previously [21,30,50]. For the experiment, a two-compartment (15 × 20 × 15 cm high) polyvinylchloride box was used. Thereby, one compartment is white and illuminated with a bulb (60 W, 40 cm above the apparatus) and the other compartment is black with a cover and grid floor. The compartments are separated by a guillotine door. During the training session (day 9), every animal was placed in the white compartment and left to explore for 5 s. Then, the door was opened, and the mouse was able to explore into the dark compartment. After it entered the dark with all its paws touching the grid floor, the door was closed, and a foot shock was delivered (0.3 mA) for 3 s using a scrambled shock generator (Lafayette Instruments, Lafayette, USA). The time to enter the dark compartment (step-through latency), and the level of sensitivity to the shock evaluated (no sign = 0, flinching reactions = 1, vocalizations = 2) were recorded. The treatments did not affect the step-through latency or shock sensitivity in the present study (data not shown). On day 10, the mice were placed in the white compartment again and the door was opened after 5 s allowing the mouse to explore the box. The step-through latency was measured up to 300 s.

Sacrifice and brain sampling. Animals were sacrificed on day 11, and their brains were collected. Hippocampus and cortex were isolated and frozen in liquid nitrogen for further evaluation. Brain samples were stored at −80°C.

Statistical analysis. Statistical analysis of weight gain and results from Y-maze assay were performed with GraphPad Prism 5.0 using one-way ANOVA (*F* value), followed by the Dunnett's *post-hoc* multiple comparison test. As passive avoidance latencies have cut-off times after 300 s, the results do not follow a Gaussian distribution. Therefore, they were analyzed using a Kruskal-Wallis non-parametric ANOVA (*H* value), followed by a Dunn's multiple comparison test. $p < 0.05$ was considered as statistically significant.

Associated content

Spectral data for the compounds and uptake experiments can be found in the supporting information.

Author contributions

The manuscript was written through contributions of all authors. All authors have given approval to the final version of the manuscript.

Funding sources

Financial support by the Bavaria California Technology Center under project number 3 [2018–2] is gratefully acknowledged. MD and TM also acknowledge support from Campus France (PHC Procope), and the German Academic Exchange Service (DAAD) with funds of the Federal Ministry of Education and Research (BMBF). SG was supported by a grant of the German Excellence Initiative to the Graduate School of Life Sciences, University of Würzburg. PM was supported by funding from NIH (RO1 AG046153, RF1 AG054714 and R41 AI104034). This publication was funded by the German Research Foundation (DFG) and the University of Wuerzburg in the funding programme Open Access Publishing.

Acknowledgment

This work was supported by the Mass Spectrometry Core of the Salk Institute with funding from NIH-NCI CCSG: P30 014195 and the Helmsley Center for Genomic Medicine. The MS data described here was gathered on a ThermoFisher Q Exactive Hybrid Quadrupole Orbitrap mass spectrometer funded by NIH grant (1S10OD021815-01).

Appendix A. Supplementary data

Supplementary data to this article can be found online at https://doi.org/10.1016/j.redox.2019.101378.

Abbreviations

GSH	glutathione
IAA	iodoacetic acid
IL6	interleukin 6
Nrf2	nuclear factor (erythroid-derived 2)-like 2
TNFα	tumor necrosis factor α

References

[1] World Alzheimer report 2018; Alzheimer's disease international, https://www.alz.co.uk/research/world-report-2018 , Accessed date: 31 July 2019.
[2] A.J. Doig, M.P. Del Castillo-Frias, O. Berthoumieu, B. Tarus, J. Nasica-Labouze, F. Sterpone, P.H. Nguyen, N.M. Hooper, P. Faller, P. Derreumaux, Why is research on amyloid-beta failing to give new drugs for Alzheimer's disease? ACS Chem. Neurosci. 8 (7) (2017) 1435–1437.
[3] P. Agostinho, R.A. Cunha, C.N. Oliveira, Oxidative stress and the pathogenesis of Alzheimer's disease, Curr. Pharmaceut. Des. 16 (25) (2010) 2766–2778.
[4] F. Pohl, P. Kong Thoo Lin, The potential use of plant natural products and plant extracts with antioxidant properties for the prevention/treatment of neurodegenerative diseases: in vitro, in vivo and clinical trials, Molecules 23 (12) (2018) 3283–3313.
[5] A. Currais, C. Chiruta, M. Goujon-Svrzic, G. Costa, T. Santos, M.T. Batista, J. Paiva, M. do Ceu Madureira, P. Maher, Screening and identification of neuroprotective compounds relevant to alzheimers disease from medicinal plants of S. Tomé e Príncipe, J. Ethnopharmacol. 155 (1) (2014) 830–840.
[6] S. Schramm, G. Huang, S. Gunesch, F. Lang, J. Roa, P. Högger, R. Sabate, P. Maher, M. Decker, Regioselective synthesis of 7-*O*-esters of the flavonolignan silibinin and sars lead to compounds with overadditive neuroprotective effects, Eur. J. Med. Chem. 146 (2018) 93–107.
[7] S. Gunesch, S. Schramm, M. Decker, Natural antioxidants in hybrids for the treatment of neurodegenerative diseases: a successful strategy? Future Med. Chem. 9 (8) (2017) 711–713.
[8] J.B. Baell, Feeling nature's pains: natural products, natural product drugs, and pan assay interference compounds (PAINS), J. Nat. Prod. 79 (3) (2016) 616–628.
[9] N.H. Gay, K. Phopin, W. Suwanjang, N. Songtawee, W. Ruankham, P. Wongchitrat, S. Prachayasittikul, V. Prachayasittikul, Neuroprotective effects of phenolic and carboxylic acids on oxidative stress-induced toxicity in human neuroblastoma SH-SY5Y cells, Neurochem. Res. 43 (3) (2018) 619–636.
[10] J.J. Yan, J.Y. Cho, H.S. Kim, K.L. Kim, J.S. Jung, S.O. Huh, H.W. Suh, Y.H. Kim, D.K. Song, Protection against beta-amyloid peptide toxicity in vivo with long-term administration of ferulic acid, Br. J. Pharmacol. 133 (1) (2001) 89–96.
[11] T. Mori, N. Koyama, M.V. Guillot-Sestier, J. Tan, T. Town, Ferulic acid is a nutraceutical beta-secretase modulator that improves behavioral impairment and Alzheimer-like pathology in transgenic mice, PLoS One 8 (2) (2013) e55774.
[12] S. Chakrabarti, M. Jana, A. Roy, K. Pahan, Upregulation of suppressor of cytokine signaling 3 in microglia by cinnamic acid, Curr. Alzheimer Res. 15 (10) (2018) 894–904.
[13] S. Schramm, S. Gunesch, F. Lang, M. Saedtler, L. Meinel, P. Högger, M. Decker, Investigations into neuroprotectivity, stability, and water solubility of 7-*O*-cinnamoylsilibinin, its hemisuccinate and dehydro derivatives, Arch. Pharm. Chem. Life Sci. 351 (11) (2018).
[14] M. Sato, K. Murakami, M. Uno, Y. Nakagawa, S. Katayama, K. Akagi, Y. Masuda, K. Takegoshi, K. Irie, Site-specific inhibitory mechanism for amyloid beta42 aggregation by catechol-type flavonoids targeting the Lys residues, J. Biol. Chem. 288 (32) (2013) 23212–23224.
[15] T. Ginex, M. Trius, F.J. Luque, Computational study of the aza-Michael addition of the flavonoid (+)-taxifolin in the inhibition of beta-amyloid fibril aggregation, Chem. Eur. J. 24 (22) (2018) 5813–5824.
[16] J. Vrba, R. Gazak, M. Kuzma, B. Papouskova, J. Vacek, M. Weiszenstein, V. Kren, J. Ulrichova, A novel semisynthetic flavonoid 7-O-galloyltaxifolin upregulates heme oxygenase-1 in RAW264.7 cells via MAPK/Nrf2 pathway, J. Med. Chem. 56 (3) (2013) 856–866.
[17] T. Inoue, S. Saito, M. Tanaka, H. Yamakage, T. Kusakabe, A. Shimatsu, M. Ihara, N. Satoh-Asahara, Pleiotropic neuroprotective effects of taxifolin in cerebral amyloid angiopathy, Proc. Natl. Acad. Sci. U.S.A. 116 (20) (2019) 10031–10038.
[18] M. Tanaka, S. Saito, T. Inoue, N. Satoh-Asahara, M. Ihara, Novel therapeutic potentials of taxifolin for amyloid-beta-associated neurodegenerative diseases and other diseases: recent advances and future perspectives, Int. J. Mol. Sci. 20 (9) (2019).
[19] A. Sgarbossa, D. Giacomazza, M. di Carlo, Ferulic acid: a hope for Alzheimer's disease therapy from plants, Nutrients 7 (7) (2015) 5764–5782.
[20] M. Prior, C. Chiruta, A. Currais, J. Goldberg, J. Ramsey, R. Dargusch, P.A. Maher, D. Schubert, Back to the future with phenotypic screening, ACS Chem. Neurosci. 5 (7) (2014) 503–513.
[21] T. Maurice, B.P. Lockhart, A. Privat, Amnesia induced in mice by centrally administered beta-amyloid peptides involves cholinergic dysfunction, Brain Res. 706 (2) (1996) 181–193.
[22] S. Tan, D. Schubert, P. Oxytosis Maher, A novel form of programmed cell death, Curr. Top. Med. Chem. 1 (6) (2001) 497–506.
[23] A. Currais, P. Maher, Functional consequences of age-dependent changes in glutathione status in the brain, Antioxidants Redox Signal. 19 (8) (2013) 813–822.
[24] J. Lewerenz, G. Ates, A. Methner, M. Conrad, P. Maher, Oxytosis/ferroptosis-(re-) emerging roles for oxidative stress-dependent non-apoptotic cell death in diseases of the central nervous system, Front. Neurosci. 12 (214) (2018).
[25] P. Maher, K. van Leyen, P.N. Dey, B. Honrath, A. Dolga, A. Methner, The role of Ca (2+) in cell death caused by oxidative glutamate toxicity and ferroptosis, Cell Calcium 70 (2018) 47–55.
[26] W.S. Yang, K.J. Kim, M.M. Gaschler, M. Patel, M.S. Shchepinov, B.R. Stockwell, Peroxidation of polyunsaturated fatty acids by lipoxygenases drives ferroptosis, Proc. Natl. Acad. Sci. U.S.A. 113 (34) (2016) 4966–4975.
[27] U. Saxena, Bioenergetics failure in neurodegenerative diseases: back to the future, Expert Opin. Ther. Targets 16 (4) (2012) 351–354.
[28] P. Maher, K.F. Salgado, J.A. Zivin, P.A. Lapchak, A novel approach to screening for new neuroprotective compounds for the treatment of stroke, Brain Res. 1173 (2007) 117–125.
[29] T. Wyss-Coray, J. Rogers, Inflammation in Alzheimer disease-a brief review of the basic science and clinical literature, Cold Spring Harbor Perspect. Med. 2 (1) (2012) a006346.
[30] D. Dolles, M. Hoffmann, S. Gunesch, O. Marinelli, J. Moller, G. Santoni, A. Chatonnet, M.J. Lohse, H.J. Wittmann, A. Strasser, M. Nabissi, T. Maurice, M. Decker, Structure-activity relationships and computational investigations into the development of potent and balanced dual-acting butyrylcholinesterase inhibitors and human cannabinoid receptor 2 ligands with pro-cognitive in vivo profiles, J. Med. Chem. 61 (4) (2018) 1646–1663.
[31] V. Lahmy, J. Meunier, S. Malmstrom, G. Naert, L. Givalois, S.H. Kim, V. Villard, A. Vamvakides, T. Maurice, Blockade of tau hyperphosphorylation and Abeta1-42 generation by the aminotetrahydrofuran derivative anavex2-73, a mixed muscarinic and sigma(1) receptor agonist, in a nontransgenic mouse model of Alzheimer's disease, Neuropsychopharmacology 38 (9) (2013) 1706–1723.
[32] M.V. Turovskaya, S.G. Gaidin, V.N. Mal'tseva, V.P. Zinchenko, E.A. Turovsky, Taxifolin protects neurons against ischemic injury in vitro via the activation of antioxidant systems and signal transduction pathways of gabaergic neurons, Mol. Cell. Neurosci. 96 (2019) 10–24.
[33] J.P. Spencer, K. Vafeiadou, R.J. Williams, D. Neuroinflammation Vauzour, Modulation by flavonoids and mechanisms of action, Mol. Asp. Med. 33 (1) (2012) 83–97.
[34] R. Gazak, P. Sedmera, M. Vrbacky, J. Vostalova, Z. Drahota, P. Marhol, D. Walterova, V. Kren, Molecular mechanisms of silybin and 2,3-dehydrosilybin antiradical activity-role of individual hydroxyl groups, Free Radic. Biol. Med. 46 (6) (2009) 745–758.
[35] A. Mattarei, L. Biasutto, F. Rastrelli, S. Garbisa, E. Marotta, M. Zoratti, C. Paradisi, Regioselective O-derivatization of quercetin via ester intermediates. An improved synthesis of rhamnetin and development of a new mitochondriotropic derivative, Molecules 15 (7) (2010) 4722–4736.
[36] R. Gazak, K. Purchartova, P. Marhol, L. Zivna, P. Sedmera, K. Valentova, N. Kato, H. Matsumura, K. Kaihatsu, V. Kren, Antioxidant and antiviral activities of silybin fatty acid conjugates, Eur. J. Med. Chem. 45 (3) (2010) 1059–1067.
[37] D. Schubert, P. Maher, An alternative approach to drug discovery for Alzheimer's disease dementia, Future Med. Chem. 4 (13) (2012) 1681–1688.
[38] J.L. Ehren, P. Maher, Concurrent regulation of the transcription factors Nrf2 and ATF4 mediates the enhancement of glutathione levels by the flavonoid fisetin, Biochem. Pharmacol. 85 (12) (2013) 1816–1826.
[39] N. Ballatori, S.M. Krance, S. Notenboom, S. Shi, K. Tieu, C.L. Hammond, Glutathione dysregulation and the etiology and progression of human diseases, Biol. Chem. 390 (3) (2009) 191–214.
[40] L. Chen, H. Teng, Z. Jia, M. Battino, A. Miron, Z. Yu, H. Cao, J. Xiao, Intracellular signaling pathways of inflammation modulated by dietary flavonoids: the most recent evidence, Crit. Rev. Food Sci. Nutr. 58 (17) (2018) 2908–2924.
[41] E.H. Kobayashi, T. Suzuki, R. Funayama, T. Nagashima, M. Hayashi, H. Sekine, N. Tanaka, T. Moriguchi, H. Motohashi, K. Nakayama, M. Yamamoto, Nrf2 suppresses macrophage inflammatory response by blocking proinflammatory cytokine transcription, Nat. Commun. 7 (2016) 11624–11638.
[42] P. Lu, T. Mamiya, L.L. Lu, A. Mouri, L. Zou, T. Nagai, M. Hiramatsu, T. Ikejima, T. Nabeshima, Silibinin prevents amyloid beta peptide-induced memory impairment and oxidative stress in mice, Br. J. Pharmacol. 157 (7) (2009) 1270–1277.
[43] X. Song, B. Zhou, P. Zhang, D. Lei, Y. Wang, G. Yao, T. Hayashi, M. Xia, S. Tashiro, S. Onodera, T. Ikejima, Protective effect of silibinin on learning and memory impairment in LPS-treated rats via ROS-BDNF-TrkB pathway, Neurochem. Res. 41 (7) (2016) 1662–1672.
[44] K. Yamada, T. Tanaka, D. Han, K. Senzaki, T. Kameyama, T. Nabeshima, Protective effects of idebenone and alpha-tocopherol on beta-amyloid-(1-42)-induced learning

and memory deficits in rats: implication of oxidative stress in beta-amyloid-induced neurotoxicity in vivo, Eur. J. Neurosci. 11 (1) (1999) 83–90.

[45] Y. Wang, Q. Wang, X. Bao, Y. Ding, J. Shentu, W. Cui, X. Chen, X. Wei, S. Xu, Taxifolin prevents beta-amyloid-induced impairments of synaptic formation and deficits of memory via the inhibition of cytosolic phospholipase A_2/prostaglandin E_2 content, Metab. Brain Dis. 33 (4) (2018) 1069–1079.

[46] S.Y. Park, H.Y. Kim, H.J. Park, H.K. Shin, K.W. Hong, C.D. Kim, Concurrent treatment with taxifolin and cilostazol on the lowering of beta-amyloid accumulation and neurotoxicity via the suppression of P-JAK2/P-STAT3/NF-kappaB/BACE1 signaling pathways, PLoS One 11 (12) (2016) e0168286.

[47] J. Meunier, V. Villard, L. Givalois, T. Maurice, The gamma-secretase inhibitor 2-[(1r)-1-[(4-chlorophenyl)sulfonyl](2,5-difluorophenyl) amino]ethyl-5-fluorobenzenebutanoic acid (BMS-299897) alleviates Abeta1-42 seeding and short-term memory deficits in the Abeta25-35 mouse model of Alzheimer's disease, Eur. J. Pharmacol. 698 (1–3) (2013) 193–199.

[48] S. Saito, Y. Yamamoto, T. Maki, Y. Hattori, H. Ito, K. Mizuno, M. Harada-Shiba, R.N. Kalaria, M. Fukushima, R. Takahashi, M. Ihara, Taxifolin inhibits amyloid-beta oligomer formation and fully restores vascular integrity and memory in cerebral amyloid angiopathy, Acta Neuropathol. Commun. 5 (26) (2017).

[49] P. Maher, Potentiation of glutathione loss and nerve cell death by the transition metals iron and copper: implications for age-related neurodegenerative diseases, Free Radic. Biol. Med. 115 (2018) 92–104.

[50] T. Maurice, M. Strehaiano, N. Simeon, C. Bertrand, A. Chatonnet, Learning performances and vulnerability to amyloid toxicity in the butyrylcholinesterase knockout mouse, Behav. Brain Res. 296 (2016) 351–360.

SUPPORTING INFORMATION

7-*O*-Esters of taxifolin with pronounced and overadditive effects in neuroprotection, anti-neuroinflammation, and amelioration of short-term memory impairment *in vivo*.

Sandra Gunesch, [a] *Carolina Kiermeier,* [a] *Matthias Hoffmann,* [a] *Wolfgang Fischer,* [b] *Antonio Pinto,* [b] *Tangui Maurice,* [c] *Pamela Maher,* [b]* *and Michael Decker* [a]*

Table of contents:

S1: HPLC chromatograms of cellular uptake experiment

a) Reference chromatogram

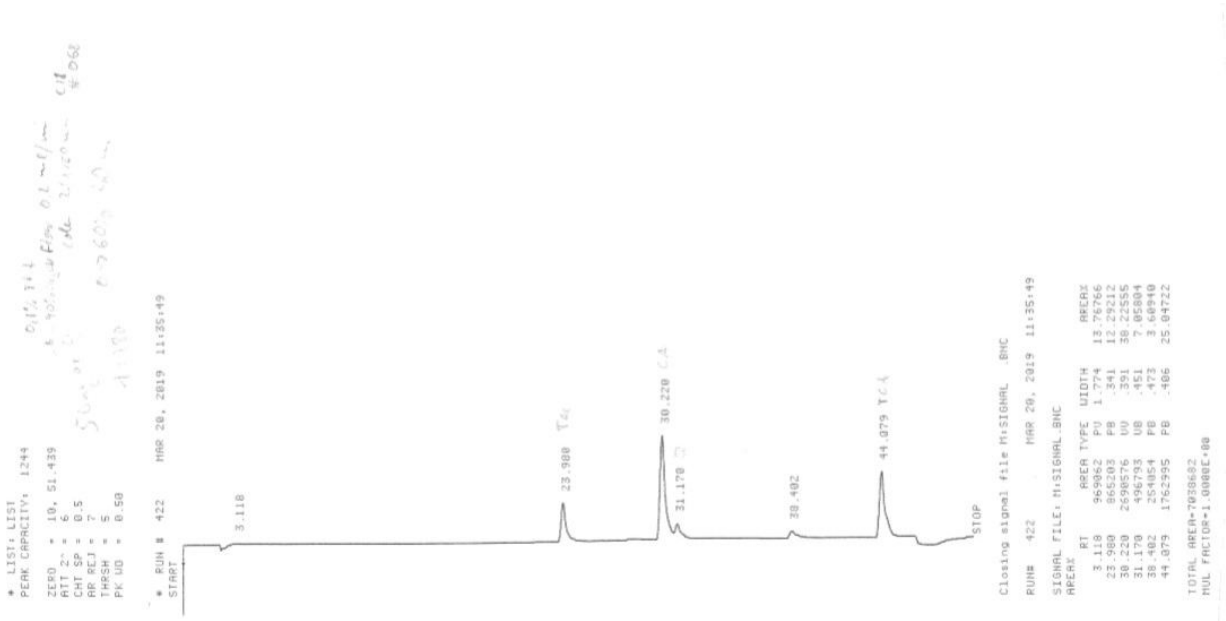

b) BV-2 cell lysate immediately after addition of 50 µM compound **1** (0 min)

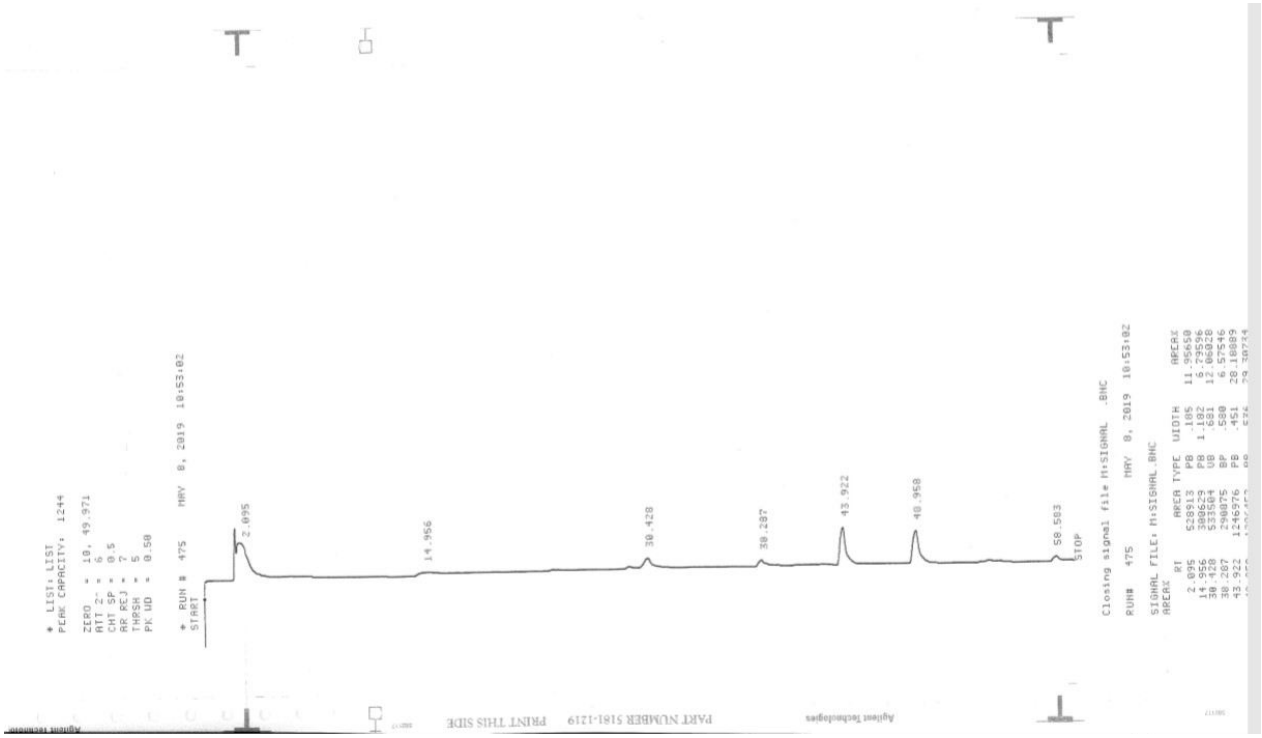

c) BV-2 cell lysate after 30 minutes incubation with 50 µM compound **1**

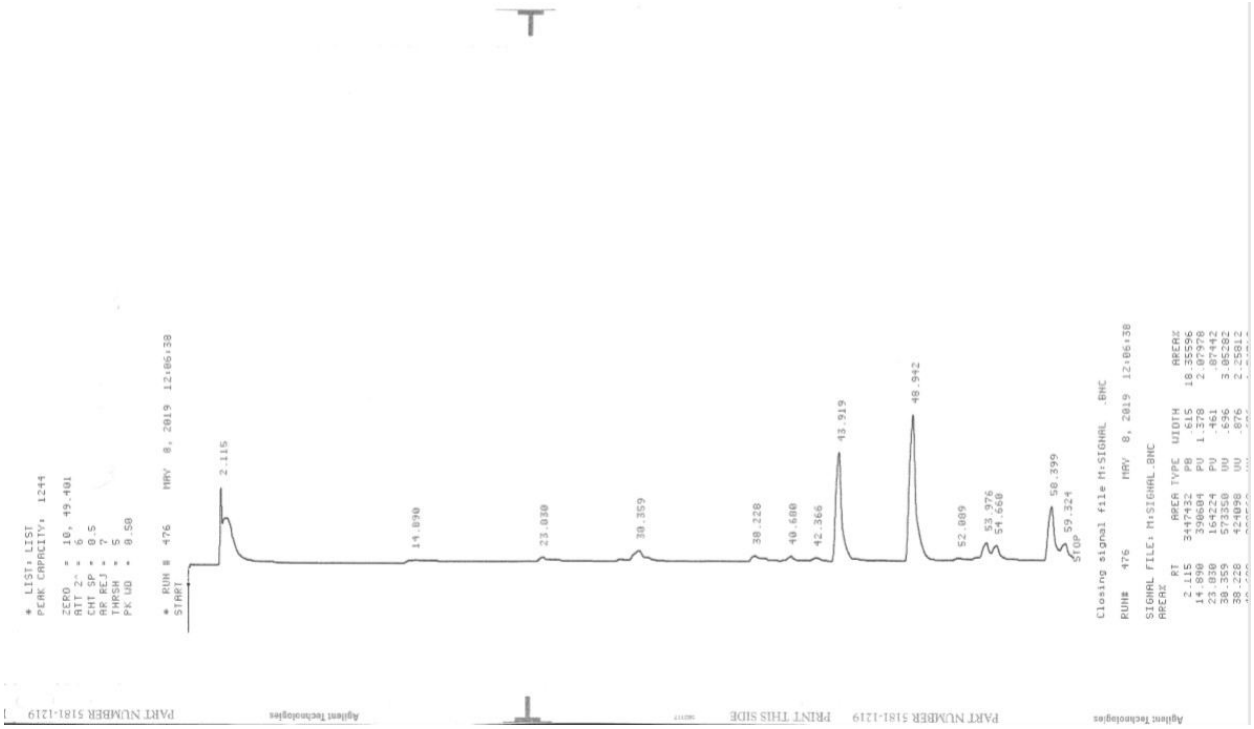

d) BV-2 cell lysate after 90 minutes incubation with 50 µM compound **1**

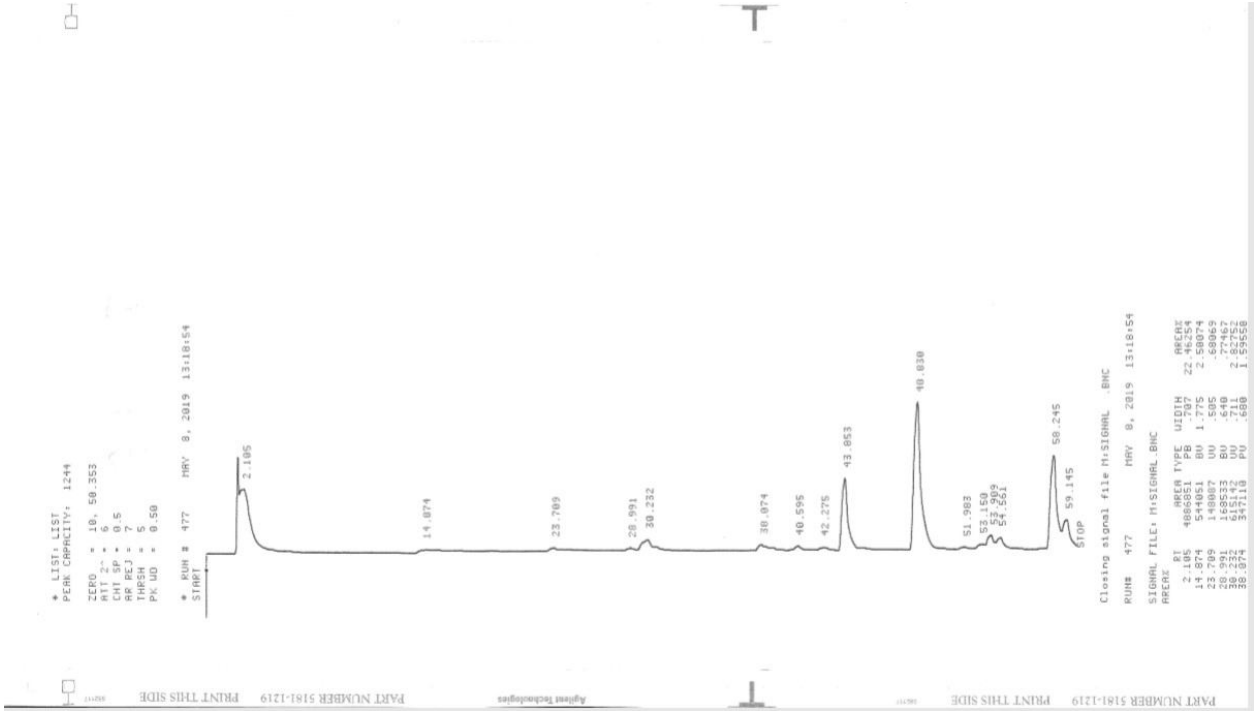

e) BV-2 cell lysate after 4 hours incubation with 50 µM compound **1**

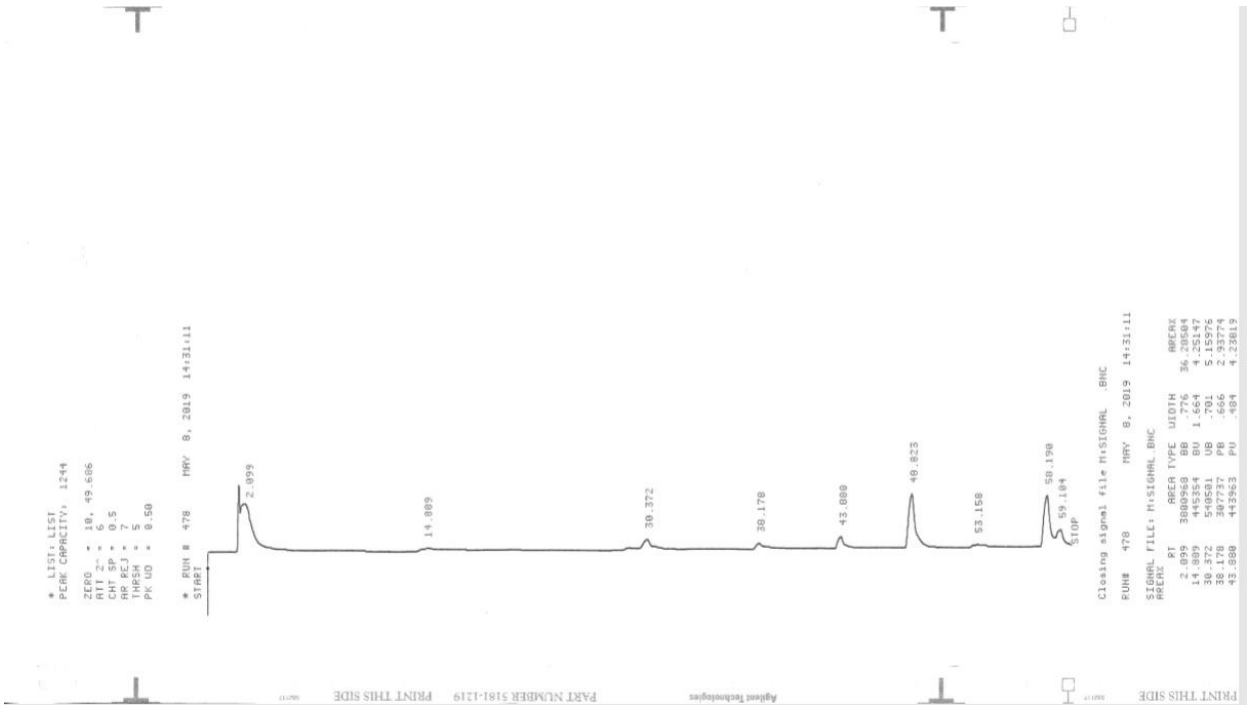

f) Medium only (blank)

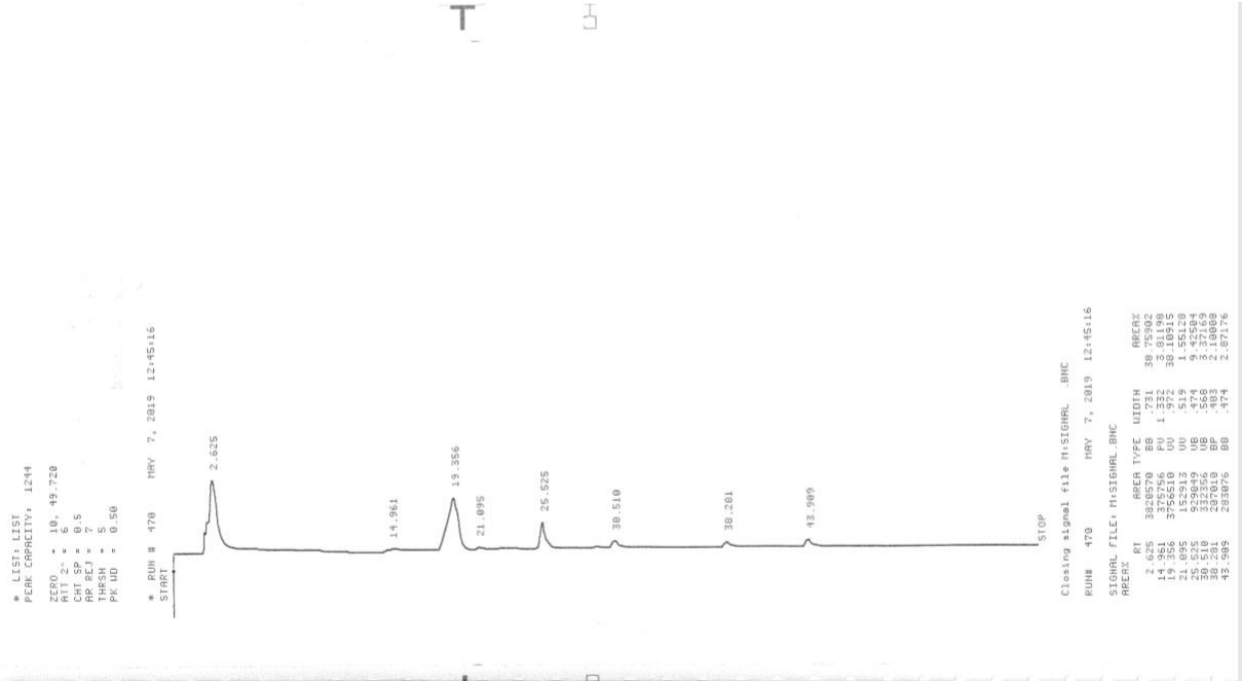

g) 30 minutes incubation of 50 µM compound **1** in medium only (without cells)

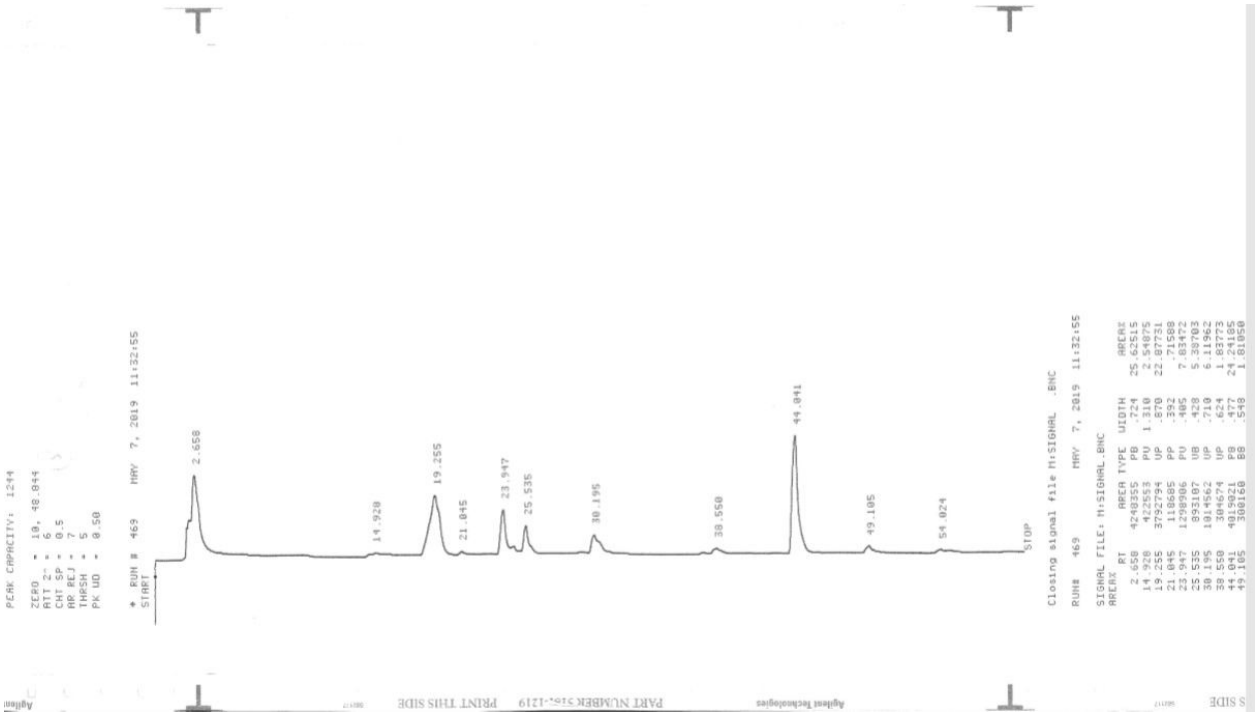

S2: Full MS spectra and MS fragmentation pattern of collected peaks

a) MS spectrum of peak 1, retention time = 43.9 min corresponding to compound **1**

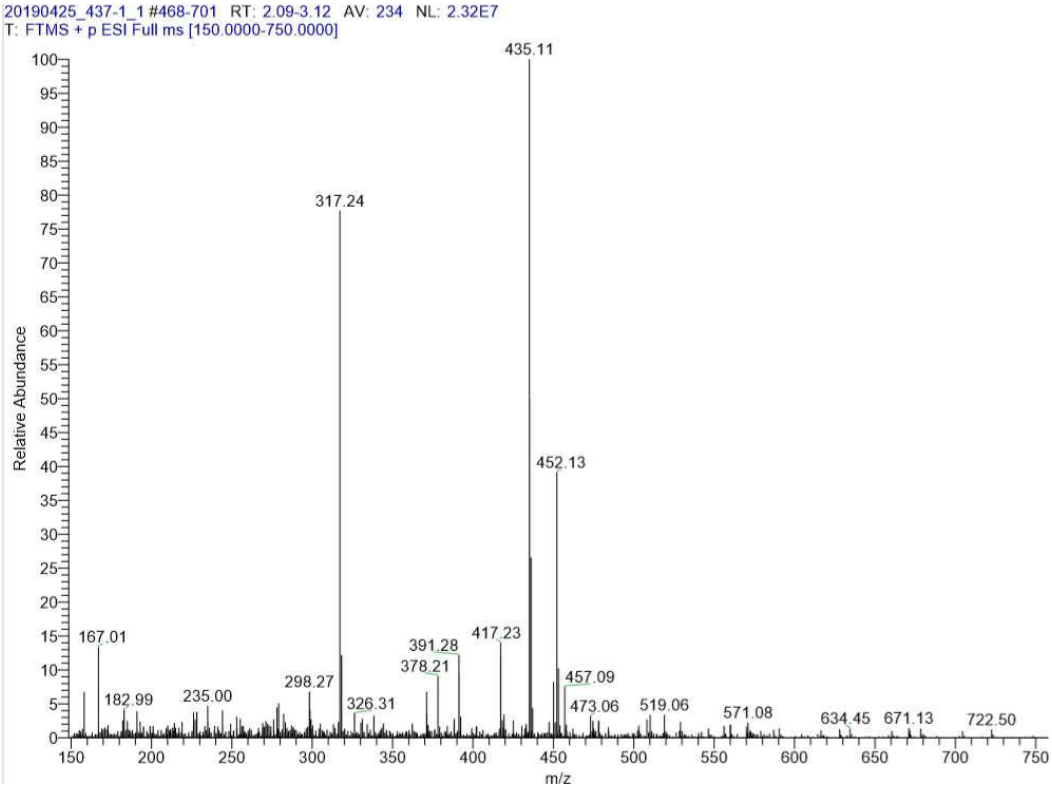

b) MS fragmentation pattern *m/z* = 435.11

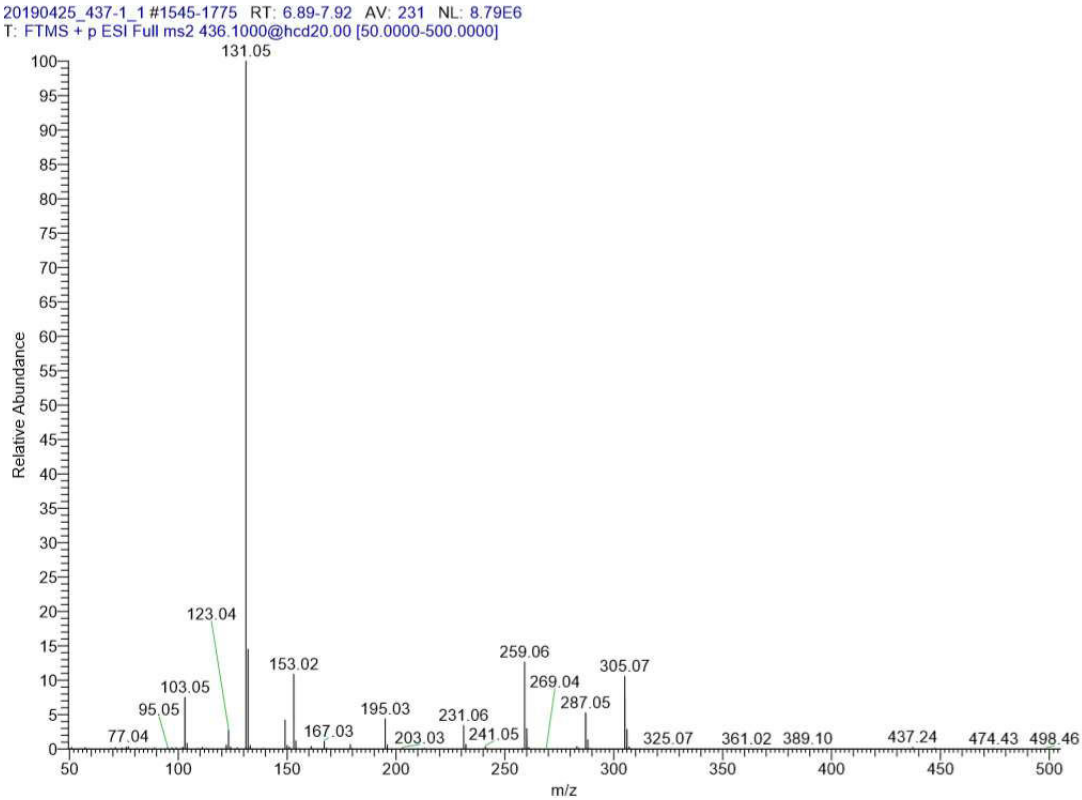

c) MS spectrum of peak 2, retention time = 48.9 min

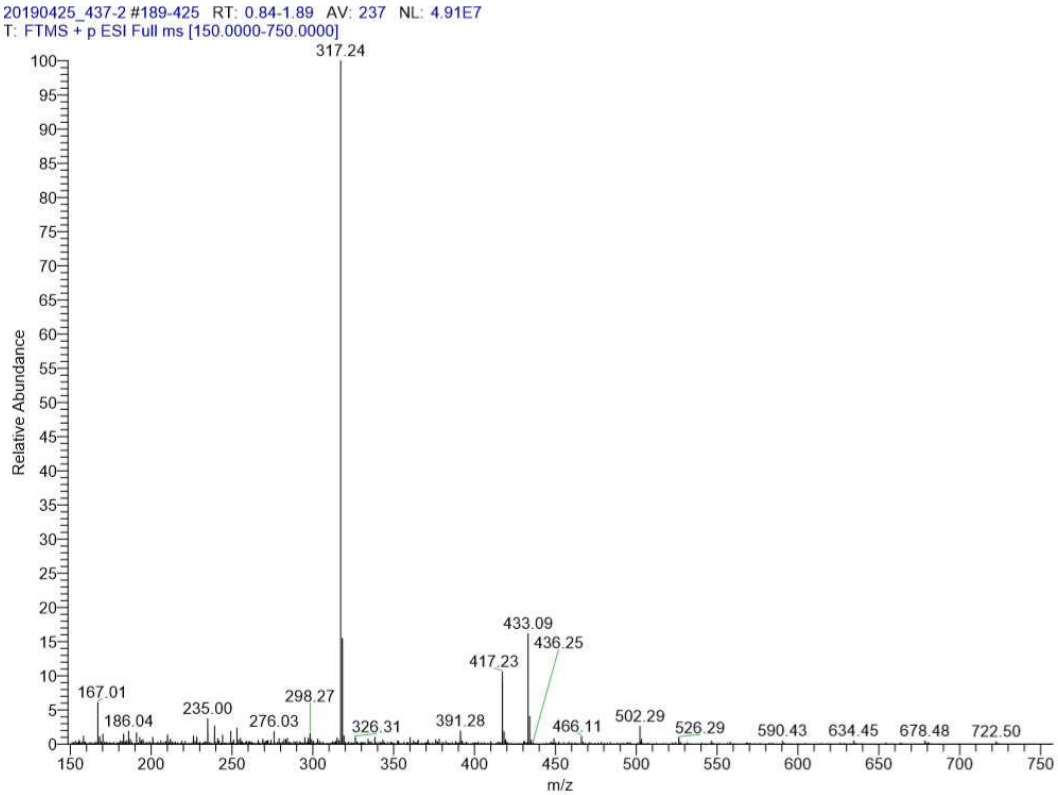

d) MS fragmentation pattern *m/z* = 435.11

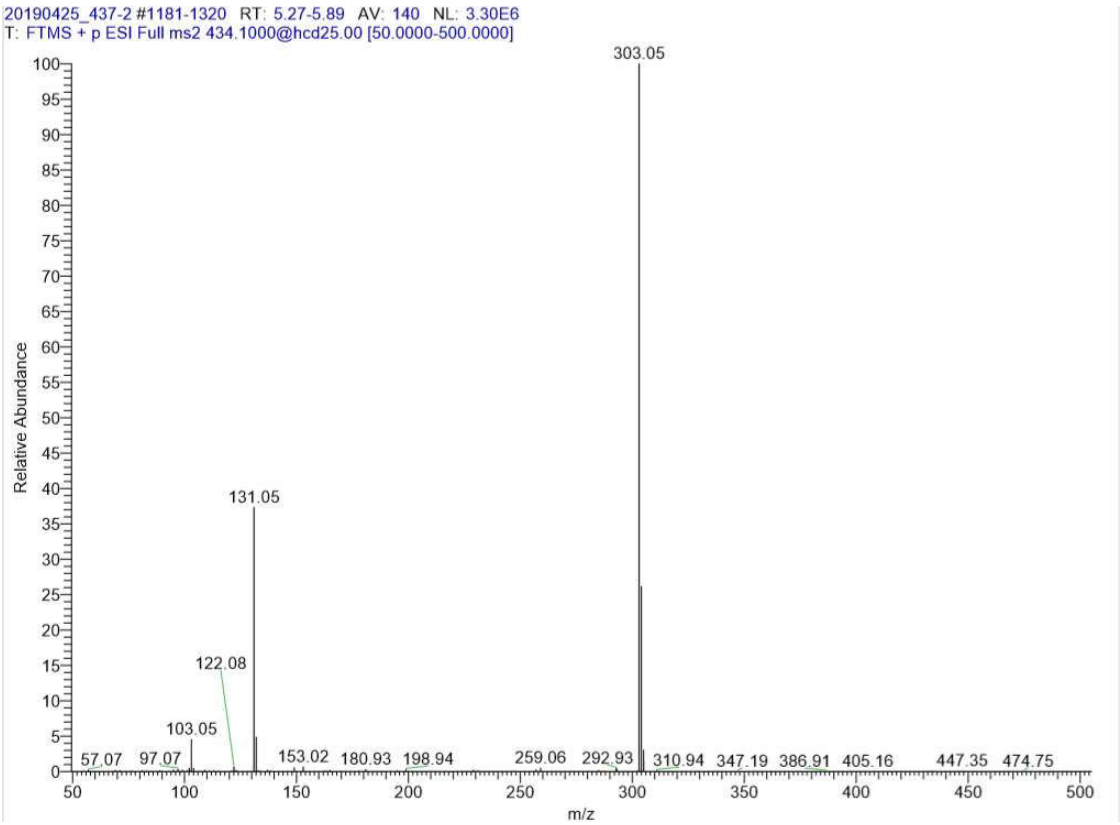

S3: LC chromatogram for purity verification

a) 7-*O*-Cinnamoyltaxifolin (**1**)

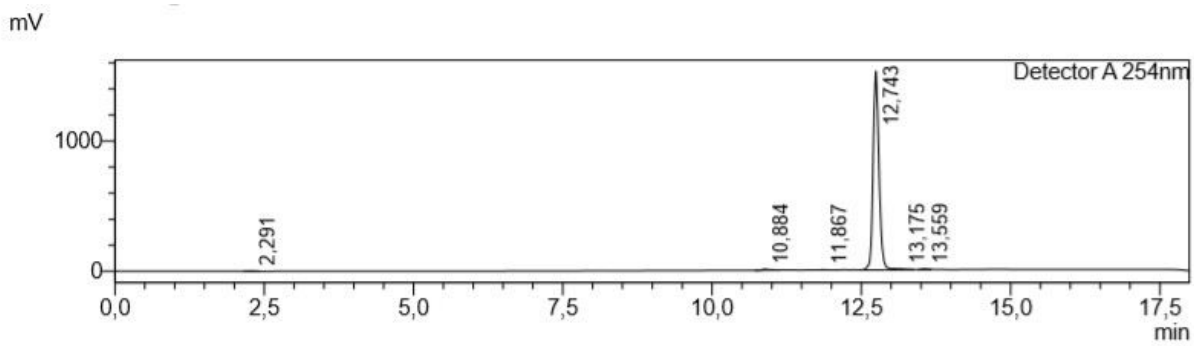

Peak Table

Detector A 254nm

Peak#	Ret. Time	Area	Height	Area%
1	2,291	20591	2788	0,191
2	10,884	72304	7475	0,672
3	11,867	11390	1918	0,106
4	12,743	10563297	1517145	98,131
5	13,175	68236	6068	0,634
6	13,559	28705	5233	0,267
Total		10764523	1540627	100,000

b) 7-*O*-Feruloyltaxifolin (**2**)

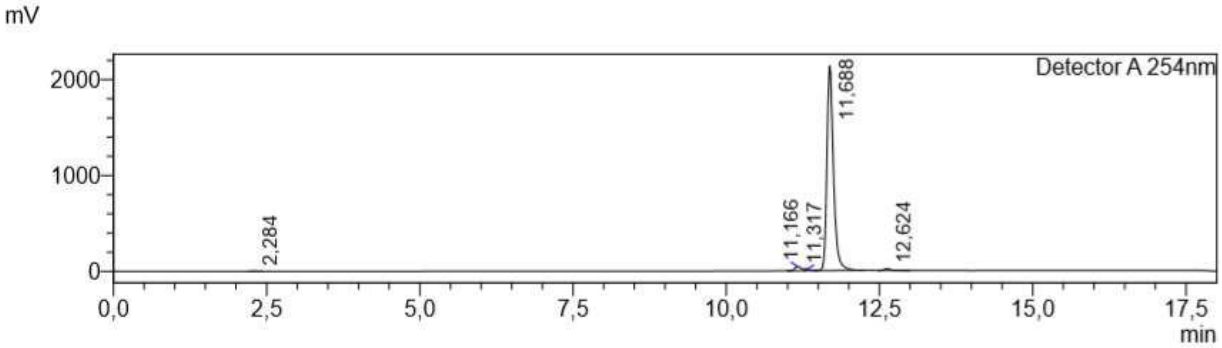

Peak Table

Detector A 254nm

Peak#	Ret. Time	Area	Height	Area%
1	2,284	12178	2290	0,074
2	11,166	338247	45724	2,063
3	11,317	90606	14234	0,553
4	11,688	15809935	2132902	96,415
5	12,624	146900	18410	0,896
Total		16397867	2213560	100,000

Appendix II:

Gunesch, S.; Soriano-Castell, D.; Lamer, S.; Schlosser, A.; Maher, P.; Decker, M. Development and application of a chemical probe based on a neuroprotective flavonoid hybrid for target identification using activity-based protein profiling. *ACS Chem. Neurosci.* **2020** (in press).

http://dx.doi.org/10.1021/acschemneuro.0c00589

ACS Chemical Neuroscience

pubs.acs.org/chemneuro Research Article

Development and Application of a Chemical Probe Based on a Neuroprotective Flavonoid Hybrid for Target Identification Using Activity-Based Protein Profiling

Sandra Gunesch, David Soriano-Castell, Stephanie Lamer, Andreas Schlosser, Pamela Maher,* and Michael Decker*

Cite This: https://dx.doi.org/10.1021/acschemneuro.0c00589 Read Online

ACCESS | Metrics & More | Article Recommendations | Supporting Information

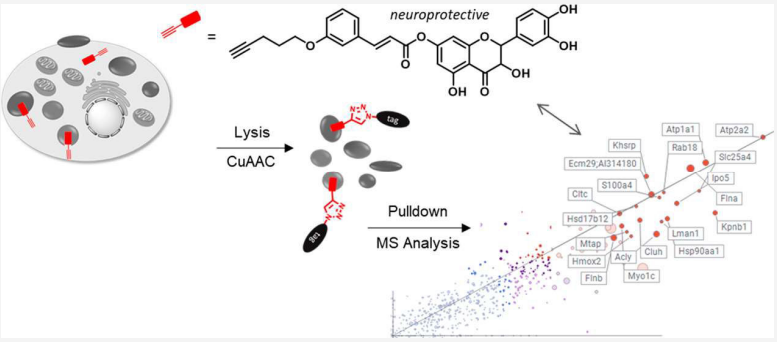

ABSTRACT: Alzheimer's disease (AD) is the most common form of dementia, and up to now, there are no disease-modifying drugs available. Natural product hybrids based on the flavonoid taxifolin and phenolic acids have shown a promising pleiotropic neuroprotective profile in cell culture assays and even disease-modifying effects *in vivo*. However, the detailed mechanisms of action remain unclear. To elucidate the distinct intracellular targets of 7-*O*-esters of taxifolin, we present in this work the development and application of a chemical probe, 7-*O*-cinnamoyltaxifolin-alkyne, for target identification using activity-based protein profiling. 7-*O*-Cinnamoyltaxifolin-alkyne remained neuroprotective in all cell culture assays. Western blot analysis showed a comparable influence on the same intracellular pathways as that of the lead compound 7-*O*-cinnamoyltaxifolin, thereby confirming its suitability as a probe for target identification experiments. Affinity pulldown and MS analysis revealed adenine nucleotide translocase 1 (ANT-1) and sarco/endoplasmic reticulum Ca^{2+} ATPase (SERCA) as intracellular interaction partners of 7-*O*-cinnamoyltaxifolin-alkyne and thus of 7-*O*-esters of taxifolin.

KEYWORDS: *Alzheimer's disease, natural product hybrids, CuAAC, neuroinflammation*

■ INTRODUCTION

Alzheimer's disease (AD) is the most common form of dementia and due to aging societies, the number of affected people is increasing dramatically.[1] AD is characterized by abnormal protein aggregation of hyperphosphorylated tau protein forming neurofibrillary tangles and amyloid β accumulation as extracellular plaques.[2] Neuroinflammation and oxidative stress are strong contributors to neurodegeneration and AD pathology.[3,4] Enhancing the pathophysiology of protein aggregation, oxidative stress and neuroinflammation may even represent key factors in AD development.[5] Currently, there are no disease-modifying drugs on the market. The only available treatments are symptomatic and cannot halt or cure the disease.[1] The complexity of AD and the lack of understanding of the details of its cause and progression are hampering drug development. It is important to broaden the knowledge about the molecular causes of the disease and focus on compounds with a pleiotropic neuroprotective profile to deal with the multifactorial nature of AD,[6] particularly as the one-target strategy has not been successful in drug discovery so far.[7]

Natural products have been used in traditional medicine and are gaining increased attention for their potential as neuroprotectants interfering with disease progression.[8−10] The well-established antioxidant features of natural products, i.e., their radical scavenging abilities, are important for neuroprotection

Received: September 8, 2020
Accepted: October 13, 2020

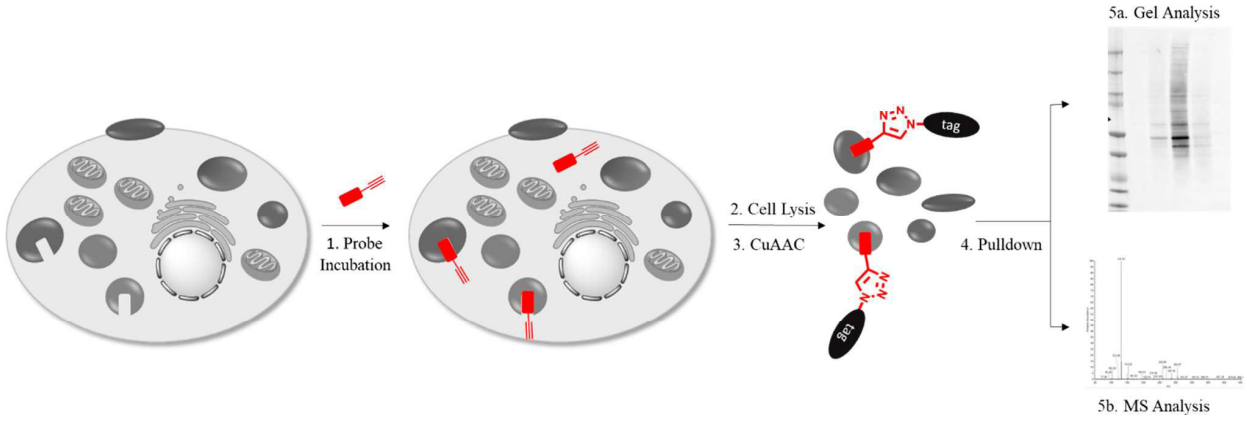

Figure 1. Workflow of the CuAAC approach for target identification. During incubation, the chemical probe binds to its native targets inside the cells. The cells are lysed and submitted to the CuAAC reaction to tag the chemical probe, which is covalently bound to its intracellular targets. After pulldown purification, target proteins are analyzed.

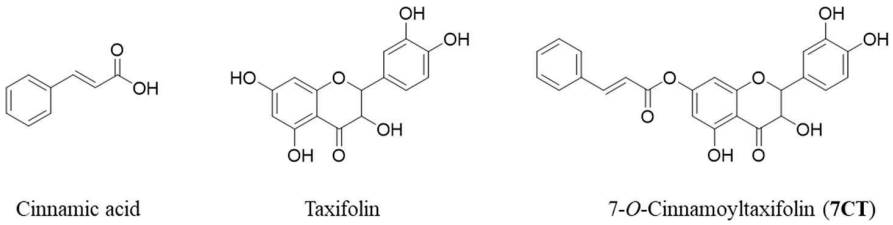

Figure 2. Chemical structures of cinnamic acid, the flavonoid taxifolin, and 7-*O*-cinnamoyltaxifolin (7CT).

induced by oxidative stress.[11] However, polyphenols as plant secondary metabolites have also shown to be neuroprotective by activating several intracellular pathways in addition to their antioxidative features.[12] The flavonoid fisetin, for example, was shown to activate the Ras-extracellular signal-regulated kinase (ERK) cascade and induced cAMP response element-binding protein (CREB) phosphorylation in rat hippocampal slices and therefore enhanced memory in mice.[13] Recently, it has been shown that the flavonoid taxifolin prevented neuroinflammation in a cerebral amyloid angiopathy mouse model by suppressing the ApoE-ERK1/2-amyloid-β precursor protein axis.[14] Phenolic acid esters of the flavonolignan silibinin are potent neuroprotectants and activate mouse microglia,[15] and esters of taxifolin upregulated the antioxidant response element (ARE) via nuclear factor (erythroid-derived 2)-like 2 (Nrf2) activation.[16,17] Even though the antioxidant and anti-inflammatory effects of these natural products are well-established and have been shown to translate into *in vivo* AD models where they ameliorated memory deficits,[13,17] the molecular mode of action and the exact intracellular targets of these compounds remain largely elusive.

To identify cellular targets of compounds, a bioorthogonal Cu(I)-catalyzed [3 + 2] azido-alkyne cycloaddition (CuAAC) approach can be used.[18−20] An alkyne tagged chemical probe of the compound of interest undergoes covalent interactions with its target proteins when incubated with cells (Figure 1). The alkyne probe binds to its native targets and can then be tagged with any azide in a CuAAC reaction. Depending on the application, tags can be fluorescent dyes or other markers for visualization and identification of target proteins. A widely used tag is biotin, as the high affinity for streptavidin is convenient for the enrichment of bound proteins and enables characterization by MS analysis.[19]

In our previous work, we showed that the 7-*O*-ester of the flavonoid taxifolin and cinnamic acid, namely, 7-*O*-cinnamoyltaxifolin (7CT), represented a highly neuroprotective compound acting in an overadditive manner (Figure 2).[17]

Specifically, at the concentrations tested, the individual components taxifolin and cinnamic acid or the equimolar mixture of both were not protective, whereas the ester hybrid 7-*O*-cinnamoyltaxifolin displayed pronounced neuroprotective activity. We observed the overadditive effect of 7-*O*-cinnamoyltaxifolin in a set of assays inducing protection against oxidative stress in neuronal HT22 cells but also investigating inhibition of inflammatory processes in BV-2 microglial cells.[17] Furthermore, the overadditive effect of 7-*O*-cinnamoyltaxifolin was translated to animals using an Aβ_{25-35}-induced memory-impaired AD mouse model where the compound was able to ameliorate short-term memory deficits.[17] The significant and overadditive effect *in vivo* of 7-*O*-cinnamoyltaxifolin showed that these natural product hybrids can be considered as a class of neuroprotective compounds with a distinct pharmacological profile. This is supported by structurally closely related 7-*O*-silibinin esters, which are sensitive to minor chemical modifications, indirectly ruling out unspecific effects underlying these properties.[15] However, to further develop the compound, it is indispensable to understand its mechanism of action and determine its intracellular targets.

The goal of this study was to design and synthesize a chemical probe of 7-*O*-cinnamoyltaxifolin suitable for target identification with the CuAAC approach. Previously, targets for xanthumol, a phytochemical of hops,[21] have been identified using this approach. Furthermore, a functional probe for flavonoid catabolites was developed by Nakashima et al. and used in the CuAAC reaction.[22] Here, we present 7-*O*-

https://dx.doi.org/10.1021/acschemneuro.0c00589
ACS Chem. Neurosci. XXXX, XXX, XXX−XXX

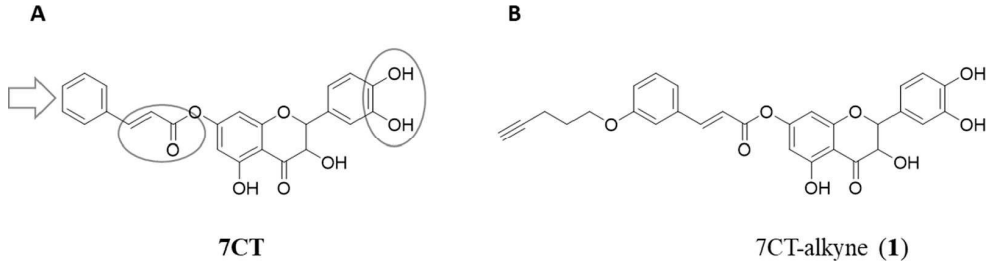

Figure 3. Chemical structures. (A) Design of the chemical probe without altering electrophilic moieties (encircled) of 7-*O*-cinnamoyltaxifolin. (B) The chemical structure of 7CT-alkyne (**1**).

Scheme 1. Synthesis of 7CT-Alkyne (1), a 7-*O*-Cinnamoyltaxifolin-Based Chemical Probe, and the Control Compound (2)[a]

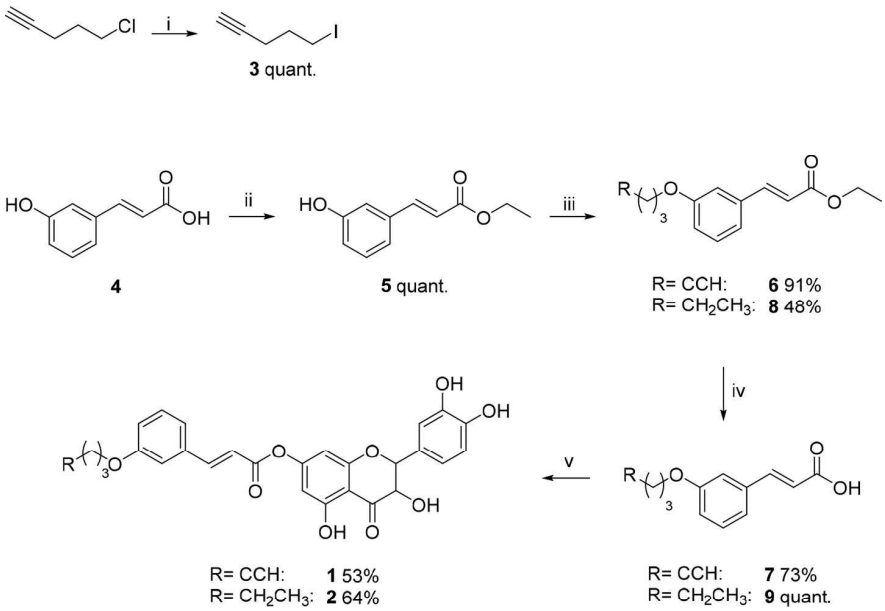

[a](i) NaI, dry acetone, reflux, overnight; (ii) H_2SO_4, ethanol, reflux, 6 h; (iii) **3**, K_2CO_3, dry acetone, 0 °C to reflux, overnight; (iv) NaOH, water, ethanol, room temperature; (v) (1) Oxalyl chloride, DMF, dry THF, rt, 30 min; (2) Taxifolin, triethylamine, rt, overnight.

cinnamoyltaxifolin-alkyne (7CT-alkyne, **1**, Figure 3B), a derivative of 7-*O*-cinnamoyltaxifolin (7CT), functioning as a chemical probe for intracellular target identification. Equivalent effects in relevant assays of neuroprotection and neuroinflammation of 7CT-alkyne **1** compared to those of 7CT proved the probes' interaction with the targets of the parent compound. Among others, ANT-1 and SERCA were identified as targets of **1** and 7CT.

■ RESULTS AND DISCUSSION

Aiming to identify intracellular targets of flavonoid esters and investigate their intracellular mode of neuroprotection, the chemical probe of 7-*O*-cinnamoyltaxifolin (7CT), compound **1**, was designed and synthesized to be used in a CuAAC reaction for affinity-based protein profiling. The suitability of **1** as a probe for 7CT was investigated in cell-based phenotypic screening assays and Western blots. Microscopic analysis of Cy3-coupled **1** suggested mitochondria as one of the subcellular locations of internalized **1**, which was supported by the identification of the mitochondrial ATP/ADP carrier ANT-1 in MS analysis of the pulldown.

Chemistry. It is of utmost importance not to alter the mode of action of the compound when designing a chemical probe for target identification purposes. For 7-*O*-cinnamoyltaxifolin, its simultaneous influence on several proteins and signaling pathways could be mediated through the Michael acceptor sites at the cinnamoyl moiety and the catechol residue, allowing covalent conjugation to proteins (Figure 3A). This is supported by comprehensive structure−activity relationship studies (SARs) on the respective silibinin ester.[15] The attack of a nucleophilic side chain, for example, of cysteinyl thiolates, to the electrophilic β-carbon could be one potential mechanism to form covalent adducts inducing cellular responses.[23] To preserve potential reactive sites in 7-*O*-cinnamoyltaxifolin, the aromatic moiety of the acid was chosen to introduce the alkyne tag necessary for CuAAC. In a previous SAR study with phenolic acid esters of silibinin[15] and also with 7-*O*-feruloyltaxifolin as a potent neuroprotectant,[17] we showed that this entity tolerates modification without loss of activity. Therefore, 7CT-alkyne (**1**) (Figure 3B) was synthesized starting from 3-hydroxy cinnamic acid (**4**). The carboxylic acid moiety was protected using ethanol to selectively react with 5-iodopentyne (**3**), which was synthesized via a Finkelstein reaction, at the aromatic hydroxyl position. Deprotection under basic conditions gave compound **7**. Regioselective esterification represents a considerable synthetic

https://dx.doi.org/10.1021/acschemneuro.0c00589
ACS Chem. Neurosci. XXXX, XXX, XXX−XXX

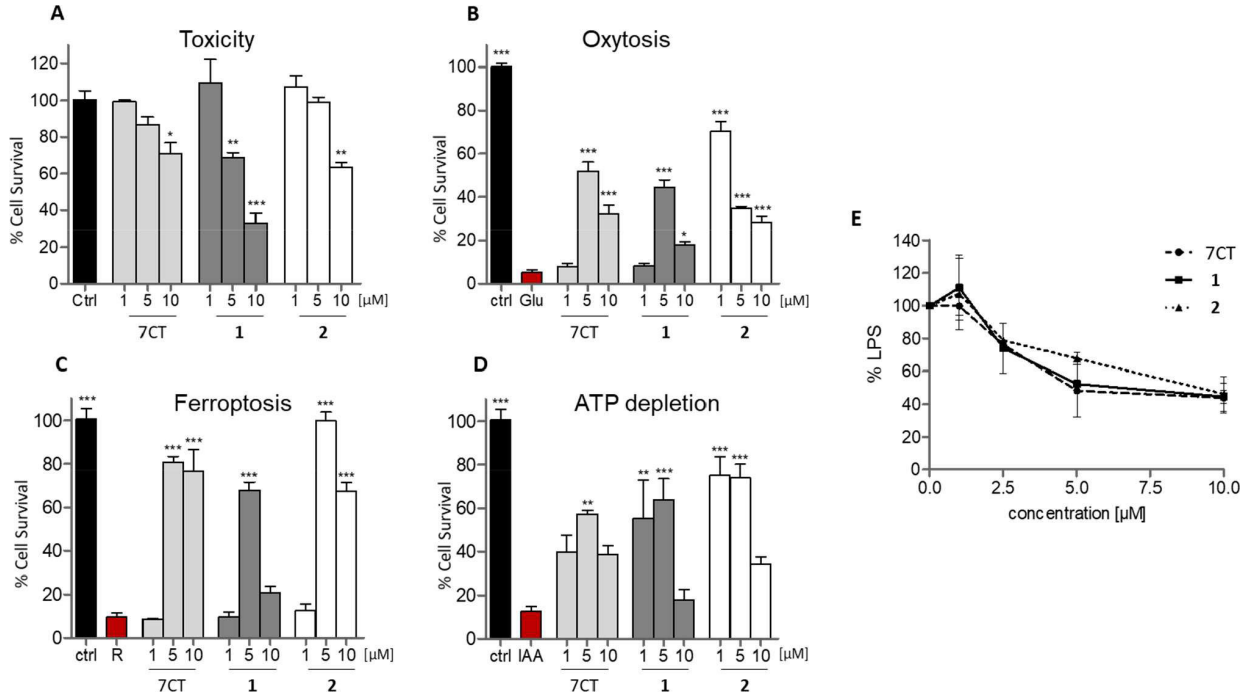

Figure 4. Phenotypic screening assays in HT22 hippocampal nerve cells and neuroinflammation in BV-2 cells. (A) Toxicity of the compounds 7CT, 7CT-alkyne (**1**), and 7CT-alkane (**2**). (B) Neuroprotective effects of 7CT, **1**, and **2** against oxytosis. Glutamate (5 mM) was used to induce toxicity (red). (C) Neuroprotection of 7CT, **1**, and **2** against ferroptosis induced by 0.3 μM RSL3 (red). (D) Neuroprotective effects of 7CT, **1**, and **2** against ATP depletion. ATP loss was induced with 20 μM iodoacetic acid (IAA, red). Data are presented as means ± SEM of three independent experiments, and results refer to untreated control cells (black). Statistical analysis was performed using One-way ANOVA followed by Dunnett's multiple comparison post-tests using GraphPad Prism 5 referring to untreated controls in part A or cells treated with the respective insult only in parts B, C, and D (red bars). Levels of significance: * $p < 0.05$; ** $p < 0.01$; *** $p < 0.001$. (E) Effects of 7CT, **1**, and **2** on NO production in LPS-induced neuroinflammation in BV-2 microglial cells. Cells were treated overnight with 50 ng/mL LPS alone or in the presence of 7CT, **1**, or **2**. Supernatants were cleared, and NO was quantified by the Griess assay. Data are given as means ± SEM and relative to BV-2 cells treated with LPS only, which was set as 100%.

challenge due to the minor differences in reactivity of the various hydroxyl groups in flavonoids. It can involve complex sequences of full protection, regioselective deprotection, esterification, and full deprotection. We previously described direct regioselective esterification for both the flavonolignan silibinin and taxifolin.[15,17] Therefore, regioselective esterification with taxifolin was achieved by forming the acid chloride of compound **7** with oxalyl chloride. *In situ* esterification under basic conditions with adjusted reaction times, as described before,[15] and extensive column purification gave the target compound 7CT-alkyne (**1**). 7CT-alkane (**2**) was synthesized as a control to compare the influence of an aliphatic modification in the aromatic position on the neuroprotective performance of the compound and served as a negative control in the CuAAC reaction. The synthetic route for compound **2** was analogous to that of compound **1**, replacing 5-iodopentyne (**3**) with 1-iodopentane in step iii (Scheme 1).

Cell Culture Assays to Confirm a Comparable Mode of Action. To validate the chemical probe, compounds **1** and **2** were subjected to phenotypic screening assays addressing different age-related stresses, as age is the major risk factor of neurodegenerative diseases.[6] Activities of the chemical probe **1** and control compound **2** were investigated in the three different assays oxytosis, ferroptosis, and ATP depletion in the murine hippocampal cell line HT22. Oxytosis is a form of programmed cell death due to oxidative stress induced by intracellular glutathione (GSH) depletion due to glutamate treatment.[24] As GSH reduction is seen in the aging brain and is accelerated in AD, this assay has a mechanistic association with aging and AD.[25] Closely related to oxytosis, if not identical, is the cell death pathway ferroptosis.[26] Here, oxidative stress is induced by direct inhibition of glutathione peroxidase 4 (GPX4) with the compound RSL3. Distinct from oxytosis, which is induced by glutamate inhibiting cysteine import by blocking system x_c^-, ferroptosis is induced downstream in the cascade. ATP depletion is of interest, as the breakdown in neuronal energy production leads to decreased energy metabolism and ATP levels in the aging brain, which is associated with nerve cell damage and death in AD.[27] To induce ATP loss, HT22 cells were treated with iodoacetic acid (IAA), an irreversible inhibitor of the glycolytic enzyme glyceraldehyde 3-phosphate dehydrogenase.

Figure 4 shows the activity of the chemical probe **1** and the control compound **2** compared to that of the lead compound 7-*O*-cinnamoyltaxifolin (7CT). Even though there is a slight increase in toxicity by the introduction of the aliphatic moiety (Figure 4A), compound **1** proved to be neuroprotective throughout all assays, as was control compound **2**. At a concentration of 5 μM, compound **1** was as protective as 7CT in the phenotypic screening assays for protection against oxytosis (Figure 4B), ferroptosis (Figure 4C), and ATP depletion (Figure 4D) proving that the compound is active and therefore suitable for use as a chemical probe for target identification.

https://dx.doi.org/10.1021/acschemneuro.0c00589
ACS Chem. Neurosci. XXXX, XXX, XXX−XXX

Furthermore, we were also interested in whether compound **1** could be effective against neuroinflammation. As shown in Figure 4E, bacterial lipopolysaccharide (LPS)-induced inflammation in BV-2 mouse microglial cells was reduced by compounds **1** and **2**. The production of nitric oxide (NO) as a proinflammatory mediator was quantified to assess inflammation. At 10 μM, the highest concentration tested, NO levels are reduced to around 45% compared to those of LPS treatment alone, confirming the anti-neuroinflammatory effect of **1** and **2**.

The results of the phenotypic screening assays and microglial activation showed that compound **1** was protective in all assays tested and was not altered in its activity compared to that of 7CT, which was of utmost importance for using **1** as a chemical probe. Compound **1** exhibited neuroprotection addressing different characteristics of neurodegeneration and aging in oxytosis, ferroptosis, ATP depletion, and neuroinflammation at low micromolar concentrations.

Intracellular Pathways Are Modified by Compound 1. The nuclear factor (erythroid-derived 2)-like 2 (Nrf2) is an important transcription factor regulating many antioxidant and detoxification enzyme genes. It is the main regulator of the antioxidant response element (ARE) and is crucial for maintaining the cellular redox balance by preventing the accumulation of reactive oxygen species (ROS) and oxidative stress, one of the hallmarks of AD.[28] It has been shown that a taxifolin ester with gallic acid upregulated Nrf2 pathway in RAW264.7 cells,[16] and we previously found 7CT to induce Nrf2 activation in microglial BV-2 cells.[17] Therefore, we asked whether compound **1** also modifies Nrf2 levels. Nuclear fractions of HT22 cells treated with compound **1** and 7CT for comparison were submitted to Western blot analysis. Figure 5 shows that compound **1** significantly induced Nrf2 upregulation. Even though 7CT seemed more potent at higher concentrations and led to nearly a 6-fold induction of Nrf2 levels at 10 μM, increased Nrf2 levels were significant for both compounds at the same concentration of 5 μM (Figure 5B).

Upregulation of Nrf2 is, therefore, one potential mechanism explaining the neuroprotective activity of the compounds. The classical mechanism for Nrf2 activation is by its interaction with Keap1. When bound to Keap1, Nrf2 is directed for proteasomal degradation. Modification on cysteine residues of Keap1, by oxidative stress, for example, leads to dissociation of the complex and translocation of Nrf2 to the nucleus where it activates several cellular responses including the ARE. However, phosphorylation of Nrf2 by various protein kinases can be an alternative mechanism of Nrf2 regulation.[29] It is known that extracellular signal-regulated protein kinase (ERK) can play a role in Nrf2 activation, and levels of ERK phosphorylation are modified by natural products.[30] Furthermore, ERK signaling is involved in cell proliferation, differentiation, and survival or promotion of cell death and therefore can be involved in neurodegeneration.[31] We were interested in whether ERK is activated by compound **1** and 7CT in HT22 cells, as modifications of mitogen-activated protein (MAP) kinases have not been investigated for 7-*O*-esters of taxifolin before. Figure 6 shows a time-course of HT22 cells incubated with 10 μM **1** or 7CT. Both compounds lead to a significant increase in ERK phosphorylation and thereby activation after 5 min (Figure 6B). The effect ceased with increased incubation times thereby excluding chronic ERK activation, which is correlated with neurodegeneration.[32] Another MAP kinase important in the context of AD is p38.

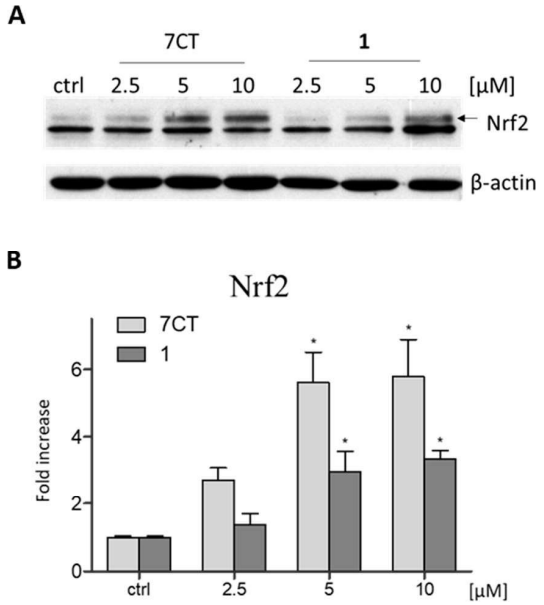

Figure 5. Western blot analysis of Nrf2. Nrf2 induction by 7CT and **1** in nuclear fractions of HT22 cells. (A) Cells were treated for 4 h with DMSO as control or with increasing concentrations of **1** or 7CT. Nuclear fractions of HT22 cells were prepared and analyzed by Western blot for Nrf2. Levels of Nrf2 were normalized to actin, and representative blots are shown. (B) Quantification of the results from three independent experiments as shown in part A. Statistical significance refers to DMSO-treated controls with * $p < 0.05$.

Postmortem brains of early stage AD patients showed increased phosphorylation of p38 which is connected to mediating Aβ-induced inflammation and impaired autophagy in neurons leading to neurodegeneration.[33−35] At a concentration of 10 μM, compound **1** and 7CT both reduce p38 phosphorylation (Figure 6C). Decreased activation was observed after 5 min of incubation and was significantly reduced for the whole time-course of 2 h. The results for activation of ERK and deactivation of p38 underline that 7CT and compound **1** modify MAP kinases. Thus, these results strengthen the reliability of compound **1** as suitable bait for target identification.

CuAAC with Cy3-Azide. The introduction of the alkyne tag in compound **1** enables the reaction of the compound with different azide carriers. As a proof of concept for the CuAAC reaction, and to visualize cellular uptake and the intracellular localization of compound **1**, we coupled **1** to an azide conjugated fluorophore Cy3. First, adducts of the chemical probe **1** with proteins of HT22 lysates were visualized by Western blot analysis. Cy3-azide was coupled to compound **1** in a CuAAC reaction, and bands were detected with an anti-Cy3 antibody. HT22 cells were incubated with increasing concentrations of 5−80 μM **1** for 4 h, lysed, and submitted to the CuAAC reaction using 20 μM Cy3-azide. Incubation of HT22 cells with **1** led to the conjugation of a wide range of proteins with increasing intensity which correlated with increasing concentrations of the compound (see Supporting Information (SI), Figure S1). In cells incubated with DMSO, no adducts were detected. This was also the case for incubation with compound **2** lacking the alkyne tag (SI, Figure S2). Therefore, Cy3-coupling and the detection of conjugated intracellular proteins bound to the probe **1** was

https://dx.doi.org/10.1021/acschemneuro.0c00589
ACS Chem. Neurosci. XXXX, XXX, XXX−XXX

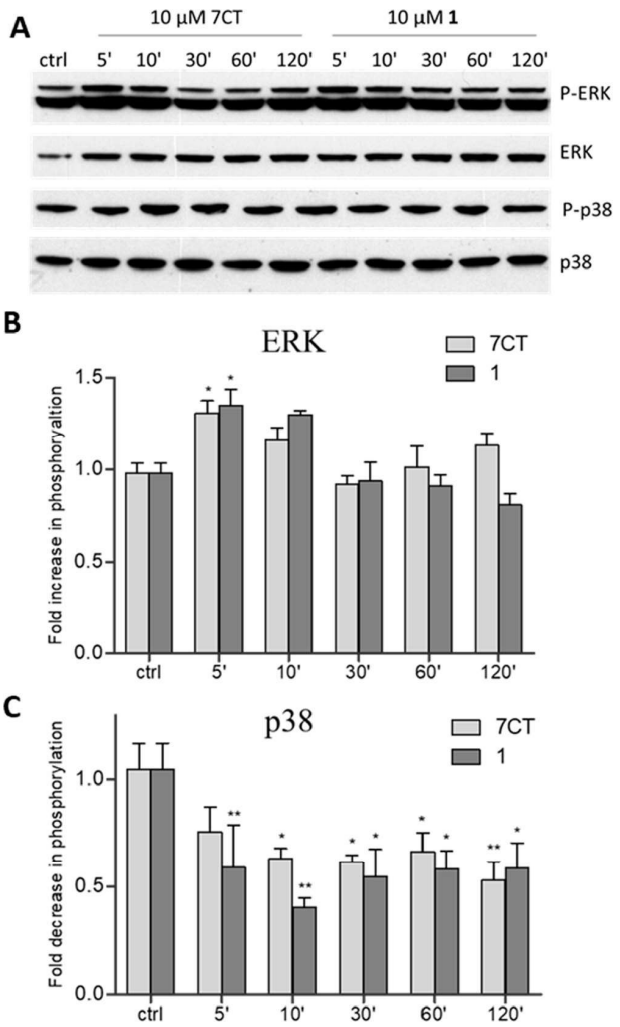

Figure 6. Time-dependent modification of MAP kinases by 7CT and **1** in HT22 cells. (A) Cells were treated for the indicated time points with 10 μM **1** or 7CT. DMSO treatment served as a control. Lysates of HT22 cells were prepared in sample buffer and analyzed by Western blot for phosphorylated ERK (P-ERK), total ERK (ERK), phosphorylated p38 (P-p38), or total p38 (p38). Levels of the phosphorylated protein were normalized to those of the total protein, and representative blots are shown. (B) Quantification of the results from three independent experiments, as shown in part A. Statistical significance refers to DMSO-treated controls with * $p < 0.05$, ** $p < 0.01$.

dependent on the presence of the alkyne moiety and not due to unspecific binding.

Microscopic Analysis. Mitochondria play a crucial role in apoptosis,[36] and in AD, neuronal cell death is associated with mitochondrial dysfunction.[37] Although the exact role of mitochondria in ferroptosis is under debate, increasing evidence strongly suggests that these organelles can also play a key role in this cell death pathway.[38−41] To determine whether compound **1** is targeting the mitochondria, we used fluorescence microscopy to analyze its intracellular location. Therefore, HT22 cells stably expressing the green fluorescent protein in mitochondria (mito-GFP) were incubated with 5 μM compound **1** or DMSO for 30 min, and after fixation, the cells were reacted with Cy3-azide in a CuAAC reaction. The specimens were then imaged by high-resolution fluorescence microscopy using an Airyscan detector.[42] As shown in Figure 7, compound **1** is found at several locations after 30 min of incubation, including in unknown structures in the perinuclear region. Importantly, the fluorescence profiles of mito-GFP and Cy3 indicate that compound **1** is also strongly enriched in mitochondria after 30 min of incubation (see graphs on the right of Figure 7). No significant signal for Cy3 was detected in control cells treated with DMSO. These results indicate that the interaction partners of compound **1** and 7CT might be associated with mitochondria.

Affinity Pulldown and MS Analysis. After demonstrating that compound **1** is suitable as a chemical probe for 7CT, due to pronounced neuroprotection by the same mode of action, the chemical probe **1** was applied for target identification in an affinity pulldown with HT22 cells. HT22 cells were incubated with 200 μM of compound **1** or DMSO as a control for 2 h before lysis and the CuAAC reaction with biotin-azide. Proteins bound by **1** and the DMSO-control lysates were purified on streptavidin magnetic beads, separated by SDS−PAGE, and analyzed by nanoLC−MS/MS after tryptic digestion in a label-free quantification. A total of 708 proteins were identified and quantified. Of these, 70 were significantly enriched in both replicates and thus classified as potential target candidates (summed significance 4; Figure 8). Two of the 70 hits were pursued further to investigate the interaction between compound **1** and 7CT and the respective identified proteins. One was the sarco/endoplasmic reticulum Ca^{2+}-ATPase (SERCA, Atp2a2), which was the protein with the highest significance in the log2 protein ratio sample/control and therefore the top target identified according to MS analysis (Figure 8). As the microscopic analysis showed localization of compound **1** in mitochondria, we were interested in mitochondrial proteins among the targets. Indeed, the mitochondrial carrier adenine nucleotide translocase 1 (ANT-1, Slc25a4) was among the top 4 most significant hits and was chosen as a second target for further examination.

ANT-1 and SERCA Are Identified in MS Analysis. Adenine nucleotide translocase-1 (ANT-1) was identified as a potential target in MS/MS analysis. This finding is supported by the microscopic analysis conducted, where colocalization of Cy3-labeled **1** with mitochondria was observed (Figure 7). ANT-1 is an ADP/ATP carrier at the inner mitochondrial membrane and the most abundant protein in mitochondria, contributing to 1−10% of total mitochondrial protein.[43] ANT-1 is the muscle and brain-specific isoform of ANT and is important for mitochondrial physiology as well as general cell function, as it transports ADP into the mitochondrial matrix and ATP into the cytoplasm, undergoing extensive conformational changes during transport.[44−46] ANT-1 is relevant as a potential pharmacological target in the context of neurodegenerative disorders, particularly for AD, as mitochondrial dysfunction is proposed to be one of the major hallmarks of the disease.[47,48] ANT-1 has been studied in the context of apoptosis as well. The carrier was characterized as a proapoptotic protein, as increased ATP export, which is important for apoptosis, is mediated by enhanced levels of ANT-1 leading to mitochondrial breakdown and the apoptotic cascade.[45,49,50] Its role in nonapoptotic forms of cell death, like ferroptosis and oxytosis covered in this work, has not been described so far. Therefore, HT22 cells transfected with ANT-1 siRNA were tested for effects on oxytosis and ferroptosis. ANT-1 knockdown protected against these insults. Significantly more cells survived treatment with glutamate as an

https://dx.doi.org/10.1021/acschemneuro.0c00589
ACS Chem. Neurosci. XXXX, XXX, XXX−XXX

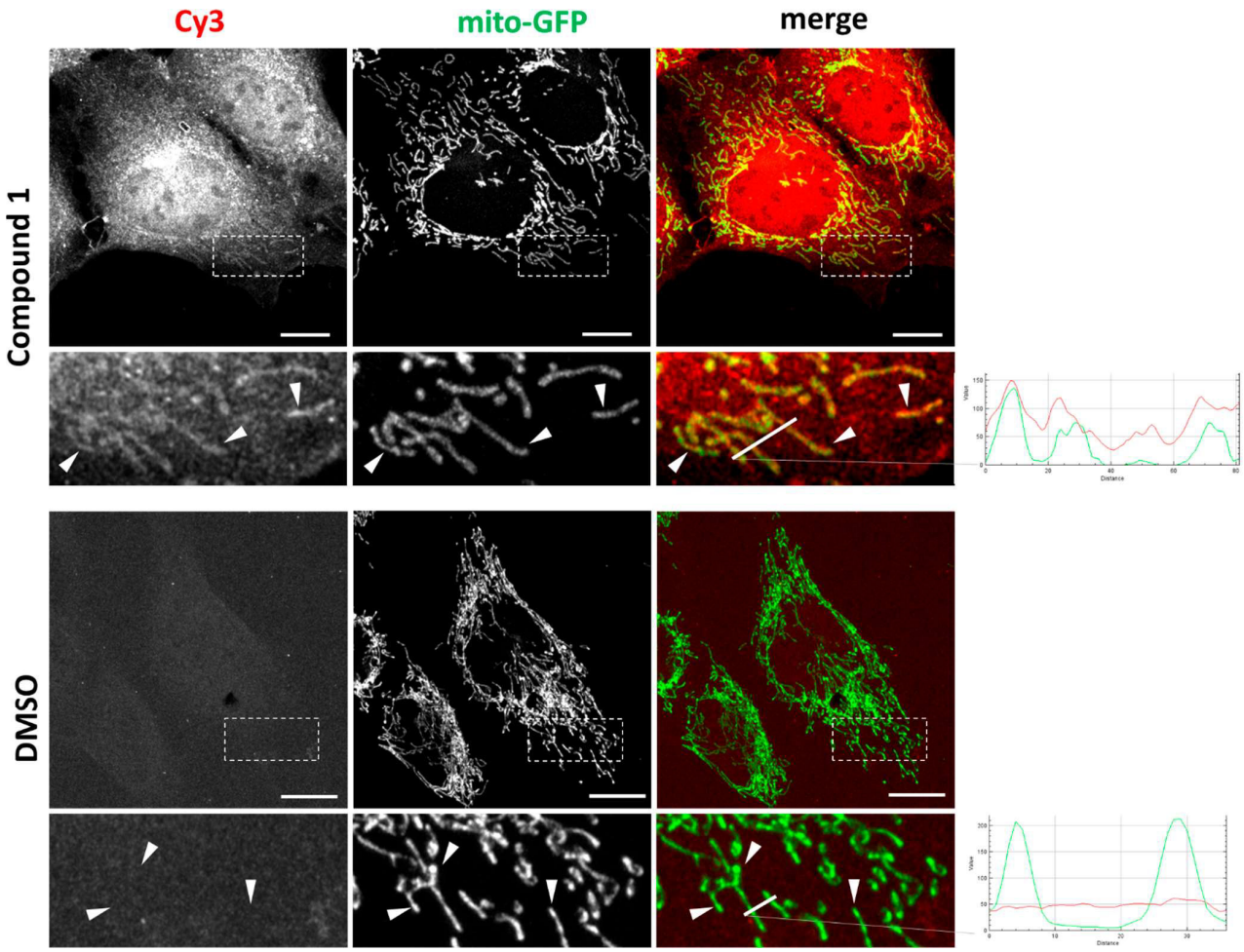

Figure 7. Microscopic analysis of HT22-mitoGFP cells with compound **1**. Representative microscopic images of HT22-mitoGFP cells incubated with 5 μM **1** or DMSO for 30 min. Red signals derive from Cy3 and correspond to adducted proteins; green signals are mitochondria-targeted GFP. Arrows indicate mitochondrial structures to note the colocalization of Cy3 staining with mitochondria in cells incubated with compound **1** compared to the absence of a signal in DMSO-treated cells. To visualize the colocalization, a line was plotted in the merged images (magnified images). Charts on the right show quantification of the fluorescence profile along this line for each channel. The *X*-axis indicates distance, and the *Y*-axis represents fluorescence intensity in arbitrary units. Bars = 10 μm.

inducer of oxytosis (Figure 9A), or erastin and RSL3 as inducers of ferroptosis (Figure 9B,C, respectively). These findings strongly support the implication of ANT-1 inhibition in the protective effect of compound **1** and consequently 7CT.

The treatment of ANT-1 knockdown cells with 7CT in oxytosis conditions induced by glutamate showed that the compound provides additional protection (Figure 9E). In the absence of 7CT, the knockdown of ANT-1 is significantly protective. However, upon treatment of 7CT, the control cells are as protected as the ANT-1 knockdown cells indicating that ANT-1 is not the exclusive target of 7CT, and other mechanisms are also involved in the protection (Figure 9E). ROS and oxidative stress lead to increased mitochondrial membrane potential (MMP).[51] It was shown that FCCP, a mitochondrial uncoupler dissipating the MMP, also protects cells from oxytosis.[52] Furthermore, a study with quercetin showed that low concentrations of the flavonoid reduced the MMP and inhibited adenine nucleotide exchange by ANT-1.[53] As the concentrations at which neuroprotection is observed in our study are in the low micromolar range, we hypothesize that **1** and 7CT could act as mild uncouplers and inhibitors of ANT-1 and thereby protect cells. It has been reported that the nucleotide exchange by ANT-1 can potentially play a role in maintaining the MMP,[54,55] but increased oxidative damage by apoptosis inducers leads to harmfully increased expression levels of ANT-1.[56,57] However, whether this is also the case for oxytosis and ferroptosis as well as the exact role of ANT-1 in these nonapoptotic pathways remains a subject of future research.

A second interaction partner identified by MS analysis was the sarco/endoplasmic reticulum Ca^{2+}-ATPase 2 (SERCA). Located in the endoplasmic reticulum (ER), the pump regulates calcium influx into the ER under ATP consumption. ER-stress concomitant with calcium dysregulation causes neuronal impairment and death and is involved in the progressive neurological decline of AD.[58] Krajnak et al. showed that activation of SERCA is neuroprotective and improves memory and cognition in APP/PS1 mice.[59] In this work, SERCA was validated as a target for 7-*O*-esters of taxifolin by knockdown experiments. In contrast to the results with ANT-1, HT22 cells treated with SERCA siRNA were not protected against glutamate-induced oxytosis (Figure 9D). However,

https://dx.doi.org/10.1021/acschemneuro.0c00589
ACS Chem. Neurosci. XXXX, XXX, XXX−XXX

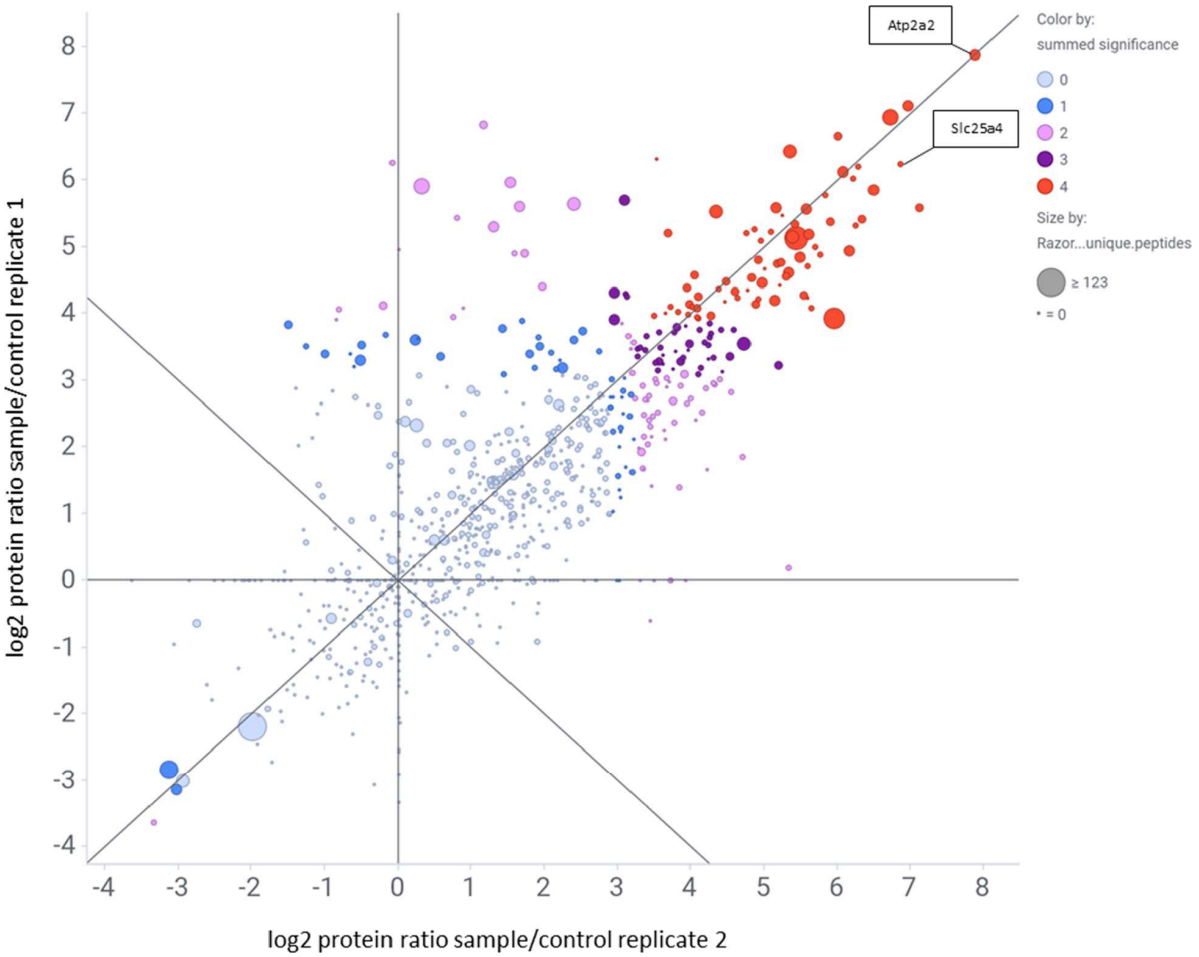

Figure 8. Mass spectrometric identification of target candidates. Log2 transformed protein ratios sample/control of two replicates are shown. Summed significance values were used to identify the best target candidates (significance 2 in both replicates = significance 4, marked in red). The size of the dots corresponds to the number of razors and unique peptides of a protein.

SERCA knockdown significantly impaired the protection by compound 7CT at the lower concentrations of 2.5 and 5 μM (Figure 9E) suggesting an important role of SERCA in the protective mechanism of 7CT. At a concentration of 10 μM 7CT, the decrease in protection by the absence of SERCA was no longer seen. Higher concentrations of 7CT likely activate other protective pathways due to the pleiotropic action of the compound and hence compensate for SERCA knockdown.

■ CONCLUSION

In summary, a chemical probe of the neuroprotective natural product hybrid 7-*O*-cinnamoyltaxifolin bearing an alkyne tag for CuAAC reaction was designed and synthesized. The probe **1** proved its suitability as a neuroprotectant in cell-based phenotypic screening assays addressing different aspects of neurodegeneration and aging. On a molecular level, Western blots were used to confirm that the parent compound and the probe act on the same pathways and to ensure that the alkyne tag was not altering the mechanisms of action. Both compounds, **1** and 7CT, induced significant upregulation of Nrf2 in HT22 nuclear fractions, increased ERK phosphorylation, and reduced phosphorylation of p38 in HT22 lysates. Microscopic analysis of **1** coupled to the fluorescent dye Cy3-azide showed efficient uptake of the compound into HT22 cells and localization in mitochondria. MS analysis after CuAAC of **1** with biotin-azide and following streptavidin purification, revealed 70 potential target candidates by MS analysis. Due to the pleiotropic mechanism of action, the identification of many interaction partners was assumed. As compound **1** carries a Michael system, which is prone to react with nucleophiles like thiols, we expected to identify proteins that were previously described to interact with electrophiles.[21] HSP90, prohibitin, and 14-3-3β are examples of such proteins. Indeed, HSP90, prohibitin and 14-3-3β were identified among others in the MS analysis of the pulldown with compound **1** (for the full list of targets, see Supporting Information). However, the top target candidate of compound **1** in MS analysis was SERCA. In addition, because microscopic analysis pointed at mitochondria as a subcellular location for compound **1**, we also looked at the top mitochondrial target candidate in the analysis which was the mitochondrial protein ANT-1. These two proteins were chosen to investigate for their relevance as targets of compound **1** and 7CT in knockdown experiments. As both proteins are crucial for cell homeostasis and survival and are for the first time shown to be modified by 7-*O*-esters of flavonoids, further work in this area should focus on the role of ANT-1 and SERCA in AD and oxytotic/ferroptotic cell death pathways as well as the

https://dx.doi.org/10.1021/acschemneuro.0c00589
ACS Chem. Neurosci. XXXX, XXX, XXX−XXX

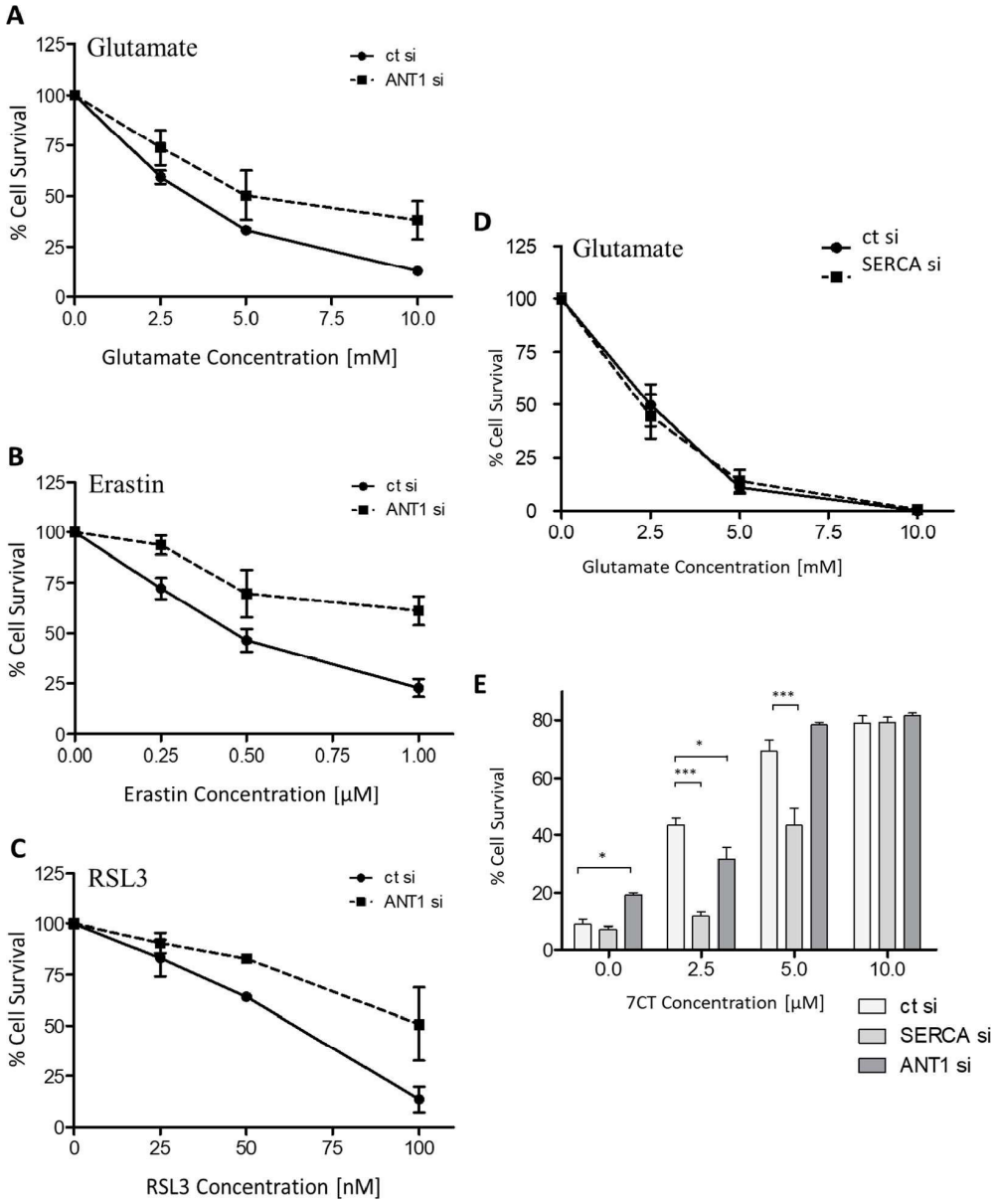

Figure 9. Transfection of HT22 cells with ANT-1 siRNA and SERCA siRNA and investigations on neuroprotection. ANT-1 knockdown leads to protection against glutamate as an inducer of oxytosis (A), and erastin (B) and RSL3 (C) as inducers of ferroptosis. (D) The transfection of HT22 cells with SERCA siRNA is not protective against glutamate-induced oxytosis. (E) ANT-1 (dark gray) and SERCA (light gray) knockdown cells were treated with increasing concentrations of 7CT in the presence of glutamate. Data are presented as means ± SEM of four independent experiments. Statistical analysis was rendered using Two-way ANOVA followed by Bonferroni posttests using GraphPad Prism 5. Levels of significance: * $p < 0.05$; ***$p < 0.001$.

identification and functional characterization of the site(s) modified by the compound. Our findings are a step toward understanding the specific interaction partners of natural product-derived compounds like 7-*O*-esters of flavonoids. The activity-based protein profiling approach with compound **1** as a chemical probe revealed several proteins as interaction partners that might also apply to other flavonoids and lead to new approaches for drug development against neurodegenerative diseases like AD.

■ METHODS

Chemical Synthesis. *General Information.* All reagents were used without further purification and bought from common commercial suppliers in reagent grade. For anhydrous reaction conditions, THF was dried before use by refluxing over sodium slices for at least 2 days under an argon atmosphere. Thin-layer chromatography was performed on silica gel 60 (alumina foils with fluorescent indicator 254 nm). UV light (254 and 366 nm) was used for detection. For column chromatography, silica gel 60 (particle size 0.040−0.063 mm) was used. Nuclear magnetic resonance (NMR) spectra were recorded with a Bruker AV-400 NMR instrument (Bruker, Karlsruhe, Germany) in a deuterated solvent. Chemical shifts are expressed in parts per million (ppm) relative to the solvent applied (2.50 ppm for 1H and 39.5 ppm for 13C in DMSO-d_6; 7.26 ppm for 1H and 77.2 ppm for 13C for $CDCl_3$; 2.05 ppm for 1H and 206.3 ppm for 13C for acetone-d_6; 4.87 ppm for 1H and 49.0 ppm for 13C for methanol-d_4). The purity of the synthesis products was

https://dx.doi.org/10.1021/acschemneuro.0c00589
ACS Chem. Neurosci. XXXX, XXX, XXX−XXX

determined by HPLC (Shimadzu Products), containing a DGU-20A3R degassing unit, an LC20AB liquid chromatograph, and an SPD-20A UV/vis detector. UV detection was measured at 254 nm. Mass spectra were obtained by an LCMS 2020 (Shimadzu Products). As a stationary phase, a Synergi 4U fusion-RP (150 mm × 4.6 mm) column was used, and as a mobile phase, a gradient of methanol/water with 0.1% formic acid was used. Parameters: A = water, B = methanol, $V(B)/(V(A) + V(B))$ = from 5 to 90% over 10 min, $V(B)/(V(A) + V(B))$ = 90% for 5 min, $V(B)/(V(A) + V(B))$ = from 90 to 5% over 3 min. The method was performed with a flow rate of 1.0 mL/min. Compounds were only used for biological evaluation if the purity was ≥95%. Melting points were determined using an OptiMelt automated melting point system (Scientific Instruments GmbH, Gilching, Germany).

General Procedure A: Protection. Acid (1.0 equiv) was dissolved in ethanol, and H_2SO_4 was added. The solution was refluxed until TLC showed full conversion. The reaction mixture was concentrated *in vacuo* and dissolved in ethyl acetate to be washed with 5% sodium hydrogen carbonate in water. The organic layers were combined, and the solvent was evaporated.

General Procedure B: Substitution. K_2CO_3 (1.5 equiv) was dissolved in dry acetone under argon and cooled to 0 °C in an ice bath when the protected acid (1.0 equiv) was added. The mixture was stirred at 0 °C for 15 min, and the respective iodine (2.0 equiv) was added. The reaction was heated to reflux for 6 h, diluted with water and 1 M HCl, extracted with ethyl acetate (3 × 30 mL), washed with brine, and dried over Na_2SO_4. The solvent was removed, and the compound was purified by silica column chromatography using 20% ethyl acetate in petroleum ether to give the compound as an oil.

General Procedure C: Deprotection. The compound was dissolved in ethanol, and 0.52 M NaOH was added. The mixture was stirred at room temperature for 5 h. The reaction was diluted with 5 mL of water and extracted with ethyl acetate twice. The aqueous layers were combined and acidified to pH 1 with 1 M HCl to be again extracted with ethyl acetate. The organic layers were combined, washed with brine, and dried over Na_2SO_4.

General Procedure D: Esterification. Acid (1.1 equiv) was dissolved in 5 mL of dry THF, and oxalyl chloride (2.0 equiv) together with catalytic amounts of DMF (4 μL) were added. The reaction was stirred at room temperature until TLC showed complete conversion of the acid to the acid chloride. The acid chloride was then added dropwise to a solution of taxifolin (1.0 equiv) and triethylamine (4.5 equiv) in dry THF and stirred at room temperature for 2 h. The reaction was quenched with water and 1 M HCl and extracted with ethyl acetate. The organic layer was combined, washed with brine, and dried over Na_2SO_4. The mixture was purified by flash column chromatography using a gradient of 4−15% acetone in dichloromethane to give the pure compound.[15,17]

*5-Iodo Pentyne (**3**).* 5-Chloro pentyne (1.0 g, 9.76 mmol, 1.0 equiv) was dissolved in dry acetone, and sodium iodine (7.3 g, 48.8 mmol, 5.0 equiv) was added; the mixture was heated to reflux overnight. The reaction was diluted with water and extracted with dichloromethane (3 × 40 mL). The organic layer was combined, washed with brine, and dried over Na_2SO_4, and the solvent was evaporated. The compound was obtained as a yellow oil (1.8 g, quantitative (quant)).

^{1}H NMR (400 MHz, $CDCl_3$): δ 3.28 (td, *J* = 6.7, 1.3 Hz, 2H), 2.34−2.26 (m, 2H), 2.01−1.92 (m, 3H) ppm.

^{13}C NMR (101 MHz, $CDCl_3$): δ 82.4 (s), 69.6 (s), 32.0 (s), 19.6 (s), 5.2 (s) ppm.

*Ethyl (E)-3-(3-Hydroxyphenyl)acrylate (**5**).* Following general procedure A, 500 mg of *trans*-3-hydroxycinnamic acid was dissolved in 15 mL of ethanol, and 5 drops of sulfuric acid were added. After 6 h, TLC showed total consumption of the educt. Compound **5** was obtained as an off-white solid (584 mg, quant).

^{1}H NMR (400 MHz, acetone-d6): δ 8.54 (s, 1H, −OH), 7.60 (d, *J* = 16.0 Hz, 1H, *H*C═CHCO), 7.26 (t, 1H, aromatic (arom)), 7.15−7.11 (m, 2H, arom), 6.93−6.90 (m, 1H, arom), 6.43 (d, *J* = 16.0 Hz, 1H, HC═C*H*CO), 4.20 (quart, 2H, OCH_2CH_3), 1.28 (t, 3H, OCH_2CH_3) ppm.

^{13}C NMR (101 MHz, acetone-d6): δ 167.0, 158.7, 145.2, 136.8, 130.9, 120.5, 119.10, 118.3, 115.4, 60.8, 14.6 ppm.

*Ethyl (E)-3-(3-(Pent-4-yn-1-yloxy)phenyl)acrylate (**6**).* Following general procedure B, **5** (300 mg, 1.5 mmol, 1.0 equiv) was reacted with **3** (605 mg, 3.12 mmol, 2.0 equiv) and K_2CO_3(311 mg, 2.25 mmol, 1.5 equiv). Compound **6** was obtained as a yellow oil (352 mg, 1.36 mmol, 91% yield).

^{1}H NMR (400 MHz, $CDCl_3$): δ 7.64 (d, *J* = 16.0 Hz, 1H, *H*C═CHCO), 7.27 (t, 1H, arom), 7.11 (m, 1H, arom), 7.05 (m, 1H, arom), 6.93−6.91 (m, 1H, arom), 6.41 (d, *J* = 16.0 Hz, 1H, HC═C*H*CO), 4.26 (quart, 2H, OCH_2CH_3), 4.08 (t, 2H, H≡$CCH_2CH_2CH_2O$), 2.40 (dt, 2H, H≡$CCH_2CH_2CH_2O$), 2.03−1.97 (m, 3H, *H*≡$CCH_2CH_2CH_2O$), 1.33 (t, 3H, OCH_2CH_3) ppm.

^{13}C NMR (101 MHz, $CDCl_3$): δ 167.0, 159.3, 144.6, 135.9, 130.0, 120.9, 118.7, 116.8, 113.6, 83.4, 69.1, 66.3, 60.6, 28.2, 15.2, 14.4 ppm.

*(E)-3-(3-(Pent-4-yn-1-yloxy)phenyl)acrylic Acid (**7**).* Following general procedure C, 290 mg **6** was dissolved in 3 mL of ethanol, and 5 mL of 0.52 M NaOH was added. The compound was obtained as a white solid (191 mg, 0.82 mmol, 73% yield).

^{1}H NMR (400 MHz, $CDCl_3$): δ 7.74 (d, *J* = 16.0 Hz, 1H, *H*C═CHCO), 7.31 (t, 1H, arom), 7.15 (d, *J* = 8.0 Hz 1H, arom), 7.08 (m, 1H, arom), 6.97 (dd, *J* = 8.0 and 2.3 Hz, 1H, arom), 6.46 (d, *J* = 16.0 Hz, 1H, HC═C*H*CO), 4.11 (t, 2H, H≡$CCH_2CH_2CH_2O$), 2.42 (td, 2H, H≡$CCH_2CH_2CH_2O$), 2.06−1.98 (m, 3H, *H*≡$CCH_2CH_2CH_2O$) ppm.

^{13}C NMR (101 MHz, $CDCl_3$): δ 172.0, 159.3, 147.0, 135.4, 130.0, 121.2, 117.5, 117.2, 113.8, 83.3, 69.0, 66.3, 28.1, 15.2 ppm.

*7-O-Cinnamoyltaxifolin-pentyne (**1**).* Following general procedure D, **7** (120 mg, 0.52 mmol, 1.1 equiv) was dissolved in 5 mL of dry THF, and 85 μL of oxalyl chloride (127 mg, 1.00 mmol, 2 equiv) and catalytic amounts of DMF were added. Taxifolin (150 mg, 0.52 mmol, 1 equiv) and triethylamine (228 mg, 2.25 mmol, 4.5 equiv) were dissolved in dry THF, and the acid chloride was added dropwise. Target compound **1** was obtained as a white foam (137 mg, 0.26 mmol, 53% yield).

^{1}H NMR (400 MHz, DMSO-d6): δ 11.73 (s, 1H, 5-OH), 9.03 (s, 2H, 3′ and 4′-OH), 7.80 (d, *J* = 16.0 Hz, 1H, ArC*H*═CH−CO), 7.40 (s, 1H, arom CA), 7.35 (d, *J* = 5.1 Hz, 2H, arom CA), 7.05−7.02 (m, 1H, arom CA), 6.93 (m, 1H, arom B-ring), 6.88 (d, *J* = 16.0 Hz, 1H, ArCH═C*H*−CO), 6.79−6.76 (m, 2H, arom B-ring), 6.45 (d, *J* = 2.0 Hz, 1H, 8-H), 6.42 (d, *J* = 2.0 Hz, 1H, 6-H), 5.92 (d, *J* = 6.2 Hz, 1H, 3-OH), 5.15 (d, *J* = 11.6 Hz, 1H, 2-H), 4.70 (dd, *J* = 11.5, 6.3 Hz, 1H, 3-H), 4.09 (t, 2H, HC≡C−CH_2−CH_2−CH_2), 2.80 (t, 1H, *H*C≡C−CH_2−CH_2−CH_2), 2.34 (td, *J* = 2.6 Hz, 2H, HC≡C−CH_2−CH_2−CH_2), 1.90 (tt, *J* = *J*′ = 6.5 Hz, 2H, HC≡C−CH_2−CH_2−CH_2) ppm.

^{13}C NMR (101 MHz, DMSO-d6): δ 199.6, 164.0, 162.0, 161.9, 158.9, 158.1, 147.2, 146.0, 145.0, 135.2, 130.1, 127.7, 121.5, 119.6, 117.7, 117.1, 115.5, 115.2, 113.8, 104.9, 102.8, 101.7, 83.7, 83.3, 71.9, 71.6, 66.2, 27.7, 14.5 ppm.

ESI: *m*/*z* calculated for $C_{29}H_{24}O_9$ $[M + H]^+$ 517.14, found 517.13; HPLC purity = 99%.

*Ethyl (E)-3-(3-(Pentyloxy)phenyl)acrylate (**8**).* Following general procedure B, **5** (500 mg, 2.6 mmol, 1.0 equiv) was reacted with 1-iodopentane (1.03 g, 5.2 mmol, 2.0 equiv) and K_2CO_3(539 mg, 3.9 mmol, 1.5 equiv). Compound **8** was obtained as an off-white oil (330 mg, 1.26 mmol, 48% yield).

^{1}H NMR (400 MHz, $CDCl_3$): δ 7.87 (d, *J* = 16.0 Hz, 1H), 7.49 (t, 1H), 7.30 (d, *J* = 7.9 Hz, 1H), 7.13 (dd, *J* = 7.9, 2.4 Hz, 1H), 6.64 (d, *J* = 16.0 Hz, 1H), 4.48 (q, *J* = 7.1 Hz, 2H), 4.18 (t, 2H), 2.01 (quint, 2H), 1.72−1.59 (m, 4H), 1.56 (t, *J* = 7.1 Hz, 3H), 1.21−1.11 (m, 3H) ppm.

^{13}C NMR (101 MHz, $CDCl_3$): δ 167.0, 159.5, 144.6, 135.8, 129.8, 120.6, 118.4, 116.7, 113.5, 68.1, 60.5, 28.9, 28.2, 22.5, 14.3, 14.0 ppm.

*(E)-3-(3-(Pentyloxy)phenyl)acrylic Acid (**9**).* Following general procedure C, 250 mg of **8** was dissolved in 5 mL of ethanol, and 5 mL of 0.52 M NaOH was added. The compound was obtained as a white solid (173 mg, 1.35 mmol, quant).

^{1}H NMR (400 MHz, $CDCl_3$): δ 7.76 (d, *J* = 15.9 Hz, 1H), 7.31 (t, *J* = 7.9 Hz, 1H), 7.13 (d, *J* = 7.7 Hz, 1H), 7.07 (s, 1H), 6.96 (dd, *J* = 8.2, 2.4 Hz, 1H), 6.44 (d, *J* = 15.9 Hz, 1H), 3.98 (t, *J* = 6.6 Hz, 2H),

https://dx.doi.org/10.1021/acschemneuro.0c00589
ACS Chem. Neurosci. XXXX, XXX, XXX−XXX

1.86−1.75 (m, 2H), 1.54−1.33 (m, 4H), 0.95 (t, J = 7.1 Hz, 3H) ppm.

^{13}C NMR (101 MHz, $CDCl_3$): δ 172.3, 159.7, 147.3, 135.5, 130.1, 121.1, 117.5, 117.4, 113.9, 68.3, 29.1, 28.3, 22.6, 14.2 ppm.

*7-O-Cinnamoyltaxifolin-pentane (**2**).* Following general procedure D, **9** (134 mg, 0.57 mmol, 1.1 equiv) was dissolved in 5 mL of dry THF, and 100 μL of oxalyl chloride (155 mg, 1.08 mmol, 2 equiv) and catalytic amounts of DMF were added. Taxifolin (164 mg, 0.54 mmol, 1 equiv) and triethylamine (278 mg, 2.75 mmol, 4.5 equiv) were dissolved in dry THF, and the acid chloride was added dropwise. Compound **2** was obtained as a white foam (181 mg, 0.35 mmol, 64% yield).

^{1}H NMR (400 MHz, DMSO-d6): δ 11.73 (s, 1H, 5-OH), 9.06 (s, 1H, 3′-OH), 9.00 (s, 1H, 4′-OH), 7.82 (d, J = 16.0 Hz, 1H, ArC*H*═CH−CO), 7.38 (s, 1H, arom H CA), 7.34−7.33 (m, 2H, arom H CA), 7.03−7.00 (m, 1H, arom H CA), 6.93 (m, 1H, arom B-ring), 6.88 (d, J = 16.0 Hz, 1H, ArCH = C*H*−CO), 6.79−6.74 (m, 2H, arom B-ring), 6.45 (d, J = 2.0 Hz, 1H, 8-H), 6.41 (d, J = 2.0 Hz, 1H, 6-H), 5.90 (d, J = 6.3 Hz, 1H, 3-OH), 5.13 (d, J = 11.6 Hz, 1H, 2-H), 4.69 (dd, J = 11.6, 6.3 Hz, 1H, 3-H), 4.01 (t, 2H, $CH_3CH_2CH_2CH_2CH_2O$), 1.72 (tt, J = J' = 6.8 Hz, 2H, $CH_3CH_2CH_2CH_2CH_2O$), 1.43−1.30 (m, 4H, $CH_3CH_2CH_2CH_2CH_2O$), 0.89 (t, 3H, $CH_3CH_2CH_2CH_2CH_2O$) ppm.

^{13}C NMR (101 MHz, DMSO-d6): δ 199.6, 164.0, 162.0 161.9, 159.1, 158.1, 147.2, 146.0, 145.0, 135.1, 130.0, 127.7, 121.3, 119.6, 117.7, 117.0, 115.5, 115.2, 113.7, 104.8, 102.8, 101.7, 83.3, 71.9, 67.6, 28.4, 27.7, 21.9, 13.9 ppm.

ESI: m/z calculated for $C_{29}H_{28}O_9$ $[M + H]^+$ 521.17, found 521.14; HPLC purity = 96%.

Cell Culture General Procedures. HT22 cells were grown in Dulbecco's Modified Eagle Medium (DMEM, Sigma-Aldrich, Munich, Germany) supplemented with 10% (v/v) fetal calf serum (FCS) and 1% (v/v) penicillin−streptomycin. BV-2 cells were grown in low-glucose DMEM (Invitrogen, Carlsbad, CA, USA) supplemented with 10% FCS and 1% (v/v) penicillin−streptomycin. Cells were subcultured every 2 days and incubated at 37 °C with 10% CO_2 in a humidified incubator.

Compounds were dissolved in dimethyl sulfoxide (DMSO, Sigma-Aldrich, Munich, Germany) as stock solutions and diluted further into 1x phosphate-buffered saline (PBS).

For determination of cell viability, a colorimetric 3-(4,5-dimethylthiazol-2-yl)-2,5- diphenyl tetrazolium bromide (MTT, Sigma-Aldrich, Munich, Germany) assay was used. MTT solution (5 mg/mL in PBS) was diluted 1:10 with medium and added to the wells after removal of the old medium. Cells were incubated for 3 h, and then lysis buffer (10% SDS) was applied. The next day, absorbance at 560 nm was determined with a multiwell plate photometer (Tecan, SpectraMax 250).

Neurotoxicity and Oxytosis in HT22 Cells. Cells (5×10^3 cells per well) were seeded into sterile 96-well plates and incubated overnight. For the neurotoxicity assay, the medium was removed, and 1, 5, 10, or 25 μM of the compound diluted with medium from a 0.1 M stock solution was added to the wells. DMSO (0.05%) in DMEM served as a control. Cells were incubated for 24 h at which neurotoxicity was determined using the colorimetric MTT assay.

For the oxytosis assay, 3×10^3 cells per well were treated with 5 mM glutamate (monosodium-*L*-glutamate, Sigma-Aldrich, Munich, Germany) together with 1, 5, or 10 μM concentrations of the respective compounds and incubated for 24 h. Cell viability was determined using the MTT assay, as described above. Results are presented as percentage of untreated control cells. Data are expressed as means ± SEM of three independent experiments. The analysis was accomplished using GraphPad Prism 5 Software applying One-way ANOVA followed by Dunnett's multiple comparison posttest. Levels of significance: * $p < 0.05$; ** $p < 0.01$; *** $p < 0.001$.

Ferroptosis in HT22 Cells. Cells (3×10^3 cells per well) were seeded into sterile 96-well plates and incubated overnight. The next day, the medium was exchanged with fresh medium, and 300 nM RSL3 was added with vehicle (DMSO) to induce oxidative stress, or together with 1, 5, or 10 μM concentrations of the respective compound for protection. After 24 h, cell viability was determined using the MTT assay. Results are presented as percentages of untreated control cells. Data are expressed as means ± SEM of three independent experiments. The analysis was accomplished using GraphPad Prism 5 Software applying One-way ANOVA followed by Dunnett's multiple comparison posttest. Levels of significance: * $p < 0.05$; ** $p < 0.01$; *** $p < 0.001$.

ATP Depletion in HT22 Cells. Cells (3×10^3 cells per well) were seeded into sterile 96-well plates and incubated overnight. The next day, medium was exchanged with fresh medium. Iodoacetic acid (IAA, 20 μM) was added with vehicle (DMSO) as a negative control, or together with 1, 5, or 10 μM concentrations of the respective compound for protection. After 2 h of incubation at 37 °C in the incubator, the medium was aspirated, and fresh medium was applied; only the compounds at the same respective concentrations were added without IAA. After 24 h, cell viability was determined using the MTT assay. Results are presented as percentages of untreated control cells. Data are expressed as means ± SEM of three independent experiments. The analysis was accomplished using GraphPad Prism 5 Software applying One-way ANOVA followed by Dunnett's multiple comparison posttest. Levels of significance: * $p < 0.05$; ** $p < 0.01$; *** $p < 0.001$.

Anti-Inflammatory Activity in BV-2 Cells. Cells (5×10^5 cells per plate) were seeded in sterile 35 mm cell culture dishes. After overnight incubation, medium was exchanged with fresh medium. The cells were pretreated with the respective compounds at the indicated concentrations for 30 min when 50 μg/mL bacterial lipopolysaccharide (LPS) was added. After 24 h of incubation, the medium was collected and spun briefly to remove floating cells, and 100 μL of the supernatant was assayed for nitrite using 100 μL of the Griess Reagent in a 96-well plate. After incubation for 10 min at room temperature, the absorbance at 550 nm was read on a microplate reader. Results are normalized to cell number as assessed by the MTT assay, as described above.

Western Blots. *Sample Preparation.* Cells (1.5×10^5HT22 cells per 35 mm dish) were grown for 24 h before treatment with the respective compounds at the indicated concentrations and incubation times. For whole lysate analysis, cells were washed twice with PBS and scraped into 100 μL of 2.5x SDS sample buffer; then, they were sonicated and boiled for 5 min.

For nuclear fractions, HT22 cells were rinsed twice in ice-cold Tris-buffered saline (TBS), scraped into ice-cold nuclear fractionation buffer (10 mM HEPES pH 7.9, 10 mM KCl, 0.1 mM EDTA, 0.1 mM EGTA, 1 mM DTT, 1 mM Na_3VO_4, 1x protease inhibitor cocktail, and 1x phosphatase inhibitor cocktail), and incubated on ice for 15 min. NP40 at a final concentration of 0.6% was added, and cells were vortexed; the nuclei were pelleted by centrifugation. Nuclear proteins were extracted by sonication of the nuclear pellet in nuclear fractionation buffer, and the extracts were cleared by additional centrifugation. Protein concentrations were quantified by the bicinchoninic acid assay (Pierce, Rockford, IL, USA) and adjusted to equal concentrations. Western blot (5x) sample buffer (74 mM Tris−HCl pH 8.0, 6.25% SDS, 10% β-mercaptoethanol, 20% glycerol) was added to a final concentration of 2.5x, and samples were boiled for 5 min.

Western Blotting. Equal amounts of protein (10−20 μg) per lane were used for SDS−PAGE. All samples were separated using 4−12% Criterion XT Precast Bis−Tris Gels (Biorad, Hercules, CA, USA). Proteins were transferred to nitrocellulose membranes, and the quality of protein measurement, electrophoresis, and transfer were checked by Ponceau S staining. Membranes were blocked with 5% skim milk in TBS-T (20 mM Tris buffer pH 7.5, 0.5 M NaCl, 0.1% Tween 20) for 1 h at room temperature and incubated overnight at 4 °C with the primary antibody diluted in 5% BSA in TBS/0.05% Tween 20. HRP-conjugated rabbit antiactin (#5125, 1/20 000), anti-Nrf2 (#sc-13032, 1/500), antiphospho ERK (#9101, 1/1000), antitotal ERK (#9102, 1/1000), antiphospho p38 (#9212, 1/1000), and antitotal p38 (#9212,1/1000) from Cell Signaling (Danvers, MA, USA) were used as the primary antibody. Subsequently, blots were washed in TBS/

https://dx.doi.org/10.1021/acschemneuro.0c00589
ACS Chem. Neurosci. XXXX, XXX, XXX−XXX

0.05% Tween 20 and incubated for 1 h at room temperature in horseradish peroxidase goat antirabbit or antimouse (Biorad) diluted 1/5000 in 5% skim milk in TBS-T. After additional washing, protein bands were detected by chemiluminescence using the Super Signal West Pico Substrate (Pierce). Autoradiographs were scanned using a Biorad GS800 scanner. Band density was measured using ImageJ. Each Western blot was repeated at least three times with independent protein samples.

CuAAC with Cy3-Azide. Cells (5×10^5 cells per 60 mm dish) were grown overnight, and then the compound or DMSO was added at the indicated concentrations and incubated for 4 h. The CuAAC reaction was performed in a final volume of 120 μL. Therefore, 100 μg of protein were adjusted to the appropriate volume with PBS, and 20 μM Cy3-azide was added followed by freshly prepared tris(2-carboxyethyl)phosphine hydrochloride (TCEP) (1 mM final concentration), tris[(1-benzyl-1H-1,2,3-triazol-4-yl)methylamine (TBTA) (0.1 mM final concentration), and copper sulfate (1 mM final concentration). The mixture was vortexed and incubated rotating at room temperature for 1 h after which the reaction was quenched by the addition of 120 μL of 5X sample buffer. The samples were submitted to SDS−PAGE, transferred to a nitrocellulose membrane, and examined according to the Western blot protocol described above with anti-Cy3 (sc-166894, 1/1000) as a primary antibody.

CuAAC in Fixed Cells for Fluorescence Microscopy. Cells (0.4×10^3 HT22 cells) stably expressing a mitochondria-targeted GFP (mito-GFP) were grown overnight on 24-well plates with coverslips. The next day, compounds were added at the indicated concentrations and incubated for 30 min at 37 °C. After we washed the cells three times for 5 min with warm PBS, the cells were fixed with freshly prepared 4% paraformaldehyde (PFA) in PBS at 37 °C for 20 min and permeabilized with 0.5% Triton X-100 in PBS at room temperature for 15 min. The CuAAC reaction mixture was prepared in an Eppendorf tube by mixing Cy3-azide (20 μM final concentration), freshly prepared tris(2-carboxyethyl)phosphine hydrochloride (TCEP) (1 mM final concentration), tris[(1-benzyl-1H-1,2,3-triazol-4-yl)methylamine (TBTA) (0.1 mM final concentration), and copper sulfate (1 mM final concentration) in PBS. The CuAAC reaction mixture was added to the permeabilized cells and incubated for 1 h at room temperature in the dark. Three additional PBS washing steps were performed before placing the coverslips on slides with mounting media. Images were acquired using a Zeiss LSM 880 Rear Port Laser Scanning Confocal and Airyscan FAST Microscope. GFP and Cy3 were excited sequentially using 488 and 561 laser lines, respectively, and collected using the corresponding filters and the Airyscan detector. The final analysis of the images was performed using ImageJ FIJI software.

CuAAC with HT22 Cells and Affinity Purification of Target Proteins. The procedure was based on Weerapana et al.[60] and Brodziak-Jarosz et al.[21] with modifications. HT22 cells were grown in 10 cm dishes to 90% confluency. Compound **1** (200 μM) or DMSO in fresh medium was added and incubated for 2 h. The cells were washed with ice-cold PBS, scraped into 2 mL of ice-cold PBS, and transferred to Eppendorf tubes. After centrifugation at 5000 rpm for one min, the cells were suspended in 500 μL of lysis buffer (TBS with 1% NP-40, pH 7.4) with protease inhibitor cocktail and left shaking for 20 min at 4 °C. Lysates were centrifuged at 14 000 rpm for 20 min at 4 °C to pellet cellular debris. The supernatant was transferred to fresh Eppendorf tubes, and the protein concentration was determined by the bicinchoninic acid method (Pierce).

The CuAAC reaction was conducted in an Eppendorf tube in a final volume of 500 μL. Protein (2000 μg) was adjusted to the needed volume with PBS and 150 μM Biotin-PEG3-azide (Sigma-Aldrich, Munich, Germany); 1 mM freshly prepared tris(2-carboxyethyl)-phosphine hydrochloride, 0.1 mM tris[(1-benzyl-1H-1,2,3-triazol-4-yl)methylamine, and 1 mM copper sulfate were added. The reaction mixture was vortexed, and then the reaction proceeded for 3 h at room temperature with gentle shaking at which time a precipitate formed. After centrifugation at 6500 *g* for 4 min at 4 °C, the supernatant was collected and immediately submitted to affinity pulldown following the procedure described below. The pellet was washed with 500 μL of ice-cold methanol and sonicated for 4 s, and after 10 min incubation rotating at 4 °C, the suspension was centrifuged at 6500 *g* for 4 min at 4 °C. The supernatant was removed, and the washing step was repeated once. For solubilization, 1 mL of 1.2% SDS in PBS was added to the pellet after the second washing step, and it was sonicated for 4 s and boiled for 5 min when the sample was transferred into a 15 mL falcon tube and diluted with 5 mL PBS to a final SDS concentration of 0.2%. For affinity purification, streptavidin magnetic beads (GE Healthcare) were used according to the manufacturer's protocol with an extended incubation time of 2 h for proteome incubation. After elution in 35 μL of 2.5x sample buffer, a methanol/chloroform extraction was rendered to prepare the samples for MS analysis. The samples were diluted in 140 μL of methanol and 35 μL of chloroform and vortexed. Milli-Q (105 μL) was added, and the mixture was vortexed again before centrifugation at 15 000 rpm for 2 min at 4 °C. The upper layer was removed, and 105 μL of methanol was added and vortexed. After another centrifugation step, the supernatant was removed, and the pellet was left to dry.

MS Analysis. *Gel Electrophoresis.* Precipitated proteins were dissolved in NuPAGE LDS sample buffer (Life Technologies), reduced with 50 mM DTT at 70 °C for 10 min, and alkylated with 120 mM Iodoacetamide at room temperature for 20 min. The separation was performed on NuPAGE Novex 4−12% Bis−Tris gels (Life Technologies) with MOPS buffer according to the manufacturer's instructions. Gels were washed three times for 5 min with water and stained for 1 h with Simply Blue Safe Stain (Life Technologies). After washing with water for 1 h, each gel lane was cut into 14 slices.

In-Gel Digestion. The excised gel bands were destained with 30% acetonitrile in 0.1 M NH_4HCO_3 (pH 8), shrunk with 100% acetonitrile, and dried in a vacuum concentrator (Concentrator 5301, Eppendorf, Germany). Digests were performed with 0.1 μg of trypsin per gel band overnight at 37 °C in 0.1 M NH_4HCO_3 (pH 8). After removing the supernatant, peptides were extracted from the gel slices with 5% formic acid, and extracted peptides were pooled with the supernatant.

NanoLC−MS/MS Analysis. NanoLC−MS/MS analyses were performed on an Orbitrap Fusion (Thermo Scientific) equipped with a PicoView Ion Source (New Objective) and coupled to an EASY-nLC 1000 (Thermo Scientific). Peptides were loaded on capillary columns (PicoFrit, 30 cm × 150 μm ID, New Objective) self-packed with ReproSil-Pur 120 C18-AQ (1.9 μm) (Dr. Maisch) and separated with a 30 min linear gradient from 3 to 30% acetonitrile and 0.1% formic acid and a flow rate of 500 nL/min.

Both MS and MS/MS scans were acquired in the Orbitrap analyzer with a resolution of 60 000 for MS scans and 7500 for MS/MS scans. HCD fragmentation with 35% normalized collision energy was applied. A Top Speed data-dependent MS/MS method with a fixed cycle time of 3 s was used. Dynamic exclusion was applied with a repeat count of 1 and an exclusion duration of 30 s; singly charged precursors were excluded from selection. The minimum signal threshold for precursor selection was set to 50 000. Predictive AGC was used with an AGC target value of 2e5 for MS scans and 5e4 for MS/MS scans. EASY-IC was used for internal calibration.

MS Data Analysis. Raw MS data files were analyzed with MaxQuant version 1.6.2.2.[61] The database search was performed with Andromeda, which is integrated into the utilized version of MaxQuant. The search was performed against the UniProt mouse database. Additionally, a database containing common contaminants was used. The search was performed with tryptic cleavage specificity with 3 allowed miscleavages. Protein identification was under the control of the false-discovery rate (FDR; < 1% FDR on protein and PSM level). In addition to MaxQuant default settings, the search was performed against the following variable modifications: Protein N-terminal acetylation, Gln to pyro-Glu formation (N-term. Gln), and oxidation (Met). Carbamidomethyl (Cys) was set as a fixed modification. Further data analysis was performed using R scripts developed in-house. LFQ intensities were used, and missing LFQ intensities in the control samples were imputed with values close to

https://dx.doi.org/10.1021/acschemneuro.0c00589
ACS Chem. Neurosci. XXXX, XXX, XXX−XXX

the baseline. Data imputation was performed with values from a standard normal distribution with a mean of the 5% quantile of the combined log10-transformed LFQ intensities and a standard deviation of 0.1. For the identification of significantly enriched proteins, mean log2 transformed protein ratios were calculated from the two replicate experiments, and boxplot outliers were identified in intensity bins of at least 300 proteins. Log2 transformed protein ratios of the sample *versus* control with values outside a 1.5x (significance 1) or 3x (significance 2) interquartile range (IQR), respectively, were considered as significantly enriched in the individual replicates. Summed significance values were used to identify best target candidates (significance 2 in both replicates = significance 4). GoTerms were added using Perseus.[62]

Transfection. HT22 cells were plated at 5×10^5 cells per dish in 60 mm tissue culture dishes and grown overnight. The cells were then transfected with 166 pmol siRNA (ANT-1 no. sc-42354; SERCA no. sc-36485, both from Santa Cruz Biotechnology) or control siRNA (no. 1027280; Quiagen) using RNAi max (Invitrogen) according to the manufacturer's instructions. After growth overnight, the cells were subcultured for analysis, as described above.

■ ASSOCIATED CONTENT

Supporting Information

The Supporting Information is available free of charge at https://pubs.acs.org/doi/10.1021/acschemneuro.0c00589.

LC−MS traces and NMR analysis of target compounds **1** and **2** and full list of identified proteins by MS analysis (PDF)

Protein ID and related information (XLSX)

■ AUTHOR INFORMATION

Corresponding Authors

Michael Decker − *Pharmaceutical and Medicinal Chemistry, Institute of Pharmacy and Food Chemistry, Julius Maximilian University of Würzburg, Am Hubland 97074, Würzburg, Germany*; orcid.org/0000-0002-6773-6245; Phone: +49 931 3189676; Email: michael.decker@uni-wuerzburg.de

Pamela Maher − *The Salk Institute for Biological Studies, La Jolla 92037, California, United States of America*; Phone: +1 858 453 4110 1932; Email: pmaher@salk.edu

Authors

Sandra Gunesch − *Pharmaceutical and Medicinal Chemistry, Institute of Pharmacy and Food Chemistry, Julius Maximilian University of Würzburg, Am Hubland 97074, Würzburg, Germany*

David Soriano-Castell − *The Salk Institute for Biological Studies, La Jolla 92037, California, United States of America*

Stephanie Lamer − *Rudolf-Virchow-Zentrum—Center for Integrative and Translational Bioimaging, Julius Maximilian University of Würzburg, 97080 Würzburg, Germany*

Andreas Schlosser − *Rudolf-Virchow-Zentrum—Center for Integrative and Translational Bioimaging, Julius Maximilian University of Würzburg, 97080 Würzburg, Germany*

Complete contact information is available at: https://pubs.acs.org/10.1021/acschemneuro.0c00589

Author Contributions

The manuscript was written through contributions of all authors. All authors have given approval to the final version of the manuscript.

Funding

Financial support by the Bavaria California Technology Center under project number 3 [2018-2] and by the German Academic Exchange Service (DAAD) with funds of the Federal Ministry of Education and Research (BmBF) under project number 57508635 is gratefully acknowledged. P.M. was supported by grants from NIH (RO1 AG046153, RF1 AG054714, and RF1 AG061296).

Notes

The authors declare no competing financial interest.

■ ACKNOWLEDGMENTS

We thankfully acknowledge support by Dr. Antonio Currais (Cellular Biology Laboratory, Salk Institute for Biological Studies) for providing HT22-mitoGFP cells.

■ ABBREVIATIONS

7CT, 7-*O*-cinnamoyltaxifolin; GSH, glutathione; IAA, iodoacetic acid

■ REFERENCES

(1) Patterson, C. *World Alzheimer Report 2018—The State of the Art of Dementia Research: New Frontiers*; Alzheimer's Disease International: London, 2018.

(2) Irvine, G. B., El-Agnaf, O. M., Shankar, G. M., and Walsh, D. M. (2008) Protein aggregation in the brain: the molecular basis for Alzheimer's and Parkinson's diseases. *Mol. Med. 14* (7), 451−464.

(3) Minter, M. R., Taylor, J. M., and Crack, P. J. (2016) The contribution of neuroinflammation to amyloid toxicity in Alzheimer's disease. *J. Neurochem. 136* (3), 457−474.

(4) Simpson, D. S. A., and Oliver, P. L. (2020) ROS Generation in Microglia: Understanding Oxidative Stress and Inflammation in Neurodegenerative Disease. *Antioxidants 9* (743), 1−27.

(5) Ismail, R., Parbo, P., Madsen, L. S., Hansen, A. K., Hansen, K. V., Schaldemose, J. L., Kjeldsen, P. L., Stokholm, M. G., Gottrup, H., Eskildsen, S. F., and Brooks, D. J. (2020) The relationships between neuroinflammation, beta-amyloid and tau deposition in Alzheimer's disease: a longitudinal PET study. *J. Neuroinflammation 17* (1), 151.

(6) Prior, M., Chiruta, C., Currais, A., Goldberg, J., Ramsey, J., Dargusch, R., Maher, P., and Schubert, D. (2014) Back to the future with phenotypic screening. *ACS Chem. Neurosci. 5* (7), 503−513.

(7) Schubert, D., and Maher, P. (2012) An alternative approach to drug discovery for Alzheimer's disease dementia. *Future Med. Chem. 4* (13), 1681−1688.

(8) Pohl, F., and Kong Thoo Lin, P. (2018) The Potential Use of Plant Natural Products and Plant Extracts with Antioxidant Properties for the Prevention/Treatment of Neurodegenerative Diseases: In Vitro, In Vivo and Clinical Trials. *Molecules 23* (12), 3283−3313.

(9) Currais, A., Chiruta, C., Goujon-Svrzic, M., Costa, G., Santos, T., Batista, M. T., Paiva, J., do Ceu Madureira, M., and Maher, P. (2014) Screening and identification of neuroprotective compounds relevant to Alzheimers disease from medicinal plants of S. Tome e Principe. *J. Ethnopharmacol. 155* (1), 830−840.

(10) Maher, P., Fischer, W., Liang, Z., Soriano-Castell, D., Pinto, A. F. M., Rebman, J., and Currais, A. (2020) The Value of Herbarium Collections to the Discovery of Novel Treatments for Alzheimer's Disease, a Case Made With the Genus Eriodictyon. *Front. Pharmacol. 11* (208), 208.

(11) Kling, B., Bücherl, D., Palatzky, P., Matysik, F.-M., Decker, M., Wegener, J., and Heilmann, J. (2014) Flavonoids, Flavonoid Metabolites, and Phenolic Acids Inhibit Oxidative Stress in the Neuronal Cell Line HT-22 Monitored by ECIS and MTT Assay: A Comparative Study. *J. Nat. Prod. 77* (3), 446−454.

(12) Dhakal, S., Kushairi, N., Phan, C. W., Adhikari, B., Sabaratnam, V., and Macreadie, I. (2019) Dietary Polyphenols: A Multifactorial Strategy to Target Alzheimer's Disease. *Int. J. Mol. Sci. 20* (20), 5090.

(13) Maher, P., Akaishi, T., and Abe, K. (2006) Flavonoid fisetin promotes ERK-dependent long-term potentiation and enhances memory. *Proc. Natl. Acad. Sci. U. S. A. 103* (44), 16568−16573.

(14) Inoue, T., Saito, S., Tanaka, M., Yamakage, H., Kusakabe, T., Shimatsu, A., Ihara, M., and Satoh-Asahara, N. (2019) Pleiotropic neuroprotective effects of taxifolin in cerebral amyloid angiopathy. *Proc. Natl. Acad. Sci. U. S. A. 116* (20), 10031−10038.
(15) Schramm, S., Huang, G., Gunesch, S., Lang, F., Roa, J., Hogger, P., Sabate, R., Maher, P., and Decker, M. (2018) Regioselective synthesis of 7-O-esters of the flavonolignan silibinin and SARs lead to compounds with overadditive neuroprotective effects. *Eur. J. Med. Chem. 146* (2018), 93−107.
(16) Vrba, J., Gazak, R., Kuzma, M., Papouskova, B., Vacek, J., Weiszenstein, M., Kren, V., and Ulrichova, J. (2013) A novel semisynthetic flavonoid 7-O-galloyltaxifolin upregulates heme oxygenase-1 in RAW264.7 cells via MAPK/Nrf2 pathway. *J. Med. Chem. 56* (3), 856−866.
(17) Gunesch, S., Hoffmann, M., Kiermeier, C., Fischer, W., Pinto, A. F. M., Maurice, T., Maher, P., and Decker, M. (2020) 7-*O*-esters of taxifolin with pronounced and overadditive effects in neuroprotection, anti-neuroinflammation, and amelioration of short-term memory impairment in vivo. *Redox Biol. 29* (2020), 101378.
(18) Speers, A. E., Adam, G. C., and Cravatt, B. F. (2003) Activity-based protein profiling in vivo using a copper(i)-catalyzed azide-alkyne [3 + 2] cycloaddition. *J. Am. Chem. Soc. 125* (16), 4686−4687.
(19) Bottcher, T., Pitscheider, M., and Sieber, S. A. (2010) Natural products and their biological targets: proteomic and metabolomic labeling strategies. *Angew. Chem., Int. Ed. 49* (15), 2680−2698.
(20) Chen, X., Wong, Y. K., Wang, J., Zhang, J., Lee, Y. M., Shen, H. M., Lin, Q., and Hua, Z. C. (2017) Target identification with quantitative activity based protein profiling (ABPP). *Proteomics 17* (3), 1600212.
(21) Brodziak-Jarosz, L., Fujikawa, Y., Pastor-Flores, D., Kasikci, S., Jirasek, P., Pitzl, S., Owen, R. W., Klika, K. D., Gerhauser, C., Amslinger, S., and Dick, T. P. (2016) A click chemistry approach identifies target proteins of xanthohumol. *Mol. Nutr. Food Res. 60* (4), 737−748.
(22) Nakashima, S., Liu, Z., Yamaguchi, Y., Saiki, S., Munemasa, S., Nakamura, T., Murata, Y., and Nakamura, Y. (2016) A novel tag-free probe for targeting molecules interacting with a flavonoid catabolite. *Biochem. Biophys. Rep. 7* (2016), 240−245.
(23) Su, C., Liu, Z., Wang, Y., Wang, Y., Song, E., and Song, Y. (2017) The electrophilic character of quinones is essential for the suppression of Bach1. *Toxicology 387* (2017), 17−26.
(24) Tan, S., Schubert, D., and Maher, P. (2001) Oxytosis: A novel form of programmed cell death. *Curr. Top. Med. Chem. 1* (6), 497−506.
(25) Currais, A., and Maher, P. (2013) Functional consequences of age-dependent changes in glutathione status in the brain. *Antioxid. Redox Signaling 19* (8), 813−822.
(26) Lewerenz, J., Ates, G., Methner, A., Conrad, M., and Maher, P. (2018) Oxytosis/Ferroptosis-(Re-) Emerging Roles for Oxidative Stress-Dependent Non-apoptotic Cell Death in Diseases of the Central Nervous System. *Front. Neurosci. 12*, 214.
(27) Saxena, U. (2012) Bioenergetics failure in neurodegenerative diseases: back to the future. *Expert Opin. Ther. Targets 16* (4), 351−354.
(28) Schmidlin, C. J., Dodson, M. B., Madhavan, L., and Zhang, D. D. (2019) Redox regulation by NRF2 in aging and disease. *Free Radical Biol. Med. 134* (2019), 702−707.
(29) Bryan, H. K., Olayanju, A., Goldring, C. E., and Park, B. K. (2013) The Nrf2 cell defence pathway: Keap1-dependent and -independent mechanisms of regulation. *Biochem. Pharmacol. 85* (6), 705−717.
(30) Qin, S., and Hou, D. X. (2016) Multiple regulations of Keap1/Nrf2 system by dietary phytochemicals. *Mol. Nutr. Food Res. 60* (8), 1731−1755.
(31) Rai, S. N., Dilnashin, H., Birla, H., Singh, S. S., Zahra, W., Rathore, A. S., Singh, B. K., and Singh, S. P. (2019) The Role of PI3K/Akt and ERK in Neurodegenerative Disorders. *Neurotoxic. Res. 35* (3), 775−795.
(32) Colucci-D'Amato, L., Perrone-Capano, C., and di Porzio, U. (2003) Chronic activation of ERK and neurodegenerative diseases. *BioEssays 25* (11), 1085−1095.
(33) Hensley, K., Floyd, R. A., Zheng, N. Y., Nael, R., Robinson, K. A., Nguyen, X., Pye, Q. N., Stewart, C. A., Geddes, J., Markesbery, W. R., Patel, E., Johnson, G. V., and Bing, G. (1999) p38 kinase is activated in the Alzheimer's disease brain. *J. Neurochem. 72* (5), 2053−2058.
(34) Sun, A., Liu, M., Nguyen, X. V., and Bing, G. (2003) P38 MAP kinase is activated at early stages in Alzheimer's disease brain. *Exp. Neurol. 183* (2), 394−405.
(35) Schnoder, L., Hao, W., Qin, Y., Liu, S., Tomic, I., Liu, X., Fassbender, K., and Liu, Y. (2016) Deficiency of Neuronal p38alpha MAPK Attenuates Amyloid Pathology in Alzheimer Disease Mouse and Cell Models through Facilitating Lysosomal Degradation of BACE1. *J. Biol. Chem. 291* (5), 2067−2079.
(36) Jeong, S. Y., and Seol, D. W. (2008) The role of mitochondria in apoptosis. *BMB reports 41* (1), 11−22.
(37) Jeong, S. (2017) Molecular and Cellular Basis of Neurodegeneration in Alzheimer's Disease. *Mol. Cells 40* (9), 613−620.
(38) Gao, M., Yi, J., Zhu, J., Minikes, A. M., Monian, P., Thompson, C. B., and Jiang, X. (2019) Role of Mitochondria in Ferroptosis. *Mol. Cell 73* (2), 354−363.
(39) Krainz, T., Gaschler, M. M., Lim, C., Sacher, J. R., Stockwell, B. R., and Wipf, P. (2016) A Mitochondrial-Targeted Nitroxide Is a Potent Inhibitor of Ferroptosis. *ACS Cent. Sci. 2* (9), 653−659.
(40) Neitemeier, S., Jelinek, A., Laino, V., Hoffmann, L., Eisenbach, I., Eying, R., Ganjam, G. K., Dolga, A. M., Oppermann, S., and Culmsee, C. (2017) BID links ferroptosis to mitochondrial cell death pathways. *Redox Biol. 12* (2017), 558−570.
(41) Basit, F., van Oppen, L. M., Schockel, L., Bossenbroek, H. M., van Emst-de Vries, S. E., Hermeling, J. C., Grefte, S., Kopitz, C., Heroult, M., HGM Willems, P., and Koopman, W. J. (2017) Mitochondrial complex I inhibition triggers a mitophagy-dependent ROS increase leading to necroptosis and ferroptosis in melanoma cells. *Cell Death Dis. 8* (3), No. e2716.
(42) Huff, J. (2015) The airyscan detector form ZEISS: confocal imaging with improved signal-to-noise ratio and super-resolution. *Nat. Methods 12*, 1−2.
(43) Brand, M. D., Pakay, J. L., Ocloo, A., Kokoszka, J., Wallace, D. C., Brookes, P. S., and Cornwall, E. J. (2005) The basal proton conductance of mitochondria depends on adenine nucleotide translocase content. *Biochem. J. 392* (2), 353−362.
(44) Liu, Y., and Chen, X. J. (2013) Adenine Nucleotide Translocase, Mitochondrial Stress, and Degenerative Cell Death. *Oxid. Med. Cell. Longevity 146860*, 1−10.
(45) Chevrollier, A., Loiseau, D., Reynier, P., and Stepien, G. (2011) Adenine nucleotide translocase 2 is a key mitochondrial protein in cancer metabolism. *Biochim. Biophys. Acta, Bioenerg. 1807* (6), 562−567.
(46) Ruprecht, J. J., King, M. S., Zögg, T., Aleksandrova, A. A., Pardon, E., Crichton, P. G., Steyaert, J., and Kunji, E. R. S. (2019) The Molecular Mechanism of Transport by the Mitochondrial ADP/ATP Carrier. *Cell 176* (3), 435−447.
(47) Wang, W., Zhao, F., Ma, X., Perry, G., and Zhu, X. (2020) Mitochondria dysfunction in the pathogenesis of Alzheimer's disease: recent advances. *Mol. Neurodegener. 15* (30), 1−22.
(48) Cadonic, C., Sabbir, M. G., and Albensi, B. C. (2016) Mechanisms of Mitochondrial Dysfunction in Alzheimer's Disease. *Mol. Neurobiol. 53* (9), 6078−6090.
(49) Bobba, A., Amadoro, G., Azzariti, A., Pizzuto, R., and Atlante, A. (2014) Extracellular ADP prevents neuronal apoptosis via activation of cell antioxidant enzymes and protection of mitochondrial ANT-1. *Biochim. Biophys. Acta, Bioenerg. 1837* (8), 1338−1349.
(50) Bauer, M. K., Schubert, A., Rocks, O., and Grimm, S. (1999) Adenine nucleotide translocase-1, a component of the permeability transition pore, can dominantly induce apoptosis. *J. Cell Biol. 147* (7), 1493−1502.

https://dx.doi.org/10.1021/acschemneuro.0c00589
ACS Chem. Neurosci. XXXX, XXX, XXX−XXX

(51) Liu, Y., and Schubert, D. (2009) The specificity of neuroprotection by antioxidants. *J. Biomed. Sci. 16* (98), 1−14.
(52) Tan, S., Sagara, Y., Liu, Y., Maher, P., and Schubert, D. (1998) The regulation of reactive oxygen species production during programmed cell death. *J. Cell Biol. 141* (6), 1423−1432.
(53) Ortega, R., and García, N. (2009) The flavonoid quercetin induces changes in mitochondrial permeability by inhibiting adenine nucleotide translocase. *J. Bioenerg. Biomembr. 41* (1), 41−47.
(54) Appleby, R. D., Porteous, W. K., Hughes, G., James, A. M., Shannon, D., Wei, Y. H., and Murphy, M. P. (1999) Quantitation and origin of the mitochondrial membrane potential in human cells lacking mitochondrial DNA. *Eur. J. Biochem. 262* (1), 108−116.
(55) Zorova, L. D., Popkov, V. A., Plotnikov, E. Y., Silachev, D. N., Pevzner, I. B., Jankauskas, S. S., Babenko, V. A., Zorov, S. D., Balakireva, A. V., Juhaszova, M., Sollott, S. J., and Zorov, D. B. (2018) Mitochondrial membrane potential. *Anal. Biochem. 552* (2018), 50−59.
(56) Ren, R., Zhang, Y., Li, B., Wu, Y., and Li, B. (2011) Effect of β-amyloid (25−35) on mitochondrial function and expression of mitochondrial permeability transition pore proteins in rat hippocampal neurons. *J. Cell. Biochem. 112* (5), 1450−1457.
(57) Song, X. B., Liu, G., Wang, Z. Y., and Wang, L. (2016) Puerarin protects against cadmium-induced proximal tubular cell apoptosis by restoring mitochondrial function. *Chem.-Biol. Interact. 260* (2016), 219−231.
(58) Unterberger, U., Höftberger, R., Gelpi, E., Flicker, H., Budka, H., and Voigtländer, T. (2006) Endoplasmic reticulum stress features are prominent in Alzheimer disease but not in prion diseases in vivo. *J. Neuropathol. Exp. Neurol. 65* (4), 348−357.
(59) Krajnak, K., and Dahl, R. (2018) A new target for Alzheimer's disease: A small molecule SERCA activator is neuroprotective in vitro and improves memory and cognition in APP/PS1 mice. *Bioorg. Med. Chem. Lett. 28* (9), 1591−1594.
(60) Weerapana, E., Speers, A. E., and Cravatt, B. F. (2007) Tandem orthogonal proteolysis-activity-based protein profiling (TOP-ABPP)—a general method for mapping sites of probe modification in proteomes. *Nat. Protoc. 2* (6), 1414−1425.
(61) Cox, J., and Mann, M. (2008) MaxQuant enables high peptide identification rates, individualized p.p.b.-range mass accuracies and proteome-wide protein quantification. *Nat. Biotechnol. 26* (12), 1367−1372.
(62) Tyanova, S., Temu, T., Sinitcyn, P., Carlson, A., Hein, M. Y., Geiger, T., Mann, M., and Cox, J. (2016) The Perseus computational platform for comprehensive analysis of (prote)omics data. *Nat. Methods 13* (9), 731−740.

https://dx.doi.org/10.1021/acschemneuro.0c00589
ACS Chem. Neurosci. XXXX, XXX, XXX−XXX

Supporting Information

Development and application of a chemical probe based on a neuroprotective flavonoid hybrid for target identification using activity-based protein profiling.

Sandra Gunesch, [a] *David Soriano-Castell,* [b] *Stephanie Lamer,* [c] *Andreas Schlosser,* [c] *Pamela Maher,* [b]* *and Michael Decker* [a]*

[a] Pharmaceutical and Medicinal Chemistry, Institute of Pharmacy and Food Chemistry, Julius Maximilian University of Würzburg, Am Hubland, 97074 Würzburg, Germany.

[b] The Salk Institute for Biological Studies, 10010 N Torrey Pines Road, La Jolla, CA 92037, United States of America.

[c] Rudolf-Virchow-Zentrum - Center for Integrative and Translational Bioimaging, Julius Maximilian University of Würzburg, 97080 Würzburg, Germany

SI 1: Western Blots, LC-MS traces, and NMR analysis of target compounds **1** and **2**.

SI 2: Full list of identified proteins by MS analysis (excel file).

Figure S1: Western blot analysis for CuAAC control of compound 1

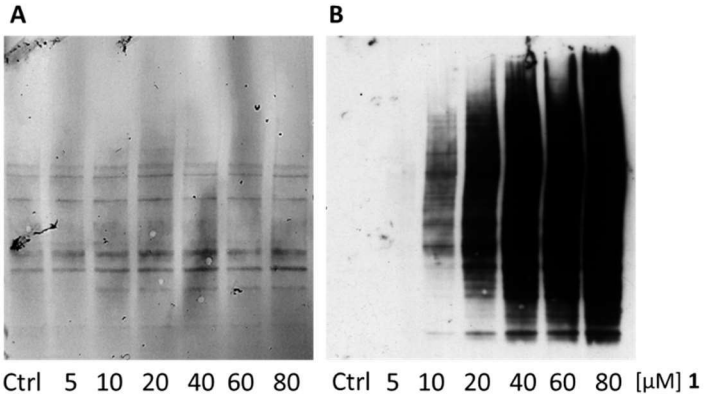

Figure S1: Western blot of HT22 cells incubated with 1 and subsequent CuAAC. A) Amido black stain of the membrane showing equal amounts of protein in each sample. B) Specific bands are detected with increasing intensity in line with the increasing concentrations of compound **1** after anti-Cy3 antibody incubation of the membrane.

Figure S2: Western blot analysis for CuAAC with compound 1 and 2

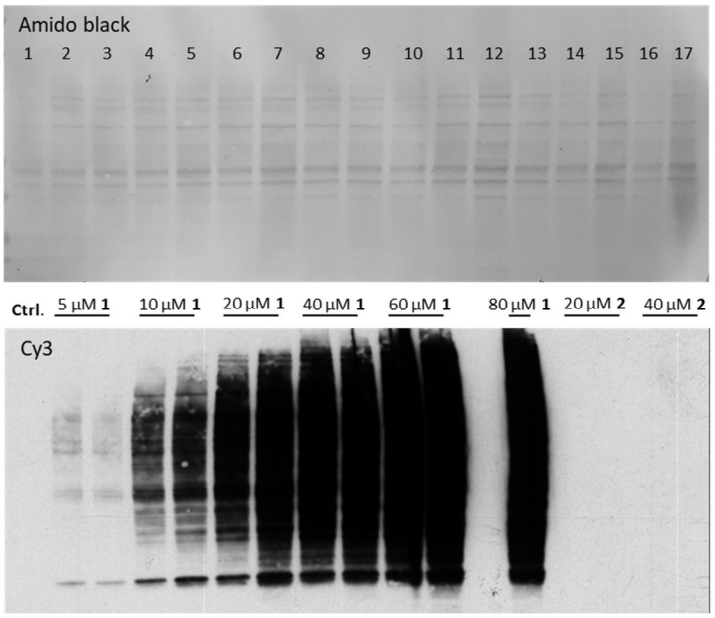

Figure S2: Western blot of HT22 cells incubated with 1 or 2 and subsequent CuAAC. Top: Amido black stain of the membrane showing equal amounts of protein in each sample. Bottom: Specific bands are detected with increasing intensity in line with the increasing concentrations of compound **1** (lanes 2-13) after anti-Cy3 antibody incubation of the membrane and lanes 14-17 show that compound **2** did not conjugate any proteins. Samples of two independent experiments are loaded for each concentration, lane 12 was deficient.

Figure S3: HPLC chromatogram of compound 1

SHIMADZU LabSolutions

Analysis Report

<Sample Information>

Sample Name	: SG-II-82		
Sample ID	:		
Data Filename	: SG-II-82.lcd		
Method Filename	: Analysis 15 cm 05-90 1mL +50-1000 Standard.lcm		
Batch Filename	: batchj.lcb		
Vial #	: 1-82	Sample Type	: Unknown
Injection Volume	: 20 uL		
Date Acquired	: 15/10/2019 18:25:24	Acquired by	: System Administrator
Date Processed	: 15/10/2019 18:43:29	Processed by	: System Administrator

<Chromatogram>

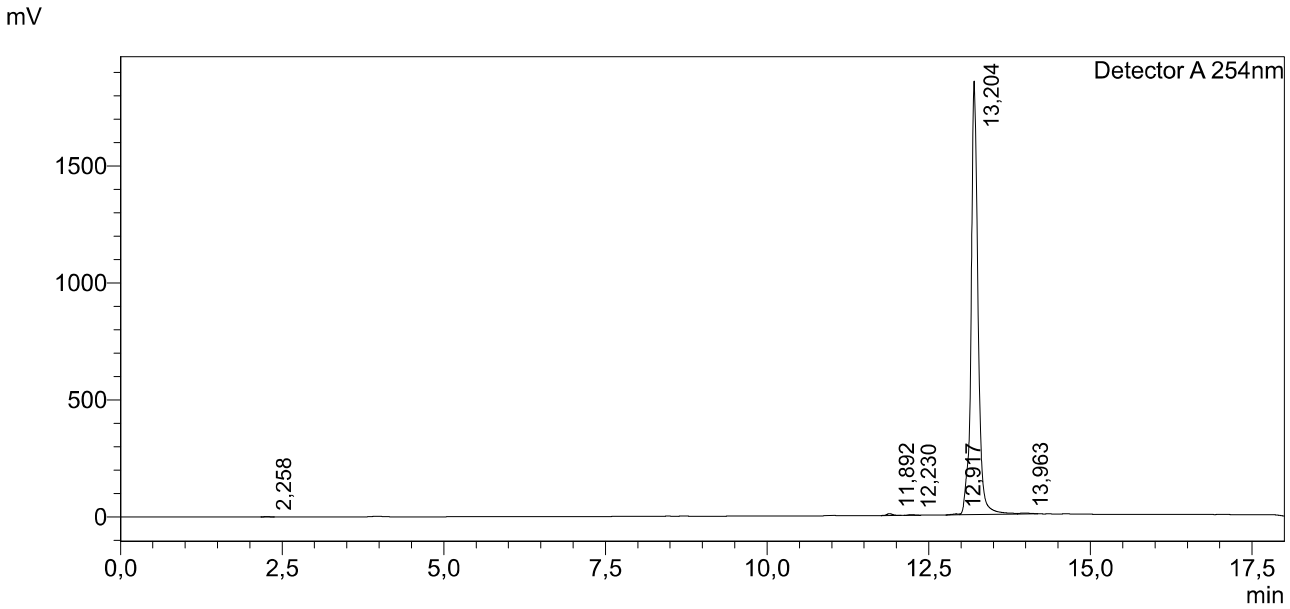

Peak Table

Detector A 254nm

Peak#	Ret. Time	Area	Height	Conc.	Unit	Mark	Name
1	2,258	9041	1822	0,065			
2	11,892	49020	7785	0,353			
3	12,230	18392	2782	0,132			
4	12,917	30213	3850	0,218			
5	13,204	13744747	1848042	98,957		V	
6	13,963	38252	3394	0,275		V	
Total		13889666	1867675				

Figure S4: 1H-NMR of compound 1

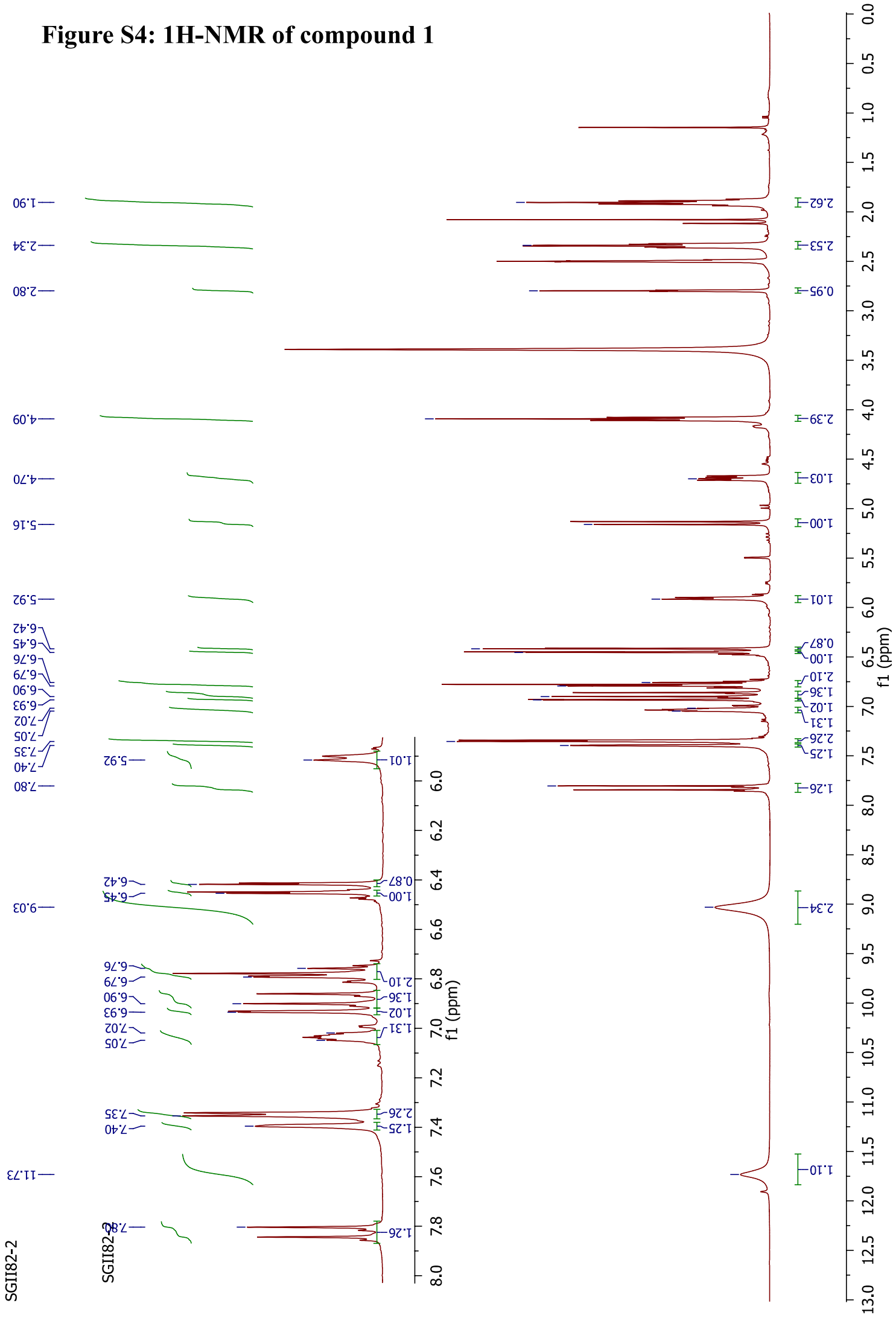

Figure S5: 13-C NMR of compound **1**

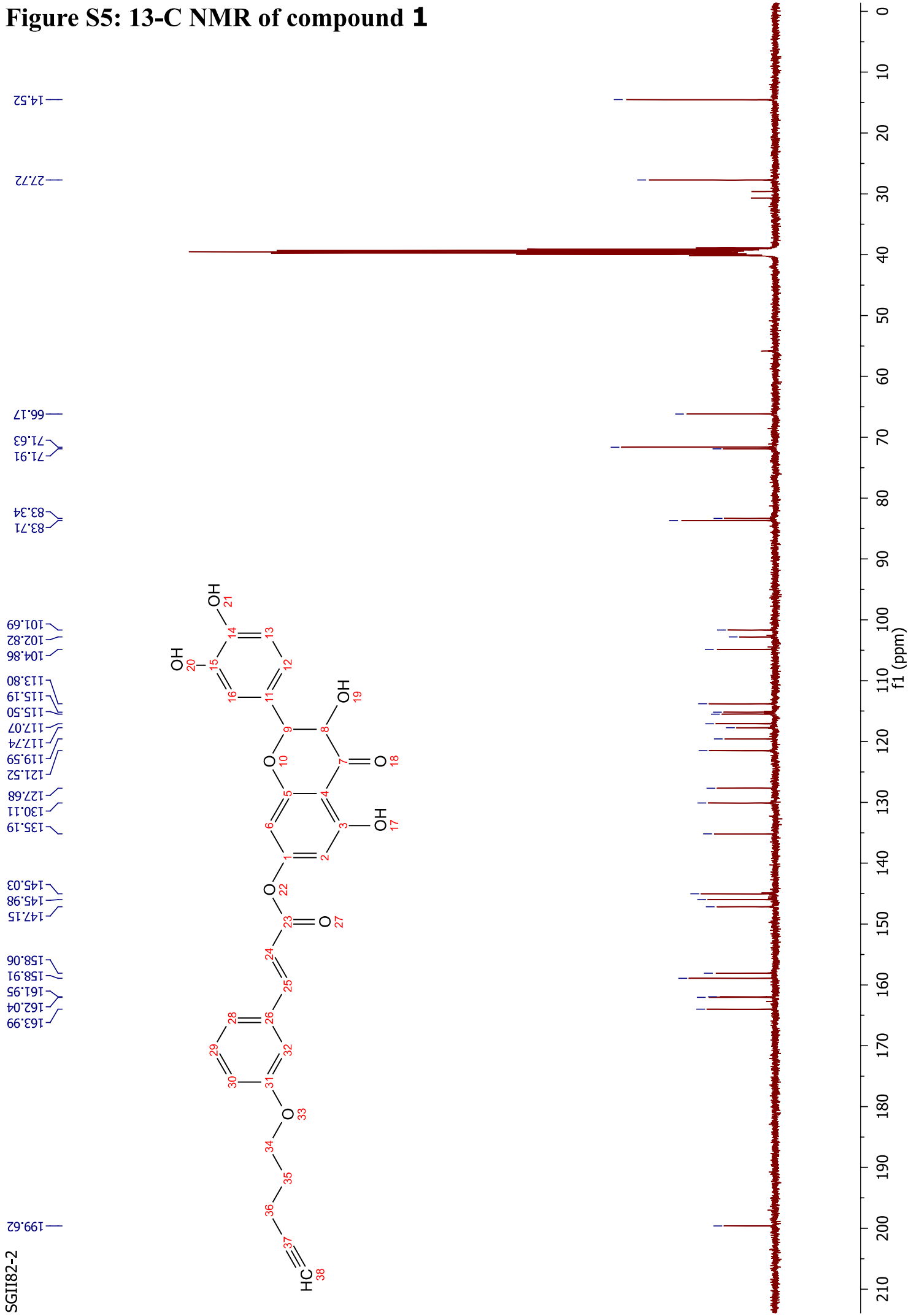

Figure S6: HPLC chromatogram of compound 2

SHIMADZU LabSolutions **Analysis Report**

<Sample Information>

Sample Name	: SG-II-83		
Sample ID	:		
Data Filename	: SG-II-83.lcd		
Method Filename	: Analysis 15 cm 05-90 1mL +50-1000 Standard.lcm		
Batch Filename	: batchj.lcb		
Vial #	: 1-68	Sample Type	: Unknown
Injection Volume	: 20 uL		
Date Acquired	: 15/10/2019 18:53:24	Acquired by	: System Administrator
Date Processed	: 15/10/2019 19:11:28	Processed by	: System Administrator

<Chromatogram>

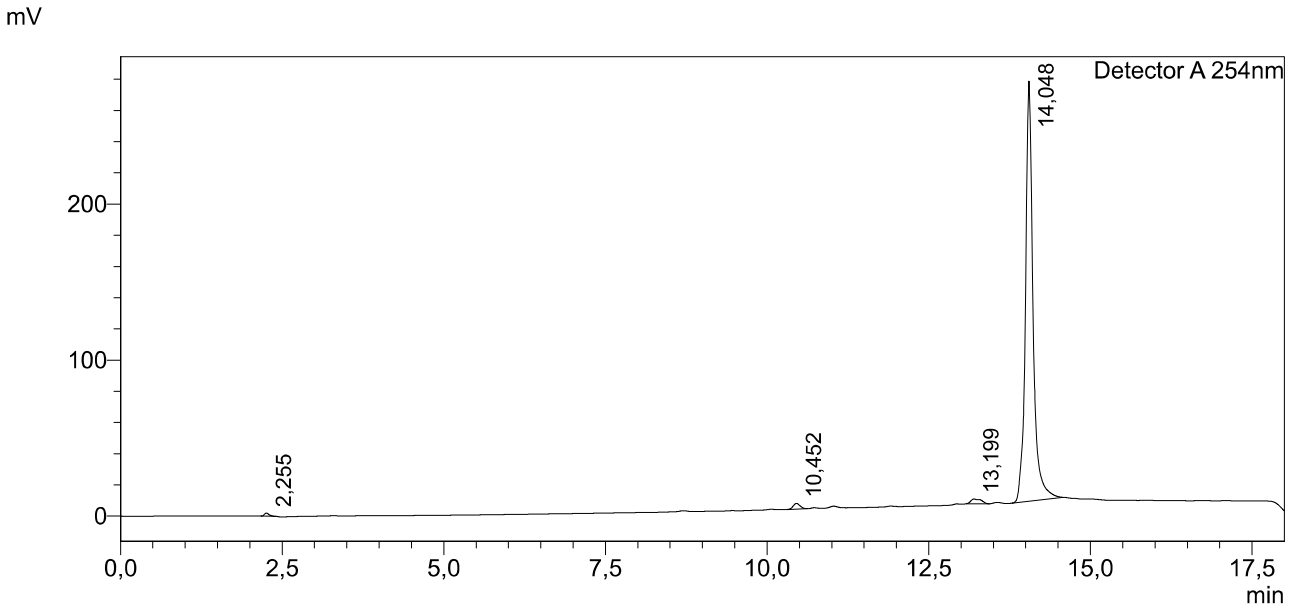

Peak Table

Detector A 254nm

Peak#	Ret. Time	Area	Height	Conc.	Unit	Mark	Name
1	2,255	10122	2050	0,447			
2	10,452	27219	3660	1,201			
3	13,199	33912	3048	1,496			
4	14,048	2195392	268690	96,856			
Total		2266645	277449				

Figure S7: 1H-NMR of compound 2

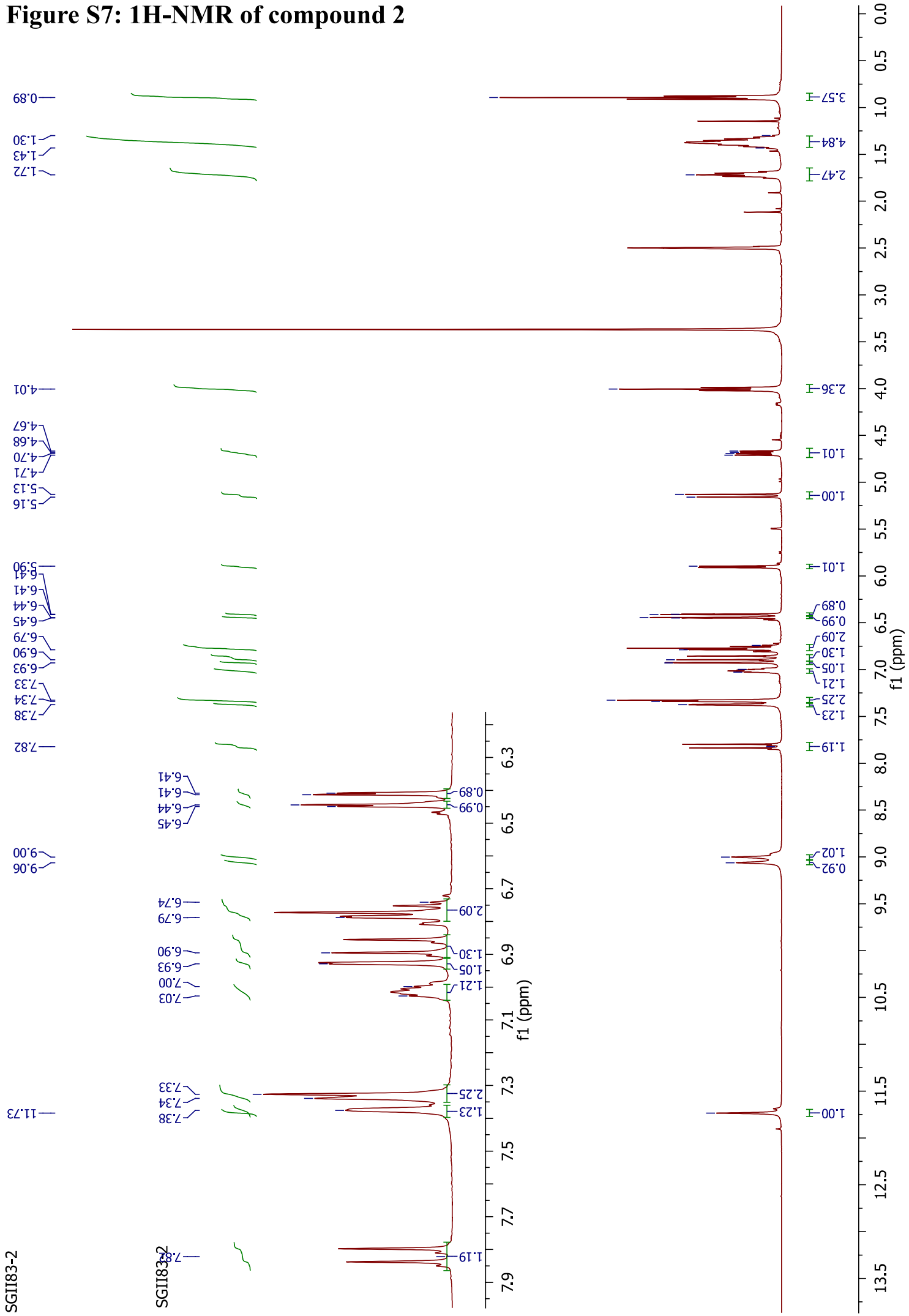

Figure S8: 13C-NMR of compound 2

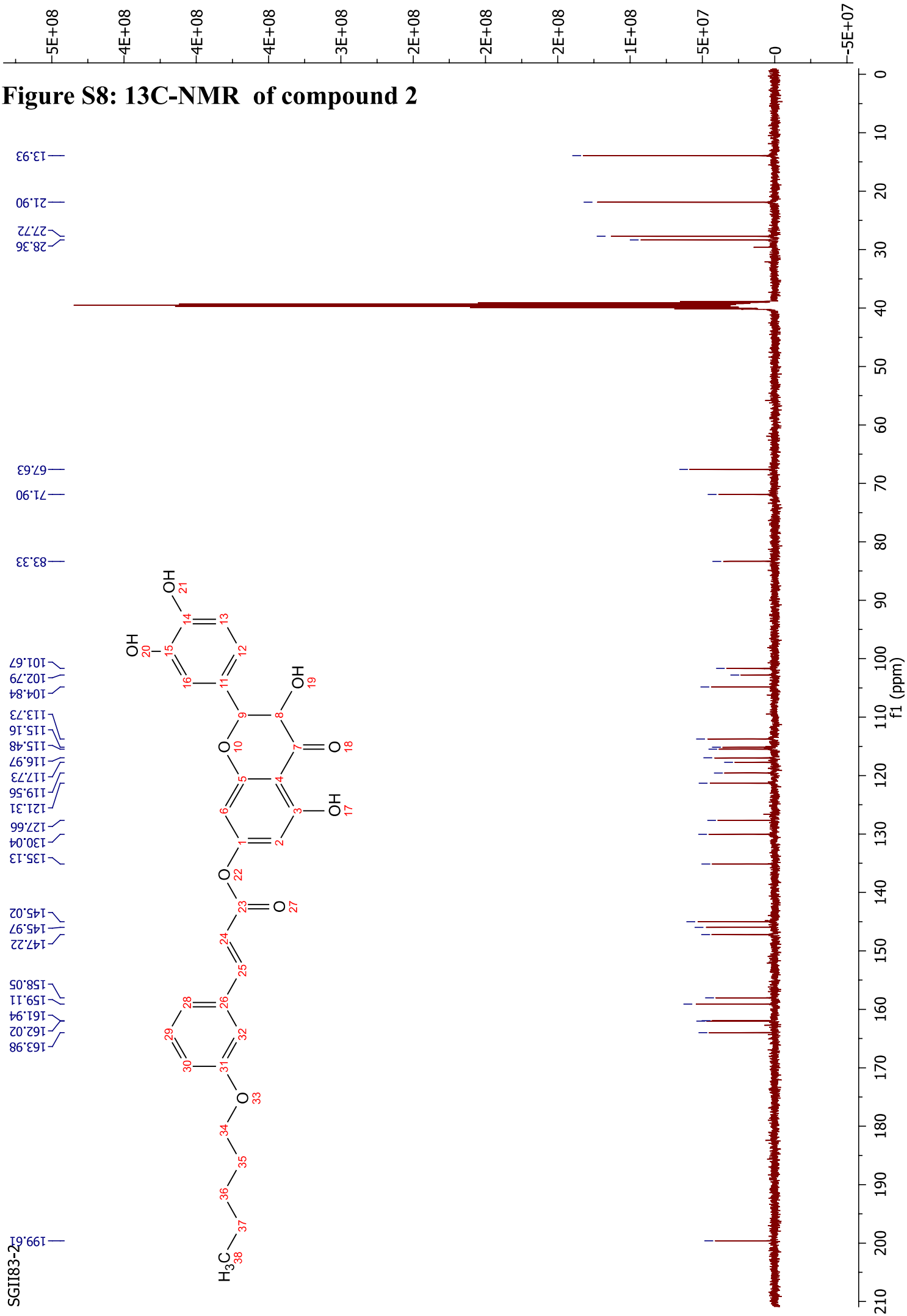

Appendix III:

Gunesch S.; Schramm, S.; Decker, M. Natural antioxidants in hybrids for the treatment of neurodegenerative diseases: a successful strategy? *Future Med. Chem.* **2017**, *9* (8), 711-713.

https://doi.org/10.4155/fmc-2017-0073

Editorial

Future Medicinal Chemistry

Natural antioxidants in hybrids for the treatment of neurodegenerative diseases: a successful strategy?

"The combination of natural antioxidants with other moieties can often lead to disadvantageous drug properties, such as high MW, and therefore low bioavailability, poor solubility, rapid metabolism and hampered blood–brain barrier penetration."

First draft submitted: 20 March 2017; Accepted for publication: 21 March 2017; Published online: 9 May 2017

Keywords: drug design • oxidative stress • reactive oxygen species

Sandra Gunesch[1], Simon Schramm[1] & Michael Decker*,[1]
[1]Pharmazeutische & Medizinische Chemie, Institut für Pharmazie & Lebensmittelchemie, Julius-Maximilians-Universität Würzburg, Am Hubland, D-97074 Würzburg, Germany
*Author for correspondence:
Tel.: +49 0 931 31 89676;
michael.decker@uni-wuerzburg.de

It is well established that oxidative stress is one of the characteristics of neurodegenerative diseases, such as Alzheimer's disease (AD) and Parkinson's disease [1]. Free radicals, that is, reactive oxygen species (ROS) and reactive nitrogen species, are damaging a variety of biomolecules like lipids, proteins and DNA. Such radicals are generated in the pathology of neurodegenerative diseases and eventually lead to neuronal cell death. They contribute to the overall pathophysiology and pathogenesis of these diseases, but are not their sole cause. In fact, it is unclear until now at which stage of the pathophysiological cascades oxidative stress occurs. Irrespective of the stage though, it is obvious that ROS enhance if not multiply the effects of the neuropathological cascades [1].

In AD, for example, pathological mechanisms mainly include hyperphosphorylation of T proteins, reduction of acetylcholine receptor levels, mitochondrial dysfunction, neuronal DNA damage, cerebral glucose hypometabolism, aggregation of β-amyloid peptides (Aβ) and oxidative stress [1,2]. With several mechanisms contributing to a complex pathological network, development of therapeutically applicable drugs is extremely challenging. A drug addressing only one biological target is probably not going to yield any success in stopping neurodegenerative diseases. Therefore, multitarget or hybrid drugs – combining two or more pharmacologically active units – that are capable of modifying several biological targets, may overcome the shortcomings of a single-target drug. Many multitarget compounds have been developed in recent years [3]. A very significant number of those compounds contain – mostly natural – antioxidants to target oxidative stress, therefore counteract the formation of ROS and are claimed to hold the potential to interfere with the neuropathological cascades [3,4]. The term 'antioxidant' is actually kind of vague and unspecific in both the chemical and biological sense and more specific terms are desirable. The combination of natural antioxidants with other moieties can often lead to disadvantageous drug properties, such as high MW, and therefore low bioavailability, poor solubility, rapid metabolism and hampered blood–brain barrier penetration. Problems typical for natural antioxidants also include rapid CYP metabolism – often 3A4 – and CYP induction.

We want to shortly discuss both the physicochemical as well as the cell-based *in vitro* assays that have been applied for assessing the 'antioxidant' properties of multitarget compounds containing antioxidant

FUTURE SCIENCE part of fsg

moieties and discuss what the outcomes of these assays actually mean, before we report on some very recent *in vivo* studies.

"A tacrine–ferulic acid hybrid...showed reduction of oxidative stress markers as well as positive effects on learning and memory in transgenic Alzheimer's disease mice"

In vitro cell-free assays

Natural antioxidants belong to very diverse chemical classes including carotenoids, vitamins C and E, stilbene derivatives, curcuminoids, phenolic acids (such as cinnamic, caffeic and ferulic acids) and flavonoids (such as quercetin, rutin and genistein). Due to this structural diversity it is assumed that they exhibit different modes of action [4]. The cell-free assays used to assess antioxidant activity *in vitro* are fairly similar in what properties they determine, namely their ability to scavenge radicals. These assays include the DPPH assay, an ABTS scavenging assay, the NBT assay and the oxygen radical absorbance capacity assay [5]. The oxygen radical absorbance capacity assay, for example, provides quantification of the test compounds' abilities to protect fluorescein from being oxidized by scavenging peroxyl radicals. Tacrine–ferulic acid hybrids, for example, show even higher values than the natural antioxidant ferulic acid by itself [6,7].

The ability of molecules to scavenge radicals determined in these assays is a prerequisite and an indication for the occurrence of effects in cell-based assays or *in vivo*, but not more than that. For that reason, more advanced cell-based assays are indispensable for better prediction of 'antioxidant' and therapeutically desirable activities *in vivo*.

In vitro cell-based assays

A variety of set-ups can be used *in vitro* to simulate disease-like conditions in cells, including oxidative stress, and to investigate the neuroprotective properties of test compounds. To quantify the protection against ROS-mediated apoptosis, cells are incubated with ROS-inducing or producing agents in the presence of the antioxidant compounds and the experimental read-out is the reduced cell viability determined in an MTT (3-[4,5-dimethylthiazol-2-yl]-2,5-diphenyltetrazolium bromide) or a chemically related assay.

Different cell lines are established that reflect the quite diverse origins of ROS. Mouse hippocampal HT-22 cells are used to study neuroprotective effects of hybrids toward ROS produced by glutamate-induced toxicity [8]. Presence of high glutamate concentrations in culture medium leads to glutathione depletion inside the cells. This causes ROS accumulation leading to cell death by apoptosis. Aβ exposure can also induce oxidative damage in cells and lead to apoptosis due to Aβ-induced mitochondrial dysfunction [9]. Protection against Aβ-induced oxidative stress through ferulic–tacrine acid hybrids was shown in PC-12 cells [10], a pheochromocytoma cell line of the rat adrenal medulla. MC-65 and SH-SY5Y are human neuroblastoma cell lines and are also applied in such assays since they derive from neuronal tissue and are therefore very suitable to investigate neurodegenerative diseases. For example, SH-SY5Y cells were used to investigate neuroprotection of tacrine–melatonin hybrids against Aβ-induced toxicity [11]. This cell line also served to investigate ROS production induced by application of hydrogen peroxide and rotenone. Rotenone specifically inhibits mitochondrial complex I leading to increased ROS formation and mitochondrial-induced apoptosis [12], whereas hydrogen peroxide causes DNA damage and lipid peroxidation, being a source of nonselective reactive oxygen species [13].

Drawbacks & first *in vivo* data

Curcumin represents a prime example for a natural product for which numerous beneficial effects have been claimed and that has also been used in hybrid molecules. A remarkable review has been published recently [14], that discusses the positive results of numerous *in vitro* assays found for this compound and derivatives thereof and the article raises some questions: low solubility, instability due to the oxidation-prone phenolic and enolic hydroxyl groups, the Michael system and its fluorescent properties, respectively, are likely leading to false-positive results *in vitro* for curcumin and curcumin-derived compounds . Albeit to a lower extent, these false positives can also occur with other natural products that, for example, possess a Michael system.

Numerous multitarget compounds containing antioxidant moieties have been claimed to be lead structures for AD therapy after their investigation in one or more of the above described *in vitro* assays (cell-free and/or cell-based). Nevertheless, only *in vivo* studies giving access to information about bioavailability, blood–brain barrier penetration and *in vivo* neuroprotection plus antineuroinflammation, are really answering the question, whether such compounds hold true therapeutic potential. Only very recently first *in vivo* data has become available [15]. A melatonin–curcumin hybrid was applied to 4-month-old transgenic mice and *in vitro* results could be confirmed *in vivo* with regard to reduction of markers of oxidative stress on the molecular level [16], even though no behavioral effects have been reported. However, a tacrine–ferulic acid hybrid described above showed reduction of oxidative stress markers as well as positive effects on learning and memory in transgenic AD mice [10].

Summary

Taken together, multitarget (hybrid) compounds and other chemical compounds containing antioxidant moieties are prone to several disadvantages: metabolic instability, false-positive results in (some – nonsuitable) *in vitro* assays and unknown modes of action. There are also problems of transferring the relevance of *in vitro* data to an *in vivo* setup. Nevertheless, this does not mean that antioxidants are not versatile and promising components of hybrids, but only specific assays for assessing the compounds' activities are suitable. The methods deemed suitable have to be carefully selected on the basis of the chemical structure of the compounds under investigation. Positive results should not be overinterpreted. The often unknown modes of action of natural antioxidants with regard to neuroprotection *in vitro* and *in vivo* still hamper the development of effective hybrid molecules.

Financial & competing interests disclosure

Financial support by the German Research Foundation (Deutsche Forschungsgemeinschaft) DFG DE 1546/6-1 and 6-3 is gratefully acknowledged. The authors have no other relevant affiliations or financial involvement with any organization or entity with a financial interest in or financial conflict with the subject matter or materials discussed in the manuscript apart from those disclosed.

No writing assistance was utilized in the production of this manuscript.

References

1 Thanan R, Oikawa S, Hiraku Y *et al.* Oxidative stress and its significant roles in neurodegenerative diseases and cancer. *Int. J. Mol. Sci.* 16(1), 193–217 (2015).

2 Karran E, De Strooper B. The amyloid cascade hypothesis: are we poised for success of failure? *J. Neurochem.* 139(Suppl. 2), 237–252 (2016).

3 Ismaili L, Romero A, do Carmo Carreiras M, Marco-Contelles J. Multi-target directed antioxidants as therapeutic agents: putting the focus on the oxidative stress. In: *Design of Hybrid Molecules for Drug Development.* Decker M (Ed.). Elsevier, Oxford, UK, 5–46 (2017).

4 Pisoschi AM, Pop A. The role of antioxidants in the chemistry of oxidative stress: a review. *Eur. J. Med. Chem.* 97, 55–74 (2015).

5 López-Alarcón C, Denicola A. Evaluating the antioxidant capacity of natural products: a review on chemical and cellular-based assays. *Anal. Chim. Acta* 763, 1–10 (2013).

6 Benchekroun M, Bartolini M, Egea J *et al.* Novel tacrine-grafted Ugi adducts as multipotent anti-Alzheimer drugs: a synthetic renewal in tacrine-ferulic acid hybrids. *ChemMedChem* 10(3), 523–539 (2015).

7 Fang L, Kraus B, Lehmann J, Heilmann J, Zhang Y, Decker M. Design and synthesis of tacrine-ferulic acid hybrids as multi-potent anti-Alzheimer drug candidates. *Bioorg. Med. Chem. Lett.* 18(9), 2905–2909 (2008).

8 Kling B, Bücherl D, Palatzky P *et al.* Flavonoids, flavonoid metabolites, and phenolic acids inhibit oxidative stress in the neuronal cell line HT-22 monitored by ECIS and MTT assay: a comparative study. *J. Nat. Prod.* 77(3), 446–454 (2014).

9 Lin MT, Beal MF. Mitochondrial dysfunction and oxidative stress in neurodegenerative diseases. *Nature* 443(7113), 787–795 (2006).

10 Pi R, Mao X, Chao X *et al.* Tacrine-6-ferulic acid, a novel multifunctional dimer, inhibits amyloid-β-mediated Alzheimer's disease-associated pathogenesis *in vitro* and *in vivo*. *PLoS ONE* 7(2), e31921 (2012).

11 Fernandez-Bachiller MI, Perez C, Campillo NE *et al.* Tacrine-melatonin hybrids as multifunctional agents for Alzheimer's disease, with cholinergic, antioxidant, and neuroprotective properties. *ChemMedChem* 4(5), 828–841 (2009).

12 Sipos I, Tretter L, Adam-Vizi V. Quantitative relationship between inhibition of respiratory complexes and formation of reactive oxygen species in isolated nerve terminals. *J. Neurochem.* 84(1), 112–118 (2003).

13 Halliwell B, Aruoma OI. DNA damage by oxygen-derived species. Its mechanism and measurement in mammalian systems. *FEBS Lett.* 281(1–2), 9–19 (1991).

14 Nelson KM, Dahlin JL, Bisson J, Graham J, Pauli GF, Walters MA. The essential medicinal chemistry of curcumin. *J. Med. Chem.* 60(5), 1620–1637 (2017).

15 Muñoz-Torrero D. Multi-target anti-Alzheimer hybrid compounds: do they work *in vivo*? In: *Design of hybrid molecules fordrug development.* Decker M (Ed.). Elsevier, Oxford, UK, 167–192 (2017).

16 Chojnacki JE, Liu K, Yan X *et al.* Discovery of 5-(4-hydroxyphenyl)-3-oxo-pentanoic acid [2-(5-methoxy-1*H*-indol-3-yl)-ethyl]-amide as a neuroprotectant for Alzheimer's disease by hybridization of curcumin and melatonin. *ACS Chem. Neurosci.* 5(8), 690–699 (2014).

Curriculum Vitae